Mechanisms of robust feature extraction in early visual processing

Dissertation for the award of the degree

Doctor rerum naturalium

of the Georg-August-Universität Göttingen

within the doctoral program *Neurosciences*

of the Georg-August University School of Science (GAUSS)

submitted by

Sebastian M. Molina-Obando

from Quito, Ecuador

Göttingen – Mainz, 2021

Thesis Advisory Committee (TAC) and Examination Board members

First referee and TAC supervisor

Silies, Marion, Prof. Dr.

Institute of Developmental Biology and Neurobiology (iDN),

Johannes Gutenberg University Mainz

Second referee and TAC supervisor

Fiala, André, Prof. Dr

Dept. of Molecular Neurobiology of Behaviour,

Schwann-Schleiden Research Centre, University of Göttingen

Third TAC supervisor

Gollisch, Tim, Prof. Dr

Dept. of Ophthalmology, Sensory Processing in the Retina,

University Medical Center Göttingen

Further members of the Examination Board

Dresbach, Thomas, Prof. Dr

Dept. of Anatomy and Embryology,

University Medical Center Göttingen

Clemens, Jan, Dr.

Neural Computation and Behavior group,

European Neuroscience Institute – Göttingen

Brett, Carter, Ph.D.

Synaptic physiology and plasticity group,

European Neuroscience Institute – Göttingen

Date of oral examination

09.02.2022

To my family and friends,

especially to Ángela, Katty and Lía.

Acknowledgements

Typing on this page as the last one to be written is a unique pleasure in the life of a Ph.D. student. Not because the hardest part is complete, but due to the happy memories that I recall. For all this I am in debt and would like to thank the following people:

Foremost, my deep gratitude to my mentor **Marion Silies**. Over the years she has been a cornerstone in my development as a scientist. I considered myself lucky to have been among her first "batch" of graduate students to whom she shared priceless lessons while establishing her Lab, first in Göttingen and later in Mainz. Thank you, Marion, for your patience, advice, enthusiasm, and integrity. With your supervision on my side, my personal pursuit of scientific knowledge has been and still is a thrilling journey.

My supervisors from the Thesis Advisory Committee, **André Fiala** and **Tim Gollisch**, for their insightful feedback during TAC meetings that shook my "roter Faden" and made it more solid. For supporting my thesis extensions that made possible to conceal my new life as a father. And for their advice to write a good thesis.

Thomas Dresbach, Jan Clemens, and **Brett Carter** for sharing their time with me as an extended thesis examination board. Their expertise in their respective fields nicely complement the evaluation of this thesis.

Current and previous staff members of the IMPRS Neuroscience office: **Sandra, Michael, Franziska, Mirja,** and **Jonas**. Their support resolving countless doubts and sharing valuable information helped in almost every step I took over the past years. Also, the GGNB office, for offering various courses that enriched my carrier.

All my colleagues from the Silies Lab. This work could not have been fulfilled without their support. I like to think about this work as a team's victory in which I was honored to take the lead. In every Lab meeting, every symposium or retreat, every lunch break, and every game night event. I would like to give some specific mentions.

To my previous and current office mates. To be around was more than enough to turn on fascinating conversations that shaped my rhetoric in both my personal and academic life. Many of the key ideas that made it to the different studies were born between the four walls of our office. I recall various "aha moments" that took my breath. **Burak,** thank you for your aid when I got stuck and for creating the fun and productive environment in the office. I have learned so many things from you but one I would like to stress: how to inspire others to become the best version of themselves. You have inspired me and continue doing so every day. **Juan**, I am grateful that you once chose to join the Silies Lab and became one of the

first students that I could supervise. During your Master thesis you made important contributions to what it became our first published paper (and the first of the Lab!). You taught me how to become a better educator which is something that I value the most. I am happy to still be part of joined projects in which you share your keen intellect. **Miriam,** our office is a brighter place because of you with the multiple meanings of this adjective: you are cheerful, clever, and promising. I am especially thankful for your countless volunteering to bring us together. **Freya,** I am happy that you chose our office to start your studies in the Lab. I cannot wait to be part of your personal journey as a fresh Ph.D. student.

To all Ph.Ds. (now postdocs!) that shared all their knowledge and skills when I first joined the Lab. They were, and still are, an important reference to me. **Luis,** for being my supervisor and accompanying me during my first steps in the Lab. I appreciate that initial guidance that contributed to my decision to stay. **Katja,** your skills in dissection rescued me from many attempts full of frustrations. You were kind to show me your mastery and let me learn from you. **Madhura**, for answering all my "one quick question" that sometimes opened a whole universe in a Slack thread. I specially value some lessons you taught me as a colleague: the gentleness while handling flies and the criticism while handling thoughts.

Elsa and **Marwa,** two very different students that allowed me to try my first methods as an educator. I hope that I could inspire you or guide you during your apprenticeship. You for sure were a guide during mine.

The irreplaceable laboratory technical support staff. I can recall many times that you offered your help even if I didn´t ask for it. And it was worth it. You made my work just better. **Jonas**, thank you for taking care of my fly stocks so many times when I couldn´t. **Christine,** thank you for your lessons in molecular biology and your outstanding good mood. **Simone, Barbara,** and **Lichi,** thank you for helping me in my adequation in the Lab when we moved to Mainz and for allowing me to practice some German with you.

All other Lab members that I haven´t had the pleasure to share projects with yet. I am sure the time will come! **Sofia, Leticia,** and **Giovanni,** for making the Martelli Lab a nice neighbor from which to learn. **Neel** and **Jackeline,** for your constant feedback about how the different data analysis pipelines could improve. You come with unbiased brand-new eyes. **Jonas P**, for your expertise on the bench and knowledge about molecular biology. **Carlotta,** for your immense knowledge about some fundamentals in sensory processing. Most of your contributions during Lab meetings re-evaluated my foundations. **Chris,** for our scientific discussions wherever and whenever they were needed. Thank you for taking the time to discuss with me and draw concepts (even on napkins if necessary) to make them clearer.

Abstract

The detection of changes in signal intensity, namely contrast, happens across senses. Visual systems extract contrast information at very early stages. The first cells to "sense" light, the photoreceptors, carry contrast information which is processed by their downstream neuronal circuitry. Visual systems have evolved to ensure robust ON and OFF detection in distinct ON- and OFF-selective or pathways. Downstream of a common photoreceptor input, the molecular mechanism to implement the split in ON and OFF pathways has been described in the vertebrate retina and involves a signal inversion in the ON pathway through inhibitory glutamatergic synapses at individual synaptic connection (Masu et al., 1995). In the first study of this thesis, using cell-type specific manipulations and pharmacogenetics, I demonstrate that the extraction of ON selectivity in *Drosophila* is rather a distributed and multisynaptic computation involving glutamatergic and GABAergic inhibitions. This raises the possibility that using more specific manipulation in other systems, including the vertebrate retina, might reveal a similar distributed coding strategy.

Contrast extraction by early visual processing serves as basis for later computations and eventually to guide motor behavior. In a dynamically changing world, rapid changes in illumination challenges proper contrast extraction in early stages when photoreceptors cannot adapt fast enough. Corrections downstream of photoreceptors are necessary to detect the same contrast equally well across distinct illuminations, namely in a luminance-invariant manner. In the second study, this thesis explores the correction mechanism behind ON and OFF luminance-invariant behaviors in *Drosophila*. In both ON and OFF pathways, luminance-sensitive signals scale contrast signals to achieve luminance-invariant behaviors. For that, distinct lamina first-order interneurons diversify and asymmetrically distribute luminance and contrast signal across pathways. This second study changes the current understanding of the role of these three first-order interneurons, previously thought to be specific inputs for either the ON or the OFF pathway.

In the first study and second study we show that contrast extraction is supported by parallel inputs, involving different inhibitory connections and distinct lamina input neurons, respectively. In the third study of this thesis, I show that a parallel input architecture leads to robust contrast extraction. Individual input pathways can be sufficient but not necessarily required to implement ON selectivity. These findings align with the idea of neuronal circuits being degenerate, in which structurally different elements can implement the same function, leading to robustness. Since comparative connectomics reveals parallel connectivity as a common trait across animals and sensory systems (Barsotti et al., 2021), a distributed feature extraction might be a general strategy present in other systems too to achieve functional robustness.

Table of content

1.   General introduction

Nervous systems of animals have evolved to detect the stimuli in their environment that are critical for their survival. For that, different sensory systems process several types of stimuli, e.g., light, odors, or air vibrations. Since these stimuli vary across time and space, various mechanisms must be in place to capture and process distinct features, e.g., absolute intensity or intensity change. At early stages, each sensory system has a specialized receptor cell that transduces the energy of the stimuli into electrochemical signals. The receptor cell is part of a neuronal circuit and pass the signals to downstream neurons which transform them in different ways. The activity -or responses- of several neurons starts to correlate with distinct stimulus features, which has led to the categorization of neurons in groups or pathways that detect specific features. Different mathematical algorithms or solutions have been suggested to explain feature detection in each pathway. For example, the detection of contrast increments (ON) or decrements (OFF) is split in two distinct pathways, where neurons depolarize either to ON or to OFF. Since all neurons receive the same input signal, a signal inversion, being the algorithm or solution, must happen in one of the pathways. Across sensory systems described so far, this signal inversion happens in the ON pathway (Chalasani et al., 2007; Masu et al., 1995). The biological mechanisms that underlie this algorithm, and if these mechanisms are similar across systems, is still being studied. This thesis will explore the molecular and cellular mechanisms for ON contrast detection in the *Drosophila* visual system, comparing them with those described in other well-known system: the vertebrate retina.

Since sensory computations are ultimately used to guide the animal's behavior, sensory systems must properly work when the world is dynamically changing. For example, the visual system allows humans to detect, and later perceive, contrast in a luminance-invariant manner, meaning independent of the background illumination (Burkhardt et al., 1984). Other animals must do that too, and neuronal correlates have been found in the cat visual system (Mante et al., 2005). However, how luminance-invariant behaviors are implemented by neuronal circuits is not fully understood. A recent study in *Drosophila* shows that visually guided OFF behavior is nearly luminance-invariant and describes a mechanism in which a luminance-sensitive neuron scales the contrast response when background luminance quickly changes. This mechanism ensures appropriate behavioral responses to contrast when background luminance is quickly changing (Ketkar et al., 2020). However, if this mechanism is also in place for invariant behavioral responses to ON contrasts it not known, and it cannot be assumed to use the same mechanism since the ON and OFF pathways

have developed several anatomical and physiological asymmetries (Behnia et al., 2014; Chichilnisky and Kalmar, 2002; Jin et al., 2011; Leonhardt et al., 2016; Ratliff et al., 2010). This thesis will explore the neuronal mechanisms implementing luminance-invariant behavior in the *Drosophila* ON pathway.

Lastly, sensory systems are known to be robust in encoding distinct features to properly guide animal's behavior. With robustness, I refer to the ability of generating the <u>same output</u> despite of challenging conditions. What type of brain architecture could implement this? Neuronal wiring similarities across animals and systems reveal parallel connectivity between neurons as one ubiquitous trait. It has been proposed that common traits reveal a common optimal architecture for brain function (Barsotti et al., 2021). However, if parallel connectivity is indeed a predictor of function has not been explored. Since the *Drosophila* ON pathway has highly interconnected neurons receiving structurally different parallel inputs (Molina-Obando et al., 2019; Takemura et al., 2013), it is a system where to analyze information flow and test functional predictions. This thesis will investigate how neuronal responses to ON can be robustly implemented by parallel inputs.

In the following sections, I first review contrast detection in the vertebrate retina and the insect optic lobe, revealing similarities and differences in anatomy and physiology that lead to a remarkably similar implementation of contrast detection. Second, I review how contrast perception/behavior is stable despite sudden changes of illumination challenging early visual processing. Third, I review the state of the art of EM reconstructions and connectomes which allow to formulate theories about how the architecture of the brain achieves robustness. Finally, I state the aims of my thesis.

1.1   Contrast detection in early visual processing

The understanding of how any feature, e.g., contrast, is detected has changed over the past decades. Every technological and scientific advance, revealing new details about the anatomy and the function of the brain, has allowed conceptualists to create new theories about how the brain process information. For example, the Golgi staining, that allows a random stain and visualization of single cells, was used by Ramón y Cajal and others to reveal the morphological diversity of neurons, as well as to trace neural circuits in many brain regions and across animals (Fischbach and Dittrich, 1989; Ramón y Cajal et al., 1915). The common observations in early experiments led to the formulation of the Neuron Doctrine, which says that the neuron is the anatomical and physiological unit of the nervous

system (Jones, 1994). The invention of the microelectrode, that allows the recording of single neuron electrical activity, led to the observation that some neuronal responses correlate with distinct features of the stimulation, and so the idea of single cells as single feature detectors was born (Martin, 1994). Looking at stimulus-response correlations of connected neurons, each located at a different level from the sensory periphery to the central brain, scientist observed that higher-order cells correlated with more complex and abstract stimulus features. For example, the responses of peripheral photoreceptors correlated with light offset, but a couple of connections later in the retina, ganglion cells responses correlated with the movement of objects (Masland, 2012). The idea of feature detection as a progressive and hierarchical process has been coined, and it is described to happen in neuronal pathways.

In the field of sensory systems, the term "pathway" normally refers to a group of interconnected neurons detecting a specific feature, although it can sometimes also refer to neurons downstream of or upstream of an neuron to highlight (Bloomfield and Dacheux, 2001; Gollisch and Meister, 2010; Livingstone and Hubel, 1988). In this thesis I use the first definition if not specified otherwise. How distinct stimulus features are encoded separately in different pathways is one relevant question in neuroscience. The split into ON and OFF pathways, for the detection of stimulus increments (ON) and decrements (OFF) is one of the most prominent examples across sensory systems, for example, in electrolocation, temperature detection, hearing, olfaction, and vision (Gallio et al., 2011; Metzner and Viete, 1996; Scholl et al., 2010; Tichy and Hellwig, 2018; Werblin and Dowling, 1969). Importantly, the split in ON and OFF pathways is described as energetically advantageous for neural processing (Gjorgjieva et al., 2014; Sterling and Freed, 2007).

For all sensory system studied to date, the ON and OFF pathways arise downstream of a common input. The input, regardless of connecting to an ON or OFF contrast selective neuron, exerts the same action, and, therefore, a specific mechanism in the contrast selective neurons must implement the split. The mechanism usually implies a signal inversion in one of the pathways involving an inhibition between the input and the downstream neurons. Known mechanisms in olfaction and vision have described the signal inversion in the ON pathway by using inhibitory glutamate receptors (Chalasani et al., 2007; Masu et al., 1995). In this section, I review how ON contrast is detected in early visual processing. I focus on two distinct visual systems where this computation has been described: the vertebrate retina and the *Drosophila* optic lobe, before drawing some similarities and differences in mechanisms between the two visual systems that lead to remarkably common implementations.

1.1.1   Contrast detection in the vertebrate retina

In this section, I will mostly focus on studies in the mouse retina due to the precise classification of the different ON and OFF contrast selective cells (Euler et al., 2014; Shekhar et al., 2016), although some evidence comes from other vertebrates such as the mudpuppy, carp or the tiger salamander.

Anatomy

The vertebrate retina comprises 10 different anatomical layers and a columnar structure where different neurons make synaptic contacts (Masland, 2012). Visual information goes from outer layer to inner layers, along which different neuronal types have been described. Briefly, retinal photoreceptors, the first neurons that process light, project their terminals into the outer plexiform layer (OPL) where they make synaptic contact with bipolar cell (BCs). BCs project from the OPL to the inner plexiform layer (IPL) to contact retina ganglion cells (RGCs), which then take the visual information out of the retina towards central brain areas (Figure 1Ai). In both the OPL and IPL, horizontal (HCs) and amacrine cells (ACs), respectively, connect the neurons laterally (Figure 1Aii).

Neighboring photoreceptors sample neighboring points in the visual space and pass the information to downstream neighboring neurons. This keeps the mapping of the visual input at all levels, a phenomenon defined as retinotopy. There are two types of photoreceptors: cones and the rods. Cone and rod pathways are highly interconnected (Rogerson et al., 2017) and make most contacts with downstream contrast-selective BCs in the OPL (Euler et al., 2014; Kato and Negishi, 1979) which exist in at least 14 different types (Euler et al., 2014). BCs types then project to the same or different IPL sublayers, with the OFF subgroup (see physiology) projecting to sublayers 1-2 and the ON subgroup to sublayers 3-5 (Figure 1Ai).

A
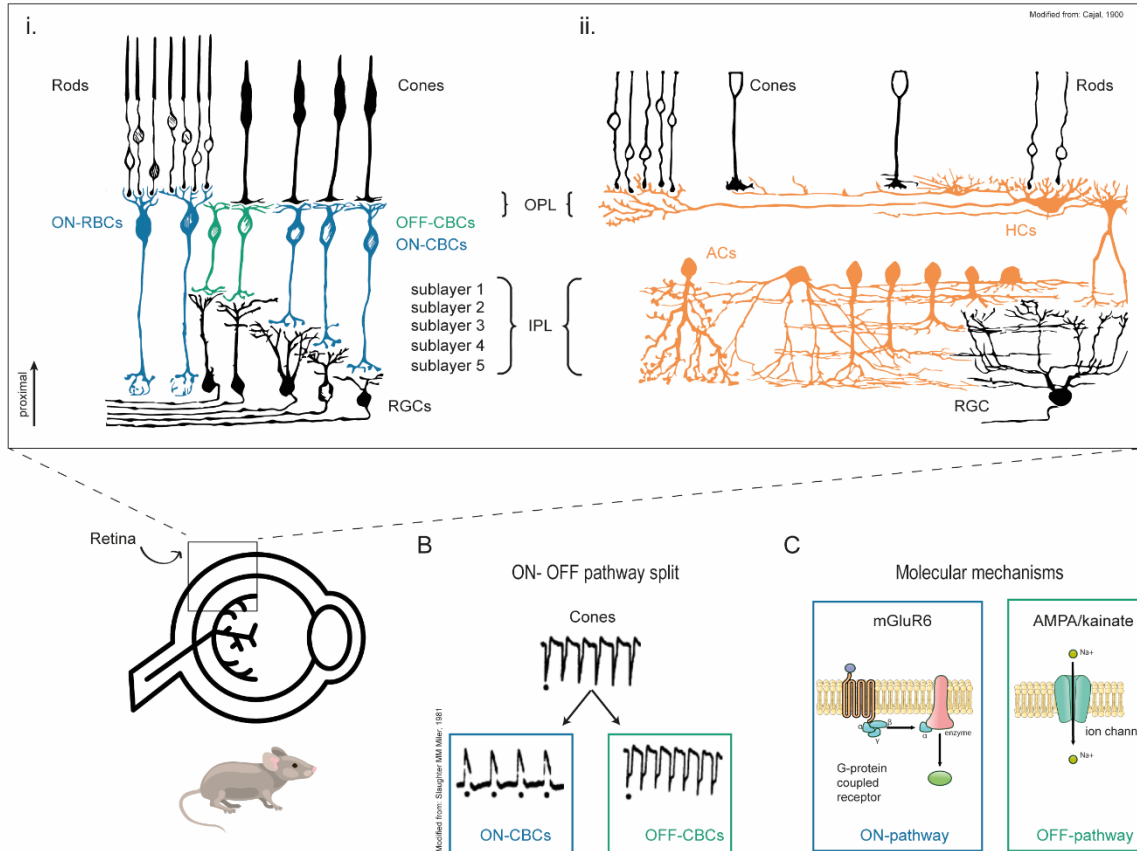
Figure 1: **The vertebrate retina.** **(A)** Layer organization and main neuronal types in the vertebrate retina. i. Neurons belonging to a feedforward signal pathways, from photoreceptors' input to retinal ganglion cells (RGCs) outpus. Highlighted are the ON- (blue) and OFF- (green) pathway bioplar cells (BCs) ii. Highlighted (orange) the horizontal (HCs) and amacrine (ACs) cells for lateral connections in the retina. **(B)** Physiological responses from photoreceptos and ON- and OFF-BCs showing the signal inversion in the ON-BCs. The black dote shows a light onset. Modified from (Miller and Slaughter, 1986). **(C)** Molecular mechanisms showing the different glutamate receptor classes in the ON and OFF pathways.

Physiology

When photons hit the photoreceptors in the retina, the photopigment rhodopsin, a transmembrane protein with a light-absorbing chromophore, absorbs their energy and changes its configuration, leading to a chemical cascade that ends up hyperpolarizing the cell (Fu and Yau, 2007). The cascade includes the activation of multiple protein complexes by one rhodopsin, leading to signal amplification. When the number of photons decreases, the process reverses and photoreceptors depolarize to OFF, leading to dark current (Hagins et al., 1970) and photoreceptors' graded potentials. Although the number of subtypes of cones and abundance vary across species (Hart, 2001; Peichl, 2005), all of them present similar characteristics having a faster response time course to a flash and less light sensitivity than rods. Importantly, different cones have different spectral sensitivity, playing an important role in daylight and color vision. Rods, on the other hand, have a slower

response time course and possess high light sensitivity, therefore playing a role for scotopic vision (Kawamura and Tachibanaki, 2008).

Downstream of photoreceptors, ON-BCs depolarize to ON due to a signal inversion introduced by metabotropic inhibitory glutamate receptors (mGluRs), whereas OFF-BCs keep the OFF polarity thanks to a sign-conserving glutamatergic excitatory synapse (Euler et al., 1996) (Figure 1B-C). The signal transduction in ON-BPs has been studied in detail (Martemyanov and Sampath, 2017). In brief, photoreceptor release glutamate onto ON-BPs dendrites, where inhibitory glutamate receptors mGluR6 are expressed. The activation of these metabotropic receptors generates a G-protein signaling cascade that leads to the closing of transient receptor potential (TRP) M1 channels and hyperpolarizes the cell. In response to light, TRPM1 channels opened by a protein complex called GAP and ON-BPs depolarize. The expression pattern of mGluR6 or the G-protein machinery exclusively localizes in the OPL (Masu et al., 1995; Vardi, 1998) where all type of BCs project their dendrites to contact photoreceptors.

All this research led to the idea that the signal inversion in the ON pathway is implemented by the glutamatergic inhibitory synapse between photoreceptors and ON-BCs. However, it is important to consider that all these studies used non-conditional knock out mice in which the gene disruption of *mGluR6* (Masu et al., 1995) or *TRPM1* (Koike et al., 2010; Morgans et al., 2009; Shen et al., 2009) affected all types of ON-BCs simultaneously. There are at least 8 types of ON-BPs downstream of photoreceptors (Euler et al., 2014; Shekhar et al., 2016; Tsukamoto and Omi, 2017). Although all of them depolarize to ON, they have different response dynamics (Ichinose et al., 2014). Moreover, ON-BCs are highly interconnected through lateral interneurons and functionally influence each other leading to an increase in functional diversity (Euler et al., 2014; Franke et al., 2017; Rogerson et al., 2017). For example, glycinergic inhibitory ACs modulate BC output in an indirect way by inhibiting GABAergic ACs (Franke et al., 2017), or ON rod bipolar cells (RBCs) feed sign-conserving signals to ON cone bipolar cell (CBC) via amacrine cells (Bloomfield and Dacheux, 2001).

1.1.2   Contrast detection in the *Drosophila* optic lobe

In this section, I mostly describe the state-of-the-art knowledge about contrast selectivity in the *Drosophila* optic lobe. Some basic notion about anatomy and physiology of photoreceptor and first-order lamina interneurons come from other insects as well, such as the blowfly.

Anatomy

The fly visual system resides in the two optic lobes at both sides of the brain, two relatively big regions containing half of the total number of neurons in the fly brain (Strausfeld, 1976). The first neuronal layer is called the retina, which has a columnar organization in which its ~800 facets cover together 180˚ of visual angle. Downstream of the retina and following the information flow from the periphery to the central brain, different neuropiles are present: the lamina, the medulla, the lobula and the lobula plate (Fischbach and Dittrich, 1989). Briefly, photoreceptors (R1-6) housed in the retina project their axons terminals to contact lamina neurons, which then project to the medulla (Figure 2Ai). Medulla neurons either stay intrinsic or project their axons to the lobula plate and/or the lobula, where they contact direction selective (DS) cells (Figure 2Aii). Additionally, the medulla also has neurons expanding horizontally across different medulla columns and present at different medulla layers (Nern et al., 2015) (Figure 2Aiii). DS cells then project to the lobula plate, where they contact lobula plate tangential cells (LPTCs), neurons that finally project out of the optic lobe (Figure 2Aiii).

The different columns in the retina are called facets or ommatidia. Each ommatidium contains eight photoreceptor cells which are categorized in two different groups based on their relative location: the inner and the outer photoreceptors (Kirschfeld, 1967). These two categories differ in the expression of specific opsins for light detection. R1 to R6 photoreceptor form the outer group and express the opsin Rh1, whereas R7 and R8 form the inner group. R7 stochastically expresses either the UV-sensitive opsins Rh3 or Rh4, and R8 expresses either the blue-absorbing Rh5 or the green-absorbing Rh6 (Franceschini et al., 1981). The inner group form part of the color vision pathway (Schnaitmann et al., 2018). The non-color photoreceptors, R1 to R6, project their axon terminals to the next neuropile, the lamina, whereas R7 and R8 photoreceptors skip the lamina and project directly to the medulla. (Figure 2Ai).

The columnar organization of the lamina is composed of cartridges, columns containing at least 12 types of lamina neurons (Tuthill et al., 2013). Six different R1-6 photoreceptors from six different neighboring ommatidia, sampling the same point in space, project to one common lamina cartridge, establishing the retinotopic map, and at the same time, increasing the number of photons detected per visual angle without compromising visual acuity, a phenomenon called neuronal superposition (Agi et al., 2014; Nilsson, 1983). From the 12 different lamina neuron types, intracolumnar lamina neurons L1 to L3 have been studied in detailed. They receive direct input from R1-6 and are considered first-order interneurons (Silies et al., 2014). L neurons project to the same or distinct medulla layers,

where they make synaptic contact with contrast-selective second-order interneurons (Silies et al., 2014). The termination of L neurons in different medulla layers suggests a split of the primary visual information into different parallel processing pathways.
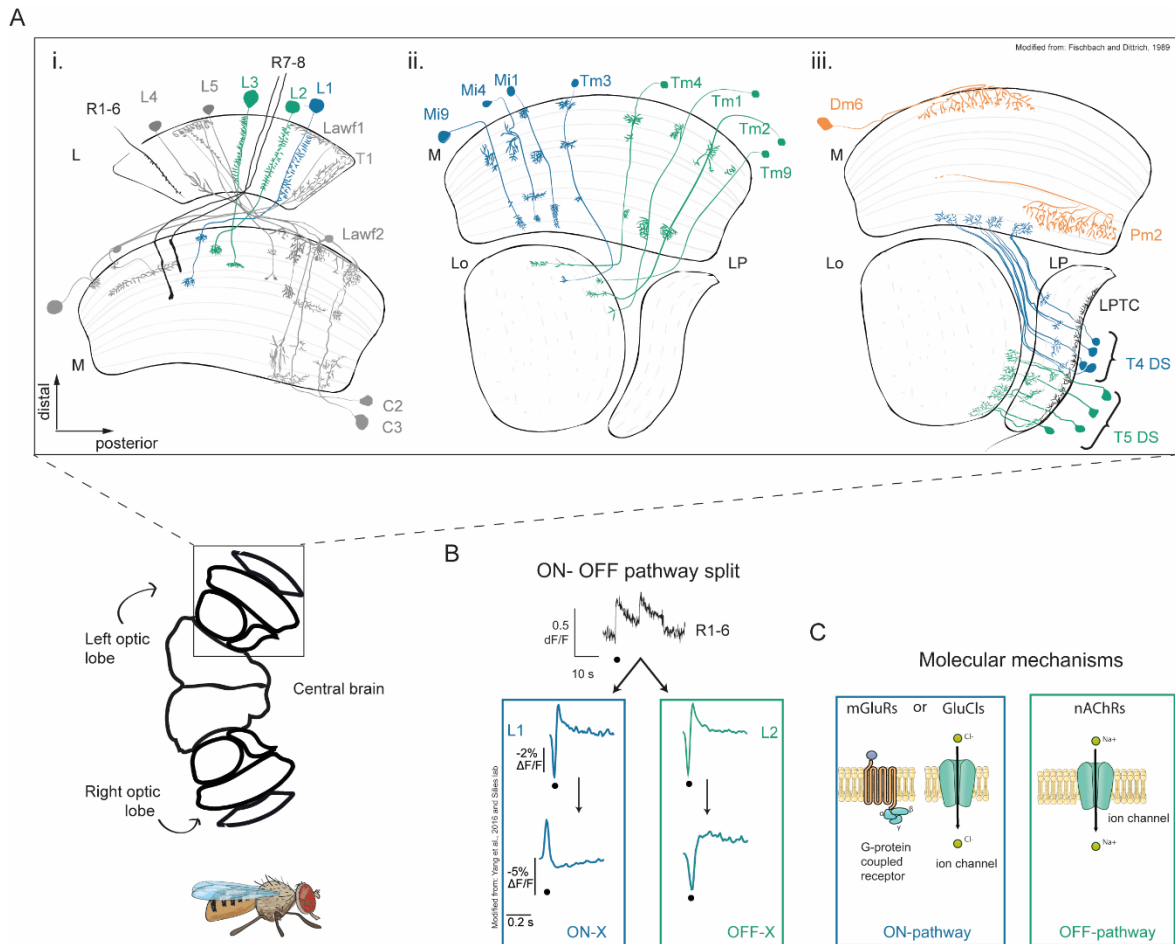
Figure 2: **The Drosophila optic lobe. (A)** Layered organization and main neuronal types in the fly optic lobe. i. Photoreceptors and lamina neurons with projections in the lamina (L) and medulla (M). Highlighted are the ON- (blue) and OFF- (green) pathway inputs ii. Medulla neurons belonging either to the ON (blue) or to the OFF (green) pathways. iii. Highlighted in orange an neuron example for the distal medulla (Dm) and proximal medulla (Pm). In blue and green are the direction-selective (DS) cells of the ON and OFF pathway, respectively. **(B)** Physiological responses from photoreceptos and ON- and OFF- medulla neurons showing the signal inversion in the ON pathway. The black dote shows a light onset. Modified from (Yang et al., 2016). **(C)** Molecular mechanisms showing the different hypothesized glutamate receptor classes in the ON and OFF ptahways. Shown are metabotropic glutamate recepertors (mGluRs), glutamate-gated chloride channels (GluCls), and nicotinic acetylcholine receptors (nAChRs).

Neighboring medulla column receive projections from neighboring lamina cartridges, maintaining retinotopy. The medulla, a neuropile bigger than the lamina, is patterned in different layers labelled from distal to proximal as M1 to M10 and hosts more than 60 different types of neurons (Fischbach and Dittrich, 1989; Morante and Desplan, 2008; Nern et al., 2015). Some medulla neurons have been described in detail (Figure 2Aii). This is the

case for intracolumnar neurons downstream of lamina (L) neurons, which have been described in the context of motion detection and have been assigned to either the ON- or the OFF-motion pathways (Borst and Helmstaedter, 2015; Silies et al., 2014; Yang and Clandinin, 2018). Thus, this classification does not necessarily match their either ON or OFF contrast selectivity but is rather based on connections to either ON- or OFF-DS neurons (Shinomiya et al., 2019; Takemura et al., 2013). For example, ON-pathway neurons Mi1, Tm3, Mi4, and C3 depolarize to ON (Arenz et al., 2017; Behnia et al., 2014; Molina-Obando et al., 2019; Strother et al., 2017; Yang et al., 2016)(Miriam Henning personal communication), whereas Mi9 depolarizes to OFF (Arenz et al., 2017; Strother et al., 2017). In the OFF-pathway, all neurons, including Tm1, Tm2, Tm4 and Tm9 depolarized to OFF (Fisher et al., 2015; Ramos-Traslosheros and Silies, 2021; Serbe et al., 2016). ON and OFF medulla neurons then contact T4 ON-DS cells in medulla layers 9-10, and T5 OFF-DS cells in the first layer of the lobula, respectively. Lobula plate T4 and T5 DS cells project their axons terminals to four distinct anatomical layers housing four anatomically defined subtypes of T4 and T5 cells (Fischbach and Dittrich, 1989; Maisak et al., 2013; Takemura et al., 2017), although a recent study, has identified a total of six functional subtypes (see physiology) (Henning et al., 2021). DS cell then connect to large lobula plate tangential cells (LPTCs) (Boergens et al., 2018; Schnell et al., 2010; Scott et al., 2002; Wei et al., 2020) which can be considered the main outputs neurons of the optic lobe projecting to central brain areas.

Physiology

Visual transduction in *Drosophila* starts at the level of photoreceptors, but fundamentally differs from phototransduction in vertebrate photoreceptors. Briefly, when a photon hits a chromophore-protein complex, known as rhodopsin, its chromophore changes its configuration from 11-cis to all-trans retinal which leads to the activated metarhodopsin state. Metarhodopsin is thermostable and can directly re-isomerize back to rhodopsin by absorption of longer wavelength light (e.g., red), which is constantly scattered by eyes pigments. In the activated state, metarhodopsin triggers a secondary chemical cascade leading to a graded depolarization. This chemical cascade amplifies the signal since one metarhodopsin can activate several G-proteins which then activate the phospholipase C (PLC) leading to the opening of calcium TRP channels (Hardie and Raghu, 2001). Fly photoreceptors increase their activity with light and release the neurotransmitter histamine onto first-order lamina interneurons (Hardie, 1989).

L1, L2 and L3 neurons express Ora transientless (Ort) receptors, a type of the histamine-gate chloride channels which leads to neuronal hyperpolarization at light onset (Davis et al.,

2020; Gengs et al., 2002). When there is no histamine release, L neurons depolarize, thus, having OFF polarity. Moreover, L neurons amplify the signal from photoreceptors (Laughlin, 1989) and L1-2 respond linearly to changes in light (Clark et al., 2011) whereas L3 rectifies and has higher responses to OFF (Silies et al., 2013). Among these three types, L1 has been described as the major input to the ON pathway, whereas L2 and L3 feed into the OFF pathway (Clark et al., 2011; Joesch et al., 2010; Rister et al., 2007; Silies et al., 2013). A recent study in the *Drosophila* OFF pathway further showed that L2 carries contrast information and L3 luminance information from photoreceptors to the downstream circuit (Ketkar et al., 2020). The different sensitivity to distinct features can be also inferred from their response dynamics: L2 responses to an OFF-light step show a strong transient component whereas L3 responses are sustained and correlate with the step luminance. L1, on the other hand, has been described as an ON-pathway sibling of L2 due to their similar physiology and transcriptome (Clark et al., 2011; Tan et al., 2015). Voltage and calcium signals of downstream medulla neurons show that they either depolarized to ON or OFF (Behnia et al., 2014; Serbe et al., 2016; Strother et al., 2017; Yang et al., 2016), indicating that ON-responding neurons downstream of L1 need to implement a signal inversion, whereas OFF responding neurons conserve the sign of their inputs (Figure 2B). Since L1 is a glutamatergic neuron (Davis et al., 2020; Takemura et al., 2011), glutamatergic inhibition must do the job (Figure 2C).

The glutamatergic identity of L1 led to the expectation that inhibitory glutamate receptors are expressed in ON selective neurons to implement the signal inversion. Metabotropic glutamate receptors (mGluRs), like in the vertebrate retina, also exist in the fly, and have the potential to exert inhibition (Davis et al., 2020; Parmentier et al., 1996). However, inhibitory glutamate-gated chloride channels (GluCla) have been reported in the *Drosophila* olfactory system, where their inhibitory role has been tested (Liu and Wilson, 2013). Both receptor types are candidates for the molecular implementation of ON selectivity in the visual system (Figure 2C). *GluClα*, the only known gene coding for GluCls receptors, is consistently expressed very high in all ON-pathway medulla neurons, whereas *mGluR* has relatively high expression only in Mi1 (Davis et al., 2020). This makes *GluClα* a better candidate but does not discard *mGluR* functional implications. For almost all ON-depolarizing medulla neurons, L1 is the main presynaptic partner (Takemura et al., 2013), and therefore, it is reasonable to think that the signal inversion is implemented in the L1-medulla neuron glutamatergic synapse. The exception is Mi4, which receives its main input from L5 and has not direct connections with L1 (Takemura et al., 2013). Although L5 has not been functionally characterized, it is expected to depolarize to ON and excite Mi4 through a cholinergic synapse (Davis et al., 2020). This is plausible since L5 does not

receive direct photoreceptor inputs and receives its main inputs from L1 (Takemura et al., 2013), making L5 another neuron where a signal inversion postsynaptic to L1 could take place.

The medulla connectome has also revealed a pervasive interconnectivity among medulla neurons, showing that every neuron is directly or indirectly connected with the rest (Takemura et al., 2013). For example, ON-pathway neurons that do have direct synaptic connections with L1, also have other direct inputs that might play an important role in their ON response. This is the case for Mi1 which receives direct inputs from Mi9, a glutamatergic neuron (Davis et al., 2020) that depolarizes to OFF (Strother et al., 2017), and therefore, can also introduce a signal inversion in Mi1. Along similar lines, there are intercolumnar glutamatergic neurons that connect OFF depolarizing neurons with other neurons in the ON pathway (Davis et al., 2020; Takemura et al., 2013). Altogether, the connectivity in the medulla suggests that ON selectivity can be implemented by multiple inputs rather than just a direct one downstream of L1.

1.1.3 Similarities and differences in the visual processing of contrast between the vertebrate retina and the *Drosophila* optic lobe

In this section I expose and stress the similarities and differences in anatomy and molecular mechanisms between the vertebrate retina and the *Drosophila* optic lobe, that lead to remarkably similar algorithms to achieve contrast selectivity during visual processing (Figure 3).

<u>An extra processing layer in the Drosophila optic lobe</u>
These two visual systems share a lot of similarities. Both systems present a similar columnar organization to preserve the spatial information from the environment in a retinotopic map in the visual circuit. This organization is preserved at all layers in the vertebrate retina as well as in the different optic lobe neuropiles. Both systems have different classes of photoreceptors that feed into color and non-color pathways. Downstream of photoreceptors, both systems split the contrast information in ON and OFF pathways, which then contact DS cells. Both systems also have cell types that laterally connect neurons at different depths. However, there is an important difference to highlight: contrast selectivity appears at different synaptic layers downstream of photoreceptors. In the vertebrate retina, cones and rods directly contact ON or OFF selective BCs. In the optic lobe instead, fly R1-

6 photoreceptors contact medulla ON or OFF selective neurons through lamina first-order interneurons. Thus, contrast selectivity happens one synapse later in the fly. Only fly R7-8 project directly to the medulla. Moreover, retinotopy, present in vertebrates at the photoreceptor layer, first appears in the insect lamina thanks to neural superposition. Thus, the visual processing of contrast and the anatomical arrangement behind retinotopy shows that the fly optic lobe possesses an extra layer for visual processing for non-color vision: the lamina (Figure 3A).
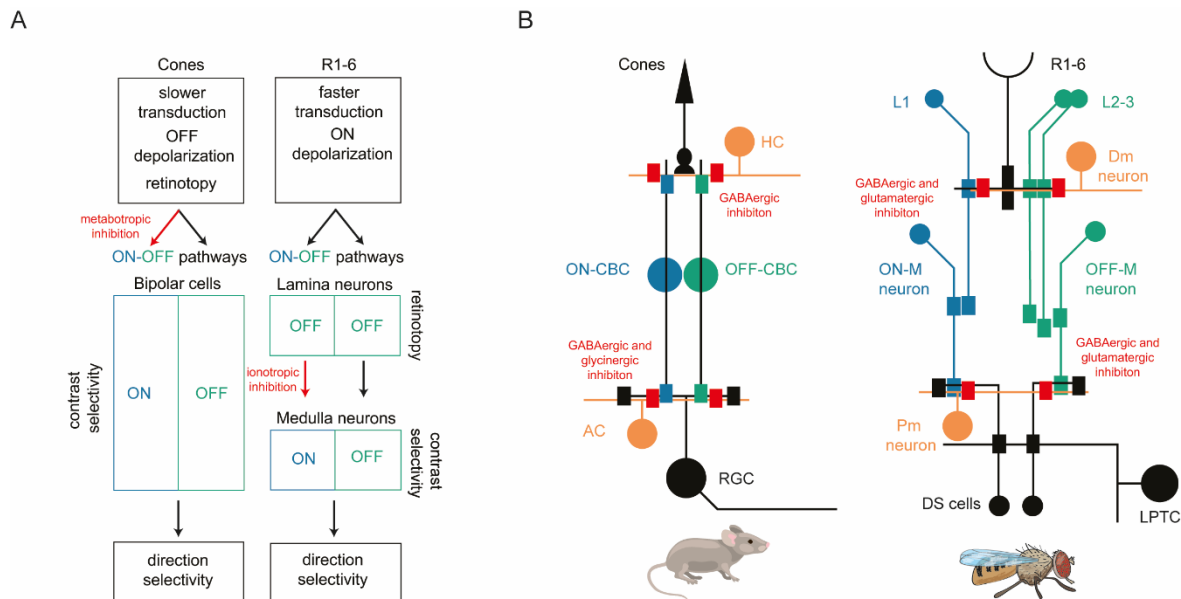
Figure 3: **The vertebrate retina vs the fly optic lobe.** Similarities and differences between the vertebrate retina and the *Drosophila* optic lobe. ON pathway in blue and OFF pathway in green **(A)**. In the vertebreate retina, cones have a slower photransduction machinery compared to the one in insects, depolarize to OFF and establish retinotopy. R1-6 photoreceptors in the fly depolarize to ON. Dowsntream of photoreceptros, ON-OFF pathways are defined. Bipolar cells in the vertebrate retina are contrast selective.The ON responses polarity in bioplar cells arise through metabotropic inhibition (red arrow). In the fly, all lamina neurons have OFF polarity and established retinotopy. Medulla neurons in the optic lobe are contrast selective. The ON responses polarity arises in medulla nuerons probably through ionotropic inhibition (red arrow). Downtream of contrast selective inputs, direction selectivity is extracted in both systems **(B)** Feeddforward neuronal connections between photoreceptors and main output cells of the vertebrate retina and the optic lobe. In the vertebrate retina, the ptahway cones> CBCs > RGCs has inhibitory lateral connections from HCs and ACs (in red). In the fly optci lobe, the pathway R1-6 > L neurons > M neuron > DS cells > LPTCs has inhibitroy lateral conections from Dm and Pm neurons (in red). HC: horrizontal cell. AC: amacrine cells. CBC: cone bipolar cell. RGC: retinal ganglion cell. Dm: dorsal medulla. Pm: proximal medulla. DS: direction selective. LPTC: lobula plate tangential cell. L: lamina, M: medulla.

Phototransduction and neuronal responses before contrast selectivity

Both systems have the same type of light sensor mechanism: the photoactivation of a chromophore that leads to active metarhodopsins, G-protein coupled receptors (GPCRs) which activate secondary messenger cascades leading to signal amplification and

photoreceptor response. Photoreceptors in both systems have graded potentials and distinct response dynamics, responding faster at higher luminance levels (Daly and Normann, 1985; Dunn et al., 2007). Vertebrate rods have a slow and sustained response dynamics, whereas cones are faster and more transient (Kawamura and Tachibanaki, 2008). Similarly, *Drosophila* photoreceptors have also transient and sustained components in their response (Hardie and Raghu, 2001) which then are differentially amplified by different lamina neuron types: L1-2 neurons are faster and more transient than L3, which has a slower and sustained response (Clark et al., 2011; Silies et al., 2013). However, there are important difference to highlight in phototransduction: whereas metarhodopsins in the vertebrate system need a long chemical process to go back to a rhodopsin state, the isomerization in insects is instantaneous relying on longer light wavelength. This shows that ON-OFF signal transduction and rhodopsin recovery from light bleaching is faster in insects. Furthermore, the G-protein signaling cascade downstream of rhodopsins leads to ON hyperpolarization in vertebrate photoreceptors, and ON depolarization in insects. Thus, vertebrate and insect photoreceptors have an opposite response polarity (Figure 3A).

Contrast selectivity: implementation of parallel ON-OFF pathways

In both systems, the implementation of parallel ON and OFF pathways relies on a signal inversion at the dendrites of ON-depolarizing neurons. The molecular mechanisms in both systems involves glutamatergic synapses, which need to be inhibitory. However, how this inhibition is molecularly introduced seems to differ across these systems. In the vertebrate retina, all photoreceptor types are glutamatergic neurons and the molecular mechanism for the split in ON and OFF pathways utilizes two distinct glutamate receptors in BCs: the inhibitory and metabotropic mGluR6 in ON-BCs and the excitatory and ionotropic AMPA/kainate receptors in OFF-BCs (Euler et al., 1996). In *Drosophila*, however, signaling in the ON pathway is glutamatergic, whereas in the OFF-pathway is cholinergic (Davis et al., 2020; Takemura et al., 2011). If the receptors are metabotropic or ionotropic is not clear, but ON-pathway neurons have higher expression of the ionotropic *GluClα* receptor and OFF-pathway neurons of the ionotropic *nAChR,* compared to metabotropic glutamatergic or cholinergic receptors (Davis et al., 2020). If indeed the signal inversion in the *Drosophila* ON pathway is ionotropic, this could give to flies further advantage in temporal resolution capabilities compared to metabotropic in the vertebrate retina, as shown to happen in chemosensation (Kaupp, 2010; Silbering and Benton, 2010) (Figure 3A).

Moreover, ON- and OFF-pathway neurons are half-wave rectified, meaning that they depolarize to its preferred contrast but suppressed responses to the opposite contrast. Therefore, pathways report complementary information. In the vertebrate retina,

rectification occurs at the synaptic release of BCs (Borghuis et al., 2013; Demb et al., 2001; Schwartz and Rieke, 2011), and the ON pathway is less rectified than the OFF pathway (Chichilnisky and Kalmar, 2002; Liang and Freed, 2010). Similarly, in *Drosophila*, rectification appears in ON- and OFF-pathway medulla neurons at the voltage to calcium transformation (Yang et al., 2016) and ON neurons appear to be less rectified than OFF (Behnia et al., 2014).

Parallel connectivity in the ON and OFF pathways

Both visual systems have lateral connections right after the synapse between photoreceptors and first-order interneurons. The interneurons laterally connecting different neuronal types, expand their dendrites at different depths, contacting both dendritic arborizations and axon terminals. For example, in the retina, HCs connect to photoreceptor terminals (feedback connections) and to both ON and OFF BCs dendrites (lateral connections) at the distal OPL, whereas ACs connect to BCs terminals (lateral connections) and to RGC dendrites (feedforward connection) at the proximal IPL (Sanes and Zipursky, 2010). Similarly, distal medulla (Dm) and proximal medulla (Pm) neurons in the optic lobe laterally connect different ON and OFF contrast selective neurons at their dendrites or axon terminals (Nern et al., 2015; Takemura et al., 2013). Thus, both systems have highly interconnected ON-OFF contrast pathways and parallel paths exist from a particular photoreceptor type to a contrast selective neuron (Figure 3B).

Lateral inhibitory circuits and neurotransmitter receptors

In both systems, lateral inhibitory connections shape responses of the vertical excitatory pathways: photoreceptors − BCs − RGCs, in the retina, and photoreceptors − L neurons − M neurons − DS cells, in *Drosophila*. This inhibition creates the inhibitory surround in the spatial receptive fields of contrast selective neurons (Dacey et al., 2000), and helps to emphasize both responses to small objects as well as the abrupt change in contrast in a spatial edge (Clark and Demb, 2016). When the neuronal receptive field moves relative the world, the spatial contrast become temporal contrast, and so, lateral inhibition also tunes responses to the temporal frequency of the stimulation. Interestingly, since the arrangement of both visual systems is columnar, and because visual signals correlate over time and space, a given neuron can predict its own response from their neighbors or from its own response history.

Moreover, in both the vertebrate retina and the fly optic lobe there are several types of inhibitory receptor channels acting at the level of contrast-selective neurons. The receptor family for all these receptors includes many types of ligand-gate chloride channels (LGCC).

In vertebrate, members of this family include GABA and glycine receptors, and in the retina, glycinergic and GABAergic ACs exist which contact ON- and OFF-BCs at the axon terminals to generate functional diversity (Franke et al., 2017). In Drosophila, there are at least 12 LGCC gene subunits, of which six have been described as neurotransmitter receptors. These receptor subunits include histamine, GABA, and glutamate receptors: *histamine-gated chloride channel 1 (HisCl1)* and *ort* code for two independent histamine-gated chloride channels, *resistance to dieldrin (rdl)* and *Lcch3* code for GABAa receptor subunits, Grd is a GABA-receptor like sequence, and GluClα is a glutamate-gated chloride channel subunit which has high homology with the vertebrate glycine receptor (Knipple and Soderlund, 2010). Furthermore, GABAergic and glutamatergic Dm and Pm neurons exist (Davis et al., 2020) and make contact to ON- and OFF- pathway neurons in the fly (Takemura et al., 2015, 2013). Thus, lateral inhibition in the vertebrate system is done by a combination of GABAergic and glycinergic inhibition, whereas in *Drosophila* it is likely GABAergic and glutamatergic (Freifeld et al., 2013) (Figure 3B).

1.2   Luminance-invariant contrast responses

Contrast detection informs animals about salient objects around them, e.g., prey to catch or predators to escape from. The magnitude of a given contrast correlates with the object's strength as a visual cue: the higher the contrast, the stronger the cue. Different contrast magnitudes are properly differentiated and animal behavior scales with them (Busse et al., 2011; Chakravarthi et al., 2016; Dakin and Turnbull, 2016; Keleş et al., 2019; Palmer et al., 2007; Rinner et al., 2005). The stable detection of the same contrast magnitude regardless of changes in background illumination is behaviorally relevant, for example, when a day gradually turns to night or when our gaze suddenly moves from one location to another within a visual scene. Luminance-invariant contrast responses have been shown at the level of perception in humans for both ON and OFF contrasts (Burkhardt et al., 1984), in neuronal responses in the vertebrate visual system (Mante et al., 2005) and, recently, in OFF contrast behavior in Drosophila (Ketkar et al., 2020). But how is it possible that visual systems "see" the same contrast equally good across diverse illumination conditions, when the illumination changes gradually or suddenly? In this section I cover the existing mechanisms in early visual processing that allow systems to adapt their contrast response to a changing background illumination, at different time scales.

Photoreceptor adaptation (gain control)

When animals navigate in the environment, they face a wide range of light intensities. In each scenery, the number of photons varies by a factor of 10^3 (Van Hateren, 1997; van Hateren and van der Schaaf, 1998) and in a day by a factor or 10^9 (Rieke and Rudd, 2009). However, photoreceptor outputs only can cover a range of 10^1-10^2 with vesicle release per second (Choi et al., 2005; Sheng et al., 2007). To solve this mismatch, the phototransduction machinery in both systems leads to photoreceptor adaptation to different range of luminances. They adapt their sensitivity to light to the mean intensity: the brighter the mean, the lesser the sensitivity to detect photons (Burkhardt, 1994; Juusola et al., 1995; Laughlin and Hardie, 1978). This leads to detect a change relative to the mean rather than an absolute change in photon. This is referred to as gain control and follows Weber law (Fechner, 1948).

The mechanism of gain control in photoreceptors are diverse but all of them share the same effect: a decrease in sensitivity to light at high illumination and an increase at low. For example, the phototransduction machinery can be altered at different levels to decrease or increase the level of dark current (Fain et al., 2001). Or the immediate downstream circuitry in which horizontal cells give inhibitory feedback to the photoreceptors at the axon terminal, decreasing photoreceptor activity when background illumination is high (Baylor et al., 1971; Thibos and Werblin, 1978). In any of those cases, adaptation times in vertebrate and fly photoreceptors are not instantaneous, taking tens of seconds to minutes to reach a fully adapted state (Burkhardt, 1994; Laughlin and Hardie, 1978). Immediately after a contrast change, vertebrate rods and cones do not respond invariant with respect to luminance: the response of cones and rods to the same just detectable light flash actually scale with background luminance rather than to be the same (Brown and Rudd, 1998). Similarly, in the fly, responses of canonical lamina monopolar cells (LMCs) to the same contrast scale with background intensity (Laughlin et al., 1987).

Post-receptor gain control

Due to the time constrains of photoreceptor adaptation, further mechanisms are required to achieve luminance-invariant contrast response under sudden changes in illumination. In the vertebrate retina, for example, RGCs adapt at lower light levels than cones, showing that there is post-receptor adaptation in the retinal circuitry. This adaptation occurs when signals are relayed from cone bipolar cells to ganglion cells (Dunn et al., 2007). In the fly visual circuit, a recent study suggests a post-receptor gain control mechanism at the circuit level downstream of lamina neurons, where luminance-sensitive responses of L3 will set a gain on contrast-sensitive signals (Ketkar et al., 2020). The exact location for this luminance-

based correction mechanisms is not known yet, but it probably takes place in synapses with downstream medulla neurons where, based on connectomics (Takemura et al., 2013), the luminance and contrast signals can first coincide. Post-receptor gain control has been also related to contrast adaptation, a mechanism that allow to shift the operating range of a neuron to properly encode luminance variance (Carandini and Heeger, 2012; Laughlin, 1981), for example, when eyes saccade from a region with little spatial structure to high spatial structure.

Behavioral measurements of luminance-invariant responses

The advantage of study luminance-invariant contrast responses in *Drosophila* is that it allows to draw a causal relationship between neuronal function and behavior, shedding light on the neuronal implementation of luminance-invariance as a feature. This is possible thanks to recordings of visually driven compensatory behaviors while manipulating neuronal activity. Compensatory behaviors are present in both mice and flies, and some of them involve the function of visual systems. For example, behaviors that are triggered by the visual displacement of the body with respect to the world, includes behaviors from mouse eye movement to compensatory head movements, referred as vestibulo-ocular reflex (Crawford and Vilis, 1991), or fly turning in the direction of the moving world, referred to as the optomotor response (Götz, 1968). The purpose of these compensations is to stabilize an image on the retina while the animal is navigating in the environment.

In flies, optomotor responses are used to compensate for unplanned self-motion and so to minimize the optic flow -or retinal movement patterns. This compensatory turning corrects any deviation from course (Götz and Wehrhahn, 1984; Mronz and Lehmann, 2008). Different optic flow patterns will elicit a different type of motion correction, for example, rotational optic how will elicit yaw turning, whereas expansion optic flow will generate translational movement (Collett, 1980; Mronz and Lehmann, 2008). Altogether, these corrections help flies to have robust steering maneuvers and avoid collision while maintaining correct flight or walking postures. Optomotor responses have been crucial to examine visual processing underlying behavior. Genetic manipulations in specific neurons in the ON and the OFF pathway have shown their behavioral relevance in the detection of moving patterns (Clark et al., 2011; Serbe et al., 2016; Silies et al., 2013; Strother et al., 2017). This way, the neuronal mechanism behind luminance-invariant responses to OFF stimuli was also investigated, using OFF edges moving on a background that suddenly changed in luminance (Ketkar et al., 2020). Although, it remains to be investigated if this mechanism can be expanded to luminance-invariant ON behaviors, optomotor behavior can be used as the experimental approach to answer it.

1.3   Connectomes and degenerate networks

All visual systems share the common goal to detect visual features in a robust fashion. Despite their anatomical differences, they utilize remarkably similar mechanisms to do so (Clark and Demb, 2016). It is often hypothesized that function -in this case feature detection- is an emergent property of neuronal connectivity. In this section, I review the latest advances (and limitations) in connectomics leading to wiring diagrams of unprecedented detail in the mouse, in the fruit fly and other animal models in neuroscience. Furthermore, I discuss degeneracy as a framework for functional robustness in neuronal networks.

<u>Connectomes</u>

The connectome era has recently begun and is revolutionizing the field of neuroscience, similarly to how the genome era did 30 years ago for all fields in biology. The information in a connectome, or wiring diagram, is required to understand how differences between brains underlie differences in behavior, as well as to theorize about the principles of brain function by identifying common neuronal motifs and their relationships. First attempts in completing a brain connectome were done thanks to electron microscopy (EM) reconstructions in *Caenorhabditis elegans* (White et al., 1986), a simple organism with just 302 neurons. Nowadays, the research has expanded, and more connectomes exists for brains or brain regions in *Drosophila melanogaster* (Ohyama et al., 2015; Scheffer et al., 2020; Zheng et al., 2018), *Mus musculus* (Bock et al., 2011; Lee et al., 2016; MICrONS Consortium et al., 2021; Rogerson et al., 2017), *Caenorhabditis elegans* (Jarrell et al., 2012; Varshney et al., 2011; Witvliet et al., 2021) and *Danio rerio* (Hildebrand et al., 2017), the four species that dominate neuroscience. Since brains are densely packed, the bigger challenge is to obtain a dataset of the right size, resolution, and completeness according to what is being studied. The complicated trajectories of neuronal processes, of distinct thickness, and all electrical and chemical contacts need to be accurately mapped. A small error, mixing processes of different neurons is fatal for the generation of a wiring diagram. Because of the different tradeoffs in brain size, resolution and completeness, different pipelines and improvements at each step have emerged over the past years.

An EM reconstruction experiment consist of different phases: 1) sample preparation, 2) tissue sectioning, 3) volume reconstruction and 4) image segmentation -consisting of synapse annotation and neuron identification. For tissue sectioning, first connectomes in *Drosophila* adults were based on serial sectioning methods (ssEM) which utilize a diamond knife to slice the tissue (Briggman and Bock, 2012) (Takemura et al., 2013, 2008). Later versions (Takemura et al., 2015, 2017) used a focused ion beam scanning (FIB-SEM) that

allows the same spatial resolution in x, y, and z, and therefore, small isotropic volumes (Xu et al., 2017). Other techniques also exist, such as GripTape transmission electron microscopy (TEM) for larger volumes (larger brains) (Graham et al., 2019). The image acquisition methods are especially relevant for large volumes to later assemble all images avoiding artifacts (Lee et al., 2019; Saalfeld et al., 2012). After data acquisition there are other computational steps, for example, all images are aligned in a single stack and then different segments and substructures across the volume need to be detected and annotated. In brain connectomics such segmentation refers to neuronal tracing and synaptic mapping, which can be done either manually (Helmstaedter et al., 2011; Schneider-Mizell et al., 2016) or automatically (Buhmann et al., 2021; Li et al., 2019; Macrina et al., 2021; Sheridan et al., 2021), for example, using the flood-filling algorithm (Januszewski et al., 2018). Efforts have been made to identify synaptic contacts automatically (Huang and Plaza, 2014) and tools have been developed to match light microscopy images of single cells to FIB-SEM segmentations like NBLAST (Costa et al., 2016). Nevertheless, due to the high amount of data even small error rates can lead to an error disaster in the whole data set. Therefore, a human proof-reading as last step is still needed, for example, using virtual reality tools like NeuTu (Zhao et al., 2018). Furthermore, connectomes can be complemented with physiology (Bock et al., 2011; Lee et al., 2016; MICrONS Consortium et al., 2021; Ohyama et al., 2015), and neurotransmitter information (Ohyama et al., 2015), also inferred from EM directly (Eckstein et al., 2020).

Degenerate networks

Animals robustly execute behavior despite changes in external or internal conditions (Lombardino and Nottebohm, 2000; Maddox, 1994; Meyer et al., 1998; Rokni et al., 2007). However, animals also behave flexibly and can adapt to external and internal changes (Ache et al., 2019; Honma et al., 2003; Okamoto and Aizawa, 2013; Roemschied et al., 2021; Skutt-Kakaria et al., 2019). Thus, flexibility refers to the ability of generating different outputs according to changing conditions, while robustness refers to the ability of generating the same output despite of changing conditions. Robustness and flexibility, seemingly contradictory concepts, lead to a better animal's performance while hunting a prey or escaping from a predator. Thus, knowing how robustness and flexibility are integrated in biological systems is fundamental to understand how they work (Heinl and Grabherr, 2017; Kitano, 2004; Meir et al., 2002). How can brains be robust and flexible at the same time? Some studies suggest that neurons are multifunctional (Li et al., 2014; Liu et al., 2018), contributing to multiple computations within one or more circuits. However, several neurons often contribute to similar computations (Beverly et al., 2011; Koo et al., 2011; Trojanowski et al., 2014). These one-to-multiple and multiple-to-one relationships are observed across

the animal kingdom (Jankowska, 2001; Leonardo, 2005; Schiller, 1996; Shih et al., 2015), and can be theoretically considered as part of a degenerate system (Edelman and Gally, 2001; Tononi et al., 1999).

Degeneracy has been formally defined as the ability of elements that are structurally different to perform a similar (or same) function -or output. (Tononi et al., 1999). The elements of a degenerate network can be thought as inputs to a convergent point where function -or output- is being evaluated. It is key to differentiate degeneracy from redundancy. In redundancy, elements are usually considered to be identical (e.g., duplicate genes) that implement the same function in parallel. Degeneracy, due to the different structure of elements, may lead to the same or different function depending on the context in which the system is. This idea is interesting because degeneracy reflects the seemingly contradictory dual role of robustness vs flexibility mentioned before. However, considering that elements are multiple and are placed in parallel, the seemingly contradiction becomes two faces of the same coin: 1) distinct components support the stability of a single output (robustness) and 2) individual components contribute to the stability of multiple distinct outputs (flexibility). Thus, elements can produce the same output in some cases and produce different outputs in other cases. Although a theoretical analysis to measure degeneracy in a biological network has been proposed (Tononi et al., 1999), I could only find studies where degeneracy has been described, not measured.

Degeneracy has been described in various biological systems, from genes and proteins networks to multicellular systems (Edelman and Gally, 2001) and suggested in some computational models explaining animal's behaviors (Clemens et al., 2021). Degeneracy has been suggested not just as a property that emerged under natural selection, but instead a prerequisite of evolution itself (Edelman and Gally, 2001). Expanding on this thought, in an engineered system, in contrast to an evolved system, redundancy prevails with no place in the design for irrelevant elements. The identical copies of an element are there as a backup it case something fails. In a system that evolved, which is not build on predictions of future failures, there are connections between elements that seem irrelevant. However, when context changes, either being a temporary change in environmental conditions or a permanent one forcing natural selection, "irrelevant" elements reveal their usage. In other words, many ways to generate the same output provide adaptability in response to unpredictable changes.

In neuroscience, degeneracy has been described in some systems. For example, looking at neural circuits generating thermotaxis behavior in *Caenorhabditis elegans* (Ikeda et al.,

2018), multiple microcircuits individually regulate distinct behavioral components (e.g., turns, reversals, curves) to achieve thermotaxis although they highly overlap. Interestingly, single cell ablation does not disrupt behavior since other cells compensate for the deficit. Moreover, at distinct ambient temperature (change in conditions), different microcircuit can regulate the same behavioral components and mediate a flexible switch between moves towards or away from the temperature source. Elements of this degenerate circuit, here cell types, contribute to behavioral flexibility -through individual regulation of distinct components-, and to robustness -through compensation upon deficits or change in conditions. In the somatogastric ganglion (STG) of the crab *Cancer borealis*, parallel pathways exist and can be viewed as part of a degenerate circuitry as they implement multiple mechanisms by which the output of the system is switched between states (Gutierrez et al., 2013).

1.4   Aims and structure of the thesis

Contrast detection is an early visual process that forms the basis of other visual computations. If contrast detection fails, other more complex computations that rely on that, e.g., motion detection, also fail. Since both signal increments and decrements must be detected, to study contrast detection is to study how ON and OFF contrast selectivity arises. In this thesis, I first aim to understand the neuronal and molecular mechanisms behind the emergence of ON selectivity in *Drosophila.* Moreover, for perception or behavior to be stable, visual systems must compute contrast relative to the mean illumination of a scene also when it abruptly changes faster that any type of neuronal adaptation. Therefore, I also aim to test if and how ON behavior becomes invariant to sudden changes in illumination. Finally, neuronal circuits need to have a common strategy for a robust implementation of contrast when environmental conditions suddenly change. Therefore, I also aim to understand if the parallel connectivity in the ON pathway can be the basis for a robust contrast detection.

I will address these aims in three studies. In the first study, I aim to reveal the molecular and the neuronal basis for ON responses in *Drosophila*. Since a glutamatergic synapse is in place between L1 and ON selective neurons, using a pharmacological approach we distinguished between the role of mGluRs and GluCls in ON selective medulla neurons Mi1 and Tm3. Then, with an expression analysis complemented with pharmacogenetic and genetic studies, we studied the specific roles of glutamate- and GABA-gated chloride

channels for the computation of ON contrast-selective responses. Finally, because the medulla connectome reveals a pervasive interconnectivity between ON-pathways neurons, we used advanced genetic tools to test if either just one direct glutamatergic input from L1 or a more distributed computation is in place to implement the signal inversion.

In <u>the second study</u>, we aimed to understand how information from photoreceptors is distributed by lamina neurons to downstream ON and OFF pathways to achieve robust behavioral responses to contrast when background luminance quickly changes. OFF behavior in Drosophila and ON-OFF perception in humans show nearly luminance invariance responses to contrast. In the *Drosophila* OFF pathway, luminance serves as a corrective signal to scale contrast computation. Since ON and OFF pathways face different environmental challenges and have evolved several structural and physiological asymmetries, we tested if luminance-invariance is a general feature present in the *Drosophila* ON pathway as well. Considering that ON behavioral responses approached luminance invariance, we determined the contrast- and luminance-sensitive inputs in the ON pathway, and which inputs were required and sufficient for ON behavior.

In <u>the third study</u>, I aimed to understand if the parallel input arrangement in the ON pathway serves for a robust implementation for ON contrast selectivity under changing conditions. Analyzing the connectome in the medulla using graph theory, I identified Mi1 as an ON-pathway hub for information flow and convergence for multiple inputs. Then, I first tested if Mi1, as a critical ON-pathway neuron, was required for ON contrast behavior under sudden changes in illumination and different contrast steps. Informed by connectomics, we then tested if parallel direct inputs of Mi1 were required for ON responses. Using connectome analysis and transsynaptic mapping of postsynaptic partners, I further revealed indirect candidate input pathways that might contribute to ON responses in Mi1. Finally, I tested if inputs that are not required for ON responses are sufficient under abrupt changes in illumination and different noise levels, as two different challenging conditions that visual systems face.

2. ON selectivity in the Drosophila visual system is a multisynaptic process involving both glutamatergic and GABAergic inhibition

Published manuscript

Authors and affiliations

Sebastian Molina-Obando[1][2][3], Juan F Vargas-Fique[1][2][3], Miriam Henning[1][2], Burak Gür[1][2][3], T Moritz Schlad[4], Junaid Akhtar[1], Thomas K Berger[4], and Marion Silies[1][2]

[1]Institute of Developmental Biology and Neurobiology, Johannes Gutenberg-Universität Mainz, Germany

[2]European Neuroscience Institute Göttingen – A Joint Initiative of the University Medical Center Göttingen and the Max-Planck-Society, Grisebachstr. 5, 37077 Göttingen, Germany

[3]International Max Planck Research School and Göttingen Graduate School for Neurosciences, Biophysics, and Molecular Biosciences (GGNB) at the University of Göttingen

[4]Center of Advanced European Research (Caesar), Bonn, Germany

Contribution statement

Conceptualization: **SMO**, MS, TB

Methodology: **SMO**, TB

Software: **SMO**, JA

Investigation: **SMO**, JVF, MH, BG, TMS

Visualization: **SMO**, JVF

Supervision: MS, TB

Writing—original draft: **SMO**, MS

Funding acquisition: MS

SMO performed most of the imaging experiments and analyzed the imaging, electrophysiological and qRT-PCR data (Figures 1,2,3,4,5,6,7,8, F2S1, F2S2, F2S3, F4S1, F4S2, F6S1), together with JVF (Figure 2, 4, 7, F2S2, F2S3). BG performed experiments (Figures 2, 7). MH performed experiments (Figure 5). TMS performed experiments (Figure 5). JA analyzed data (Figures 3, F3S1, F4S2). **SMO** and JFV composed the figures. **SMO** and MS wrote the manuscript.

RESEARCH ARTICLE

ON selectivity in the *Drosophila* visual system is a multisynaptic process involving both glutamatergic and GABAergic inhibition

Sebastian Molina-Obando[1,2,3], Juan Felipe Vargas-Fique[1,2,3], Miriam Henning[1,2], Burak Gür[1,2,3], T Moritz Schladt[4], Junaid Akhtar[1], Thomas K Berger[4,5], Marion Silies[1,2]*

[1]Institute of Developmental Biology and Neurobiology, Johannes Gutenberg-Universität Mainz, Mainz, Germany; [2]European Neuroscience Institute Göttingen – A Joint Initiative of the University Medical Center Göttingen and the Max-Planck-Society, Göttingen, Germany; [3]International Max Planck Research School and Göttingen Graduate School for Neurosciences, Biophysics, and Molecular Biosciences (GGNB) at the University of Göttingen, Göttingen, Germany; [4]Department of Molecular Sensory Systems, Center of Advanced European Studies and Research (caesar), Bonn, Germany; [5]Institute of Physiology and Pathophysiology, Philipps-Universität Marburg, Marburg, Germany

***For correspondence:**
msilies@uni-mainz.de

Abstract Sensory systems sequentially extract increasingly complex features. ON and OFF pathways, for example, encode increases or decreases of a stimulus from a common input. This ON/OFF pathway split is thought to occur at individual synaptic connections through a sign-inverting synapse in one of the pathways. Here, we show that ON selectivity is a multisynaptic process in the *Drosophila* visual system. A pharmacogenetics approach demonstrates that both glutamatergic inhibition through GluClα and GABAergic inhibition through Rdl mediate ON responses. Although neurons postsynaptic to the glutamatergic ON pathway input L1 lose all responses in *GluClα* mutants, they are resistant to a cell-type-specific loss of *GluClα*. This shows that ON selectivity is distributed across multiple synapses, and raises the possibility that cell-type-specific manipulations might reveal similar strategies in other sensory systems. Thus, sensory coding is more distributed than predicted by simple circuit motifs, allowing for robust neural processing.
DOI: https://doi.org/10.7554/eLife.49373.001

Introduction

Animals rely on their sensory systems to process behaviorally relevant information. One common feature of sensory systems is the sequential processing of information to extract complex features from simple inputs. For example, in the visual system, photoreceptors detect light and then downstream neurons progressively extract distinct features, such as contrast, direction of motion, form, or specific objects (*Gollisch and Meister, 2010*; *Livingstone and Hubel, 1988*). Sensory pathways diverge into pathways that become selective for increasingly specific features.

One prominent example is the split into ON and OFF pathways, where individual neurons become selective to either increases (ON) or decreases (OFF) in a signal. Such an ON/OFF dichotomy enables more efficient coding of stimuli in the visual system (*Gjorgjieva et al., 2014*) and occurs

eLife digest We rely on our senses to capture information about the world around us. Sense organs convert sensory information – such as light or sound waves – into patterns of neuronal activity. In the mammalian retina, for example, specialized neurons called photoreceptors detect individual photons of light as they hit the back of the eye. The photoreceptors then pass on this information to neurons called bipolar cells for further processing.

During darkness, all photoreceptors release the same chemical signal onto bipolar cells, namely a molecule called glutamate. But bipolar cells respond to glutamate in different ways depending on which proteins are present in their outer membrane. So-called ON cells respond to glutamate by decreasing their activity, and thus effectively become more active when light levels increase. By contrast, OFF cells respond to glutamate by increasing their activity. This ON/OFF binary code enables later stages of the visual system to detect more complex visual features, such as shape and movement.

A new study in fruit flies, however, suggests that the ON/OFF code may be more complex than previously thought. While fruit fly eyes look very different to our own, the two have much in common. By studying fruit flies, researchers can also take advantage of a variety of genetic and pharmacological tools to manipulate cells and neuronal circuits.

Using such tools, Molina-Obando et al. show that the ON/OFF signal separation in fruit flies uses two different molecular mechanisms. The first involves a gene called GluCl-alpha, which encodes a receptor for glutamate. The second involves a gene called Rdl, which encodes a receptor for another brain chemical, GABA. Deleting the gene for GluCl-alpha from the entire fly brain prevented ON cells from responding to an increase in light levels. However, deleting this gene from specific ON cells alone did not. This suggests that flies can use more than one type of neuronal connection to detect an increase in light. Moreover, if one pathway fails, the other can take over. This makes the system more robust.

The results of Molina-Obando et al. are consistent with findings from anatomical studies that have mapped connections between neurons. Future studies should explore whether the same mechanisms exist in other sensory systems, and other animals. These experiments could take advantage of the molecular tools developed as part of the current work, which allow precise manipulation of neural networks.
DOI: https://doi.org/10.7554/eLife.49373.002

across many different species and sensory modalities, such as vision, olfaction, audition, thermosensation, and electrolocation (*Bennett, 1971*; *Gallio et al., 2011*; *Scholl et al., 2010*; *Tichy and Hellwig, 2018*; *Werblin and Dowling, 1969*). Examples of how the split into ON and OFF pathways is implemented in sensory information processing have already been described. In the vertebrate retina, ON and OFF pathways split downstream of glutamatergic photoreceptors where ionotropic glutamate receptors on OFF bipolar cells maintain the sign of the response in the OFF pathway, and the metabotropic glutamate receptor mGluR6, located on ON bipolar cells, inverts the sign in the ON pathway (*Koike et al., 2010*; *Masu et al., 1995*; *Vardi, 1998*). In the olfactory system of *C. elegans*, an odor response can be split into parallel pathways in which glutamate-gated chloride channels mediate the ON response (*Chalasani et al., 2007*). While these transformations are thought to occur at specific synapses, connectomics data reveals that neural circuits are intricate and that many of the possible neuronal connections are realized (*Eichler et al., 2017*; *Takemura et al., 2013*; *Zheng et al., 2018*). This argues that important signal transformations might actually be distributed across wider circuit motifs.

In the *Drosophila* visual system, ON and OFF pathways functionally split in the first order lamina interneurons, but the physiological specialization occurs one synaptic layer further downstream. In brief, information travels from the retina, which houses the photoreceptors, through three optic ganglia: the lamina, the medulla, and the lobula complex, comprising lobula and lobula plate (*Figure 1A*). Contrast is encoded by the transient response of photoreceptors, and downstream lamina neurons amplify the contrast-sensitive signal component (*Laughlin, 1989*). Then, distinct ON and OFF pathways are required to detect contrast increments and decrements, respectively
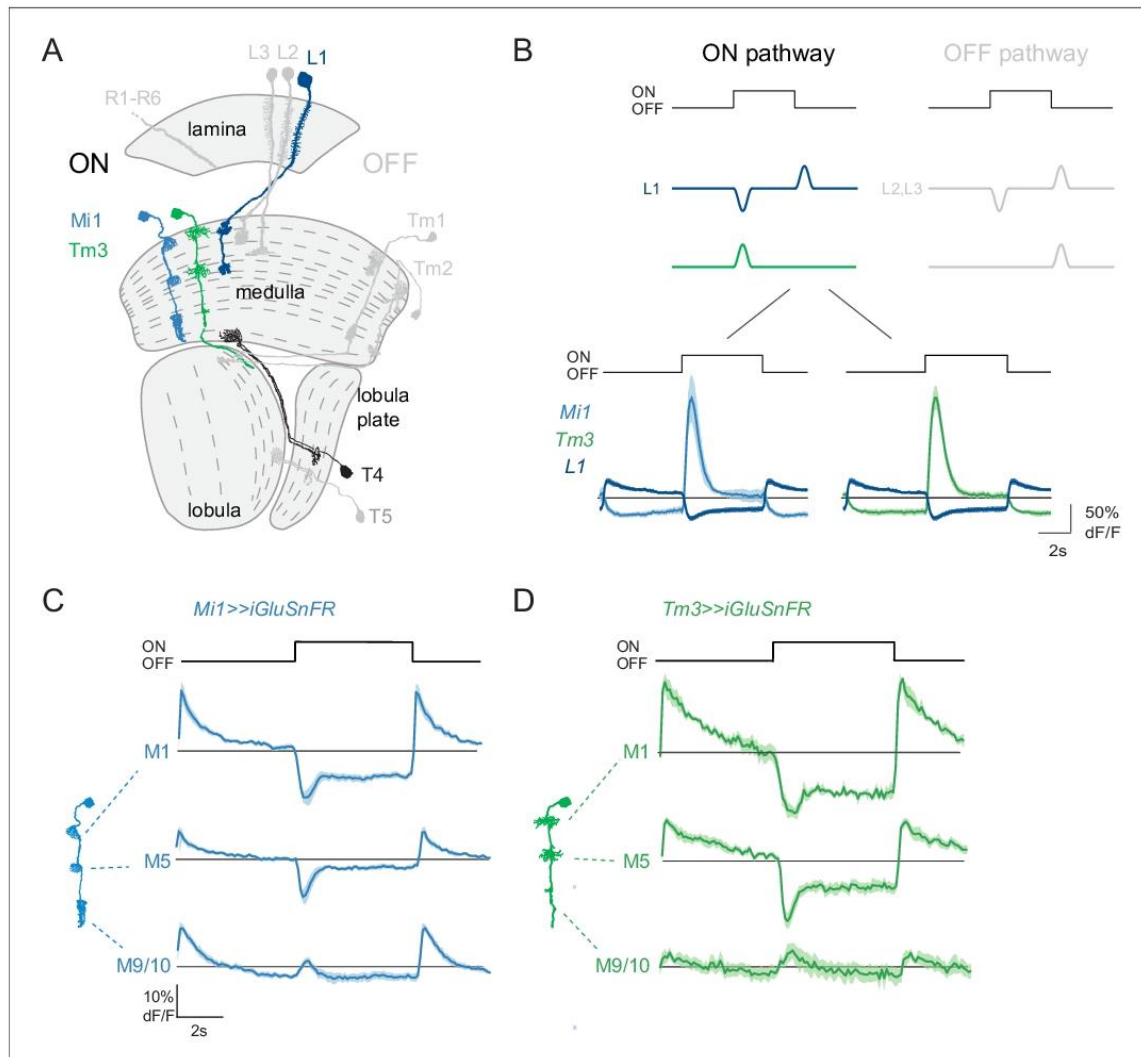
Figure 1. ON pathway medulla neurons that receive graded, glutamatergic input. (A) Schematic of the fly visual system, highlighting major neurons of the ON (colored) and OFF (gray) pathways. Visual information travels from the photoreceptors (R1–R6) through the lamina, medulla and lobula complex (lobula + lobula plate). In the ON pathway, the L1 input and its two major postsynaptic targets Mi1 and Tm3 are highlighted, as well as their common target, the T4 ON-direction-selective cell. (B) Top: Schematic representation of the signal transformations that occur at the lamina-to-medulla neuron synapse. In the ON pathway, a sign inversion is required downstream of linear lamina neuron inputs. Bottom: In vivo calcium signals in response to 5 s full-field flashes. L1 calcium signals (dark blue, n = 6 [99]) are of the opposite sign to the calcium signal in its major postsynaptic partners Mi1 (light blue, n = 5 [89]) and Tm3 (green, n = 7 [84]). (C,D) In vivo iGluSnFR signals in response to 5 s long full-field flashes at the dendrites of Mi1 (C, n = 9[278] in layer M1, n = 9[250] in M5) and Tm3 (D, n = 6[137] in layer M1, n = 6[141] in M5), or at the output region of these neuron types in medulla layers M9/10 (n = 9[326] for Mi1 in C, n = 6[161] for Tm3 in D). All traces show mean ± SEM. Sample sizes are given as number of flies [number of cells].
DOI: https://doi.org/10.7554/eLife.49373.003

(*Joesch et al., 2010*; *Strother et al., 2014*). In the lamina, L1 is the major input to the ON pathway, whereas L2 and L3 feed into the OFF pathway (*Clark et al., 2011*; *Joesch et al., 2010*; *Rister et al., 2007*; *Silies et al., 2013*). The assignment of L1, L2, and L3 to ON and OFF pathways originates from neuronal silencing studies (*Clark et al., 2011*; *Joesch et al., 2010*; *Silies et al., 2013*). However, all lamina neurons receiving direct input from photoreceptors depolarize to the offset of light and hyperpolarize to the onset of light (*Clark et al., 2011*; *Laughlin, 1989*; *Silies et al., 2013*; *Uusitalo et al., 1995*), thus passing on information about both ON and OFF (*Figure 1B*). Voltage or calcium signals in most downstream medulla neurons then selectively report only one type of contrast polarity. The major ON pathway medulla neurons Mi1 and Tm3, for example, selectively respond with depolarization or an increase in calcium signal to ON (*Figure 1B*; *Behnia et al., 2014*; *Strother et al., 2017*; *Yang et al., 2016*). In the OFF pathway, most neurons instead selectively respond to OFF stimuli, retaining the response polarity of their lamina inputs (*Figure 1B*; *Behnia et al., 2014*; *Serbe et al., 2016*; *Yang et al., 2016*). Therefore, ON selectivity requires a sign inversion between the L1 input and its postsynaptic partners Mi1 and Tm3. Previous work suggested that the L1 input to the ON pathway is glutamatergic, whereas L2 and L3, the two major inputs to the OFF pathway, are cholinergic (*Davis et al., 2018*; *Takemura et al., 2011*). This suggests that glutamate might also be used as an inhibitory neurotransmitter to implement ON/OFF dichotomy in the fly visual system. However, the molecular and cellular mechanisms implementing this signal transformation are not known in *Drosophila* visual circuitry.

Connectomics data has generated predictions about core circuit motifs (*Shinomiya et al., 2014*; *Takemura et al., 2013*). In the ON pathway, L1 makes the largest number of synapses with the medulla intrinsic Mi1 neuron and the transmedullary Tm3 interneurons (*Figure 1A*; *Takemura et al., 2013*). However, L1 has many other outputs, and Mi1 and Tm3 many additional inputs, such as indirect L1 input via L5, or the GABAergic neuron C2, among others (*Takemura et al., 2013*). Thus, coding in the visual system could be distributed across parallel pathways. One synaptic layer downstream, Mi1 and Tm3 medulla neurons project to T4, the first direction-selective cells of the ON pathway (*Figure 1A*; *Fisher et al., 2015a*; *Maisak et al., 2013*). This core visual circuit motif appears to be surprisingly resilient to perturbations. While genetic silencing of Mi1 or Tm3 leads to some deficits in ON edge motion detection (*Ammer et al., 2015*; *Strother et al., 2017*), these flies are not ON motion blind, arguing that other neurons must also play a role in motion detection. Mi4 and Mi9 have now been added to the ON pathway (*Takemura et al., 2017*). These cell types are modulated by octopamine, but silencing Mi4 or Mi9 individually has only subtle phenotypes (*Strother et al., 2018*; *Strother et al., 2017*). In the OFF pathway, combinatorial block of more than one cell type aggravates behavioral deficits (*Fisher et al., 2015a*; *Serbe et al., 2016*; *Silies et al., 2013*). This is also already true for the lamina neuron inputs L1, L2 and L3 neurons (*Silies et al., 2013*). This could argue that individual neurons might have distinct, but overlapping tuning properties (*Serbe et al., 2016*; *Tuthill et al., 2013*). Alternatively, encoding of a single aspect of a feature might already be distributed across parallel pathways.

Here, we show that ON selectivity in the *Drosophila* visual system is mediated by a glutamate-gated chloride channel, GluClα, and that all ON responses are lost upon pharmacological block or genetic loss of GluClα in the entire brain. At the same time, ON responses are robust to cell-type-specific perturbations of GluClα in individual neurons postsynaptic to L1, arguing for the existence of parallel functional pathways. Furthermore, we found that GABAergic inhibition also plays a role in mediating ON responses downstream of the glutamatergic L1 input. Together, our results indicate that ON selectivity is a multisynaptic computation that depends on both glutamatergic and GABAergic inhibition. This suggests that a seemingly simple computation can be implemented in a multisynaptic manner, allowing for greater functional robustness.

Results

ON pathway medulla neurons receive graded, glutamatergic input

To test if medulla neurons in the ON pathway receive glutamatergic input resembling the L1 response, we used the genetically encoded glutamate sensor iGluSnFR (*Marvin et al., 2013*; *Richter et al., 2018*). We selectively expressed iGluSnFR in the two major postsynaptic targets of L1: the medulla neurons Mi1 and Tm3. Using in vivo two-photon imaging, we measured visually

evoked responses on Mi1 and Tm3 dendrites reflecting their glutamatergic inputs in medulla layers M1 and M5. We also recorded iGluSnFR signals in the neurons' output layer, M9/10. In M1 and M5, both Mi1 and Tm3 neurons showed an increase in iGluSnFR signal in response to light OFF and a decrease in iGluSnFR signal in response to light ON, showing that rectification happens downstream of the glutamatergic input (*Figure 1C,D*). These signals were of the same polarity as intracellular calcium signals recorded within the presynaptic L1 axon terminals, and of the opposite polarity to calcium signals in the same layers of Mi1 and Tm3 (*Figure 1B–D*). In the proximal medulla (layer M9/10), Mi1 and Tm3 neurons showed weak iGluSnFR signals that increased in response to both light ON and OFF (*Figure 1C,D*). This data shows that the major postsynaptic targets of L1 receive glutamatergic input that provides information about both ON and OFF signals, which is in line with graded inputs coming from the L1 input to the ON pathway. Other glutamatergic inputs might further shape medulla neuron properties in the proximal medulla.

ON responses are lost at PTX concentrations affecting GABA$_A$Rs and GluCls

We hypothesized that glutamatergic inhibition mediates the sign inversion between the dendritic extracellular glutamate signals and intracellular calcium or voltage signals measured in these neurons (*Figure 1*; *Behnia et al., 2014*). Glutamatergic inhibition can be mediated either by metabotropic glutamate receptors or by ionotropic glutamate-gated chloride channels (*Collins et al., 2012*; *Cully et al., 1996*; *Liu and Wilson, 2013*; *Parmentier et al., 1996*). To determine which of these receptor types mediates ON responses, we recorded in vivo calcium signals in response to visual stimuli in the two major postsynaptic partners of L1 while pharmacologically inhibiting each of the two receptor classes. When flies expressing GCaMP6f in Mi1 neurons were shown 5 s full-field flashes, Mi1 showed a transient increase in calcium signals in response to the ON step that decayed to reach a plateau response within 2 s (*Figure 2—figure supplement 1A*). Bath application of 2-Methyl-6-(phenylethenyl) pyridine hydrochloride (MPEP), a selective blocker of metabotropic glutamate receptors, to the same flies did not reduce the responses to visual light flashes in Mi1 neurons (*Figure 2—figure supplement 1A,B*). Before drug application, Tm3 responses to ON flashes showed a transient light response. Similar to Mi1, Tm3 responses were not affected by MPEP application (*Figure 2—figure supplement 1C,D*).

We next applied picrotoxin (PTX), a drug that is known to inhibit glutamate-gated chloride channels at high concentrations (*Cully et al., 1996*; *Etter et al., 1999*), but which also affects GABA$_A$Rs at much lower concentration (*Takeuchi and Takeuchi, 1969*). In vivo studies in *Drosophila* had previously used concentrations of 1–5 μM PTX to effectively block GABA-gated hyperpolarization in the olfactory system and GABAergic inhibition in *Drosophila* visual system neurons (*Fisher et al., 2015b*; *Wilson and Laurent, 2005*). In contrast, 100 μM PTX was used to block GluCls in the olfactory system (*Liu and Wilson, 2013*). Upon bath application of 100 μM PTX, visual responses were completely abolished in Mi1 neurons (*Figure 2A*). Surprisingly, when we tested the effect of low concentrations (2.5 μM) of PTX, ON responses were also lost in Mi1 (*Figure 2A*). To test this effect more precisely, we used a range of PTX concentrations and observed a loss of visual responses at concentrations ranging from 2.5 μM to 100 μM PTX in Mi1 (*Figure 2B*). When we performed the same experiments in Tm3, we again found all ON responses to be eliminated in 100 μM PTX and strongly reduced at low concentrations of PTX (*Figure 2C,D*). This effect was consistent across all medulla layers (*Figure 2A–D*, *Figure 2—figure supplement 2A–D*). Dendritic Mi1 and Tm3 regions even showed a small decrease in calcium in response to light at the highest PTX concentrations (*Figure 2—figure supplement 2A–D*).

To evaluate if the PTX effect is ON-pathway selective and to measure the compound effect on ON and OFF pathway responses, we next imaged calcium signals in the direction-selective T4 and T5 axon terminals, the stage at which many medulla neuron inputs converge. When we measured flash responses in T4/T5 cells expressing GCaMP6f, these neurons hardly showed any response to full-field flashes before toxin application, due to surround inhibition (*Figure 2E,F*; *Fisher et al., 2015a*). Upon bath application of 2.5 μM PTX, these flash responses were disinhibited, and T4/T5 neurons responded with an increase in calcium signal to both light ON and OFF (*Figure 2E,F*; *Fisher et al., 2015b*). Thus, T4/T5 neurons still show flash responses under conditions in which all responses of their predominant Mi1 and Tm3 inputs are abolished (*Figure 2A–D*). This suggests,
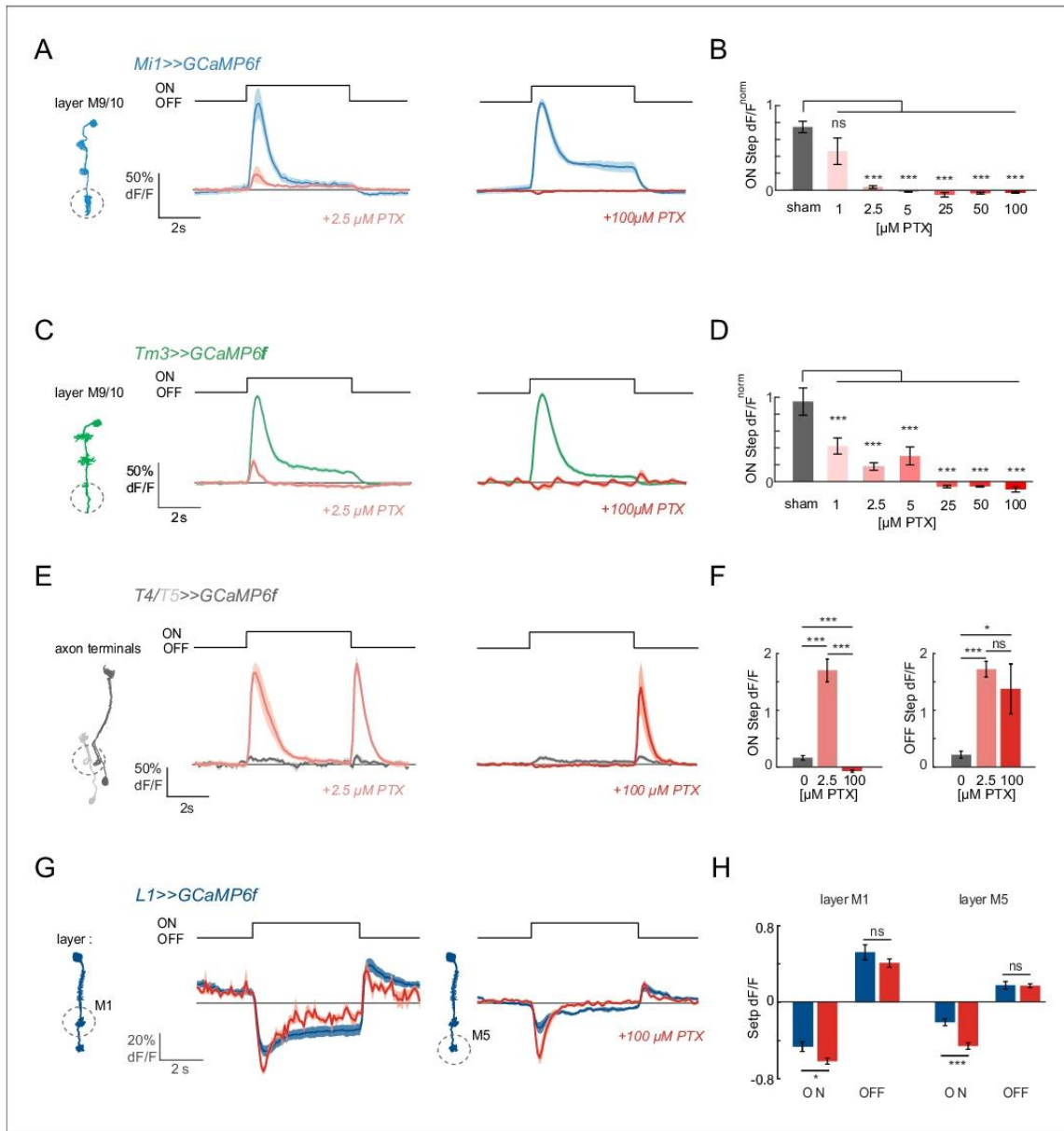
Figure 2. ON responses are abolished by PTX concentrations affecting GABA$_A$Rs and GluCls. (**A**) In vivo calcium signals recorded in layer M9/10 of Mi1 neurons, before (blue) and after (light red) PTX application. (**B**) Bar plot showing the quantification of the effect of PTX at various concentrations. A two-tailed Student t test was performed for each concentration against the sham control. Sample sizes were as follows: sham, n = 5 (89); 1 μM PTX, n = 5 (68); 2.5 μM PTX, n = 8 (102); 5 μM PTX, n = 5 (64); 25 μM PTX, n = 4 (30); 50 μM PTX, n = 5 (87); 100 μM PTX, n = 5 (89). (**C**) In vivo calcium signals recorded in layer M9/10 of Tm3 neurons, before (green) and after (light red) PTX application. (**D**) Bar plots showing the quantification of the effect of PTX at various concentrations. A two-tailed Student t test was performed for each concentration against the sham control. Sample sizes were as follows: sham, n = 7 (84); 1 μM PTX, n = 8 (108); 2.5 μM PTX, n = 9 (127); 5 μM PTX, n = 7 (74); 25 μM PTX, n = 5 (64); 50 μM PTX, n = 5 (51); 100 μM PTX, n = 6

Figure 2 continued on next page

Figure 2 continued

(92). (**E**) In vivo calcium signals in response to full-field flashes recorded in the axon terminals of T4/T5 neurons (n = 9 [229]), before (gray) and after (red) PTX application. (**F**) Bar plots showing the quantification of the results in (**E**). (**G**) In vivo calcium signals recorded in layer M1 (n = 6 [99]) and M5 (n = 6 [103]) of L1 neurons, before (dark blue) and after (red) 100 μM PTX application. (**H**) Bar plot showing the quantification of the data shown in (**G**). All traces show mean ± SEM. Sample sizes are given as number of flies (number of cells). *p<0.05, **p<0.01, ***p<0.001, tested with a one-way ANOVA and a post-hoc unpaired t-test with Bonferroni-Holm correction for multiple comparisons in (**B,D,F**), and a paired Student *t* test in (**H**).

DOI: https://doi.org/10.7554/eLife.49373.004

The following source data and figure supplements are available for figure 2:

Source data 1. Table 1 contains all mean ± s.e.m.

DOI: https://doi.org/10.7554/eLife.49373.011

Figure supplement 1. Blocking metabotropic glutamate receptors does not abolish ON responses.

DOI: https://doi.org/10.7554/eLife.49373.005

Figure supplement 1—source data 1. Table 1 contains all mean ± s.e.m.

DOI: https://doi.org/10.7554/eLife.49373.006

Figure supplement 2. ON responses are abolished by PTX concentrations affecting GABA$_A$Rs and GluCls.

DOI: https://doi.org/10.7554/eLife.49373.007

Figure supplement 2—source data 1. Table 1 contains all mean ± s.e.m.

DOI: https://doi.org/10.7554/eLife.49373.008

Figure supplement 3. The glutamatergic input onto Mi1 and Tm3 dendrites is still present upon PTX application.

DOI: https://doi.org/10.7554/eLife.49373.009

Figure supplement 3—source data 1. Table 1 contains all mean ± s.e.m.

DOI: https://doi.org/10.7554/eLife.49373.010

that at least under low PTX concentrations, other neurons (*Takemura et al., 2017*) and a lack of local inhibition (*Mauss et al., 2015*) can contribute to T4 responses.

After increasing the concentration of PTX to 100 μM within the same fly, all ON responses were abolished (*Figure 2E,F*), showing that T4 no longer receives any functional inputs at high PTX concentrations. In contrast, OFF responses were unaffected relative to the 2.5 μM phenotype (*Figure 2E,F*), arguing that the effect on the ON pathway is specific. This is in line with the idea that glutamate-gated chloride channels mediate ON responses in the visual system.

Importantly, the L1 input still responded to visual stimuli even at the highest PTX concentrations used (*Figure 2G,H*) and the iGluSnFR signal on the dendrites of Mi1 or Tm3 were largely unaltered, or even slightly increased at concentrations at which all Mi1 and Tm3 calcium responses were abolished (*Figure 2—figure supplement 3*), demonstrating that the glutamatergic input to the ON pathway was still intact. Taken together, our findings show that a systemic disruption of glutamate-gated chloride channels abolishes ON responses in Mi1 and Tm3, and suggest that GABA$_A$ receptors might play a role in mediating ON responses at the L1 to Mi1/Tm3 synapses in the fly visual system.

Glutamate- and GABA-gated chloride channels are broadly expressed in the visual system

To explore the possibility that both glutamate- and GABA-gated chloride channels mediate ON selectivity, we first looked at the expression of candidate genes. The only glutamate-gated chloride channel in the fly genome is encoded by the *GluClα* gene. A GluClα protein tagged with GFP (GluClα$^{MI02890.GFSTF.2}$) was found to be widely expressed in the visual system, including the lamina, medulla, lobula and lobula plate (*Figure 3A*). Expression was stronger in some proximal medulla layers, but the broad expression of this GFP trap did not allow expression to be assigned to specific cell types (*Figure 3A*). Two recently published cell-type-specific RNA sequencing datasets allowed us to assess candidate gene expression at cellular resolution (*Davis et al., 2018*; *Konstantinides et al., 2018*). *GluClα* mRNA was strongly expressed in all major ON pathway medulla neurons: Mi1, Tm3, Mi4, and Mi9 (*Figure 3B*, *Figure 3—figure supplement 1*). Furthermore, *GluClα* was also expressed in OFF pathway neurons (Tm1, Tm2, Tm4, and Tm9), albeit weaker in Tm9 (*Figure 3B*, *Figure 3—figure supplement 1*). The metabotropic glutamate receptor mGluR did not show expression in all ON pathway medulla neurons (*Figure 3B*, *Figure 3—figure supplement 1*), consistent with mGluR not playing a broad role in mediating ON selectivity (*Figure 2—figure supplement 1*). Of the three genes known to encode GABA$_A$Rs, *Grd* mRNA was not detectable
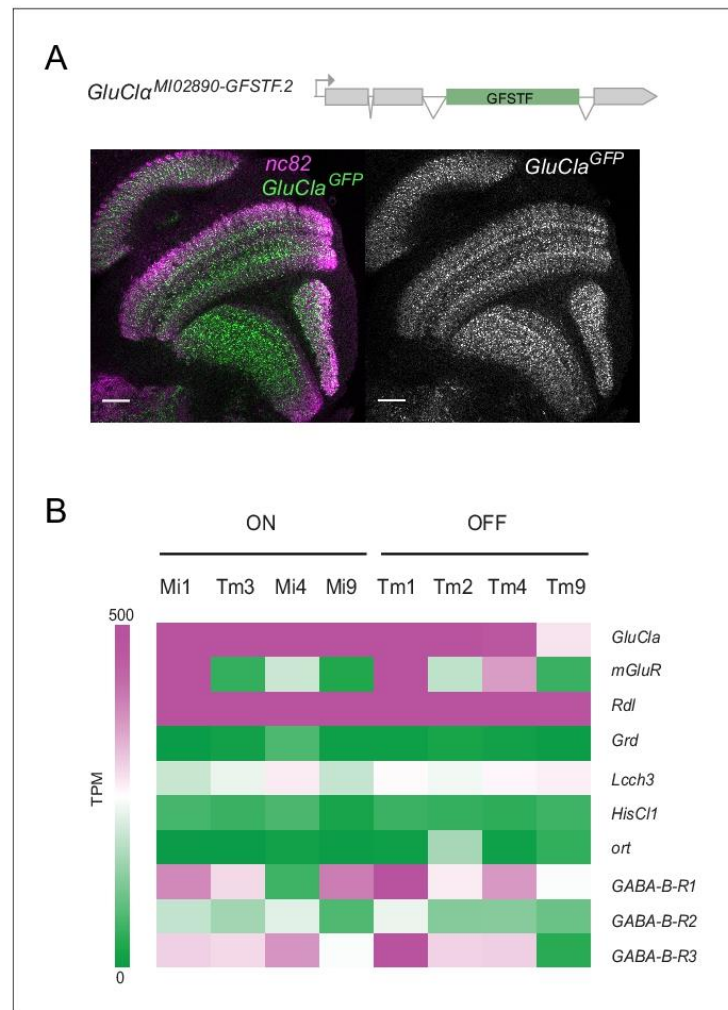
Figure 3. *GluClα* and *Rdl* are broadly expressed in the visual system. (**A**) Confocal cross-section of the visual system of a fly carrying a GFP exon trap within the *GluClα* locus (GluClα^MI02890.GFSTF.2). The neuropil is marked with nc82 (magenta) and endogenous GFP is in green/gray. Scale bar is 20 μm. (**B**) Expression levels shown as TPM (transcripts per kilobase million) values of inhibitory glutamate, GABA and histamine receptors. RNAseq data are from ***Davis et al. (2018)*** (GEO accession number: GSE 116969). Expression in the four most prominent medulla interneurons of the ON and OFF pathways are depicted.
DOI: https://doi.org/10.7554/eLife.49373.012
The following figure supplement is available for figure 3:

Figure supplement 1. *GluClα* and *Rdl* are broadly expressed in the visual system.
DOI: https://doi.org/10.7554/eLife.49373.013

in medulla neurons and *Lcch3* was only weakly expressed. Interestingly, the *Rdl* gene was strongly expressed in all major ON and OFF pathway medulla interneurons (***Figure 3B***). Thus, the glutamate- and GABA-gated chloride channel *GluClα* and *Rdl* are widely expressed in the visual system, including all ON pathway medulla neurons.

A PTX-insensitive GABA$_A$R allele partially rescues ON responses

We next wanted to determine whether the PTX-induced loss of responses was due to inhibition of the glutamate receptor GluClα, the GABA receptor Rdl, or both. We therefore added molecular specificity to the pharmacological approach using alleles that are insensitive to PTX. For *Rdl*, a single point mutation has been described that leaves channel function intact but renders GABA$_A$R insensitive to PTX (*Ffrench-Constant et al., 1993*). We hypothesized that if ON responses are mediated by the Rdl receptor, the PTX-insensitive *Rdl^{MDRR}* allele should rescue the effect of PTX on visual responses in ON pathway medulla neurons. To ensure that Rdl channels were exclusively composed of the PTX-insensitive Rdl^{MDRR} subunit, experiments were performed in trans to an *Rdl* null mutant (*Rdl^1/Rdl^{MDRR}*), or in homozygosity (*Rdl^{MDRR}/Rdl^{MDRR}*). We tested rescue of visual responses by the *Rdl^{MDRR}* mutant at 2.5 µM PTX, as this was the lowest toxin concentration that resulted in a loss of ON responses in both Mi1 and Tm3. We individually quantified the amplitude of the maximum response to the ON step, the amplitude of the plateau response, and the integrated response during the ON step (*Figure 4—figure supplement 1A*).

Control Mi1 neurons showed significantly reduced Mi1 peak responses and an eliminated sustained component upon application of PTX (2.5 µM), similar to PTX application in wild type (*Figure 4A*, *Figure 4—figure supplement 1B*). Importantly, when channels were only composed of the *Rdl^{MDRR}* insensitive subunit, Mi1 responses were partially rescued and the sustained component of the response was present (*Figure 4B,C Figure 4—figure supplement 1C*). Whereas the rescue of the peak ON response was only significant in layer M1 (*Figure 4C*), the integrated response or the plateau response were also prominently rescued in other layers (*Figure 4—figure supplement 1D*). In Tm3 neurons, PTX application also significantly reduced ON responses in controls (*Figure 4D*). This response was partially rescued by the presence of the PTX insensitive *Rdl^{MDRR}* allele (*Figure 4E*). This effect was again strongest in layer M1 (*Figure 4E,F*, *Figure 4—figure supplement 1E–G*). The fact that the *Rdl^{MDRR}* allele does not fully rescue all ON responses in Mi1 or Tm3 suggests that PTX might also be acting on *GluClα* in this context. At the same time, our findings argue that responses in medulla neurons Mi1 and Tm3 are indeed mediated at least in part by the GABA$_A$ receptor Rdl.

All lamina neurons downstream of photoreceptors were shown to be GABA negative by immunostaining, whereas the lamina feedback neurons C2 and C3 are GABA positive (*Kolodziejczyk et al., 2008*). RNAseq data support this notion, since L1 expresses high levels of genes involved in glutamate synthesis and does not express any GABA synthesis enzymes (*Figure 4—figure supplement 2A*; *Davis et al., 2018*). Expression of the vesicular GABA transporter dVGAT appears high, but this gene is highly expressed in all neurons, and could be non-specific. Furthermore, although it has been shown that neurons can maintain inhibitory signaling via uptake of GABA (*Tritsch et al., 2014*), this requires expression of the plasma membrane GABA transporter Gat, which is again not expressed in L1 (*Figure 4—figure supplement 2A*). Finally, GABA immunostaining is not visible in the terminals or cell bodies of L1 neurons, but can be seen in C2/C3 neurons (*Figure 4—figure supplement 2B,C*; *Kolodziejczyk et al., 2008*). Thus, there is no evidence for L1 co-releasing GABA in addition to glutamate. This suggests that visual responses to ON stimuli in Mi1 and Tm3 do not arise solely through a monosynaptic connection with the L1 inputs as previously thought (*Figure 4Gi*), but that a GABAergic synapse involving Rdl is likely involved in circuitry upstream of Mi1 and Tm3. In summary, Rdl-dependent circuits parallel to the glutamatergic L1 to medulla neuron synapse can also mediate ON responses (*Figure 4Gii*).

A PTX-insensitive GluClα partially rescues ON responses

We next wanted to test if and to what degree *GluClα* contributes to visual ON responses. No PTX-insensitive *GluClα* allele has been isolated in *Drosophila*, but the crystal structure of *GluClα* has been solved for the *C. elegans* homolog and the amino acid side chains interacting with the toxin have been identified (*Hibbs and Gouaux, 2011*). PTX interacts with specific residues of the M2 transmembrane alpha helix (*Figure 5A*; *Hibbs and Gouaux, 2011*). We aligned the M2 amino acid sequences of histamine, glutamate or GABA-gated chloride channels from different species (*D. melanogaster*, *C. elegans*, *M. domestica*) with known PTX sensitivities (*Cully et al., 1994*; *Ffrench-Constant et al., 1993*; *Hirata et al., 2008*; *Horoszok et al., 2001*; *Zheng et al., 2002*). This region is highly conserved among different channels and among species, with the exception of a single variable amino
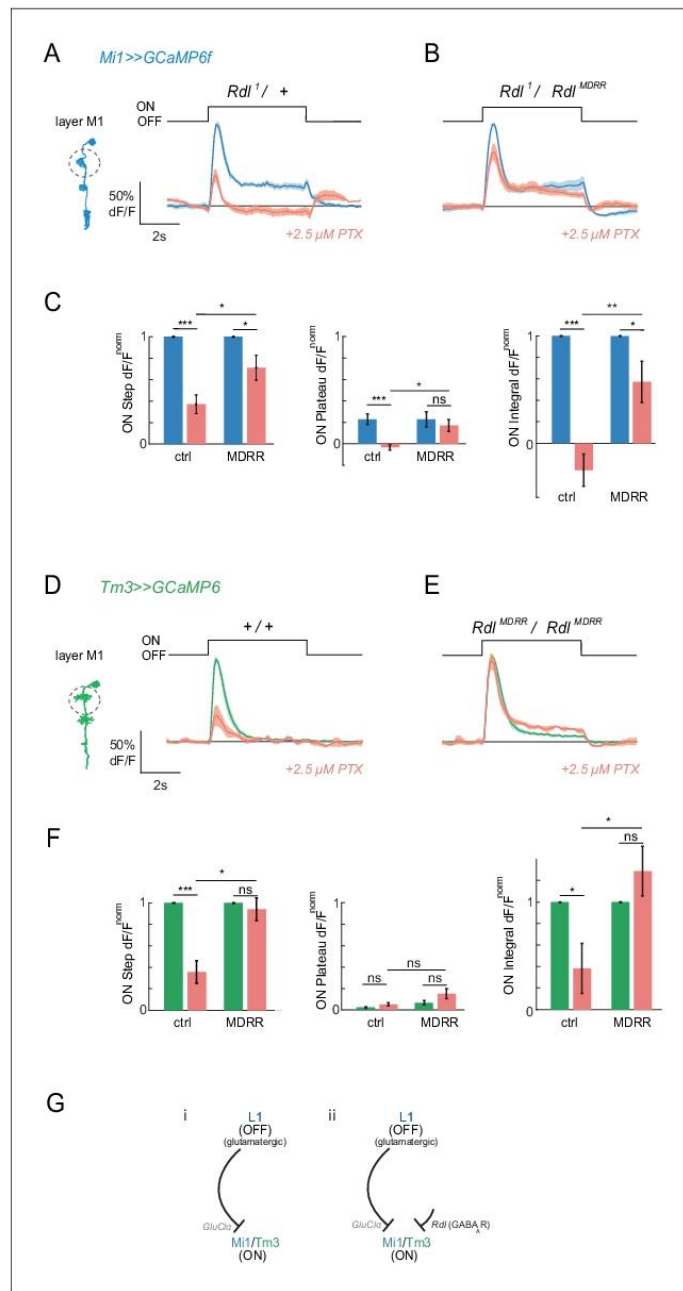
Figure 4. Pharmacogenetics shows that ON responses are partially mediated by the GABA$_A$R Rdl. (**A,B**) In vivo calcium signals in response to full-field flashes recorded in layer M1 of Mi1 neurons. Figure shows traces before (blue) and after (red) 2.5 µM PTX application in heterozygous $Rdl^1/+$ controls (A, n = 7 (58)), or flies only expressing the PTX-insensitive Rdl^{MDRR} allele (Rdl^1/Rdl^{MDRR}) (B, n = 8 (77)). (**C**) Bar plots showing the quantification of the
Figure 4 continued on next page

Figure 4 continued

normalized ON step, ON plateau and ON integral of the data shown in (**A,B**). *p<0.05, **p<0.01, ***p<0.001, tested with an unbalanced two-way ANOVA, corrected for multiple comparisons. (**D,E**) In vivo calcium signals in response to full-field flashes recorded in the layer M1 of Tm3 neurons. Genotypes: ctrl = Rdl^1/+ and 1 = Rdl^1/ Rdl^{MDRR}. Figure shows traces before (green) and after (red) PTX application +/+ controls (D, 1 = 5[34]), or flies only expressing the PTX-insensitive Rdl^{MDRR} allele (Rdl^{MDRR}/Rdl^{MDRR}) (E, n = 5[46]). (**F**) Bar plots showing the quantification of the traces shown in (**D,E**). All traces show mean ± SEM. Sample sizes are given as number of flies (number of cells). *p<0.05, **p<0.01, ***p<0.001, tested with an unbalanced two-way ANOVA, corrected for multiple comparisons. (**G**) Schematic summarizing the results. Our results suggest that ON-selectivity does not arise solely through glutamate-gated chloride channels as initially thought (i). The GABA$_A$R Rdl is required for ON-responses in a pathway parallel to the monosynaptic L1-Mi1/Tm3 connection (ii).
DOI: https://doi.org/10.7554/eLife.49373.014

The following source data and figure supplements are available for figure 4:

Source data 1. Table 1 contains all mean ± s.e.m.
DOI: https://doi.org/10.7554/eLife.49373.018

Figure supplement 1. Pharmacogenetics shows that ON responses are partially mediated by the GABA$_A$R Rdl.
DOI: https://doi.org/10.7554/eLife.49373.015

Figure supplement 1—source data 1. Table 1 contains all mean ± s.e.m.
DOI: https://doi.org/10.7554/eLife.49373.016

Figure supplement 2. L1 neurons are not GABAergic.
DOI: https://doi.org/10.7554/eLife.49373.017

acid, corresponding to amino acid S278 in *D. melanogaster* GluClα (red, *Figure 5B*). The identity of this single amino acid correlates strongly with the PTX sensitivity of the channel (*Figure 5B*). Mutations in this amino acid have been shown to change the PTX sensitivity of the channel. For example, the A > S substitution in the *D. melanogaster* GABA$_A$R allele Rdl^{MDRR} exhibits reduced sensitivity to PTX (*Figure 4*, *Ffrench-Constant et al., 1993*; *Fisher et al., 2015a*).

This prompted us to generate a potentially PTX-insensitive version of GluClα by introducing a point mutation leading to an S278T exchange. We first characterized mutant $GluClα^{S278T}$ heterologously in *Xenopus* oocytes. Two-electrode voltage-clamp recordings of wild type GluClα-expressing oocytes revealed fast activating and rapidly inactivating glutamate-induced currents, similar to inhibitory glutamate currents recorded in vivo in honeybees (*Barbara et al., 2005*). This current was sensitive to PTX (*Figure 5C,E*). Expression of the $GluClα^{S278T}$ mutant led to glutamate-induced currents that were less inactivating compared to wild-type GluClα controls. Importantly, the glutamate-induced currents in the $GluClα^{S278T}$ mutant were insensitive to PTX (*Figure 5D,E*).

We next generated $GluClα^{S278T}$ mutant flies, targeting the endogenous GluClα gene locus using CRISPR/Cas9-based genome editing (see Materials and methods for details). In the absence of toxin, $GluClα^{S278T}$ flies responded to visual stimuli with the typical peak and plateau response, arguing that the altered kinetics of the $GluClα^{S278T}$ mutant observed in oocytes was not a problem under these stimulus conditions (*Figure 6A,B*). We then tested if the $GluClα^{S278T}$ allele could rescue PTX-induced phenotypes in vivo in the visual system. Because the PTX-insensitive Rdl^{MDRR} allele rescued visual responses only partially at 2.5 μM, we first tested if GluClα could also account for a loss of responses at such low PTX concentrations previously thought to only block GABA$_A$Rs. Upon application of low concentrations of PTX (2.5 μM), calcium responses were lost in Mi1 neurons of heterozygous GluClα controls carrying a deficiency (Df) uncovering the GluClα locus (*Figure 6A*). In flies only expressing the $GluClα^{S278T}$ and no wild type protein, the ON responses were partially rescued. The rescue was specifically prominent for the step response, which was significantly rescued by $GluClα^{S278T}$ in all medulla layers (*Figure 6B,C*, *Figure 6—figure supplement 1A–C*). This shows that GluClα in vivo is sensitive to lower concentrations of PTX than previously thought, arguing that there is no specific concentrations to only block Rdl, and highlighting the usefulness of these PTX-insensitive alleles for molecular specificity. Furthermore, the rescue by $GluClα^{S278T}$ demonstrates that GluClα mediates ON responses in Mi1 in the fly visual system.

When testing if $GluClα^{S278T}$ could also rescue Tm3 responses in the presence of the toxin, this batch of 2.5 μM PTX gave a comparably mild phenotype in heterozygous controls (*Figure 6D*). The integrated ON response was still significantly rescued in a $GluClα^{S278T}$ background in layer M1
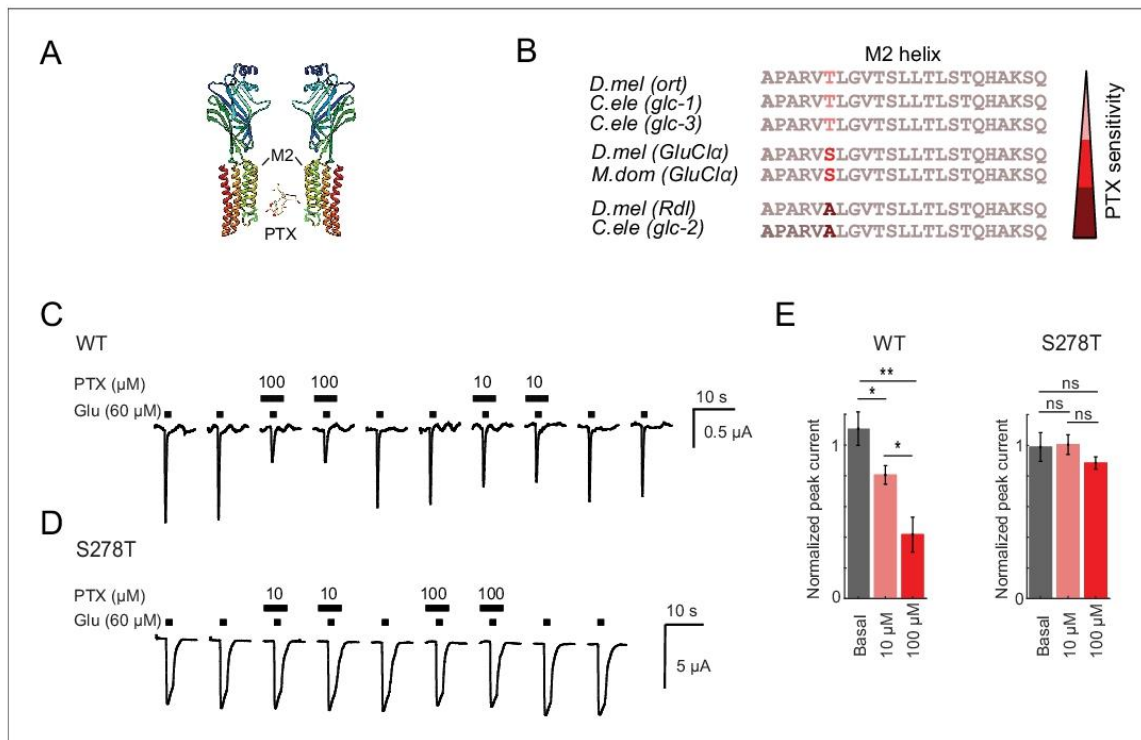
Figure 5. A *GluClα* allele insensitive to picrotoxin. (**A**) 3D protein structure of *Drosophila melanogaster* GluClα binding PTX, obtained by homology modeling with its *C. elegans* homolog GluClα using the Protein Homology/analogY Recognition Engine Phyre 2. (*Kelley et al., 2015*). The PTX structure was obtained from DrugBank, identification number DB00466. Structures were edited using Chimera 1.13, (*Pettersen et al., 2004*). (**B**) Alignment of the M2 helix of different ligand-gated chloride channel. The histamine-gated chloride channel *ort* (*Zheng et al., 2002*), the glutamate-gated chloride channels *glc-1*, *glc-2*, *glc-3*, *GluClα*, (*Cully et al., 1996*; *Cully et al., 1994*; *Horoszok et al., 2001*), and the GABA$_A$R *Rdl*. PTX sensitivities are indicated as shades of red. *D.mel = Drosophila melanogaster, C.ele = Caenorhabditis elegans, M.dom = Musca domestica*. (**C,D**) Two-electrode voltage-clamp recordings at a holding potential of −70 mV from *X. laevis* oocytes expressing wild type (**C**) or S278T (**D**) *GluClα*. Currents were evoked by glutamate wash in (lower bars) in the absence or presence of 10 μM or 100 μM picrotoxin (upper bars). (**E**) Mean peak-current amplitudes of the glutamate-evoked response in the presence (red) and absence (gray) of picrotoxin, normalized to the peak-current amplitude evoked by glutamate after picrotoxin wash out. Bars show mean ± SEM. *p<0.05, **p<0.01, tested with a one-way ANOVA and a post-hoc unpaired t-test with Bonferroni-Holm correction for multiple comparisons. Sample sizes: WT n = 6 and S278T n = 4 for 10 μM, and WT n = 6 and S278T n = 6 for 100 μM PTX.

DOI: https://doi.org/10.7554/eLife.49373.019

The following source data is available for figure 5:

Source data 1. Table 1 contains all mean ± s.e.m.

DOI: https://doi.org/10.7554/eLife.49373.020

(*Figure 6E,F*). In other medulla layers, 2.5 μM PTX more prominently blocked the peak Tm3 ON response in controls, but not in a *GluClα^{S278T}*-insensitive background (*Figure 6—figure supplement 1D–F*). This shows that *GluClα^{S278T}* also partially mediates ON responses in Tm3.

At high concentrations of PTX (100 μM), the PTX-insensitive *GluClα^{S278T}* allele did not rescue ON responses in either Mi1 or Tm3 (*Figure 6—figure supplement 1G–L*). This could suggest that GluClα^{S278T} does not confer PTX sensitivity at such high PTX concentrations in vivo. Alternatively, if GluClα^{S278T} was fully insensitive, this would further argue that PTX blocks other channels that are required for ON responses, and would thus underline the importance of Rdl. While we cannot fully distinguish between these two possibilities, we argued that if the loss of Mi1 and Tm3 responses
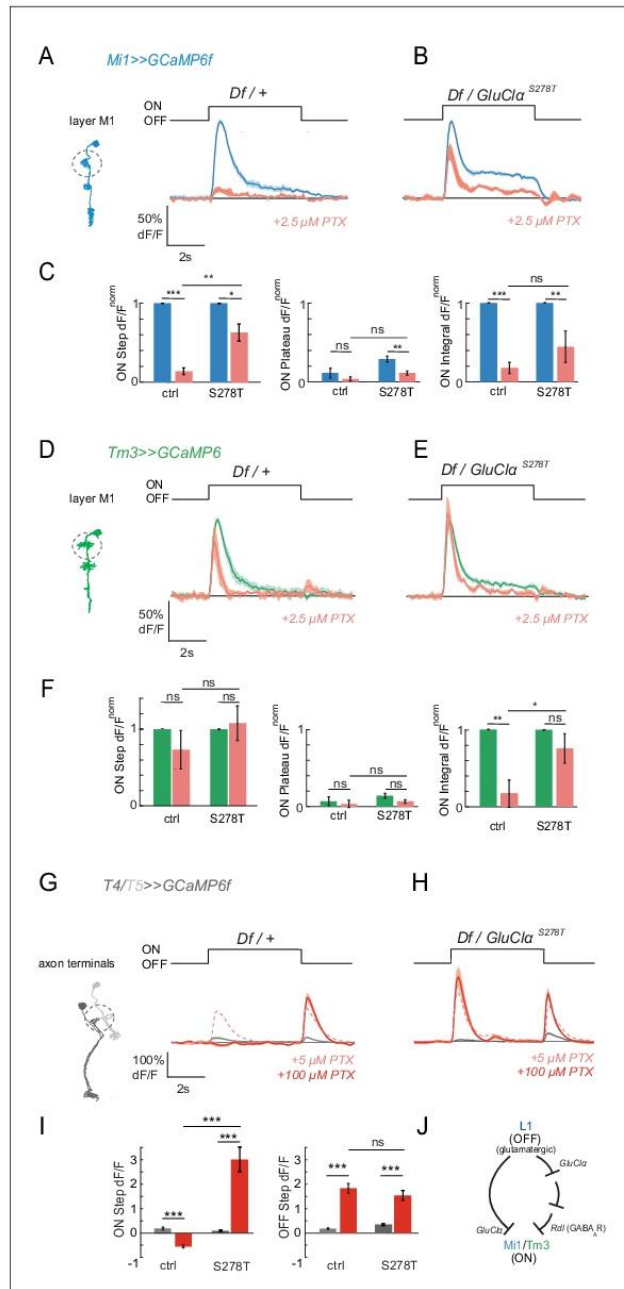
Figure 6. Pharmacogenetics shows that ON responses are mediated by *GluClα*. (**A,B**) In vivo calcium signals in response to full-field flashes recorded in layer M1 of Mi1 neurons. Figure shows traces before (blue) and after (red) 2.5 μM PTX application in heterozygous *GluClα^{Df}*/+ deficient controls (A, n = 5 [63]), as well as flies only expressing the PTX-insensitive *GluClα^{S278T}* allele (*GluClα^{S278T}*/*GluClα^{Df}*).(B, n = 5 [47]). (**C**) Bar plots showing the
Figure 6 continued on next page

Figure 6 continued

quantification of the data from (**A,B**). *p<0.05, **p<0.01, ***p<0.001, tested with an unbalanced two-way ANOVA, corrected for multiple comparisons. (**D,E**) In vivo calcium signals in response to full-field flashes recorded in the layer M1 of Tm3 neurons. Figure shows traces before (green) and after (red) PTX application in heterozygous $GluCl\alpha^{Df}/+$ deficient controls (D, n = 5 [30]), as well as flies only expressing the PTX-insensitive $GluCl\alpha^{S278T}$ allele ($GluCl\alpha^{S278T}/GluCl\alpha^{Df}$) (E, n = 5 [40]). (**F**) Bar plots showing the quantification of the data shown in (**D,E**). *p<0.05, **p<0.01, ***p<0.001, tested with an unbalanced two-way ANOVA, corrected for multiple comparisons. (**G,H**) In vivo calcium signals in response to full-field flashes recorded in T4/T5 axon terminals. Figure shows traces before (gray) and after (red) 100 µM PTX application in heterozygous $GluCl\alpha^{Df}/+$ deficient controls (G, n = 10[440]), as well as flies only expressing the PTX-insensitive $GluCl\alpha^{S278T}$ allele ($GluCl\alpha^{S278T}/GluCl\alpha^{Df}$) (H, n = 5[192]). The pink dotted line shows responses after the application of 5 µM PTX. (**I**) Bar plots showing the quantification of the data shown in (**G,H**). *p<0.05, **p<0.01, ***p<0.001. Statistics was done using an unbalanced two-way ANOVA, corrected for multiple comparisons. All traces show mean ± SEM. Sample sizes are given as number of flies (number of cells). (**J**) Schematic summarizing the results. Our results provide support for a combinatorial role of glutamatergic and GABAergic inhibition in mediating ON responses. Since GluClα is likely to be the receptor on all neurons postsynaptic to L1, Rdl could function downstream of GluClα.

DOI: https://doi.org/10.7554/eLife.49373.021

The following source data and figure supplements are available for figure 6:

Source data 1. Table 1 contains all mean ± s.e.m.
DOI: https://doi.org/10.7554/eLife.49373.024
Figure supplement 1. Pharmacogenetics shows that ON responses are mediated by *GluClα*.
DOI: https://doi.org/10.7554/eLife.49373.022
Figure supplement 1—source data 1. Table 1 contains all mean ± s.e.m.
DOI: https://doi.org/10.7554/eLife.49373.023

were due to the role of Rdl, $GluCl\alpha^{S278T}$ might still rescue the 100 µM PTX phenotype in T4/T5. As we showed above, unlike Mi1 and Tm3 responses, ON responses in T4/T5 were specifically blocked by high but not low concentrations of PTX (***Figure 2E,F***). To test if $GluCl\alpha^{S278T}$ can rescue T4/T5 responses at high concentrations, we recorded calcium signals in T4/T5 cells in a $GluCl\alpha^{S278T}$ background. Indeed, ON responses to full-field light flashes in 100 µM PTX were rescued (***Figure 6G–I***). Although this experiment does not tell us which cell types this rescue is coming from, this data shows that GluClα^{S278T} can be effective to rescue responses in some cell types at high PTX concentrations in vivo. Thus, the use of the toxin-insensitive $GluCl\alpha^{S278T}$ mutant demonstrates that $GluCl\alpha$ also mediates ON responses in vivo in the fly visual system. Together, our data provides support for a combinatorial role of glutamatergic and GABAergic inhibition in mediating ON responses. Because of the glutamatergic L1 input, GluClα is likely to be the receptor on all neurons postsynaptic to L1 (***Figure 6J***). Rdl could function downstream of GluClα. This suggests that a pathway parallel to a monosynaptic glutamatergic circuit can also mediate ON responses in Mi1 and Tm3 (***Figure 6J***).

The sign inversion in the ON pathway is a multisynaptic computation that depends on GluClα

Our findings lead to a model in which *GluClα* mediates responses to glutamatergic inputs in neurons downstream of L1 and in which a GABAergic pathway additionally drives responses in the ON pathway medulla neurons Mi1 and Tm3 (***Figure 6J***). Given that there is no evidence for L1 being GABAergic, Mi1 and Tm3 responses might not depend solely on monosynaptic L1 input. If this hypothesis is correct, *GluClα* should not exclusively function in a cell-autonomous manner in neurons downstream of L1, suggesting that Mi1 and Tm3 might still be able to respond to ON signals when *GluClα* function is only disrupted within the respective cell type. However, since pharmacological perturbations always targeted the entire visual system, more specific targeting would be required to address this possibility.

To test the above hypothesis, we generated a *GluClα* loss-of-function specifically in either Mi1 or Tm3. We inserted a FlpStop exon (***Fisher et al., 2017***) in the non-disrupting orientation ($GluCl\alpha^{FlpStop.ND}$), in which splicing occurs normally unless the FlpStop exon is inverted by Flp recombinase expression (***Fisher et al., 2017***). Upon pan-neuronal inversion of the FlpStop cassette into the non-disrupting orientation ($GluCl\alpha^{FlpStop.D}$) quantification of *GluClα* expression levels using
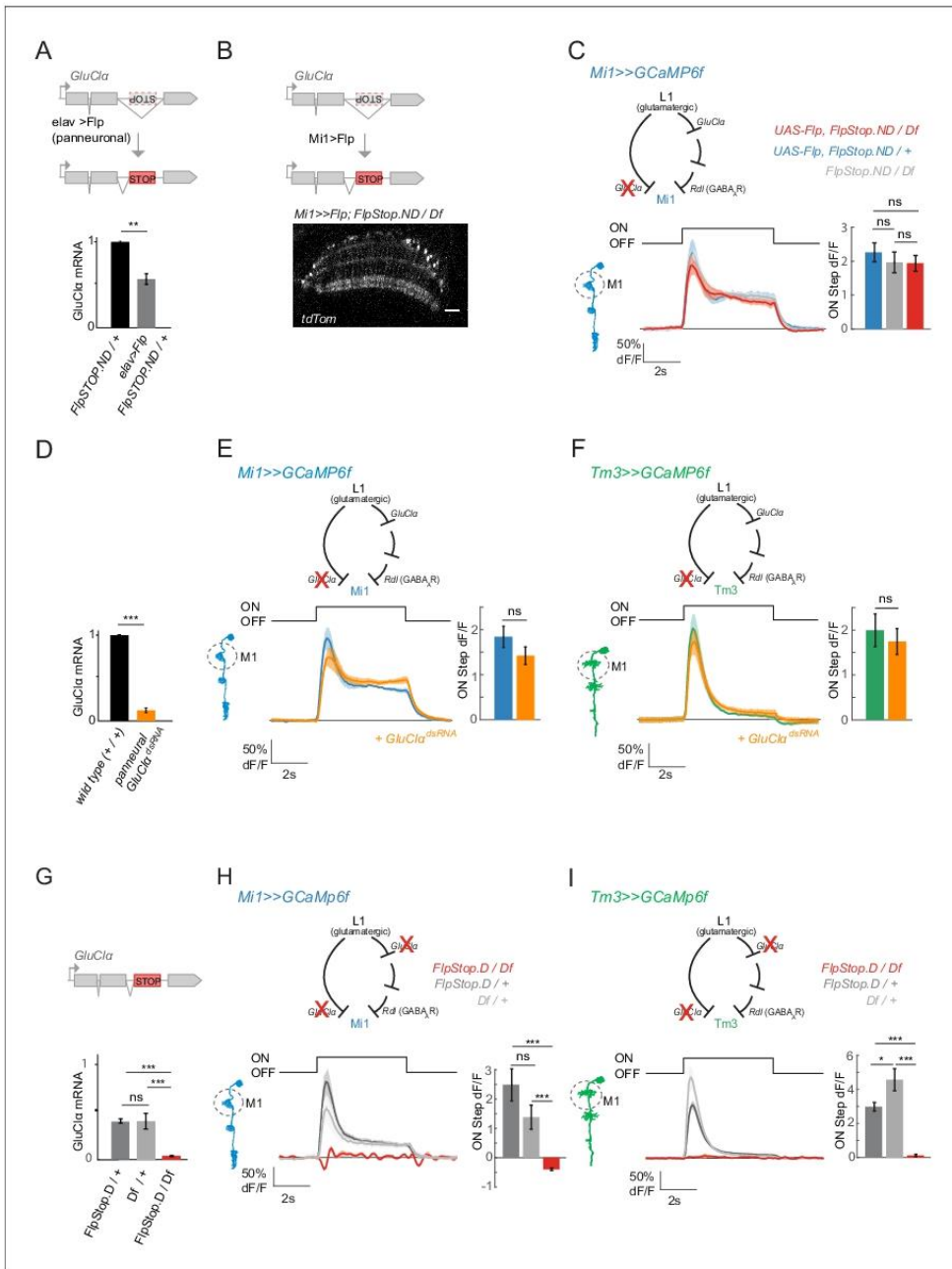
Figure 7. ON selectivity is a multisynaptic computation mediated by *GluClα*. (**A**) Schematic illustrating inversion of the *GluClα* FlpStop exon in all neurons by panneuronal expression of Flp recombinase using elav-Gal4. qRT-PCR results show *GluClα* mRNA levels relative to the GAPDH housekeeping gene, normalized to controls. (**B**) The FlpStop exon in the non-disrupting (ND) orientation was inverted specifically in Mi1 neurons by cell-type-specific expression of Flp recombinase. This is visualized via expression of tdTom signal, and is specific to and broad in Mi1. (**C**) In vivo

Figure 7 continued on next page

Figure 7 continued

calcium signals recorded in a cell-type-specific Mi1 *GluClα* loss-of-function. Calcium signals were recorded in layer M1 of *GluClα* mutant Mi1 neurons (n = 5 (136)) (red), and heterozygous controls (n = 5[166], n = 5[139]) (blue, gray). The bar plot shows quantification of the ON step. (**D**) qRT PCR results quantifying pan neuronal knockdown of *UAS-GluClα*^{RNAi} using elav-Gal4, normalized to control. (**E,F**) In vivo calcium signals upon cell-type-specific *GluClα* knockdown. Calcium signals in response to full-field flashes were recorded in layer M1 of (**E**) Mi1 control (n = 8[229]) or *Mi1 >>GluClα*^{RNAi} (n = 6 [215]) or of (**F**) Tm3 control (n = 8[150]) and *Tm3 >>GluClα*^{RNAi} (n = 6[146]). Bar plot show quantification. (**G**) qRT PCR results quantifying *GluClα* mRNA levels in heterozygous *GluClα*$^{Flp.Stop.D/+}$ and *GluClα*$^{Df/+}$, as well as the homozygous mutant *GluClα*$^{Flp.Stop.D/Df}$. (**H,I**) In vivo calcium signals recorded in a full *GluClα*$^{FlpStop.D}$ mutant background (red). Heterozygous *GluClα*$^{FlpStop.D}$ controls are in blue (Mi1, n = 5 (117)) or green (Tm3, n = 8 (275)), heterozygous Df controls are in gray (Mi1, n = 5[142]; Tm3, n = 5[198]) and the experimental condition is in red (Mi1, n = 9 [134]; Tm3, n = 5[96]). Bar plots show quantification of the ON step response. All traces show mean ± SEM. All sample sizes are shown as number of flies (number of cells). Statistics was done using an unpaired Student *t* test for comparison in (**A,D,E,F**), and a one-way ANOVA and a post-hoc unpaired t-test with Bonferroni-Holm correction for multiple comparisons in (**C,G,H,I**). *p<0.05, **p<0.01, ***p<0.001.

DOI: https://doi.org/10.7554/eLife.49373.025

The following source data is available for figure 7:

Source data 1. Table 1 contains all mean ± s.e.m.
DOI: https://doi.org/10.7554/eLife.49373.026

qRT-PCR showed that transcription was disrupted by half when the FlpStop exon was inverted in a heterozygous background, arguing for a full loss of function in *GluClα*$^{FlpStop.D}$ (*Figure 7A*).

To selectively disrupt *GluClα* function in Mi1 neurons, we expressed Flp recombinase in Mi1 (*Figure 7B*). Expression of tdTomato, a marker for the FlpStop inversion event, further confirmed efficient inversion of the cassette (*Figure 7B*). When we recorded calcium signals in Mi1 in this cell-type-specific FlpStop background, visual responses to ON flashes were still present in Mi1 neurons and did not differ from controls (*Figure 7C*). To corroborate these findings, we next used cell-type-specific RNAi. Pan-neuronal expression of *GluClα*^{dsRNA} reduced *GluClα* mRNA to 16.4 ± 7.4% of controls (*Figure 7D*). When knocking down *GluClα* in either Mi1 or Tm3, ON responses were again not abolished and did not differ significantly from controls (*Figure 7E,F*). These results demonstrate that ON selectivity is not mediated monosynaptically, but that pathways parallel to the L1-Mi1 or L1-Tm3 connection might be sufficient to mediate ON responses.

Our results argue that ON responses are encoded in a multi-synaptic fashion. Because L1 is the major input to the ON pathway and is glutamatergic (*Figure 4—figure supplement 2A*; *Takemura et al., 2011*), all ON responses might still depend on *GluClα* at the first synapse postsynaptic to L1. This leads to the hypothesis that Mi1 or Tm3 responses would be lost in a full *GluClα* mutant background. To test this, we used a FlpStop allele inserted in the disrupting orientation. In this background, expression should be fully disrupted in all cells normally expressing *GluClα*. Quantification of expression levels of *GluClα* using qRT-PCR showed that transcription was fully disrupted in *GluClα*$^{FlpStop.D}$ (3.7 ± 0.6% mRNA compared to wild type, *Figure 7G*). Furthermore, in heterozygous animals, *GluClα*$^{FlpStop.D}$ transcripts were reduced roughly by half (40.1 ± 2.2%) and to the same amount as in a *GluClα* deficiency (40.2 ± 8.2%) lacking the entire gene locus (*Figure 7G*). These findings confirm that *GluClα*$^{FlpStop.D}$ is a null allele.

GluClα$^{FlpStop.D}$ mutant flies eclosed but showed locomotor deficits. The viability of the *GluClα* mutant allowed us to conduct calcium imaging experiments in this null mutant background. Whereas Mi1 and Tm3 neurons in heterozygous *GluClα* mutant or deficient flies responded normally to light flashes, Mi1 and Tm3 responses were both dramatically affected in full *GluClα* mutants. No increase in calcium signal was detectable in *GluClα* null mutants, and light responses were largely absent in all layers (*Figure 7H,I*). Instead, Mi1 even showed a small and transient decrease in calcium signal in response to light ON, which could potentially be attributed to the additional presence of excitatory glutamate receptors or reveal inputs from the OFF pathway (*Figure 7H*). Thus, normal ON responses are lost whenever *GluClα* function is disrupted in the entire visual system, but not when it is disrupted in a cell-type-specific manner. These data are further consistent with the results of pharmacological experiments in wild type and PTX-insensitive alleles. Taken together, these results demonstrate that ON selectivity is a multisynaptic computation that is robust to perturbations at individual synapses.

GluClα mediates all ON but not OFF responses in direction-selective cells

To generalize the role of *GluClα* function for ON responses, we next asked how the output of the system is affected in a full *GluClα* loss-of-function by recording T4/T5 responses in the *GluClα*$^{FlpStop.D}$ mutant. When imaging flies expressing GCaMP6f in both T4 and T5, individual cell type responses can be separated by showing individual moving ON and OFF edges that activate T4 and T5, respectively (*Figure 8A*; *Fisher et al., 2015b*; *Maisak et al., 2013*). T4/T5 neurons project to one of the four layers of the lobula plate, and the four layers show distinct directional tuning. In heterozygous controls, T4/T5 neurons responded to both moving ON and OFF edges and the four layers responded preferentially to front to back (layer A), back to front (layer B), upward (layer C), and downward (layer D) motion (*Figure 8A*). Responses to ON edges were completely abolished for motion in all directions in the *GluClα* null mutant, showing that all T4 inputs depend on *GluClα* (*Figure 8B,C*). In contrast, T4/T5 neurons still responded to OFF edges moving in different directions (*Figure 8A–D*). Both response amplitude and direction selectivity of the OFF response were unaffected in *GluClα* mutants (*Figure 8D*).

When recording responses to light flashes, T4/T5 axon terminals also no longer showed an increase in calcium in response to the ON step. Interestingly, the calcium signal even decreased, indicating inhibition (*Figure 8E,G*). Inhibition was previously shown to be an important part of motion computation (*Fisher et al., 2015a*; *Gruntman et al., 2018*; *Haag et al., 2016*; *Leong et al., 2016*; *Salazar-Gatzimas et al., 2016*). This could argue that, in the absence of all ON inputs, feed-forward inhibition onto T4 is revealed. Alternatively, T5 neurons might have lost rectification and respond to ON with a decrease in calcium. To distinguish between these two possibilities, we recorded flash responses in layer M10 of the medulla. Here, T4 and T5 projections do not overlap and calcium signals will stem exclusively from T4 dendrites. We found that T4 dendrites also show a negative calcium signal in response to ON (*Figure 8F,H*), revealing that this inhibition is present in T4 neurons but masked in the presence of *GluClα*. Furthermore, there was an increase in calcium signal during OFF in T4 dendrites (*Figure 8F*), suggesting a loss of *GluClα*-dependent inhibition that is normally active during OFF. Taken together, our results show that *GluClα* function is critical for ON selectivity in the fly visual system.

Discussion

In this study, we have identified the mechanisms underlying splitting of the ON and OFF pathways in the *Drosophila* visual system. As expected from the major input to the ON pathway being glutamatergic, broad *GluClα* function is required for all ON responses in medulla neurons or downstream direction-selective cells. However, individual cell types downstream of the glutamatergic L1 input are resilient to a cell-type-specific loss of *GluClα*, demonstrating that ON selectivity is computed in a distributed manner. We further show that both the glutamate-gated chloride channel *GluClα* and the GABA-gated chloride channel *Rdl* are widely expressed in the visual system and together mediate ON responses. Thus, ON selectivity is a multisynaptic computation that is established across distributed circuits.

ON selectivity is mediated by both glutamatergic and GABAergic inhibition

Our work shows that visual responses in the first ON-selective neuron of the *Drosophila* visual system uses a combination of *GluClα* and *Rdl* receptors. This reveals a new biophysical mechanism through which ON and OFF pathway dichotomy can be established. While pharmacology can be used to deduce the function of specific molecular mechanisms, these approaches are often not specific to one protein. GluCls and GABARs belong to the same receptor family of ligand-gated chloride channels and have closely related structure and phylogeny (*Betz, 1990*; *Lynagh et al., 2015*). All known noncompetitive antagonists like Picrotoxin, γ-HCH, dieldrin, EBOB and fibronil target both receptor types although the actions are weaker in GluCls compared to GABARs (*Eguchi et al., 2006*). Along these lines, PTX was thought to affect GABA$_A$ receptor at low concentrations, and additionally affect GluCls at high concentrations in vitro and in vivo (*Liu and Wilson, 2013*; *McCavera et al., 2009*; *Takeuchi and Takeuchi, 1969*; *Wilson and Laurent, 2005*). Here, the use of PTX-insensitive alleles
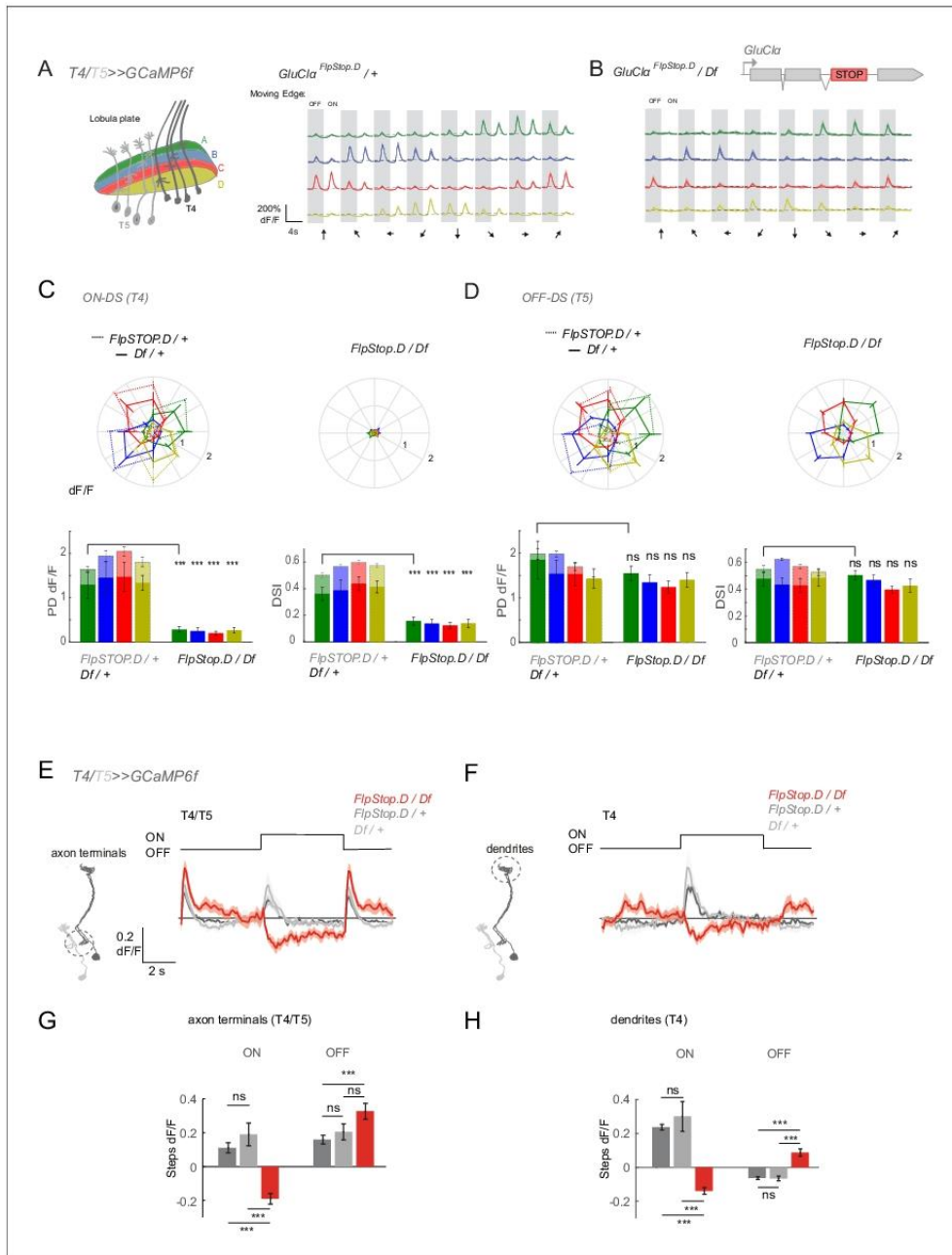
Figure 8. *GluClα* mediates ON but not OFF direction-selective responses. (A–D) In vivo calcium signals recorded in direction-selective T4/T5 neurons. (A,B) Schematic of T4 and T5 axon terminal innervating the four anatomical layers in the lobula plate (left). Visually evoked calcium signals recorded from all four layers in response to OFF and ON moving edges in eight different directions in heterozygous controls (A, n = 8 [62/60/59/50]) and a full *GluClα* mutant background, *GluClα*^FlpStop.D^/Df (B, n = 9 [69/73/70/64]). (C,D) Polar plots showing the calcium signals in response to moving ON (C) or

Figure 8 continued

OFF (**D**) edges. Genotypes are as indicated. Bar plots show the quantification of the preferred direction (PD) response and the direction selectivity index (DSI) for each layer. Sample size shows number of flies (number of cells in layers A/B/C/D) (**E,F**) Calcium signals in response to full-field flashes recorded in T4/T5 axon terminals in the lobula plate (**E**) or T4 dendrites in the medulla (**F**). (**G,H**) Bar plots show the quantification of the ON or OFF response in T4/T5 axon terminals (**G**) or T4 dendrites (**H**). Heterozygous *GluClα*^{*FlpStop.D*} (n = 8 (225/40)) and *GluClα*^{*Df*} (n = 8 [141/36]) controls are in gray and the *GluClα*^{*FlpStop.D*}/Df mutant (n = 5 [198/22]) is in red in (**E–H**). All traces show mean ± SEM. Sample size are given as number of number of flies (number of ROIs). Statistical comparisons were done using an unpaired Student *t* test in (**C,D**), and a one-way ANOVA and a post-hoc unpaired t-test with Bonferroni-Holm correction for multiple comparisons in (**G,H**), ***p<0.001.

DOI: https://doi.org/10.7554/eLife.49373.027

The following source data is available for figure 8:

Source data 1. Table 1 contains all mean ± s.e.m.

DOI: https://doi.org/10.7554/eLife.49373.028

for glutamate and GABA-gated chloride channels allowed us to deduce that, in vivo, *GluClα* is already blocked by PTX at lower concentrations than previously thought, and that both *GluClα* and *Rdl* play critical roles for ON responses in the *Drosophila* visual system. These pharmacogenetic experiments using toxin-insensitive alleles prove to be a powerful tool to unambiguously assign specific effects to individual channels.

One benefit of the use of two inhibitory transmitter systems might be the distribution of sensory coding across parallel synapses. GluClα and Rdl also appear to have very different channel dynamics (*Cully et al., 1996*; *Ffrench-Constant et al., 1993*). Interestingly, PTX-insensitive *GluClα* and *Rdl* alleles predominantly rescue different aspects of the visual responses. Whereas *GluClα*^{*S278T*} predominantly rescued the peak response in all medulla layers, *Rdl*^{*MDRR*} mainly rescued the plateau response. This is consistent with our results and with previous oocyte recordings revealing that GluClα is fast desensitizing (*Figure 5*; *Cully et al., 1996*). It is also consistent with in vivo recordings of inhibitory glutamate currents in the honeybee (*Barbara et al., 2005*). In contrast, GABA receptors stay open throughout the period in which the transmitter is present (*Ffrench-Constant et al., 1993*). Thus, the use of different inhibitory receptors might allow different aspects of a temporally structured stimulus to be encoded. This is consistent with the finding that two different types of inhibition are also in place in the vertebrate retina. There, GABAergic and glycinergic inhibition diversify the response properties of bipolar cells through a direct influence on temporal and spatial features (*Franke et al., 2017*).

While both receptors appear to be broadly expressed in many cell types of the visual system, they could be co-expressed with different transporters and channels, and interact with different molecular partners, further diversifying their role. Another common strategy to generate functional diversity is the bringing together of different receptor subunits with certain homology. Both mammalian GlyR and GABA_A receptors can function as hetero-oligomers made up of different subunits and thus generating functional diversity (*Betz, 1990*). There are at least three different GluCl subtypes in *C. elegans* that can be combined (*Cully et al., 1994*; *Horoszok et al., 2001*). In *Drosophila*, only one gene coding for a glutamate-gated chloride channel has been identified. Although alternative splicing and post-transcriptional modifications could alter channel function, all known isoforms are identical in their functional domains. However, heteropentameric channels composed of mixed Rdl and GluClα subunits have been suggested biochemically (*Ludmerer et al., 2002*). Such a potential presence of hybrid channels might also explain the higher in vivo sensitivity of GluClα to PTX in some cell types (*Figure 6*, S7). Finally, two distinct inhibitory transmitter systems might be suitable for individual changes during evolution, allowing for adaptation to specific contextual constraints.

ON selectivity is a multisynaptic computation

Our experiments revealed that *GluClα* is not exclusively required in a cell-autonomous manner for ON responses, since loss of *GluClα* function in Mi1 or Tm3 individually does not lead to a loss of ON responses. It is unlikely that this is due to an incomplete loss of function, since independent genetic tools (FlpStop and RNAi) that both disrupted *GluClα* expression substantially at the mRNA level (*Figure 7*) gave the same result. Furthermore, the same FlpStop allele effectively abolished all ON responses when *GluClα* function was disrupted within its entire expression pattern. Additionally, a PTX-resistant Rdl channel can mediate ON responses in a PTX background, although L1 is not

GABAergic. Together, these results suggest that ON selectivity is not a monosynaptic computation, but that parallel functional pathways can even compensate for the loss of the major synaptic connection that links L1 directly to Mi1 or Tm3. Thus, the emergence of ON selectivity is more distributed than suggested by minimal core circuit motifs. One synaptic layer further downstream, optogenetic activation of Mi1 and Tm3 most strongly contributes to T4/T5 responses (*Strother et al., 2017*). However, our data further show that T4/T5 neurons still respond to ON stimuli when both Mi1 and Tm3 responses are completely blocked by PTX, arguing that other neurons also significantly contribute to T4/T5 responses under visual stimulation and suggesting that coding is again more distributed at this stage.

Based on connectomics, one can speculate about candidates for the implementation of these parallel circuit motifs between L1 and Mi1 and Tm3. The lamina neuron L5 and the GABAergic feedback neurons C2 and C3 receive L1 inputs and could be part of an interconnected local microcircuit (*Takemura et al., 2013*). Intercolumnar neurons, not present in the current connectome datasets, like Pm or Dm neurons, might also be involved and are likely glutamatergic (*Davis et al., 2018*; *Raghu and Borst, 2011*). In fact, there are close to 100 cell types in the visual system and ~60 medulla neurons, but their role is so far unknown. Sensory pathway splits in the periphery are one of the most fundamental steps in sensory processing. Turning this into a process that parallel pathways can achieve might make this important feature extraction step robust to perturbations.

GluClα mutants reveal GABAergic inhibition onto T4 dendrites

T4 flash responses in a *GluClα*-deficient background show an increase in calcium signal during the OFF epoch and a decrease during the ON epoch (*Figure 8*). For a long time, the mechanisms that generate direction-selective responses in T4/T5 neurons were thought to rely on feedforward excitatory mechanisms (*Fisher et al., 2015b*; *Silies et al., 2014*; *Yang and Clandinin, 2018*). Recently, it was suggested that these direction-selective cells in the fly visual system also implement mechanisms that rely on null-direction suppression (*Haag et al., 2016*; *Leong et al., 2016*; *Salazar-Gatzimas et al., 2016*). Whereas electrophysiological recordings showed inhibition in T4 when the trailing edge of the receptive field was specifically stimulated (*Gruntman et al., 2018*), whole-cell recording experiments of T4/T5 neurons are daunting and this is the first time that calcium imaging data directly reveals inhibition in response to single ON flashes. Since glutamatergic inhibition via GluClα was disrupted in this experimental context, our data suggests that this is due to GABAergic inhibition. Several neuronal candidates could make inhibitory synapses onto T4 dendrites. Based on connectomics and neurotransmitter identity, neurons like Mi4, C3, CT1 or TmY15 give direct input and are GABAergic (*Meier and Borst, 2019*; *Takemura et al., 2017*). Alternatively, this decrease in calcium signal in T4 might come from a lack of excitatory inputs in a GluClα mutant background. Interestingly, Mi1 and Tm3 themselves show inhibition in response to light when GluClα is blocked. However, this effect is more pronounced at their dendrites than in their output layer and shows different kinetics. Our work might thus help uncover a GABAergic inhibitory input to T4 that is more strongly apparent in the absence of Mi1 and Tm3 excitation, and could ultimately reveal the circuit implementation for the inhibitory component of T4/T5 receptive fields (*Leong et al., 2016*; *Salazar-Gatzimas et al., 2016*). Furthermore, our data also reveals an increase in calcium during OFF stimulation. The major inputs to T4 are themselves rectified (*Behnia et al., 2014*). However, rectification in T4 might not be purely inherited by its inputs but also further strengthened at the T4 dendrites. Our findings thus suggest that glutamatergic inhibition contributes to establishing or maintaining contrast selectivity in T4.

Evolutionary advantages of glutamatergic ionotropic inhibition

Both *GluClα* and *Rdl* are ionotropic ligand-gated receptors. While ionotropic receptors also implement the ON and OFF pathway split in *C. elegans* chemosensation (*Chalasani et al., 2007*), examples in vertebrate vision, olfaction and gustation require metabotropic receptors (*Chandrashekar et al., 2006*; *Masu et al., 1995*; *Nei et al., 2008*). Ionotropic receptors appear to be more common in insects than in vertebrates (*Silbering and Benton, 2010*). Furthermore, glutamate-gated chloride channels have independently arisen three times within invertebrate clades and are present in arthropods, molluscs and flatworms (*Lynagh et al., 2015*), arguing for a strong evolutionary benefit. Ionotropic receptors mediate rapid transduction events at scales smaller than a

millisecond, whereas metabotropic ones are in the millisecond to second range and last longer, from seconds to several minutes, due to an enzymatic secondary cascade previous to channel opening (*Betz, 1990*; *Shiells, 1994*). The evolutionary choice of the specific glutamatergic inhibitory system needs to match the sensory processing speed required for accurate behavioral responses in these species. For example, at the photoreceptor level, invertebrate phototransduction is faster than vertebrate phototransduction thanks to sophisticated molecular strategies (*Hardie and Raghu, 2001*; *Katz and Minke, 2009*). Also, the latency of olfactory sensory neurons responses in mammals is longer than that observed in insects (*Sato et al., 2008*; *Silbering and Benton, 2010*). One advantage that metabotropic receptors have over ionotropic receptors is further amplification of the signal (*Shiells, 1994*). The distributed circuit architecture proposed here might therefore strengthen signaling in a system that uses ionotropic signaling.

Potential implications for sensory processing in other systems

Here we showed that ON selectivity is not a monosynaptic process as described in other systems (*Chalasani et al., 2007*; *Masu et al., 1995*). Although acute pharmacological block or a systemic loss of function of GluClα abolished all ON responses in different neurons, cell-type-specific mutants retained intact ON responses, revealing that sensory coding is distributed in the fly visual system. This not only highlights the power of fly genetics but sheds new light onto the mechanisms of ON selectivity in other systems, since conclusions about ON and OFF pathway splits being mediated by specific monosynaptic processes in systems such as the vertebrate retina or the *C. elegans* chemosensory system relied on systemic loss-of-function approaches (*Chalasani et al., 2007*; *Masu et al., 1995*). Several of these systems allow for cell-type-specific manipulations using genetic approaches. It will be interesting to revisit these systems and ask if coding is similarly distributed across multiple synapses in different sensory systems and organisms.

Materials and methods

Key resources table

Reagent type (species) or resource	Designation	Source or reference	Identifiers	Additional information
Strain, strain background (*Drosophila melanogaster*)	*Mi1 >> GCaMP6f*	Bloomington Drosophila Stock Center	$w+$; $R19F01$-$p65ADZp^{attP40}$ / +; $R71D01$-$ZpGdbd^{attP2}$/UAS-GCaMP6f	*Figures 1, 2* and *7* *Figure 2—figure supplement 1*
Strain, strain background (*Drosophila melanogaster*)	*Tm3 >> GCaMP6f*	Bloomington Drosophila Stock Center	$w+$; $R38C11$-$p65ADZp^{attP40}$ / +; $R59C10$-$ZpGdbd^{attP2}$/UAS- GCaMP6f	*Figures 1, 2* and *7* *Figure 2—figure supplement 1*
Strain, strain background (*Drosophila melanogaster*)	*L1 >> GCaMP6f*	Bloomington Drosophila Stock Center	w^{+}; $L1[c202]$-Gal4 / +; UAS-GCaMP6f / +	*Figure 1, 2*
Strain, strain background (*Drosophila melanogaster*)	*Mi1 >> iGluSnFR*	Bloomington Drosophila Stock Center	$w+$; $R19F01$-$p65ADZp^{attP40}$ / +; $R71D01$-$ZpGdbd^{attP2}$/UAS iGluSnFR A184A ^{attP2}	*Figure 1,* *Figure 2—figure supplement 3*
Strain, strain background (*Drosophila melanogaster*)	*Tm3 >> iGluSnFR*	Bloomington Drosophila Stock Center	$w+$; $R38C11$-$p65ADZp$ [attP40] / +; $R59C10$-$ZpGdbd^{attP2}$/UAS iGluSnFR A184A^{attP2}	*Figure 1,* *Figure 2—figure supplement 3*

Continued on next page

Continued

Reagent type (species) or resource	Designation	Source or reference	Identifiers	Additional information
Strain, strain background (*Drosophila melanogaster*)	T4/T5 >> GCaMP6f	Bloomington Drosophila Stock Center	w^+; R64G09-LexA^{attP40}, lexAop2-IVS-GCaMP6f-p10$^{su(Hw)attP5}$ / +; + / +	*Figure 2, Figure 8*
Strain, strain background (*Drosophila melanogaster*)	GluClα $^{MI02890\text{-}GFSTF.2}$	Bloomington Drosophila Stock Center	y^1 w^*; Mi{PT-GFSTF.2} GluClα $^{MI02890\text{-}GFSTF.2}$/TM6C, Sb^1 Tb^1	*Figure 3*
Antibody	Anti-GFP (chicken polyclonal)	Abcam	Cat# ab13970, RRID:AB_300798	IF (1:2000) *Figure 3, Figure 4—figure supplement 2*
Antibody	Anti-Bruchpilot (mouse monoclonal nc82)	DSHB	Cat# nc82, RRID:AB_2314866	IF (1:25) *Figure 3*
Antibody	Alexa Fluor 488-conjugates AffinityPure Goat Anti-Chicken IgG	Jackson Immuno Research Labs	Cat# 103-545-155, RRID:AB_2337390	IF (1:200) *Figure 3*
Antibody	Alexa Fluor 594-conjugates AffinityPure Goat Anti-Mouse IgG	Jackson Immuno Research Labs	Cat# 115-585-206, RRID:AB_2338886	IF (1:200) *Figure 3*
Strain, strain background (*Drosophila melanogaster*)	Mi1 >> GCaMP6f, Rdl^1/+ control	Bloomington Drosophila Stock Center	w^+; R19F01-LexA^{attP40} lexAop2-IVS-GCaMP6f-p10$^{su(Hw)attP5}$ / +; Rdl^1 / +	*Figure 4, Figure 4—figure supplement 1*
Strain, strain background (*Drosophila melanogaster*)	Tm3 >> GCaMP6f, +/+ control	Bloomington Drosophila Stock Center	w^+; R13E12-LexA^{attP40}, lexAop2-IVS-GCaMP6f-p10$^{su(Hw)attP5}$ / +; + / +	*Figure 4, Figure 4—figure supplement 1*
Strain, strain background (*Drosophila melanogaster*)	Mi1 >> GCaMP6f, Rdl^1/RdlMD$^{MD\text{-}RR}$ *	Bloomington Drosophila Stock Center	w^+; R19F01-LexA^{attP40}, lexAop2-IVS-GCaMP6f-p10$^{su(Hw)attP5}$ / +; Rdl^1/RdlMD$^{MD\text{-}RR}$	*Figure 4, Figure 4—figure supplement 1*
Strain, strain background (*Drosophila melanogaster*)	Tm3 >> GCaMP6f, Rdl$^{MD\text{-}RR}$/RdlMD$^{MD\text{-}RR}$ *	Bloomington Drosophila Stock Center	w^+; R13E12-LexA^{attP40}, lexAop2-IVS-GCaMP6f-p10$^{su(Hw)attP5}$ / +; Rdl$^{MD\text{-}RR}$/RdlMD$^{MD\text{-}RR}$	*Figure 4, Figure 4—figure supplement 1*
Strain, strain background (*Drosophila melanogaster*)	C2,C3 >> GFP	Bloomington Drosophila Stock Center	w+/UAS-CD8::GFP; R20C11 -p65ADZp^{attP40}/UAS-2xEGFP; R48D11-ZpGdbd^{attP2}/+	*Figure 4—figure supplement 2*
Strain, strain background (*Drosophila melanogaster*)	L1 >> GFP	Bloomington Drosophila Stock Center	w^+/UAS-CD8::GFP; L1[c202]-Gal4/UAS-2xEGFP; + / +	*Figure 4—figure supplement 2*
Antibody	Anti-GABA (rabbit polyclonal)	Sigma-Aldrich	Cat# A2052, RRID:AB_477652	IF (1:200) *Figure 4—figure supplement 2*
Antibody	Alexa Fluor 594-conjugates AffiniPure Goat Anti-Rabbit IgG	Jackson Immuno Research Labs	Cat# 111-585-003, RRID:AB_2338059	IF (1:200) *Figure 6*
Strain, strain background (*Drosophila melanogaster*)	Mi1 >> GCaMP6f, GluClα^{Df}/+ control	Bloomington Drosophila Stock Center	w^+; R19F01-LexA^{attP40}, lexAop2-IVS-GCaMP6f-p10$^{su(Hw)attP5}$ / +; Df(3R)ED6025/ +	*Figure 6, Figure 6—figure supplement 1*

Continued on next page

Continued

Reagent type (species) or resource	Designation	Source or reference	Identifiers	Additional information
Strain, strain background (*Drosophila melanogaster*)	*Tm3 >> GCaMP6f, GluClα^{Df}/+ control*	Bloomington Drosophila Stock Center	*w $^{+}$; R13E12-LexA^{attP40}, lexAop2-IVS-GCaMP6f-p10$^{su(Hw)attP5}$ / +; Df(3R)ED6025/ +*	*Figure 6, Figure 6—figure supplement 1*
Strain, strain background (*Drosophila melanogaster*)	*Mi1 >> GCaMP6f, GluClα^{S278T}/GluClα^{Df}*	This paper	*w $^{+}$; R19F01-LexA^{attP40}, lexAop2-IVS-GCaMP6f-p10$^{su(Hw)attP5}$ / +; Df(3R)ED6025/GluClα^{S278T}*	*Figure 6, Figure 6—figure supplement 1 More information in the Materials and methods section under 'Molecular biology'*
Strain, strain background (*Drosophila melanogaster*)	*Tm3 >> GCaMP6f, GluClα^{S278T}/GluClα^{Df}*	This paper	*w $^{+}$; R13E12-LexA^{attP40}, lexAop2-IVS-GCaMP6f-p10$^{su(Hw)attP5}$ / +; ; Df(3R)ED6025/ GluClα^{S278T}*	*Figure 6, Figure 6—figure supplement 1 More information in the Materials and methods section under 'Molecular biology'*
Strain, strain background (*Drosophila melanogaster*)	*T4/T5 >> GCaMP6f, GluClα^{Df}/+ control*	Bloomington Drosophila Stock Center	*w^{+}; R64G09-LexA^{attP40}, lexAop2-IVS-GCaMP6f-p10$^{su(Hw)attP5}$ / +; ; Df(3R)ED6025 / +*	*Figure 6, Figure 6—figure supplement 1*
Strain, strain background (*Drosophila melanogaster*)	*T4/T5 >> GCaMP6f, GluClα^{S278T}/GluClα^{Df}*	This paper	*w^{+}; R64G09-LexA^{attP40}, lexAop2-IVS-GCaMP6f-p10$^{su(Hw)attP5}$ / +; ; Df(3R)ED6025/ GluClα$^{S278T\ CRISPR}$*	*Figure 6, Figure 6—figure supplement 1 More information in the Materials and methods section under 'Molecular biology'*
Strain, strain background (*Drosophila melanogaster*)	*Mi1 >> Flp,GCaMP6f; GluClα$^{FlpStop.ND}$/GluClα^{Df}*	This paper	*w+; R19F01-p65ADZp^{attP40}/UAS-GCaMP6f, UAS-Flp; R71D01-ZpGdbd^{attP2}, GluClα^{Df}/GluClα$^{FlpStop.ND}$*	*Figure 7 More information in the Materials and methods section under 'Generation of transgenic lines'*
Strain, strain background (*Drosophila melanogaster*)	*Mi1 >> Flp,GCaMP6f; GluClα$^{FlpStop.ND}$ / +(Heterozygous control)*	This paper	*w+; R19F01-p65ADZp^{attP40}/UAS-GCaMP6f, UAS-Flp; R71D01-ZpGdbd^{attP2}/GluClα$^{FlpStop.ND}$*	*Figure 7 More information in the Materials and methods section under 'Generation of transgenic lines'*
Strain, strain background (*Drosophila melanogaster*)	*Mi1 >> GCaMP6f; GluClα$^{FlpStop.ND}$/GluClα^{Df} (No Flp control)*	This paper	*w+; R19F01-p65ADZp^{attP40}/UAS-GCaMP6f; R71D01-ZpGdbd^{attP2}, GluClα^{Df} / ; GluClα$^{FlpStop.ND}$*	*Figure 7 More information in the Materials and methods section under 'Generation of transgenic lines'*
Strain, strain background (*Drosophila melanogaster*)	*Mi1 >> GCaMP6f, GluClα^{dsRNA}*	Bloomington Drosophila Stock Center	*w+; R19F01-p65ADZp^{attP40}/P{y[+t7.7] v[+t1.8]=TRiP.HMC03585}^{attP40}; R71D01-ZpGdbd^{attP2}/UAS-GCaMP6f*	*Figure 7*
Strain, strain background (*Drosophila melanogaster*)	*Tm3 >> GCaMP6f, GluClα^{dsRNA}*	Bloomington Drosophila Stock Center	*w+; R38C11-p65ADZp^{attP40}/P{y[+t7.7] v[+t1.8]=TRiP.HMC03585}^{attP40}; R59C10-ZpGdbd^{attP2}/ UAS-GCaMP6f*	*Figure 7*

Continued on next page

Continued

Reagent type (species) or resource	Designation	Source or reference	Identifiers	Additional information
Strain, strain background (*Drosophila melanogaster*)	*Mi1 >> GCaMP6f, GluClα$^{FlpStop.D}$ / +*	This paper	*w $^+$; R19F01-LexA^{attP40}, lexAop2-IVS-GCaMP6f-p10$^{su(Hw)attP5}$ / +; ; GluClα$^{FlpStop.D}$ / +*	*Figure 7* More information in the Materials and methods section under 'Generation of transgenic lines'
Strain, strain background (*Drosophila melanogaster*)	*Mi1 >> GCaMP6f, GluClα^{Df} / +*	Bloomington Drosophila Stock Center	*w $^+$; R19F01-LexA^{attP40}, lexAop2-IVS-GCaMP6f-p10$^{su(Hw)attP5}$ / +; ; Df(3R)ED6025/GluClα^{WT}*	*Figure 7*
Strain, strain background (*Drosophila melanogaster*)	*Mi1 >> GCaMP6f, GluClα$^{FlpStop.D}$/GluClα^{Df} ** *	This paper	*w $^+$; R19F01-LexA}^{attP40}, lexAop2-IVS-GCaMP6f-p10$^{su(Hw)attP5}$ / +; ; Df(3R)ED6025/GluClα$^{FlpStop.D}$*	*Figure 7* More information in the Materials and methods section under 'Generation of transgenic lines'
Strain, strain background (*Drosophila melanogaster*)	*Tm3 >> GCaMP6f, GluClα$^{FlpStop.D}$ / +*	This paper	*w $^+$; R13E12-LexA^{attP40}, lexAop2-IVS-GCaMP6f-p10$^{su(Hw)attP5}$ / +; GluClα$^{FlpStop.D}$ / +^{T}*	*Figure 7* More information in the Materials and methods section under 'Generation of transgenic lines'
Strain, strain background (*Drosophila melanogaster*)	*Tm3 >> GCaMP6f, GluClα^{Df} / +*	Bloomington Drosophila Stock Center	*w $^+$; R13E12-lexA}^{attP40}, lexAop2-IVS-GCaMP6f-p10$^{su(Hw)attP5}$ / +; ; Df(3R)ED6025/ +*	*Figure 7*
Strain, strain background (*Drosophila melanogaster*)	*Tm3 >> GCaMP6f, GluClα^{Df} ** *	This paper	*w $^+$; R13E12-LexA^{attP40}, lexAop2-IVS-GCaMP6f-p10$^{su(Hw)attP5}$ / +; ; Df(3R)ED6025/GluClα$^{FlpStop.D}$*	*Figure 7* More information in the Materials and methods section under 'Generation of transgenic lines'
Strain, strain background (*Drosophila melanogaster*)	*T4/T5 >> GCaMP6f, GluClα$^{FlpStop.D}$ / +*	This paper	*w$^+$; R64G09-LexA^{attP40}, lexAop2-IVS-GCaMP6f-p10$^{su(Hw)attP5}$ / +; GluClα$^{FlpStop.D}$ / +*	*Figure 8* More information in the Materials and methods section under 'Generation of transgenic lines'
Strain, strain background (*Drosophila melanogaster*)	*T4/T5 >> GCaMP6f, GluClα^{Df} / +*	Bloomington Drosophila Stock Center	*w$^+$; R64G09-LexA^{attP40}, lexAop2-IVS-GCaMP6f-p10$^{su(Hw)attP5}$ / +; ; Df(3R)ED6025/ +*	*Figure 8*
Strain, strain background (*Drosophila melanogaster*)	*T4/T5 >> GCaMP6f, GluClα$^{FlpStop.D}$/GluClα^{Df} ** *	This paper	*w$^+$; R64G09-LexA^{attP40}, lexAop2-IVS-GCaMP6f-p10$^{su(Hw)attP5}$ / +; ; Df(3R)ED6025/GluClα$^{FlpStop.D}$*	*Figure 8* More information in the Materials and methods section under 'Generation of transgenic lines'
Chemical compound, drug	*Picrotoxin*	Sigma Aldrich	P1675_SIGMA	*Figures 2, 4, 5* and *6* *Figure 2—figure supplements 2* and *3, Figure 4—figure supplement 1, Figure 6—figure supplement 1*
Chemical compound, drug	*MPEP*	Abcam	Ab120008	*Figure 2—figure supplement 1*

Continued on next page

Continued

Reagent type (species) or resource	Designation	Source or reference	Identifiers	Additional information
Sequence-based reagent	GluCla_forward	This paper	ACCAAACTGC TGCAAGAC	*qRT-PCR* **Figure 7** *More information in the Materials and methods section under 'Molecular biology'*
Sequence-based reagent	GluCla_reverse	This paper	GATATGTGCTCC AGTAGACC	*qRT-PCR* **Figure 7** *More information in the Materials and methods section under 'Molecular biology'*
Sequence-based reagent	GAPDH2_forward	This paper	GATGAGGAGGT CGTTTCTAC	*qRT-PCR* **Figure 7** *More information in the Materials and methods section under 'Molecular biology'*
Sequence-based reagent	GAPDH2_reverse	This paper	GTACTTGATC AGGTCGATG	*qRT-PCR* **Figure 7** *More information in the Materials and methods section under 'Molecular biology'*
Software, algorithm	MATLAB R2017a	The MathWorks Inc.50 Natick, MA	Custom scripts	*Codes are available in the* **Source code 1**

*We used different allelic combinations for the Rdl^{MDRR} insensitive allele when imaging Mi1 (Rdl^{MD-RR}/Rdl^1) or Tm3 ($Rdl^{MD-RR}/RdlMD^{MD-RR}$). While the use of the Rdl^1 null mutant is genetically cleaner, application of low concentrations of PTX has weaker phenotypes in genetic backgrounds carrying the Rdl^1 allele than in wild type, possibly due to homeostatic mechanisms (**Figure 2A,B**, **Figure 4A**). The 2.5 µM PTX phenotype was even weaker in Tm3, and did not leave a margin to look for rescue by Rdl^{MDRR}, which is why we instead used two copies of the Rdl^{MDRR} allele, which has a PTX phenotype similar to wild type in heterozygosity.

**$GluCla^{FlpStop.D}/Df$ mutant larvae failed to crawl out of the food, but adult flies could be obtained after saving pupae from the food.

Drosophila strains and fly husbandry

Flies were raised at 25°C and 55% humidity on molasses-based food on a 12:12 hr light:dark cycle. Imaging experiments were done at room temperature (20°C). Genotypes of all *Drosophila* strains used for experiments are listed in the Key Resources Table.

Immunohistochemistry and confocal microscopy

Female flies were dissected 3–5 days after eclosion. Brains were removed in dissection solution and fixed in 2% paraformaldehyde in phosphate buffered lysine (PBL) for 50 min at room temperature. Subsequently, the brains were washed 3x for 5 min in phosphate buffered saline containing 0.3% Triton X-100 (PBT) adjusted to pH 7.2. For antibody staining, the samples were blocked in 10% normal goat serum (NGS, Fisher Scientific GmbH, Schwerte, Germany) in PBT for 30 min at room temperature followed by incubation for 24 hr at 4°C in the primary antibody solution (mouse mAb nc82,1:25, DSHB; chicken anti-GFP,1:2000, Abcam ab13970; rabbit anti-GABA, 1:200, Sigma-Aldrich, A2052). Primary antibodies were removed by washing in PBT 3 times for 5 min and the brains were incubated in the secondary antibody (anti-chicken-Alexa488, anti-mouse-Alexa594, anti-rabbit-Alexa594, all 1:200, Dianova) in the dark at 4°C overnight. The samples were further washed with PBT (3 × 5 min) and mounted in Vectashield (Vector Laboratories, Burlingame).

Serial optical sections were taken on a Zeiss LSM710 microscope (Carl Zeiss Microscopy GmbH, Germany) equipped with an oil immersion Plan-Apochromat 40x (NA = 1.3) objective and using the Zen 2 Blue Edition software (Carl Zeiss Microscopy, LLC, United States). Z-stack images were taken at 1 µm intervals and 512 × 512 pixel resolution. Confocal stacks were rendered into two-

dimensional images using Fiji (*Schindelin et al., 2012*). The images were then further processed using Illustrator CS5.1 (Adobe) or Inkscape version 0.92.1 (The Inkscape Team).

Generation of transgenic lines

Transgenic lines carrying the FlpStop cassette (*Fisher et al., 2017*) for conditional gene control were generated according to standard procedures. In brief, embryos carrying the Mi02890 insertion (*y[1] w[*]; Mi{y[+mDint2]=MIC}GluClα^MI02890^/TM3,Sb^1^*) were injected with the FlpStop cassette and PhiC31 integrase. Embryos were dechorionated in 50% bleach (DanKlorix) for 3 min, followed by washing in a buffer (100 mM NaCl, 0.02% Triton X-100) for 3 min. Injections were done on a Nikon AZ100 microscope using a FemtoJet 4i (Eppendorf AG, Hamburg, Germany). The injection mix (20 µl) consisted of 10 µg of the FlpStop construct, 6 µg of helper DNA (pBS130 containing the PhiC31 integrase) and 4 µl of 5x injection buffer (25 mM KCl, 0.5 mM NaH_2PO_4, pH 6.8, 1% phenol red [Sigma Aldrich]). Injection needles were pulled from quartz glass microcapillaries (10 cm length, 1.0 mm outside diameter, 0.5 mm inside diameter, Sutter Instruments, USA) using a P-2000 micropipette puller (Sutter Instruments, USA). Needles were sharpened using a capillary grinder (Bachofer, Germany). After injection, embryos were covered with 10S Voltalef oil and incubated at 18°C until larval hatching. Successful recombinase-mediated cassette exchange was scored by the loss of the yellow marker (y[+]) of the MiMIC cassette and verified by single fly PCR, testing for the loss of the MiMIC cassette and the orientation of the inserted FlpSTOP cassette, as in *Fisher et al. (2017)*.

Molecular biology

GluClα PTX-insensitive allele

To generate a PTX-insensitive GluClα allele, (seamless), CRISPR/Cas9-based genome editing was used to introduce the S278T mutation. Mutagenesis was performed by Well genetics (Taiwan) using the following guide RNA (gRNA): ATCATGGGTATCATTCTGGC[TGG]. In brief, the gRNA was cloned into a U6 promoter plasmid. Cassette-inverted PBacDsRed containing two PBac terminals, 3xP3-DsRed and two homology arms with point mutation S278T was cloned into pUC57-Kan as donor template for repair. GluClα-targeting gRNAs and hs-Cas9 were supplied in DNA plasmids, together with donor plasmid for microinjection into embryos of control strain w1118. F1 flies carrying the selection marker 3xP3-DsRed were validated by genomic PCR and sequencing. Subsequently, the 3x-P3 dsRed selection marker was removed using tub-PBac\T transposase (BDSC# 8285), and successful mutagenesis and 3xP3-dsRed removal was confirmed by PCR and sequencing.

qRT-PCR

For RNA extraction, ten adult fly brains per biological replicate were dissected in PBS. RNA extraction was performed using the RNeasy Mini Kit (Qiagen). The RNA quality was confirmed by the presence of both 18S and 28S ribosomal peaks and the lack of evidence of RNA degradation (RNA integrity number >5) (Fragment Analyser, Agilent). cDNA synthesis was done using SuperScript VILO kit and master mix (Thermo Fisher Scientific). For the qRT-PCR, three biological and three technical replicates were used per genotype. For each sample, 1 µl of cDNA (1:8 dilution) was mixed with 7 µl H_2O, 10 µl SYBR Green MM and 1 µl forward and 1 µl reverse primers for a given gene. Standard curves for every primer pair were taken at least once in each experiment. For run-to-run variations, each 96-well plate contained positive and negative controls in the same chosen dilution as the experimental samples. The qRT-PCR analysis software (Light Cycler 480) determined the Ct values for each technical replicate using the first peak of the second derivative method. The mean of three readings was used to estimate Ct values for each biological replicate. The Delta-Delta Ct method was used to calculate relative transcript levels: % Transcript difference = $2^{([Ct\ ND\ target\ gene\ -\ Ct\ ND\ reference\ gene]\ -\ [Ct\ D\ target\ gene\ -\ Ct\ D\ reference\ gene])}$. For presentation purposes, all observations were normalized to the mean transcript level of the WT genotype. The housekeeping gene *GAPDH2* was used as reference gene for relative mRNA quantification of *GluClα* levels. Primers were designed to amplify a product spanning the two exons flanking the intron containing the FlpStop cassette, *GluClα* exons 18 and 19, resulting in a 137 bp long amplicon. All primers were tested for primer efficiency using serial dilutions of the WT control, and efficiency values are noted next to each primer pair below.

GluCla_forward: ACCAAACTGCTGCAAGAC

GluCla_reverse: GATATGTGCTCCAGTAGACC
(Efficiency: 1.91)
GAPDH2_forward: GATGAGGAGGTCGTTTCTAC
GAPDH2_reverse: GTACTTGATCAGGTCGATG
(Efficiency: 1.96)

RNA-seq

Raw sequencing reads and TPM tables from published datasets were taken from (*Konstantinides et al., 2018*; GSE 103772) and (*Davis et al., 2018*; GSE 116969). To estimate transcript abundance, we used Kallisto (v0.43.1; *Bray et al., 2016*) to pseudo-align reads to dm6 annotation (ENSEMBLE release 91 derived from FlyBase release version 2017_04). The TPM matrix was processed further in R studio (R version 3.4.4). The TPMs were summarized at the level of genes averaged across cell type replicates. Heat maps of the gene expression in selected cell types was generated using MultiExperiment Viewer (MeV) 4.9.0 (*Howe et al., 2011*).

In vivo two-photon imaging

Fly preparation, experimental setup and data acquisition

Female flies aged 2 to 5 days were used for calcium imaging experiments, with the exception of *GluCla* cell-type-specific disruption experiments in which the flies were 8 to 10 days old. Flies were anesthetized on ice and then glued with a UV-sensitive glue (Bondic) onto a custom-made microscope holder containing a hole fitting head and thorax of the fly. To expose the brain, the cuticle on the back of the head was removed using breakable razor blades and fine forceps. During imaging, the flies were perfused with a carboxygenated saline containing 103 mM NaCl, 3 mM KCl, 5 mM TES, 1 mM NaH_2PO_4, 4 mM $MgCl_2$, 1.5 mM $CaCl_2$, 10 mM trehalose, 10 mM glucose, 7 mM sucrose, and 26 mM $NaHCO_3$. The pH of the saline equilibrated near 7.3 when bubbled with 95% O_2/5% CO_2. Imaging experiments were performed on a Bruker Investigator two-photon microscope (Bruker, Madison, WI, USA), equipped with a 25x/1.1 objective (Nikon, Minato, Japan). The excitation laser (Spectraphysics Insight DS+) was set to 920 nm in order to excite GCaMP6f, applying 5–15 mW of power to the sample. Emitted light was sent through an SP680 short pass filter, a 560 lpxr dichroic filter and a 525/70 emission filter. Data was acquired using the PrairieView software at a frame rate of ~10–15 Hz and around 3-5x zoom depending on the cell type.

Pharmacology

All pharmacological agents were stored, handled, and disposed of as indicated in the corresponding SDS and/or information sheets. MPEP was purchased from Abcam (ab120008) and PTX from Sigma Aldrich (R284556). All toxins were first dissolved in water and kept as concentrated stock solutions at −20°C for a maximum of 2 months. For experiments, toxin stock solutions were allowed to equilibrate to room temperature and diluted to the appropriate concentrations in the calcium imaging solution. This solution was then used for a maximum of 3 days, stored at 4°C. All toxins were bath applied. No perfusion was used before or after toxin application. The toxin was allowed to penetrate for 10 min before the start of experiments. The same regions of interest (ROIs) were imaged before and after toxin application to allow paired comparisons for toxin effects.

Visual stimulation

Visual stimuli were generated using custom-written software using C++ and OpenGL, and presented using a LightCrafter 4500 (Texas Instruments, Texas, USA) running at a frame rate of 100 Hz. The imaging and the visual stimulus presentation were synchronized as described in *Freifeld et al. (2013)*. Stimulus light was filtered with a 482/18 bandpass and ND1.0 neutral density filter and projected onto an 8 cm x 8 cm rear projection screen positioned in front of the fly and spanning a visual angle of 60 in azimuth and elevation.

Periodic full-field flashes

Periodic, alternating full-contrast ON and OFF flashes covering the whole screen, each lasting 5 s, were presented to the flies. Each stimulus epoch was presented for ~7 trials.

Moving OFF and ON edges

The stimulus consisted of 100% contrast moving bright or dark edges moving at a velocity of 20°/s in eight directions covering 360°. All stimuli were presented in random order with at least three repetitions per stimulus.

Data analysis

All data processing was performed offline using MATLAB R2017a (The MathWorks Inc, Natick, MA). To correct for motion artifact, individual images were aligned to a reference image composed of a maximum intensity projection of the first 30 frames. The average intensity for manually selected ROIs was computed for each imaging frame and background subtracted to generate a time-trace of the response. ROI identities were kept for matching identical ROIs before and after toxin application for paired analysis. All responses and visual stimuli were interpolated at 10 Hz and trial averaged. Neural responses are shown as relative fluorescence intensity changes over time ($\Delta F/F_0$). The mean and the standard error of the mean (SEM) were calculated across flies after averaging over ROIs for each fly. A two-tailed Student t test for paired or unpaired (independent) samples was used for statistical analysis between two groups. For comparisons between more than two groups in which one independent variable was manipulated (here: PTX concentrations), one-way ANOVA followed by two-tailed t-test with Bonferroni-Holm correction for multiple comparisons was used. For multiple comparisons between groups in which two independent variables were manipulated (here: PTX concentration and genotype), an unbalanced two-way ANOVA followed by Tukey's Honestly Significant Difference Procedure for multiple comparisons was used. For all the data, normality was tested with a Lilliefors test.

Full-field flashes

To calculate $\Delta F/F_0$, the mean of the whole trace was used as F_0. Step responses were calculated as the difference between the mean response 500 ms before the onset of the stimulus and the peak $\Delta F/F_0$ during the stimulus epoch. Plateau responses were calculated as the difference between the mean response 500 ms before the onset of the stimulus and the mean of the last 500 ms of the stimulus epoch. Integrated responses were calculated as the sum of all values during the 5 s of the ON stimulus epoch. For Mi1 and Tm3, only ROI responses that were positively correlated with the stimulus (Pearson's Correlation Coefficient >0) were used for subsequent analysis (see also *Fisher et al., 2015a*). To discard noisy ROIs, a standard deviation threshold of 0.2 was set during the 2 s before the onset of visual stimulation. For pharmacological experiments, an absolute threshold of 0.5 $\Delta F/F_0$ was used to identify well-responding ROIs. The identical ROIs were analyzed after toxin application (paired data). When control and experimental conditions were not paired, no threshold was applied. When experimental (and respective controls) conditions in preliminary data showed a full loss of response, no absolute threshold was applied and the recordings were obtained blinded to the experimenter. For T4/T5 single ROI responses, no correlation filter was applied since both response polarities were expected. For iGluSnFR recordings, only the response threshold was applied.

Moving ON and OFF edges

To calculate $\Delta F/F_0$, the mean of the last second of the intermediate gray epoch was used as F_0. ROI trial average was done per epoch (one specific direction of movement and contrast change). The mean response across ROIs was calculated after aligning traces by their maximum responses. Response amplitudes were calculated as the difference between the mean response 500 ms before the onset of the stimulus and the maximum during the stimulus epoch. The direction selectivity index was calculated as PD-ND/PD, where PD is the maximum response among all responses to the different directions of motion and ND is the response to the null direction of motion defined as 180° from the preferred direction.

Electrophysiological recordings of heterologously expressed GluClα constructs

For electrophysiological recordings, GluClα constructs (isoform O, NP_001287409) were heterologously expressed in *Xenopus laevis* oocytes. Oocytes were harvested from our own colony. Frogs were housed according to the German law of animal protection and the district veterinary office.

eLIFE Research article   Neuroscience

Oocytes were harvested following standard procedures and in agreement with the animal testing approval 84–02.04.2016.A077.

GluClα constructs were cloned in the pGEMHE vector. The vector was linearized with NheI and transcribed using the T7 mMessage mMachine kit (Ambion, Austin, TX). *Xenopus* oocytes were injected with 50 nl RNA (0.01–0.2 μg/μl) and incubated at 14–16°C for 1–2 days in ND96 medium containing (in mM): 96 NaCl, 2 KCl, 1.8 CaCl$_2$, 1 MgCl$_2$, 10 4-(2-hydroxyethyl) piperazine-1-ethane-sulfonic acid (HEPES), 5 Na-pyruvate, and 100 mg/l gentamicin, adjusted to pH 7.5 with NaOH.

Electrophysiological experiments were performed at room temperature (22–25°C). Oocytes were placed in an RC-3Z recording chamber (Warner Instruments, Hamden, CT) under a Discovery V8 stereoscope (Zeiss, Oberkochen, Germany) and continuously perfused with ND96 by a PC-controlled gravity-driven system with a flux rate of 7 ml/min. Electrodes were pulled from 1.5 mm thick borosilicate glass capillaries (Hilgenberg, Malsfeld, Germany) on a DMZ puller (Zeitz Instruments GmbH, Martinsried, Germany) and filled with 3 M KCl. The resulting initial electrode resistance was 0.5–5 MΩ in ND96. Currents were recorded in the two-electrode voltage-clamp mode at a holding potential of −70 mV with a Gene Clamp 500 amplifier (Molecular Devices, San Jose, CA), connected via a USB-6341 acquisition board (National Instruments, Austin, TX) to a PC running WinWCP (Strathclyde, University of Glasgow, UK). L-glutamate was dissolved in ND96 and was repeatedly applied for 20 s, with an interstimulus interval of 1–2 min to ensure full recovery from desensitization. Picrotoxin stock solution was first prepared in dimethyl sulfoxide (DMSO) and then diluted in ND96.

The peak current amplitude of the glutamate-evoked response, in the presence of the antagonist, was normalized to the mean peak current amplitude evoked by glutamate after picrotoxin wash-out. Data are shown as the mean ± SD. N indicates the number of cells. Data was analyzed with Igor Pro (Wavemetrics, Portland, OR). An unpaired *t* test was used for statistical analysis of the residual current between WT and the S278T mutant allele.

Author contributions

Sebastian Molina-Obando, Conceptualization, Data curation, Formal analysis, Investigation, Methodology, Writing—original draft; Juan Felipe Vargas-Fique, Formal analysis, Investigation, Writing—review and editing; Miriam Henning, Burak Gür, Formal analysis, Investigation; T Moritz Schladt, Investigation; Junaid Akhtar, Formal analysis, Writing—review and editing; Thomas K Berger, Conceptualization, Formal analysis, Investigation, Methodology, Writing—original draft; Marion Silies, Conceptualization, Data curation, Supervision, Funding acquisition, Writing—original draft, Project administration

Author ORCIDs
Sebastian Molina-Obando ⓘ http://orcid.org/0000-0003-1222-723X
Burak Gür ⓘ http://orcid.org/0000-0001-8221-9767
Marion Silies ⓘ https://orcid.org/0000-0003-2810-9828

Additional files

Supplementary files
• Source code 1. Data analysis and statistics.
DOI: https://doi.org/10.7554/eLife.49373.029
• Transparent reporting form DOI: https://doi.org/10.7554/eLife.49373.030

Data availability
All data generated or analyzed during this study are included in the manuscript and supporting files.

The following previously published datasets were used:

Author(s)	Year	Dataset title	Dataset URL	Database and Identifier
Konstantinides N, Kapuralin K, Fadil C, Barboza L, Satija R, Desplan C	2018	RNA sequencing of *Drosophila melanogaster* optic lobe cell types.	https://www.ncbi.nlm.nih.gov/geo/query/acc.cgi?acc=GSE103772	NCBI Gene Expression Omnibus, GSE103772
Davis FP, Nern A, Picard S, Reiser MB, Rubin GM, Eddy SR, Henry GL	2019	A genetic, genomic, and computational resource for exploring neural circuit function	https://www.ncbi.nlm.nih.gov/geo/query/acc.cgi?acc=GSE116969	NCBI Gene Expression Omnibus, GSE116969

References

Ammer G, Leonhardt A, Bahl A, Dickson BJ, Borst A. 2015. Functional specialization of neural input elements to the Drosophila ON motion detector. *Current Biology* **25**:2247–2253. DOI: https://doi.org/10.1016/j.cub.2015.07.014, PMID: 26234212

Barbara GS, Zube C, Rybak J, Gauthier M, Grünewald B. 2005. Acetylcholine, GABA and glutamate induce ionic currents in cultured antennal lobe neurons of the honeybee, Apis mellifera. *Journal of Comparative Physiology A* **191**:823–836. DOI: https://doi.org/10.1007/s00359-005-0007-3, PMID: 16044331

Behnia R, Clark DA, Carter AG, Clandinin TR, Desplan C. 2014. Processing properties of ON and OFF pathways for Drosophila motion detection. *Nature* **512**:427–430. DOI: https://doi.org/10.1038/nature13427, PMID: 25043016

Bennett MV. 1971. Electrolocation in fish. *Annals of the New York Academy of Sciences* **188**:242–269. DOI: https://doi.org/10.1111/j.1749-6632.1971.tb13102.x, PMID: 4331616

Betz H. 1990. Ligand-gated ion channels in the brain: the amino acid receptor superfamily. *Neuron* **5**:383–392. DOI: https://doi.org/10.1016/0896-6273(90)90077-S, PMID: 1698394

Bray NL, Pimentel H, Melsted P, Pachter L. 2016. Near-optimal probabilistic RNA-seq quantification. *Nature Biotechnology* **34**:525–527. DOI: https://doi.org/10.1038/nbt.3519, PMID: 27043002

Chalasani SH, Chronis N, Tsunozaki M, Gray JM, Ramot D, Goodman MB, Bargmann CI. 2007. Dissecting a circuit for olfactory behaviour in Caenorhabditis elegans. *Nature* **450**:63–70 . DOI: https://doi.org/10.1038/nature06292, PMID: 17972877

Chandrashekar J, Hoon MA, Ryba NJ, Zuker CS. 2006. The receptors and cells for mammalian taste. *Nature* **444**:288–294. DOI: https://doi.org/10.1038/nature05401, PMID: 17108952

Clark DA, Bursztyn L, Horowitz MA, Schnitzer MJ, Clandinin TR. 2011. Defining the computational structure of the motion detector in Drosophila. *Neuron* **70**:1165–1177. DOI: https://doi.org/10.1016/j.neuron.2011.05.023, PMID: 21689602

Collins B, Kane EA, Reeves DC, Akabas MH, Blau J. 2012. Balance of activity between LN(v)s and glutamatergic dorsal clock neurons promotes robust circadian rhythms in Drosophila. *Neuron* **74**:706–718. DOI: https://doi.org/10.1016/j.neuron.2012.02.034, PMID: 22632728

Cully DF, Vassilatis DK, Liu KK, Paress PS, Van der Ploeg LH, Schaeffer JM, Arena JP. 1994. Cloning of an avermectin-sensitive glutamate-gated chloride channel from Caenorhabditis elegans. *Nature* **371**:707–711. DOI: https://doi.org/10.1038/371707a0, PMID: 7935817

Cully DF, Paress PS, Liu KK, Schaeffer JM, Arena JP. 1996. Identification of a *Drosophila melanogaster* glutamate-gated chloride channel sensitive to the antiparasitic agent avermectin. *Journal of Biological Chemistry* **271**:20187–20191. DOI: https://doi.org/10.1074/jbc.271.33.20187, PMID: 8702744

Davis FP, Nern A, Picard S, Reiser MB, Rubin GM, Eddy SR, Henry GL. 2018. A genetic, genomic, and computational resource for exploring neural circuit function. *bioRxiv*. DOI: https://doi.org/10.1101/385476

Eguchi Y, Ihara M, Ochi E, Shibata Y, Matsuda K, Fushiki S, Sugama H, Hamasaki Y, Niwa H, Wada M, Ozoe F, Ozoe Y. 2006. Functional characterization of musca glutamate- and GABA-gated chloride channels expressed independently and coexpressed in xenopus oocytes. *Insect Molecular Biology* **15**:773–783. DOI: https://doi.org/10.1111/j.1365-2583.2006.00680.x, PMID: 17201770

Eichler K, Li F, Litwin-Kumar A, Park Y, Andrade I, Schneider-Mizell CM, Saumweber T, Huser A, Eschbach C, Gerber B, Fetter RD, Truman JW, Priebe CE, Abbott LF, Thum AS, Zlatic M, Cardona A. 2017. The complete connectome of a learning and memory centre in an insect brain. *Nature* **548**:175–182. DOI: https://doi.org/10.1038/nature23455, PMID: 28796202

Etter A, Cully DF, Liu KK, Reiss B, Vassilatis DK, Schaeffer JM, Arena JP. 1999. Picrotoxin blockade of invertebrate glutamate-gated chloride channels: subunit dependence and evidence for binding within the pore. *Journal of Neurochemistry* **72**:318–326. DOI: https://doi.org/10.1111/jnc.1999.72.1.318, PMID: 9886084

Ffrench-Constant RH, Rocheleau TA, Steichen JC, Chalmers AE. 1993. A point mutation in a Drosophila GABA receptor confers insecticide resistance. *Nature* **363**:449–451. DOI: https://doi.org/10.1038/363449a0, PMID: 8389005

Fisher YE, Leong JC, Sporar K, Ketkar MD, Gohl DM, Clandinin TR, Silies M. 2015a. A class of visual neurons with wide-field properties is required for local motion detection. *Current Biology* **25**:3178–3189. DOI: https://doi.org/10.1016/j.cub.2015.11.018, PMID: 26670999

Fisher YE, Silies M, Clandinin TR. 2015b. Orientation selectivity sharpens motion detection in Drosophila. *Neuron* **88**:390–402. DOI: https://doi.org/10.1016/j.neuron.2015.09.033, PMID: 26456048

Fisher YE, Yang HH, Isaacman-Beck J, Xie M, Gohl DM, Clandinin TR. 2017. FlpStop, a tool for conditional gene control in *Drosophila*. *eLife* **6**:e22279. DOI: https://doi.org/10.7554/eLife.22279, PMID: 28211790

Franke K, Berens P, Schubert T, Bethge M, Euler T, Baden T. 2017. Inhibition decorrelates visual feature representations in the inner retina. *Nature* **542**:439–444. DOI: https://doi.org/10.1038/nature21394, PMID: 28178238

Freifeld L, Clark DA, Schnitzer MJ, Horowitz MA, Clandinin TR. 2013. GABAergic lateral interactions tune the early stages of visual processing in Drosophila. *Neuron* **78**:1075–1089. DOI: https://doi.org/10.1016/j.neuron.2013.04.024, PMID: 23791198

Gallio M, Ofstad TA, Macpherson LJ, Wang JW, Zuker CS. 2011. The coding of temperature in the Drosophila brain. *Cell* **144**:614–624. DOI: https://doi.org/10.1016/j.cell.2011.01.028, PMID: 21335241

Gjorgjieva J, Sompolinsky H, Meister M. 2014. Benefits of pathway splitting in sensory coding. *Journal of Neuroscience* **34**:12127–12144. DOI: https://doi.org/10.1523/JNEUROSCI.1032-14.2014, PMID: 25186757

Gollisch T, Meister M. 2010. Eye smarter than scientists believed: neural computations in circuits of the retina. *Neuron* **65**:150–164. DOI: https://doi.org/10.1016/j.neuron.2009.12.009, PMID: 20152123

Gruntman E, Romani S, Reiser MB. 2018. Simple integration of fast excitation and offset, delayed inhibition computes directional selectivity in Drosophila. *Nature Neuroscience* **21**:250–257. DOI: https://doi.org/10.1038/s41593-017-0046-4, PMID: 29311742

Haag J, Arenz A, Serbe E, Gabbiani F, Borst A. 2016. Complementary mechanisms create direction selectivity in the fly. *eLife* **5**:e17421. DOI: https://doi.org/10.7554/eLife.17421, PMID: 27502554

Hardie RC, Raghu P. 2001. Visual transduction in Drosophila. *Nature* **413**:186–193. DOI: https://doi.org/10.1038/35093002, PMID: 11557987

Hibbs RE, Gouaux E. 2011. Principles of activation and permeation in an anion-selective Cys-loop receptor. *Nature* **474**:54–60. DOI: https://doi.org/10.1038/nature10139, PMID: 21572436

Hirata K, Ishida C, Eguchi Y, Sakai K, Ozoe F, Ozoe Y, Matsuda K. 2008. Role of a serine residue (S278) in the pore-facing region of the housefly L-glutamate-gated chloride channel in determining sensitivity to noncompetitive antagonists. *Insect Molecular Biology* **17**:341–350. DOI: https://doi.org/10.1111/j.1365-2583.2008.00806.x, PMID: 18651916

Horoszok L, Raymond V, Sattelle DB, Wolstenholme AJ. 2001. GLC-3: a novel fipronil and BIDN-sensitive, but picrotoxin-insensitive, L-glutamate-gated chloride channel subunit from *Caenorhabditis elegans*. *British Journal of Pharmacology* **132**:1247–1254. DOI: https://doi.org/10.1038/sj.bjp.0703937, PMID: 11250875

Howe EA, Sinha R, Schlauch D, Quackenbush J. 2011. RNA-Seq analysis in MeV. *Bioinformatics* **27**:3209–3210. DOI: https://doi.org/10.1093/bioinformatics/btr490, PMID: 21976420

Joesch M, Schnell B, Raghu SV, Reiff DF, Borst A. 2010. ON and OFF pathways in Drosophila motion vision. *Nature* **468**:300–304. DOI: https://doi.org/10.1038/nature09545, PMID: 21068841

Katz B, Minke B. 2009. Drosophila photoreceptors and signaling mechanisms. *Frontiers in Cellular Neuroscience* **3**. DOI: https://doi.org/10.3389/neuro.03.002.2009, PMID: 19623243

Kelley LA, Mezulis S, Yates CM, Wass MN, Sternberg MJ. 2015. The Phyre2 web portal for protein modeling, prediction and analysis. *Nature Protocols* **10**:845–858. DOI: https://doi.org/10.1038/nprot.2015.053, PMID: 25950237

Koike C, Numata T, Ueda H, Mori Y, Furukawa T. 2010. TRPM1: a vertebrate TRP channel responsible for retinal ON bipolar function. *Cell Calcium* **48**:95–101. DOI: https://doi.org/10.1016/j.ceca.2010.08.004, PMID: 2084671 9

Kolodziejczyk A, Sun X, Meinertzhagen IA, Nässel DR. 2008. Glutamate, GABA and acetylcholine signaling components in the Lamina of the Drosophila visual system. *PLOS ONE* **3**:e2110. DOI: https://doi.org/10.1371/journal.pone.0002110, PMID: 18464935

Konstantinides N, Degabriel S, Desplan C. 2018. Neuro-evo-devo in the single cell sequencing era. *Current Opinion in Systems Biology* **11**:32–40. DOI: https://doi.org/10.1016/j.coisb.2018.08.001, PMID: 30886939

Laughlin SB. 1989. The role of sensory adaptation in the retina. *The Journal of Experimental Biology* **146**:39–62. PMID: 2689569

Leong JC, Esch JJ, Poole B, Ganguli S, Clandinin TR. 2016. Direction selectivity in Drosophila emerges from Preferred-Direction enhancement and Null-Direction suppression. *Journal of Neuroscience* **36**:8078–8092. DOI: https://doi.org/10.1523/JNEUROSCI.1272-16.2016, PMID: 27488629

Liu WW, Wilson RI. 2013. Glutamate is an inhibitory neurotransmitter in the Drosophila olfactory system. *PNAS* **110**:10294–10299. DOI: https://doi.org/10.1073/pnas.1220560110, PMID: 23729809

Livingstone M, Hubel D. 1988. Segregation of form, color, movement, and depth: anatomy, physiology, and perception. *Science* **240**:740–749. DOI: https://doi.org/10.1126/science.3283936, PMID: 3283936

Ludmerer SW, Warren VA, Williams BS, Zheng Y, Hunt DC, Ayer MB, Wallace MA, Chaudhary AG, Egan MA, Meinke PT, Dean DC, Garcia ML, Cully DF, Smith MM. 2002. Ivermectin and nodulisporic acid receptors in *Drosophila* Melanogaster contain both gamma-aminobutyric acid-gated rdl and glutamate-gated GluCl alpha chloride channel subunits. *Biochemistry* **41**:6548–6560. DOI: https://doi.org/10.1021/bi015920o, PMID: 1200 9920

Lynagh T, Beech RN, Lalande MJ, Keller K, Cromer BA, Wolstenholme AJ, Laube B. 2015. Molecular basis for convergent evolution of glutamate recognition by pentameric ligand-gated ion channels. *Scientific Reports* **5**. DOI: https://doi.org/10.1038/srep08558, PMID: 25708000

Maisak MS, Haag J, Ammer G, Serbe E, Meier M, Leonhardt A, Schilling T, Bahl A, Rubin GM, Nern A, Dickson BJ, Reiff DF, Hopp E, Borst A. 2013. A directional tuning map of Drosophila elementary motion detectors. *Nature* **500**:212–216. DOI: https://doi.org/10.1038/nature12320, PMID: 23925246

Marvin JS, Borghuis BG, Tian L, Cichon J, Harnett MT, Akerboom J, Gordus A, Renninger SL, Chen TW, Bargmann CI, Orger MB, Schreiter ER, Demb JB, Gan WB, Hires SA, Looger LL. 2013. An optimized fluorescent probe for visualizing glutamate neurotransmission. *Nature Methods* **10**:162–170. DOI: https://doi.org/10.1038/nmeth.2333, PMID: 23314171

Masu M, Iwakabe H, Tagawa Y, Miyoshi T, Yamashita M, Fukuda Y, Sasaki H, Hiroi K, Nakamura Y, Shigemoto R, Takada M, Nakamura K, Nakao K, Katsuki M, Nakanishi S. 1995. Specific deficit of the ON response in visual transmission by targeted disruption of the mGluR6 gene. *Cell* **80**:757–765. DOI: https://doi.org/10.1016/0092-8674(95)90354-2, PMID: 7889569

Mauss AS, Pankova K, Arenz A, Nern A, Rubin GM, Borst A. 2015. Neural circuit to integrate opposing motions in the visual field. *Cell* **162**:351–362. DOI: https://doi.org/10.1016/j.cell.2015.06.035, PMID: 26186189

McCavera S, Rogers AT, Yates DM, Woods DJ, Wolstenholme AJ. 2009. An ivermectin-sensitive glutamate-gated chloride channel from the parasitic nematode *Haemonchus contortus*. *Molecular Pharmacology* **75**:1347–1355. DOI: https://doi.org/10.1124/mol.108.053363, PMID: 19336526

Meier M, Borst A. 2019. Extreme compartmentalization in a Drosophila amacrine cell. *Current Biology* **29**:1545–1550. DOI: https://doi.org/10.1016/j.cub.2019.03.070, PMID: 31031119

Nei M, Niimura Y, Nozawa M. 2008. The evolution of animal chemosensory receptor gene repertoires: roles of chance and necessity. *Nature Reviews Genetics* **9**:951–963. DOI: https://doi.org/10.1038/nrg2480, PMID: 1 9002141

Parmentier ML, Pin JP, Bockaert J, Grau Y. 1996. Cloning and functional expression of a *Drosophila* metabotropic glutamate receptor expressed in the embryonic CNS. *The Journal of Neuroscience* **16**:6687–6694. DOI: https://doi.org/10.1523/JNEUROSCI.16-21-06687.1996, PMID: 8824309

Pettersen EF, Goddard TD, Huang CC, Couch GS, Greenblatt DM, Meng EC, Ferrin TE. 2004. UCSF Chimera?A visualization system for exploratory research and analysis. *Journal of Computational Chemistry* **25**:1605–1612. DOI: https://doi.org/10.1002/jcc.20084, PMID: 15264254

Raghu SV, Borst A. 2011. Candidate glutamatergic neurons in the visual system of Drosophila. *PLOS ONE* **6**: e19472. DOI: https://doi.org/10.1371/journal.pone.0019472, PMID: 21573163

Richter FG, Fendl S, Haag J, Drews MS, Borst A. 2018. Glutamate signaling in the fly visual system. *iScience* **7**: 85–95. DOI: https://doi.org/10.1016/j.isci.2018.08.019, PMID: 30267688

Rister J, Pauls D, Schnell B, Ting CY, Lee CH, Sinakevitch I, Morante J, Strausfeld NJ, Ito K, Heisenberg M. 2007. Dissection of the peripheral motion channel in the visual system of Drosophila melanogaster. *Neuron* **56**:155–170. DOI: https://doi.org/10.1016/j.neuron.2007.09.014, PMID: 17920022

Salazar-Gatzimas E, Chen J, Creamer MS, Mano O, Mandel HB, Matulis CA, Pottackal J, Clark DA. 2016. Direct measurement of correlation responses in Drosophila elementary motion detectors reveals fast timescale tuning. *Neuron* **92**:227–239. DOI: https://doi.org/10.1016/j.neuron.2016.09.017, PMID: 27710784

Sato K, Pellegrino M, Nakagawa T, Nakagawa T, Vosshall LB, Touhara K. 2008. Insect olfactory receptors are heteromeric ligand-gated ion channels. *Nature* **452**:1002–1006. DOI: https://doi.org/10.1038/nature06850, PMID: 18408712

Schindelin J, Arganda-Carreras I, Frise E, Kaynig V, Longair M, Pietzsch T, Preibisch S, Rueden C, Saalfeld S, Schmid B, Tinevez J-Y, White DJ, Hartenstein V, Eliceiri K, Tomancak P, Cardona A. 2012. Fiji: an open-source

platform for biological-image analysis. *Nature Methods* **9**:676–682 . DOI: https://doi.org/10.1038/nmeth.2019, PMID: 22743772

Scholl B, Gao X, Wehr M. 2010. Nonoverlapping sets of synapses drive on responses and off responses in auditory cortex. *Neuron* **65**:412–421. DOI: https://doi.org/10.1016/j.neuron.2010.01.020, PMID: 20159453

Serbe E, Meier M, Leonhardt A, Borst A. 2016. Comprehensive characterization of the major presynaptic elements to the Drosophila OFF motion detector. *Neuron* **89**:829–841. DOI: https://doi.org/10.1016/j.neuron.2016.01.006, PMID: 26853306

Shiells R. 1994. Retinal synapses. Glutamate receptors for signal amplification. *Current Biology* **4**:917–918. DOI: https://doi.org/10.1016/S0960-9822(00)00204-9, PMID: 7850428

Shinomiya K, Karuppudurai T, Lin TY, Lu Z, Lee CH, Meinertzhagen IA. 2014. Candidate neural substrates for off-edge motion detection in Drosophila. *Current Biology* **24**:1062–1070. DOI: https://doi.org/10.1016/j.cub.2014.03.051, PMID: 24768048

Silbering AF, Benton R. 2010. Ionotropic and metabotropic mechanisms in chemoreception: 'chance or design'? *EMBO Reports* **11**:173–179. DOI: https://doi.org/10.1038/embor.2010.8, PMID: 20111052

Silies M, Gohl DM, Fisher YE, Freifeld L, Clark DA, Clandinin TR. 2013. Modular use of peripheral input channels tunes motion-detecting circuitry. *Neuron* **79**:111–127. DOI: https://doi.org/10.1016/j.neuron.2013.04.029, PMID: 23849199

Silies M, Gohl DM, Clandinin TR. 2014. Motion-detecting circuits in flies: coming into view. *Annual Review of Neuroscience* **37**:307–327. DOI: https://doi.org/10.1146/annurev-neuro-071013-013931, PMID: 25032498

Strother JA, Nern A, Reiser MB. 2014. Direct observation of ON and OFF pathways in the Drosophila visual system. *Current Biology* **24**:976–983. DOI: https://doi.org/10.1016/j.cub.2014.03.017, PMID: 24704075

Strother JA, Wu ST, Wong AM, Nern A, Rogers EM, Le JQ, Rubin GM, Reiser MB. 2017. The emergence of directional selectivity in the visual motion pathway of Drosophila. *Neuron* **94**:168–182. DOI: https://doi.org/10.1016/j.neuron.2017.03.010, PMID: 28384470

Strother JA, Wu ST, Rogers EM, Eliason JLM, Wong AM, Nern A, Reiser MB. 2018. Behavioral state modulates the ON visual motion pathway of *Drosophila*. *PNAS* **115**:E102–E111. DOI: https://doi.org/10.1073/pnas.1703090115, PMID: 29255026

Takemura SY, Karuppudurai T, Ting CY, Lu Z, Lee CH, Meinertzhagen IA. 2011. Cholinergic circuits integrate neighboring visual signals in a Drosophila motion detection pathway. *Current Biology* **21**:2077–2084. DOI: https://doi.org/10.1016/j.cub.2011.10.053, PMID: 22137471

Takemura SY, Bharioke A, Lu Z, Nern A, Vitaladevuni S, Rivlin PK, Katz WT, Olbris DJ, Plaza SM, Winston P, Zhao T, Horne JA, Fetter RD, Takemura S, Blazek K, Chang LA, Ogundeyi O, Saunders MA, Shapiro V, Sigmund C, et al. 2013. A visual motion detection circuit suggested by Drosophila connectomics. *Nature* **500**:175–181. DOI: https://doi.org/10.1038/nature12450, PMID: 23925240

Takemura SY, Nern A, Chklovskii DB, Scheffer LK, Rubin GM, Meinertzhagen IA. 2017. The comprehensive connectome of a neural substrate for 'ON' motion detection in Drosophila. *eLife* **6**:e24394. DOI: https://doi.org/10.7554/eLife.24394, PMID: 28432786

Takeuchi A, Takeuchi N. 1969. A study of the action of picrotoxin on the inhibitory neuromuscular junction of the crayfish. *The Journal of Physiology* **205**:377–391. DOI: https://doi.org/10.1113/jphysiol.1969.sp008972, PMID: 5357245

Tichy H, Hellwig M. 2018. Independent processing of increments and decrements in odorant concentration by ON and OFF olfactory receptor neurons. *Journal of Comparative Physiology A* **204**:873–891. DOI: https://doi.org/10.1007/s00359-018-1289-6, PMID: 30251036

Tritsch NX, Oh W-J, Gu C, Sabatini BL. 2014. Midbrain dopamine neurons sustain inhibitory transmission using plasma membrane uptake of GABA, not synthesis. *eLife* **3**: e01936. DOI: https://doi.org/10.7554/eLife.01936

Tuthill JC, Nern A, Holtz SL, Rubin GM, Reiser MB. 2013. Contributions of the 12 neuron classes in the fly Lamina to motion vision. *Neuron* **79**:128–140. DOI: https://doi.org/10.1016/j.neuron.2013.05.024, PMID: 23849200

Uusitalo RO, Juusola M, Weckström M. 1995. Graded responses and spiking properties of identified first-order visual interneurons of the fly compound eye. *Journal of Neurophysiology* **73**:1782–1792. DOI: https://doi.org/10.1152/jn.1995.73.5.1782, PMID: 7623079

Vardi N. 1998. Alpha subunit of go localizes in the dendritic tips of ON bipolar cells. *The Journal of Comparative Neurology* **395**:43–52. DOI: https://doi.org/10.1002/(SICI)1096-9861(19980525)395:1<43::AID-CNE4>3.0.CO;2-H, PMID: 9590545

Werblin FS, Dowling JE. 1969. Organization of the retina of the mudpuppy, Necturus maculosus. II. intracellular recording. *Journal of Neurophysiology* **32**:339–355. DOI: https://doi.org/10.1152/jn.1969.32.3.339, PMID: 4306897

Wilson RI, Laurent G. 2005. Role of GABAergic inhibition in shaping odor-evoked spatiotemporal patterns in the Drosophila antennal lobe. *Journal of Neuroscience* **25**:9069–9079. DOI: https://doi.org/10.1523/JNEUROSCI.2070-05.2005, PMID: 16207866

Yang HH, St-Pierre F, Sun X, Ding X, Lin MZ, Clandinin TR. 2016. Subcellular imaging of voltage and calcium signals reveals neural processing in Vivo. *Cell* **166**:245–257. DOI: https://doi.org/10.1016/j.cell.2016.05.031, PMID: 27264607

Yang HH, Clandinin TR. 2018. Elementary motion detection in *Drosophila*: algorithms and mechanisms. *Annual Review of Vision Science* **4**:143–163. DOI: https://doi.org/10.1146/annurev-vision-091517-034153, PMID: 29949723

Zheng Y, Hirschberg B, Yuan J, Wang AP, Hunt DC, Ludmerer SW, Schmatz DM, Cully DF. 2002. Identification of two novel *Drosophila* Melanogaster histamine-gated chloride channel subunits expressed in the eye. *Journal of Biological Chemistry* **277**:2000–2005. DOI: https://doi.org/10.1074/jbc.M107635200, PMID: 11714703

Zheng Z, Lauritzen JS, Perlman E, Robinson CG, Nichols M, Milkie D, Torrens O, Price J, Fisher CB, Sharifi N, Calle-Schuler SA, Kmecova L, Ali IJ, Karsh B, Trautman ET, Bogovic JA, Hanslovsky P, Jefferis G, Kazhdan M, Khairy K, et al. 2018. A complete electron microscopy volume of the brain of adult Drosophila Melanogaster. *Cell* **174**:730–743. DOI: https://doi.org/10.1016/j.cell.2018.06.019, PMID: 30033368

eLIFE
elifesciences.org

Figures and figure supplements

ON selectivity in the *Drosophila* visual system is a multisynaptic process involving both glutamatergic and GABAergic inhibition
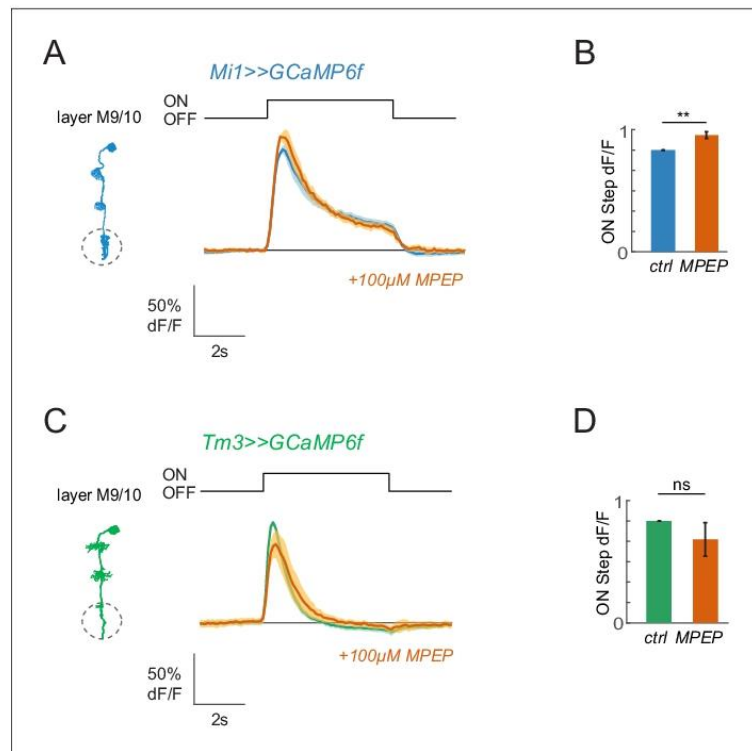
Sebastian Molina-Obando *et al*

Figure 2—figure supplement 1. Blocking metabotropic glutamate receptors does not abolish ON responses. (**A, C**) GCaMP6f signals in response to 5 s full-field flashes in layer M9/10 before (blue for Mi1, green for Tm3) and after (orange) application of 100 μM MPEP. The same cells were imaged before and after drug application. Sample sizes were n = 5 (58)±MPEP for Mi1, and n = 5 (40)±MPEP for Tm3. (**B,D**) Bar plots showing the quantification of the ON step. *p<0.05, **p<0.01, ***p<0.001, tested with paired Student *t* test. All traces and bar plots show mean ± SEM. Sample sizes are given as n = number of flies (number of cells).
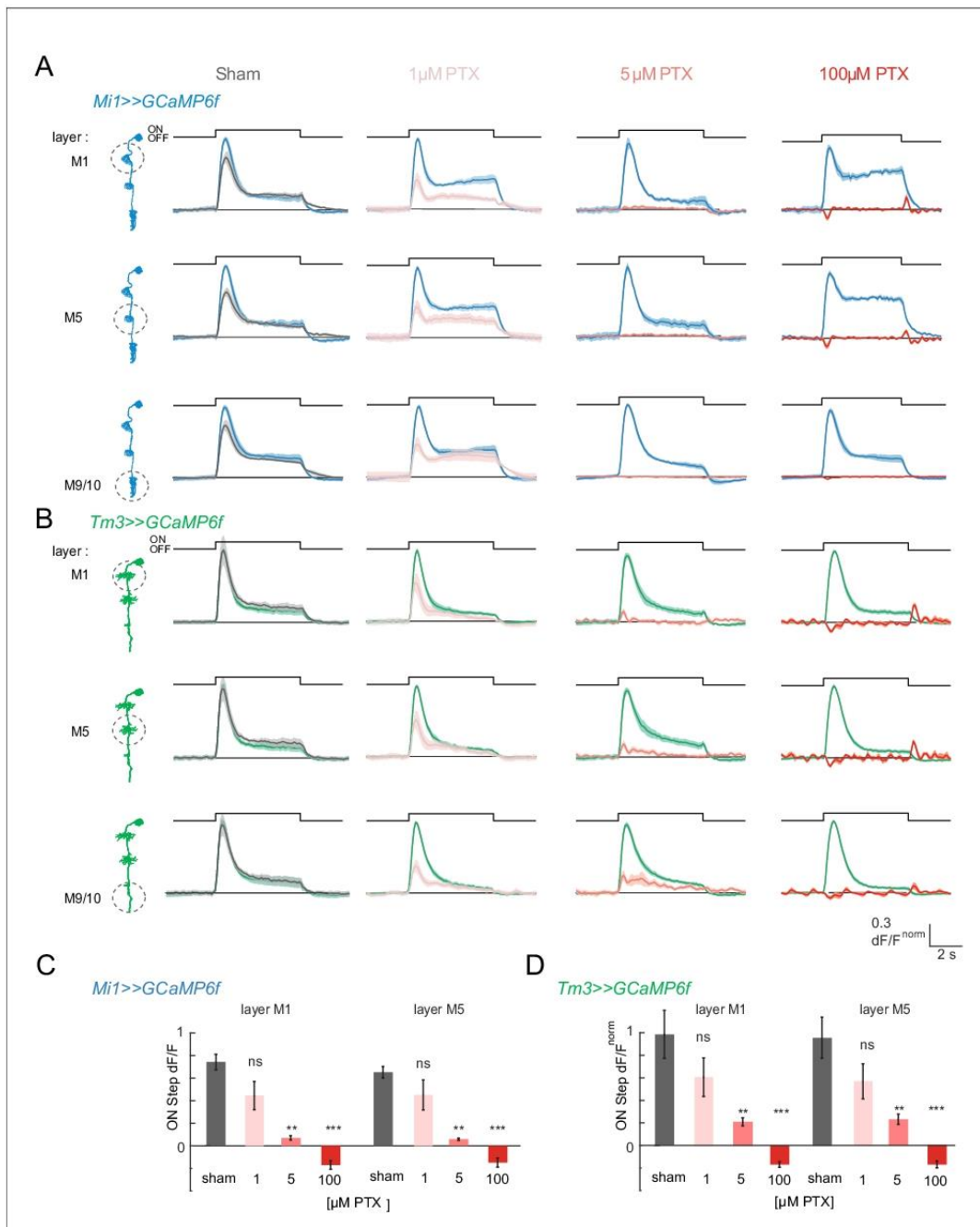DOI: https://doi.org/10.7554/eLife.49373.005

Figure 2—figure supplement 2. ON responses are abolished by PTX concentrations affecting GABA$_A$Rs and GluCls. (**A,B**) In vivo GCaMP6f signals recorded in layers M1, M5 and M9/10 of Mi1 (**A**) and Tm3 (**B**) neurons, before (blue, green) and after (gray, red) application of 0 (sham), 1, 5 or 100 µM *Figure 2—figure supplement 2 continued on next page*

eLIFE Research article

Figure 2—figure supplement 2 continued

PTX. (**C,D**) Bar plot showing the quantification of the ON step in (**A,B**). Sample sizes: sham, n = 5 (89); 1 µM, n = 5 (68); 5 µM, n = 5 (64); 100 µM, n = 5 (89). All traces show mean ± SEM. All sample sizes are given as number of flies (number of cells). *: $p<0.05$, **: $p<0.01$, ***: $p<0.001$, tested with a one-way ANOVA and a post-hoc unpaired t-test with Bonferroni-Holm correction for multiple comparisons.
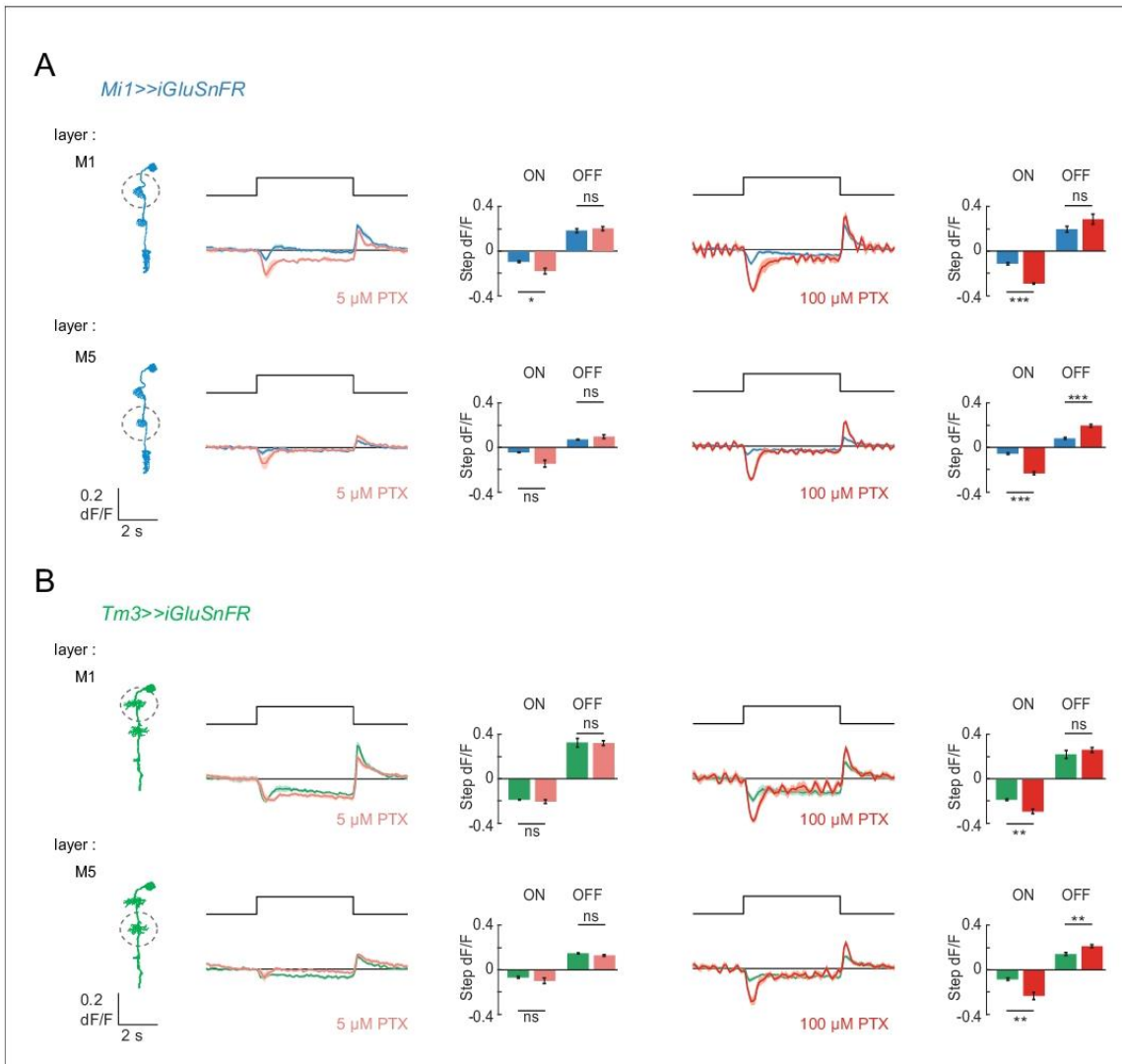
Figure 2—figure supplement 3. The glutamatergic input onto Mi1 and Tm3 dendrites is still present upon PTX application. (**A,B**) In vivo iGluSnFR signals recorded in layers M1 and M5 of Mi1 (**A**) or Tm3 (**B**) neurons, before (blue) and after application of either 5 or 100 µM PTX (light red/red). Bar plots showing the quantification of the ON and OFF response. **p<0.01, ***p<0.001, tested with paired Student *t* test. Sample sizes were N = 5 (64/67) for Mi1 in 5 µM PTX, N = 6 (72/72) for Mi1 in 100 µM PTX, N = 5 (62/60) for Tm3 in 5 µM PTX, and N = 5 (60/63) for Tm3 in 100 µM PTX, given as N = number of flies (number of cells in M1/M5). All traces show mean ± SEM.
DOI: https://doi.org/10.7554/eLife.49373.009
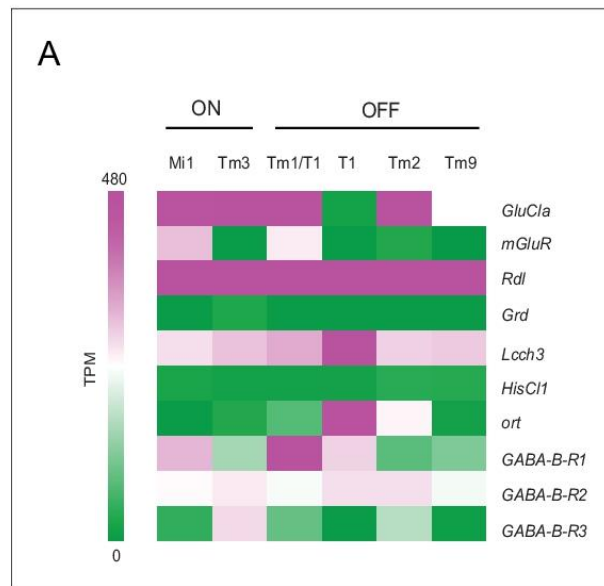
Figure 3—figure supplement 1. *GluClα* and *Rdl* are broadly expressed in the visual system. (**A**) Expression levels shown as TPM (transcripts per kilobase million) values of candidate glutamate, GABA and histamine receptors. RNAseq data are from *Konstantinides et al. (2018)* (GEO accession number: GSE103772). Expression in all available medulla interneurons in the data set of the major ON and OFF pathways components is depicted.

DOI: https://doi.org/10.7554/eLife.49373.013
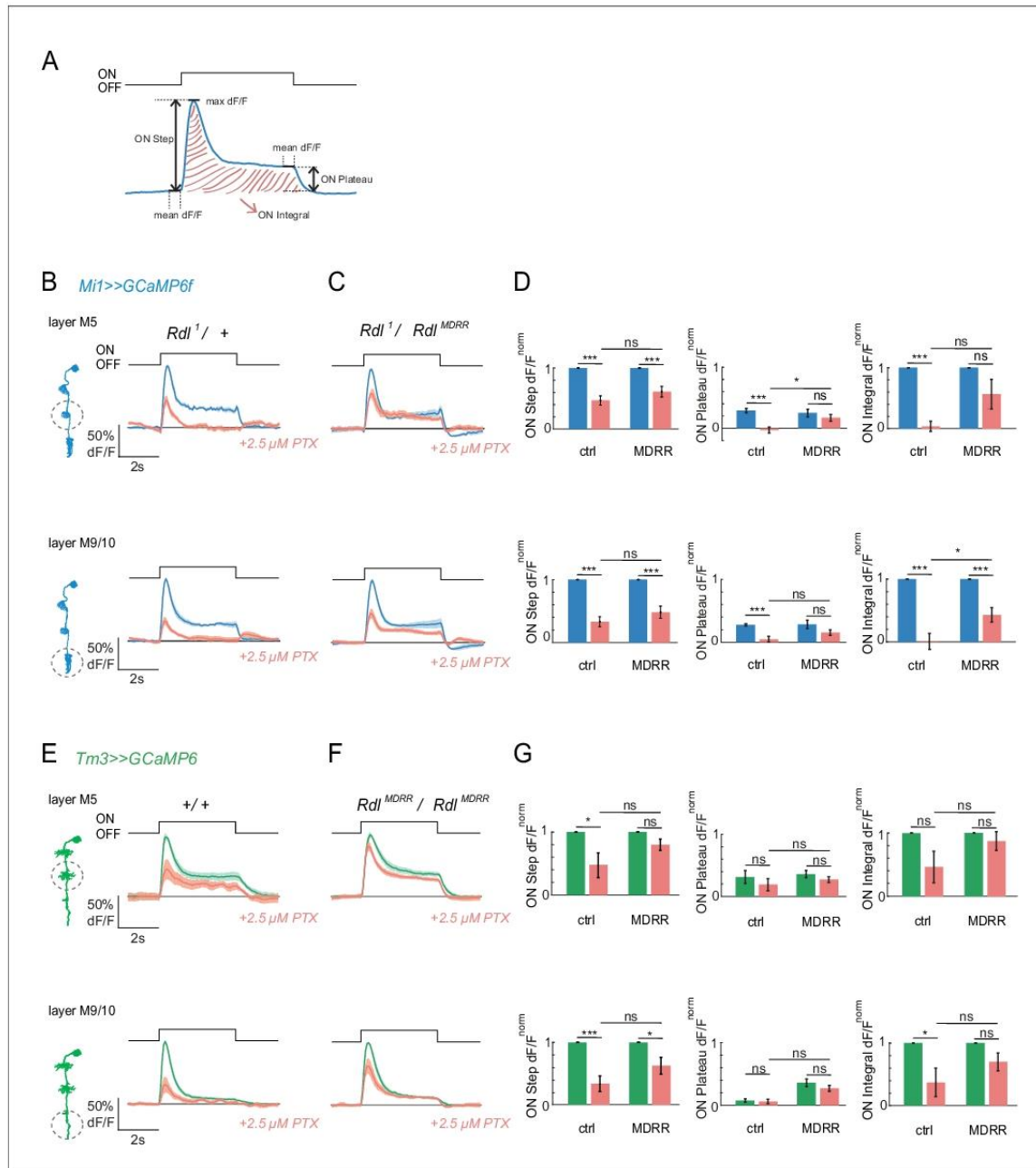
Figure 4—figure supplement 1. Pharmacogenetics shows that ON responses are partially mediated by the GABA_AR Rdl. (**A**) Schematics showing the quantification of the step response, the plateau response and the integrated response. (**B,C**) In vivo calcium signals in response to full-field stimulation recorded in layers M5 and M9/10 of Mi1 neurons. Figure shows traces before (blue) and after (red) application of 2.5 μM PTX in heterozygous Rdl^1/+

Figure 4—figure supplement 1 continued on next page

Figure 4—figure supplement 1 continued

controls (A, n = 7[55]/[78]), or flies only expressing the PTX-insensitive Rdl^{MDRR} allele (Rdl^1/Rdl^{MDRR}) (B, n = 8[76]/[90]). (**D**) Bar plots showing the quantification of the data from (**A**, **B**). (**E,F**) In vivo calcium signals in response to full-field flashes recorded in the layers M5 and M9/10 of Tm3 neurons. Figure shows traces before (green) and after (red) PTX application in wild type (+/+) (D, n = 5[36]/[47]), or flies only expressing the PTX-insensitive Rdl^{MDRR} allele (Rdl^{MDRR}/Rdl^{MDRR}) (E, n = 5[57]/[57]). (**G**) Bar plots showing the quantification of data from (**D,E**). All traces show mean ± SEM. Sample sizes are given as number of flies [number of cells in M5/M9/10], *p<0.05, ***p<0.001, tested with an unbalanced two-way ANOVA, corrected for multiple comparisons.
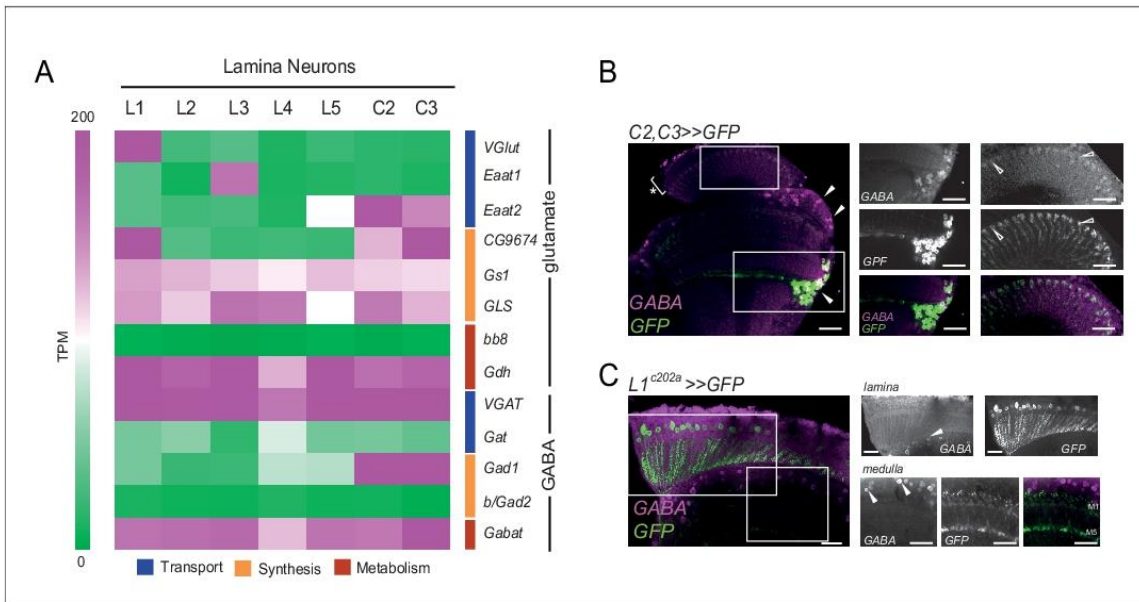
Figure 4—figure supplement 2. L1 neurons are not GABAergic. (**A**) Expression levels shown as TPM values of genes related to the synthesis, transport and release of the neurotransmitters glutamate and GABA. RNAseq data are from ***Davis et al. (2018)*** (GEO accession number: GSE 116969). Expression in the lamina neurons L1, L2, L3, L4, L5, C2 and C3. (**B,C**) Confocal images of the fly visual system of a fly expressing C2/C3 >> GFP (**B**) or L1 >>GFP (**C**) and marked with anti-GFP (green/gray) and anti-GABA (magenta/gray). C2/C3 are known GABAergic cell types and serve as positive controls. (**B**) The GABA staining shows GABA-positive signal in medulla cell bodies and C2/C3 cell bodies (filled arrowheads), as well as in C2/C3 axon terminals in the lamina (open arrowheads), but not in the lamina cortex (asterisk). (**C**) L1 cell bodies and medulla layers M1 and M5 housing the L1 axon terminals do not show specific anti-GABA signal whereas some medulla neuron cell bodies are GABA-positive (filled arrowheads). White boxes mark approximate location of the individual images to the left. Note that the medulla image in (**C**) is from a different brain. Scale bars are 20 µm.
DOI: https://doi.org/10.7554/eLife.49373.017

Figure 6—figure supplement 1. Pharmacogenetics shows that ON responses are mediated by *GluClα*. (A,B) In vivo calcium signals in response to full-field flashes recorded in layers M5 and M9/1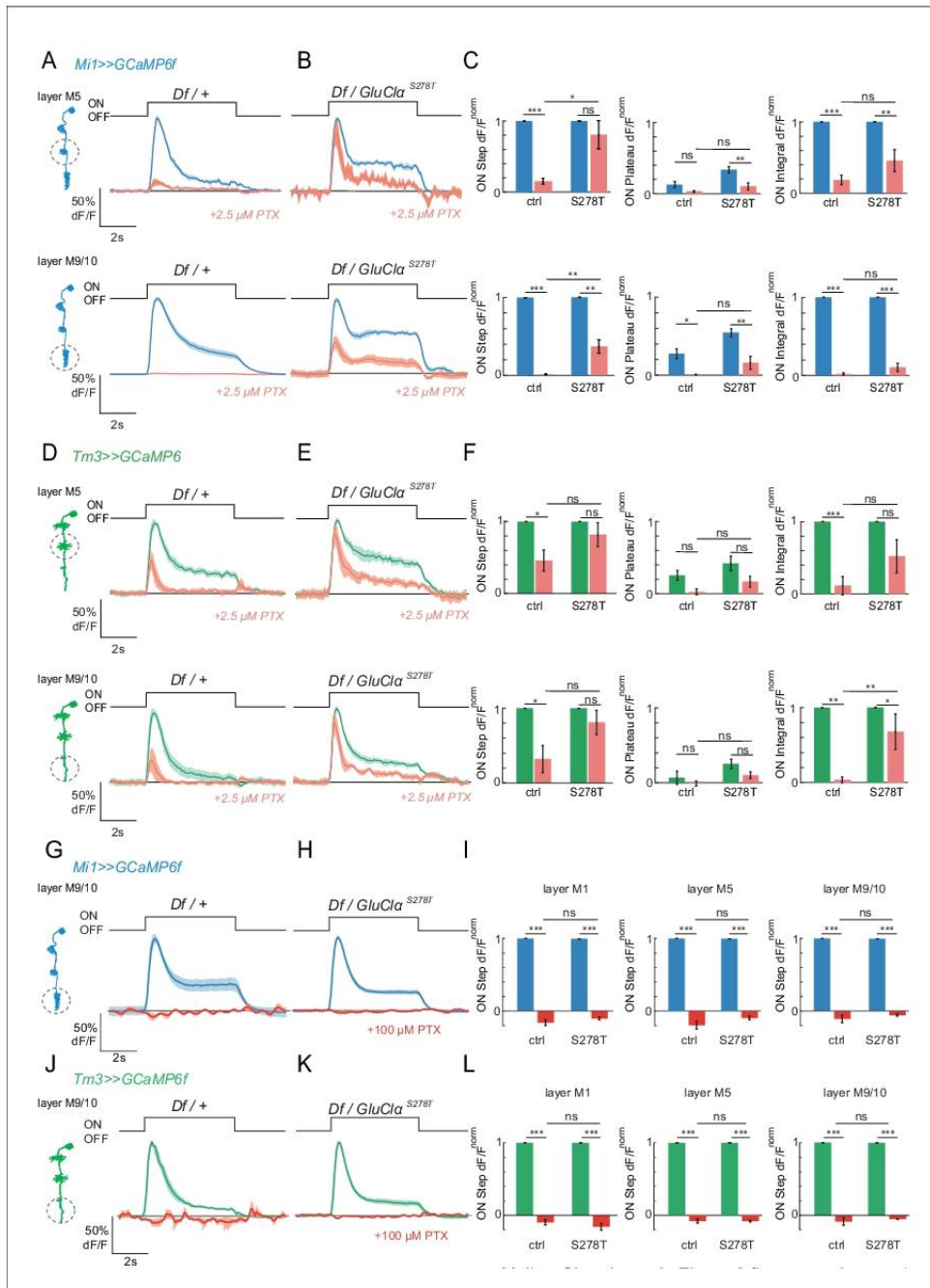0 of Mi1 neurons. Figure shows traces before (blue) and after (red) application of 2.5 µM PTX in *Figure 6—figure supplement 1 continued on next page*

Figure 6—figure supplement 1 continued

heterozygous *GluClα^{Df}/+* controls (A, n = 5[44]/[63]), or flies only expressing the PTX-insensitive *GluClα^{S278T}* allele (*GluClα^{S278T}/GluClα^{Df}*) (B, n = 5 [49]/[47]). Sample sizes are given as number of flies (number of cells in M5/M9/10). (**C**) Bar plots showing the quantification of the data shown in (**A,B**). (**D,E**) In vivo calcium signals in response to full field stimulation recorded in layers M5 and M9/10 of Tm3 neurons. Shown are traces before (green) and after (red) PTX application in heterozygous *GluClα^{Df}/+* controls (D, n = 5 [33]/[30]), or flies only expressing the PTX-insensitive *GluClα^{S278T}/GluClα^{Df}*) (E, n = 5 [37]/[40]). Sample sizes are given as number of flies [number of cells in M5/M9/10]. (**F**) Bar plots showing the quantification of the normalized data from (**D,E**). (**G,H,J,K**) In vivo calcium signals in response to full-field flashes recorded in layer M9/10 of Mi1 (**G,H**) or Tm3 (**J,K**) neurons. Figure shows traces before (blue/green) and after (red) application of 100 µm PTX in heterozygous *GluClα^{Df}/+* controls (G, n = 5[54]; J, n = 4[73]), or flies only expressing the PTX-insensitive *GluClα^{S278T}* allele (*GluClα^{S278T}/GluClα^{Df}*) (H, n = 6[78]; K, n = 5[57]). (**I,L**) Bar plots showing the quantification for Mi1 (**I**) and Tm3 (**L**). Sample sizes are shown as number of flies [number of cells]. All traces show mean ± SEM. *p<0.05, **p<0.01, ***p<0.001, tested with an unbalanced two-way ANOVA, corrected for multiple comparisons in (**C,F,I,L**).

DOI: https://doi.org/10.7554/eLife.49373.022

3. First-order visual interneurons distribute distinct contrast and luminance information across ON and OFF pathways to achieve stable behavior

Manuscript under review

Authors and affiliations

Madhura Ketkar*[1,2], Burak Gür*[1,2], **Sebastian Molina-Obando***[1,2], Carlotta Martelli[1] and Marion Silies[1]

* these authors contributed equally to this work

[1] Institute of Developmental Biology and Neurobiology, Johannes-Gutenberg University Mainz, 55128 Mainz, Germany.

[2] Göttingen Graduate School for Neurosciences, Biophysics, and Molecular Biosciences (GGNB) and International Max Planck Research School (IMPRS) for Neurosciences at the University of Göttingen, 37077 Göttingen, Germany

Abstract

The accurate processing of contrast is the basis for all visually guided behaviors. Visual scenes with rapidly changing illumination challenge contrast computation, because adaptation is not fast enough to compensate for such changes. Yet, human perception of contrast is stable even when the visual environment is quickly changing. The fruit fly Drosophila also shows nearly luminance invariant behavior for both ON and OFF stimuli. To achieve this, first-order interneurons L1, L2 and L3 all encode contrast and luminance differently, and distribute information across both ON and OFF contrast-selective pathways. Behavioral responses to both ON and OFF stimuli rely on a luminance-based correction provided by L1 and L3, wherein L1 supports contrast computation linearly, and L3 non-linearly amplifies dim stimuli. Therefore, L1, L2 and L3 are not distinct inputs to ON and OFF pathways but the lamina serves as a separate processing layer that distributes distinct luminance and contrast information across ON and OFF pathways to support behavioral performance in varying conditions.

Introduction

Across species, contrast information forms the basis of visual computations. For our perception to be stable, our eyes must compute contrast relative to the mean illumination of a scene. In natural environments, illumination changes by several orders of magnitude not only from dawn to dusk, but also at much faster timescales as our eyes saccade across a scene or we quickly move from sun to shade (Frazor and Geisler, 2006; Mante et al., 2005; Rieke and Rudd, 2009).Thus, the computation of contrast needs to be invariant to rapid changes in luminance, such that visual perception of a given contrast remains constant. This is accomplished by human perception, and neuronal responses in the cat lateral geniculate nucleus (LGN) display contrast constancy at rapid time scales (Burkhardt et al., 1984; Mante et al., 2005). However, contrast encoding in photoreceptors is not luminance invariant when the stimulus changes more rapidly than photoreceptor adaptation (Laughlin and Hardie, 1978; Normann and Werblin, 1974).

The visual OFF pathway in fruit flies, sensitive to contrast decrements, also displays contrast-constant behavior (Ketkar et al., 2020) , allowing to investigate the underlying mechanisms. In the OFF pathway, luminance information itself is maintained postsynaptic to photoreceptors, and is crucial for the accurate estimation of contrast, resulting in contrast-constant behavior. Luminance serves as a corrective signal that scales contrast computation when background luminance quickly changes (Ketkar et al., 2020). The requirement of such a corrective signal can be theoretically expected regardless of ON and OFF contrast polarities, since the adaptational constraints in dynamic environments challenge both contrast polarities. However, the ON and OFF pathways are not mere sign-inverted versions of each other since they face different environmental challenges (Clark et al., 2014; Ruderman, 1994) and have evolved several structural and physiological asymmetries (Chichilnisky and Kalmar, 2002; Jin et al., 2011; Leonhardt et al., 2016; Ratliff et al., 2010). It is thus not clear if this luminance invariance is a general feature of all visual pathways, and how luminance and contrast information are distributed across visual pathways to establish contrast constancy is not known.

Drosophila melanogaster offers a promising model system to study the pathway-specific function of luminance since the ON and OFF motion pathways have been well characterized on the cellular, circuit and behavioral levels (Behnia et al., 2014; Yang and Clandinin, 2018). In the fly visual system, neurons were assigned to distinct ON or OFF pathways based on physiological properties (Molina-Obando et al., 2019; Serbe et al., 2016; Shinomiya et al., 2019; Silies et al., 2013; Strother et al., 2017), anatomical connectivity (Shinomiya et al.,

2014; Takemura et al., 2015, 2013, 2017), and behavioral function (Clark et al., 2011; Silies et al., 2013). ON and OFF contrast selectivity first arises two synapses downstream of photoreceptors, in medulla neurons (Fischbach and Dittrich, 1989; Serbe et al., 2016; Silies et al., 2013; Strother et al., 2017; Yang et al., 2016). They receive photoreceptor information through the lamina neurons L1-L3, which project to specific medulla layers (Meinertzhagen and O'Neil, 1991; Strother et al., 2014). Although L1-L3 all show the same response polarity and hyperpolarize to light onset and depolarize to light offset, L1 projects to layers where it mostly connects to ON-selective medulla neurons. Similarly, L2 and L3 project to layers where OFF-selective medulla neurons get most of their inputs (Shinomiya et al., 2014; Takemura et al., 2015, 2013). L1 is thus thought to be the sole major input of the ON pathway, whereas L2 and L3 are considered the two major inputs of the OFF pathway (Figure 1A) (Clark et al., 2011; Joesch et al., 2008; Shinomiya et al., 2019). Among these, L2 is contrast-sensitive, but cannot support contrast constancy alone if photoreceptor adaptation is insufficient. Instead, contrast constancy in OFF-motion guided behavior is ensured by a corrective signal from luminance-sensitive L3 neurons (Ketkar et al., 2020). It is not known whether ON-motion driven behavior also requires luminance information and whether L1 can provide it along with its contrast signal (Figure 1B).

Contrast and luminance are both encoded by the transient and sustained response components in both vertebrates and invertebrate photoreceptors (Laughlin and Hardie, 1978; Normann and Perlman, 1979; Normann and Werblin, 1974; Shapley and Enroth-Cugell, 1984), which are captured differentially by their downstream neurons. In the vertebrate retina, many different types of first order interneurons, bipolar cells, exist. Although they are generally thought to capture the contrast component of the photoreceptors response, luminance information has been shown be preserved in post-photoreceptor visual circuitry post of the retina (Awatramani and Slaughter, 2000; Ichinose and Hellmer, 2016; Ichinose and Lukasiewicz, 2007; Odermatt et al., 2012; Oesch and Diamond, 2011). As suggested by their sustained response component, different degrees of luminance-sensitivity exists across bipolar cell types (Baden et al., 2016; Euler et al., 2014). Furthermore, ON and OFF contrast selectivity emerges at the bipolar cell layer, where ON selectivity emerges through glutamatergic inhibition (Masu et al., 1995). These ON and OFF bipolar cells also split anatomically, as they innervate different layers (Euler et al., 2014).

Together, many parallels exist between the Drosophila visual system and the vertebrate retina, including the response properties of photoreceptors, the layered organization and the existence of ON and OFF pathways (Clark and Demb, 2016; Mauss et al., 2017). However, in contrast to the vertebrate retina, fewer first order interneuron types distribute

contrast and luminance information, and contrast selectivity itself clearly only occurs one synapse further downstream, where neurons postsynaptic to lamina neurons are either ON or OFF selective. Comparing the vertebrate retina with the insect visual system, it is unclear how just three first order interneurons distribute their different physiological properties across visual pathways.

Here, we show that luminance and contrast information is distributed to and is of behavioral relevance for both ON and OFF pathways. In vivo calcium imaging experiments reveal that each first order interneuron is unique in its contrast and luminance encoding properties. Whereas L2 is purely contrast sensitive, L1 encodes both contrast and luminance in distinct response components. L1 linearly scales with luminance, whereas the luminance-sensitive L3 non-linearly amplifies dim light. Behavioral experiments further show that these differential luminance- and contrast- encoding properties translate into distinct behavioral roles. In the ON pathway, L1 and L3 both provide luminance information for higher luminance invariance than possible by the contrast input alone. Furthermore, L2, known as the OFF-pathway contrast input, provides contrast information to the ON pathway, in addition to L1. Surprisingly, both L1 and L3 neurons are necessary and sufficient for OFF behavior. These findings indicate that L1 L2, and L3 do not constitute ON- or OFF-specific inputs. Instead, the three first-order interneurons encode luminance and contrast differentially and contribute to computations in both ON and OFF pathways. Together, our data reveal how luminance and contrast information are distributed to both ON and OFF pathways to approach luminance invariance, a core computation of visual systems.

Results
L1 responses to contrast do not explain ON behavior

Luminance-invariant behavioral responses have been observed in multiple species (Burkhardt et al., 1984; Silies et al., 2014), highlighting their ethological relevance. In *Drosophila*, luminance-invariant behavior has been shown in response to OFF stimuli, where a dedicated luminance-sensitive pathway scales contrast-sensitive inputs to achieve luminance invariance in behavior (Ketkar et al., 2020). The ON pathway is thought to have just one prominent input, L1. We thus asked if luminance invariance is achieved in the ON pathway and if the contrast-sensitive input L1 can explain such invariance. For this purpose, we compared turning behavior of walking flies with the responses of L1. Behavioral responses were measured in a fly-on-a-ball assay. Flies were shown moving ON edges of different luminance but the same 100% Michelson contrast. Fly turning responses were

highly similar across luminances, with low-luminance edges eliciting slightly larger turning responses than brighter edges (Figure 1C).

We wondered if the sole ON pathway input L1 can directly drive this behavior. To test this, we examined the contrast responses of L1 to moving ON edges with comparable parameters and overlapping luminance values as those used in the behavioral assay (Figure 1D). We recorded L1 *in vivo* calcium responses to visual stimuli from its axon terminals expressing GCaMP6f using two-photon microscopy. As described previously, L1 responded negatively to contrast increments, in line with the inverted response polarity of lamina neurons (Figure 1D) (Clark et al., 2011; Laughlin and Hardie, 1978; Yang et al., 2016). The absolute response amplitude of the L1 calcium signals scaled with luminance and did not co-vary with the behavioral response (Figure 1E). We performed linear regression across calcium signals at different luminances and quantified the slope to extract the luminance dependency of the responses. L1 signals and behavioral responses had opposite luminance dependencies (Figure 1E). Thus, the observed behavior, approaching luminance invariance, cannot be explained solely by contrast inputs from L1, suggesting that the ON pathway additionally gets luminance-sensitive input.
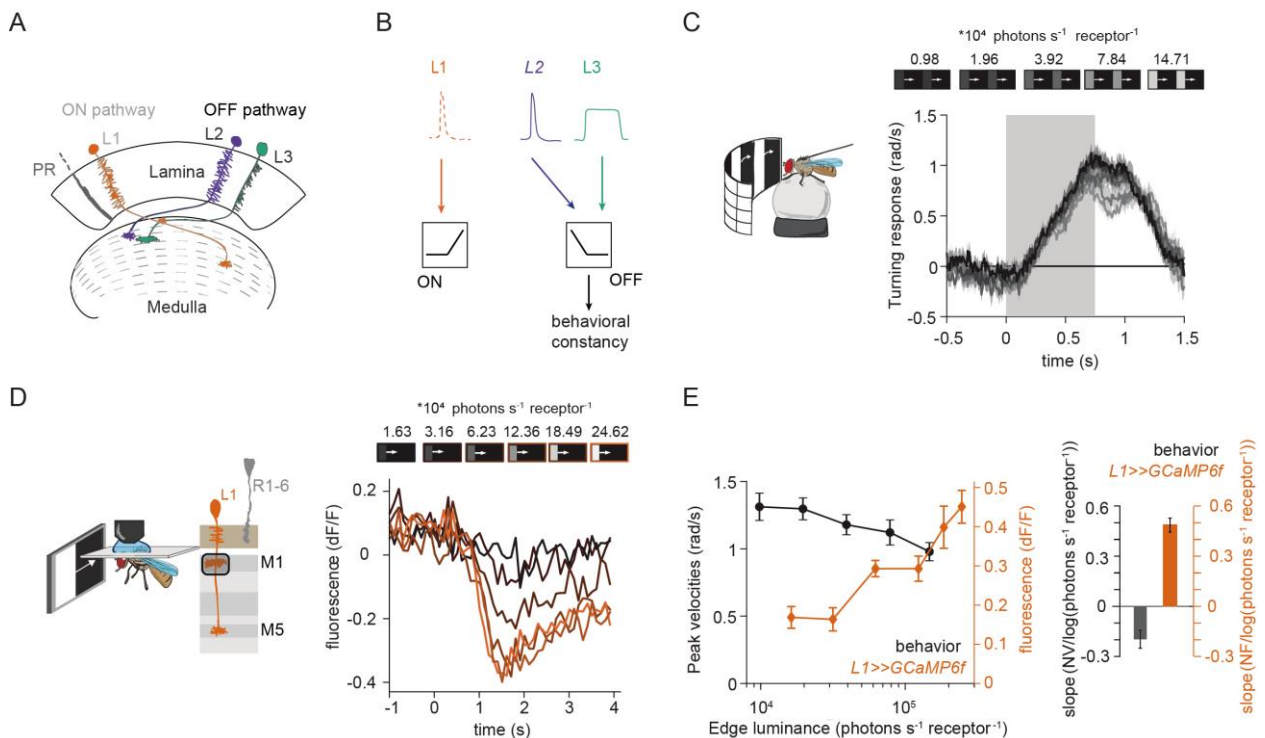
Figure 1: L1 responses to contrast do not explain ON behavior across luminance. (A) Schematic of lamina neurons projecting from the lamina to the medulla. L1 is considered the main input to the ON pathway, whereas L2 and L3 are thought to provide input to the OFF pathway. **(B)** Transient L2 and sustained L3 neurons provide contrast and luminance information, respectively, to the OFF pathway to guide contrast-constant behavior (Ketkar et al., 2020). L1 is thought to have physiological properties very similar to L2 (Clark et al., 2011) and provides contrast information to the ON selective pathway. **(C)** Turning response to multiple moving ON edges, displayed on an LED arena that surrounds a fly walking on an air-cushioned ball. The edge luminance takes

five different values, and the background is dark (~0 luminance), all resulting in 100% contrast. Turning responses are color-coded according to the edge luminance. The gray box indicates motion duration. n = 10 flies. **(D)** *In vivo* calcium signals of L1 axon terminal in medulla layer M1 in response to moving ON edges of six different luminances. Calcium responses of single L1 axon terminal are shown. **(E)** Left: Absolute step responses of L1 are plotted together with peak turning velocities calculated from (C). Behavioral and calcium traces are aligned by maximum response. Right, slope quantification of luminance dependency for normalized behavior and L1 fluorescence signals. NV = normalized peak velocity, NF = normalized fluorescent signal. Traces and plots in C and E show mean ± SEM.

L1 neuronal responses carry a luminance-sensitive component

To explore the sources of luminance information in first-order interneurons, we measured calcium signals in L1, L2 and L3. Flies were shown a staircase stimulus with luminance going sequentially up and down. L1 and L2 showed positive and negative transient responses when luminance stepped down and up, respectively (Figure 2A), consistent with their contrast sensitivity (Clark et al., 2011; Silies et al., 2013). L2 did not show any sustained component. L3 showed sustained responses to OFF steps and was non-linearly tuned to stimulus luminance, responding strongly to the darkest stimulus. Intriguingly, L1 showed a transient component followed by a sustained component, suggesting that it encodes luminance in addition to contrast (Figure 2A). The sustained components of L1 response were negatively correlated with luminance, such that the baseline calcium signal at each step sequentially increased with decreasing stimulus luminance. Thus, in addition to L3, L1 also maintains luminance information postsynaptically to photoreceptors.
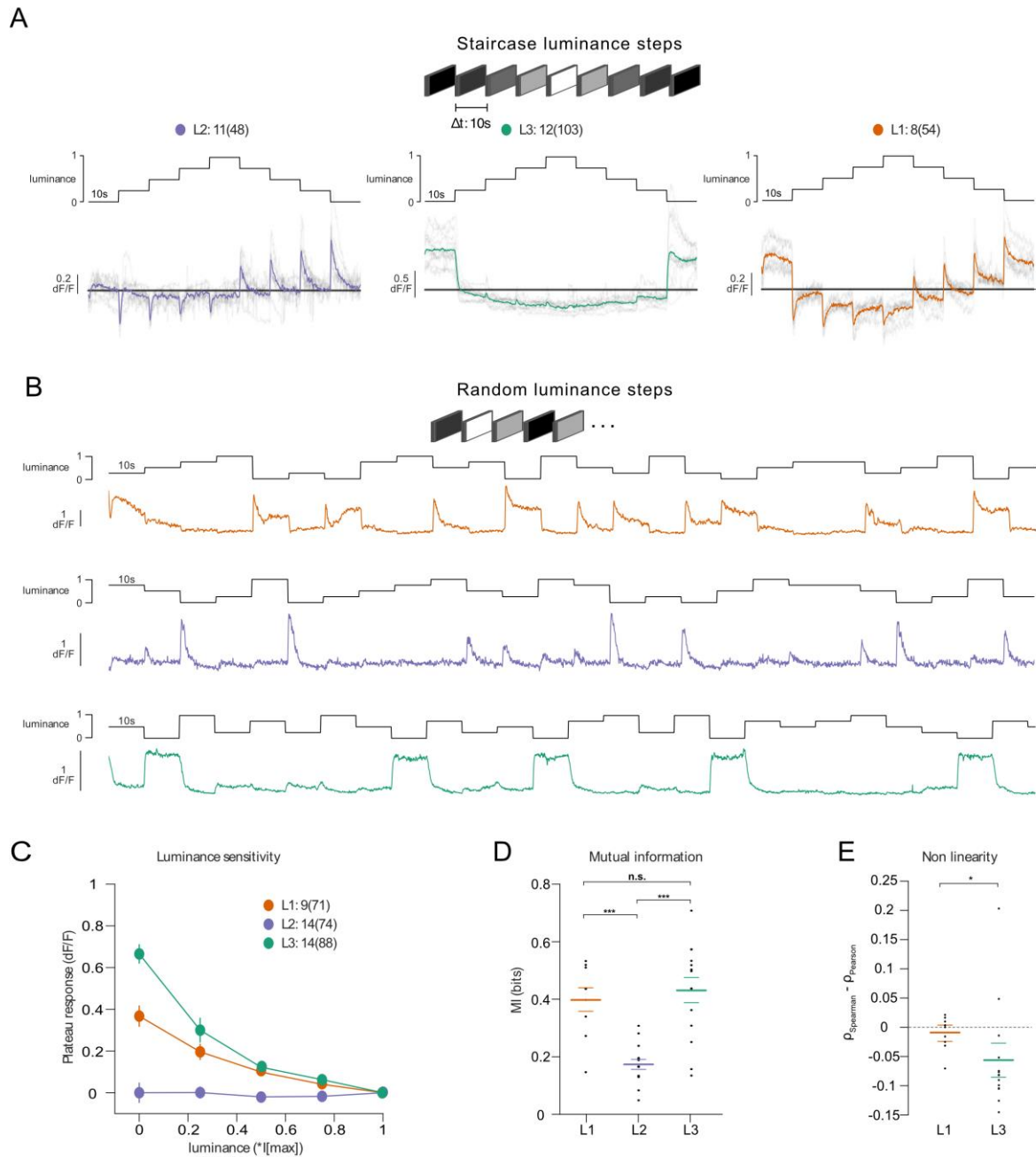
Figure 2: Lamina neuron types L1-L3 are differently sensitive to contrast and luminance. (A) Schematic of the 'staircase' stimulus. Luminance sequentially steps up through five values and then sequentially steps down. Shown below are the plateau calcium responses of L1 (orange), L2 (purple) and L3 (green) axon terminals, plotted against luminance. Colored traces shown the mean response, grey traces show individual fly means. **(B)** Example calcium traces of single L1, L2 and L3 axon terminals to a stimulus comprising 10 s full-field flashes varying randomly between five different luminances. **(C)** Plateau responses of the three neuron types, quantified from the responses to the stimulus in (B). **(D)** Mutual information between luminance and calcium signal, ***$p < 0.001$, one-way ANOVA followed by multiple comparison test corrected with Bonferroni. **(E)** Non-linearity quantification of luminance-dependent signals of L1 and L3 in (C), *$p < 0.05$, tested by a wilcoxon rank sum test.

To explicitly compare luminance information across the three input neurons, we measured responses to randomized luminance and calculated the mutual information between

stimulus and the sustained response component (Figure 2B-D). As for the staircase stimulus, L2 transient responses returned to baseline within the 10s of the stimulus presentation, whereas both L1 and L3 displayed sustained components that varied with luminance (Figure 2B,C). Sustained response components in L1 and L3 carried similar mutual information with luminance, and both were higher than L2 (Figure 2D). Interestingly, the luminance-sensitive response components of L1 and L3 scaled differently with luminance. We quantified non-linearity using the difference of Pearson's linear and Spearman's correlation between response and luminance. This value will approach zero if the relationship is linear and increase or decrease if non-linear, depending on the sign of correlation between luminance and response. L1 responses were more linear with respect to luminance than L3 responses, which selectively amplified low luminance (Figure 2E). Thus, the two luminance-sensitive neurons carry different types of luminance information.

L1 is not required but sufficient for ON behavior across luminances

Since the canonical ON pathway input L1 is also found to carry luminance information, we hypothesized that it plays a role in mediating the observed behavior. To test this, we silenced L1 outputs while measuring ON behavior using Shibire[ts] (Kitamoto, 2001). Silencing L1 severely reduced turning responses when different ON contrasts were interleaved, consistent with previous behavioral studies that identified L1 as the major input to the ON pathway (Clark et al., 2011; Silies et al., 2013) (Supp. Figure 1A-D). However, L1 silencing had little effect on responses to 100% contrast at varying luminance, suggesting the existence of other ON pathway inputs (Figure 3A,B). To explicitly test if and how L1 silencing changed the luminance dependence of behavioral responses, we quantified the slope of peak turning velocities across different background luminances (Figure 3C). The slopes were slightly negative for both the control and L1-silenced conditions, and did not differ significantly between conditions, suggesting another luminance input masking the L1 contribution. To test this possibility, we asked if L1 is sufficient for ON behavior in dynamically changing luminance conditions. We measured behavioral responses after functionally isolating L1 from other circuitry downstream of photoreceptors. To achieve this, we selectively rescued expression of the histamine-gated chloride channel Ort in *ort*-mutant flies, which otherwise lack communication between photoreceptors and their postsynaptic neurons. Behavioral responses of *ort* mutant control flies were absent, indicating that ON-motion behavior fully depends on Ort (Figure 3D). Heterozygous *ort* controls turned with the moving 100% contrast ON edges at all luminances (Figure 3E). Flies in which *ort* expression was rescued in L1 responded to ON motion at all luminances, and indistinguishable from controls (Figure 3F), showing that L1 can mediate normal turning behavior to ON edges at all luminances. This data confirms L1's general importance in the ON pathway and additionally highlights its behaviorally relevant role of its luminance-sensitive component.
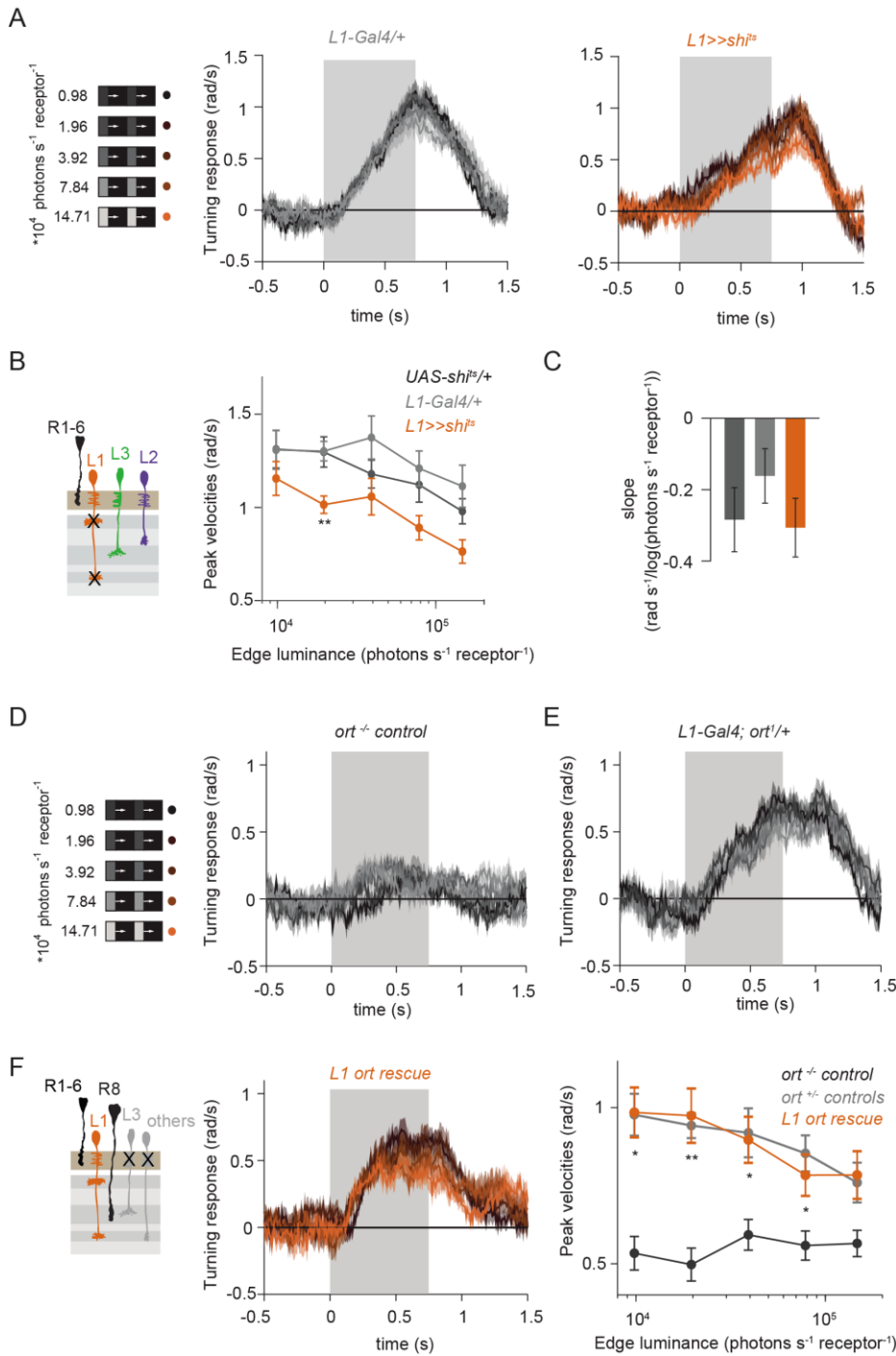
Figure 3: L1 is not required but sufficient for ON behavior across luminance. (A) Turning responses of L1-silenced flies (blue) and their specific Gal4 control (gray) to moving 100% contrast ON edges at five different luminances. **(B)** Peak velocities quantified for each of the five edges during the motion period, also including the control *UAS-shi^{is}/+*, **p < 0.01, two-tailed Student's t tests against both controls. **(C)** Relationship of the peak velocities with luminance, quantified as slopes of the linear fits to the data in (B). Sample sizes are n = 10 flies for each genotype. **(D-E)** Schematic of the stimulus (same as in A) and turning responses of the *ort* null mutant (*ort^{-/-}* controls, D) and heterozygous *ort* controls (*ort^{+/-}* controls, E). **(F)** Schematic of the L1 ort rescue genotype and turning responses of L1 ort rescue flies (left). Peak turning velocities of L1 ort rescue flies and the respective controls (right); *p<0.05, **p < 0.01, two-tailed Student's t tests against both controls. The gray box region in (A,D,E,F) indicates motion duration. Traces and plots show mean ± SEM.

L1 and L3 together provide luminance signals required for ON behavior

Our data suggest the existence of a second luminance input to the ON pathway. In the OFF pathway, the luminance-sensitive L3 neuron provides the necessary luminance-based correction to achieve contrast constancy (Ketkar et al., 2020). Connectomics data suggest that L3 could provide input to the ON pathway as well (Takemura et al., 2013). To test the hypothesis that L3 also provides a luminance signal to approach luminance-invariant ON responses, we measured behavioral responses to a set of 100% contrast ON edges at five different luminances while silencing L3 synaptic outputs (Figure 4A,B). Interestingly, unlike controls, L3-silenced flies responded stronger to all ON edges, revealing an unexplored, inhibitory role of L3. However, the responses of L3-silenced flies were still highly similar across luminances. This demonstrates that, like L1, L3 is not alone required for the near-invariant ON pathway behavior. Unlike controls, L3 silenced flies did not show a slight increase in turning amplitude at lower edge luminance, also reflected in the differences in their slopes (Figure 4C), suggesting that L3 inputs to the ON pathway also contribute to behavior in a luminance-dependent manner. To further explore this, we next asked if L3 is sufficient for ON behavior and functionally isolated L3 from another circuitry. L3 rescue flies turned to ON edges at all luminances tested (Figure 4D) and significantly rescued turning behavior at low luminances compared to *ort* mutant flies (Figure 4E), showing that L3 is sufficient for ON behavior at low luminances. This further reflects L3's nonlinear preference for dim light seen at the physiological level (Ketkar et al., 2020), (Figure 2C).

We found that L3 is a second luminance input to the ON pathway that, together with L1, supports luminance-invariant responses in ON behavior. To test this, we silenced the outputs of both L1 and L3 simultaneously while measuring ON behavior across luminance. Flies still turned to the moving ON edges. However, turning responses of flies lacking both L1 and L3 functional outputs were no longer luminance invariant and turned less than controls in a luminance-dependent manner (Figure 4F,G). Intriguingly, behavioral responses now scaled positively with the edge luminance (Figure 4H), qualitatively recapitulating the LMC contrast-sensitive responses. Thus, L1 and L3 can together account for the luminance information available to the ON pathway. To analyze the extent of the individual contributions of L1 and L3, we compared L1 and L3 ort rescues by computing rescue efficiency, defined as the fraction of the difference between positive and negative control behaviors. Whereas L1 fully rescued turning behavior to ON edges at all luminances, L3 significantly rescued turning behavior selectively at low luminances (Figure 4I). Taken together, L1 and L3 both provide distinct types of luminance information to the ON pathway (Figure 4J). Because flies lacking both of these neurons still respond to ON contrast, our data suggest the existence of an unidentified contrast input.
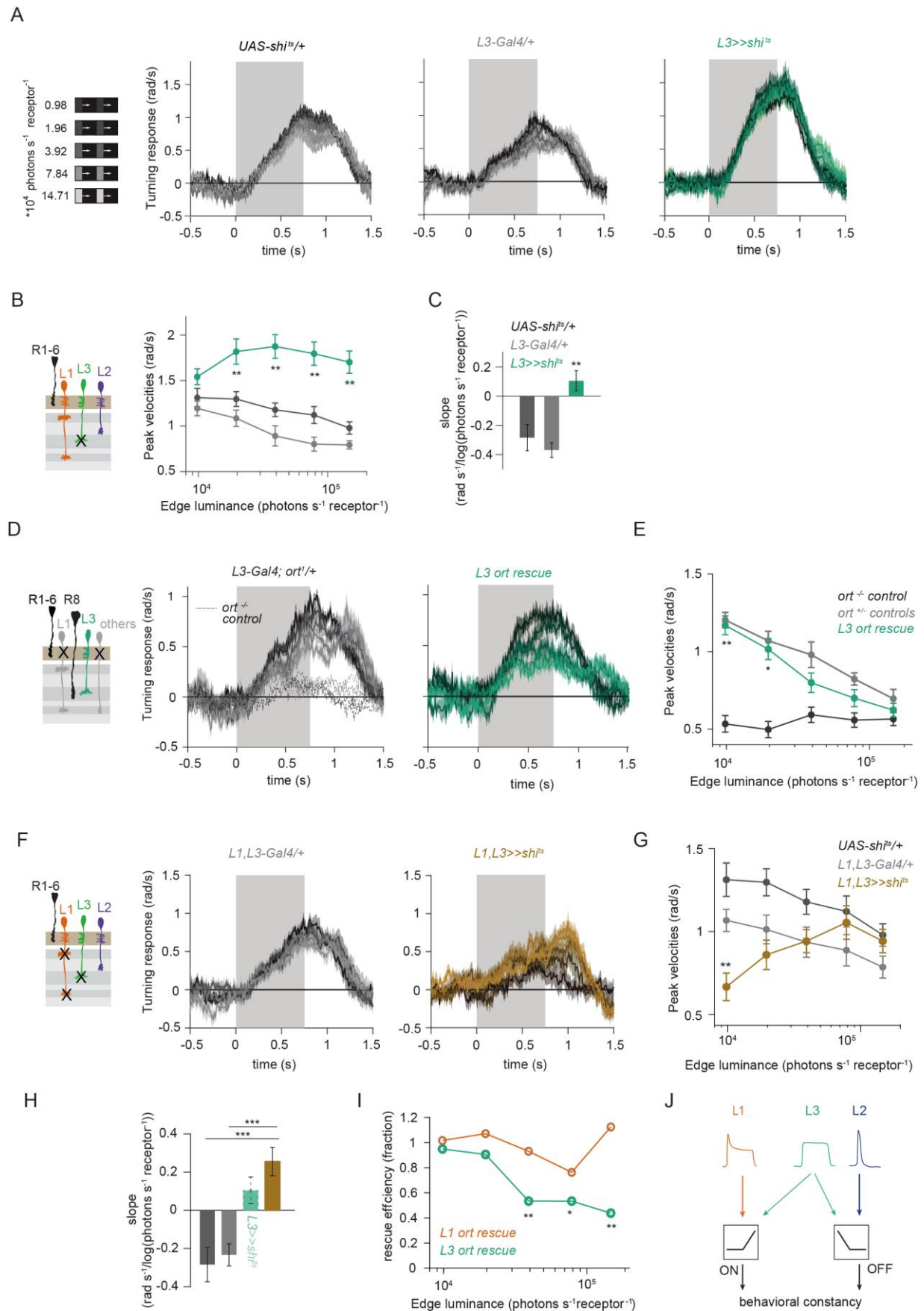
Figure 4: L1 and L3 together provide luminance signals required for ON behavior. (A) Turning velocities of the controls (gray) and L3-silenced flies (green) in response to five moving ON edges of 100% contrast. The gray box region indicates motion duration. **(B)** Peak turning velocities for five ON edges quantified during the

motion period, **p < 0.01, two-tailed Student's t tests against both controls. **(C)** Relationship of the peak velocities with luminance, quantified as slopes of the linear fits to the data in (B). Fitting was done for individual flies. Sample sizes are n = 10 (*UAS-shi^{ts}/+,L3>>shi^{ts}*) and n = 8 (*L3^{0595}-Gal4/+*). **(D)** Schematic of the L3 *ort* rescue genotype and turning responses of the heterozygous control (gray) and rescue (green) flies. **(E)** Peak turning velocities, *p<0.05, **p < 0.01, two-tailed Student's t tests against both controls. **(F)** Turning responses of flies where L1 and L3 were silenced together (golden brown) and their specific Gal4 control (gray), color-coded according to ON edge luminance. The same five moving ON edges of 100% contrast as in Figure 2A were shown. Responses of the other control *UAS-shi^{ts}/+* to these stimuli have been included in Figure 1C. **(G)** Peak velocities quantified for each of the five edges during the motion period, also including the control *UAS-shi^{ts}/+*, **p < 0.01, two-tailed Student's t tests against both controls. **(H)** Relationship of the peak velocities with luminance, quantified as slopes of the linear fits to the data in (G). Slopes from the L3-silenced flies (green, dashed) responding to the same stimuli (Figure 3C) are included again for comparison. Fitting was done for individual flies. Sample sizes are n = 10 (*UAS-shi^{ts}/+*and *L1,L3>>shi^{ts}*) and n = 7 (*L1^{c2025}-Gal4/+;L3^{0595}-Gal4/+*). **(I)** Efficiency of the L1 and L3 behavioral rescue, calculated for each edge luminance as (*rescue - ort^{-/-} control*) / (*ort^{+/-} control - ort^{-/-}* control). *p<0.05, **p < 0.01, permutation test with 1000 permutations over the *L1 ort rescue* and *L3 ort rescue* flies. **(J)** Summary schematic. The ON pathway in addition to the OFF pathway receives a prominent input from L3. Like the OFF pathway, the ON pathway drives contrast constant behavior. Traces and plots show mean ± SEM.

The contrast-sensitive L2 provides input to the ON pathway

Besides L1 and L3, the remaining input downstream of photoreceptors is the contrast-sensitive L2 neuron, which provides strong inputs to OFF-pathway neurons (Takemura et al., 2013). To explore the possibility of L2 also being an ON pathway input, we silenced L2 outputs either individually or together with L1. L2-silenced flies showed only slightly reduced turning to all ON edges as compared to controls (Figure 5A,B) similarly to silencing L1 alone (Figure 3A,B). However, when L1 and L2 were silenced together, fly turning responses were fully disrupted across conditions (Figure 5C,D). Moreover, these flies did not turn to other ON contrasts steps either (Supp. Figure 2). This shows that L2, together with L1, is required for ON behavioral responses across different contrasts and luminances. Altogether, L1, L2 and L3 are all ON-pathway inputs.
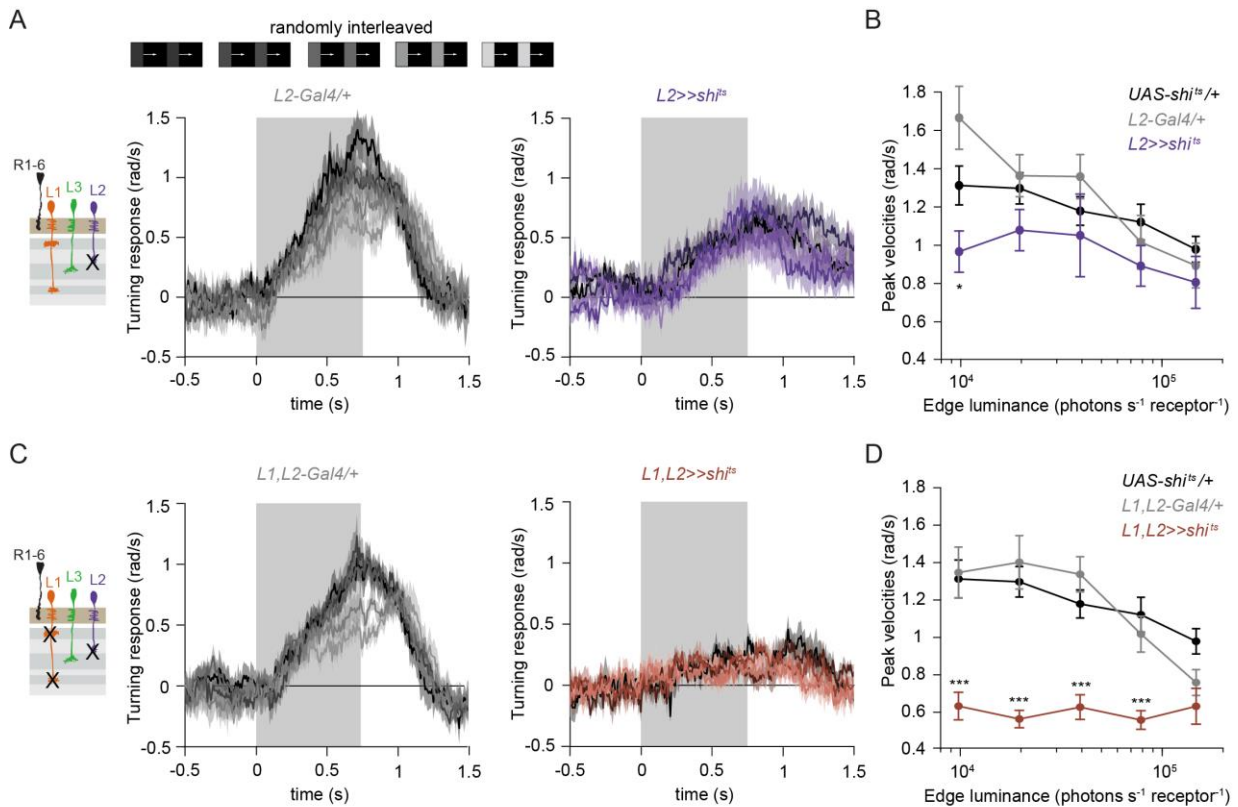
Figure 5: The contrast-sensitive L2 provides input to the ON pathway. (A) Turning responses of flies where L2 was silenced (purple) and their specific Gal4 control (gray), color-coded according to 100% contrast ON edge at five different luminances. Sample sizes are n = 9 *(L2^{21Dhh}>>shi^{ts})* and n = 6 (*L2^{21Dhh}-Gal4/+*). **(B)** Peak velocities quantified for each of the five edges during the motion period, *p < 0.05, two-tailed Student's t tests against both controls. **(C)** Turning responses of flies where L1 and L2 were silenced together (brown) and their specific Gal4 control (gray), color-coded according to ON edge luminance. Sample sizes are n = 9 *(L1^{c2025},L2^{21Dhh}>>shi^{ts})* and n = 8 (*L1^{c2025}-Gal4/+;L2^{21Dhh}-Gal4/+*). **(D)** Peak velocities quantified for each of the five edges during the motion period, ***p < 0.001, two-tailed Student's t tests against both controls. Traces and plots show mean ± SEM.

L1 is also an OFF-pathway input

Given that three lamina neuron inputs encode visual stimuli differently and that all of them convey information to the ON pathway, we next asked if L1 could also contribute to OFF-pathway function. To test this, we silenced L1 neurons while showing moving OFF edges, all of -100% contrast, and moving across five different background luminances. Control flies turned similarly under all conditions, showing luminance-invariant responses (Figure 6A). Previous work showed that L3 is required to achieve luminance invariance by scaling behavioral responses when background luminance turned dark (Ketkar et al., 2020). Similarly, when L1 was silenced, behavioral responses were no longer invariant across luminance, but flies turned less to -100% contrast at low luminance as compared to high luminance (Figure 6A,B). Underestimation of the dim OFF stimuli by L1-silenced flies was not as strong as by L3-silenced flies (Ketkar et al., 2020), again highlighting the specialized

role of L3 in dim light (Figure 6B). These data demonstrate that L1 luminance inputs are required for luminance-invariant OFF behavior. Since L1 carries both contrast and luminance information, it could be also sufficient to drive OFF behavior. To test this, we measured behavioral responses to OFF edges in L1 ort rescue flies. Heterozygous *ort* controls showed turning responses to -100% OFF edges at five different luminances (Figure 6C). As described previously (Ketkar et al., 2020), *ort* null mutants were not completely blind to this OFF-edge motion stimulus and responded especially at high luminance but very little at low luminances. L1 ort rescue flies responded similarly to positive controls, rescuing OFF edges at low luminances (Figure 6D). Therefore, L1 is even sufficient to guide OFF behavior under the same conditions that were previously described for L3 (Ketkar et al., 2020). Taken together, these findings reveal that the lamina neurons L1 and L3 provide behaviorally relevant but differentially encoded luminance information to both ON and OFF pathways. In sum, our data uncover L1, L2 and L3 as important inputs for both ON and the OFF pathways, relevant for visually guided behaviors across luminances (Figure 6E).
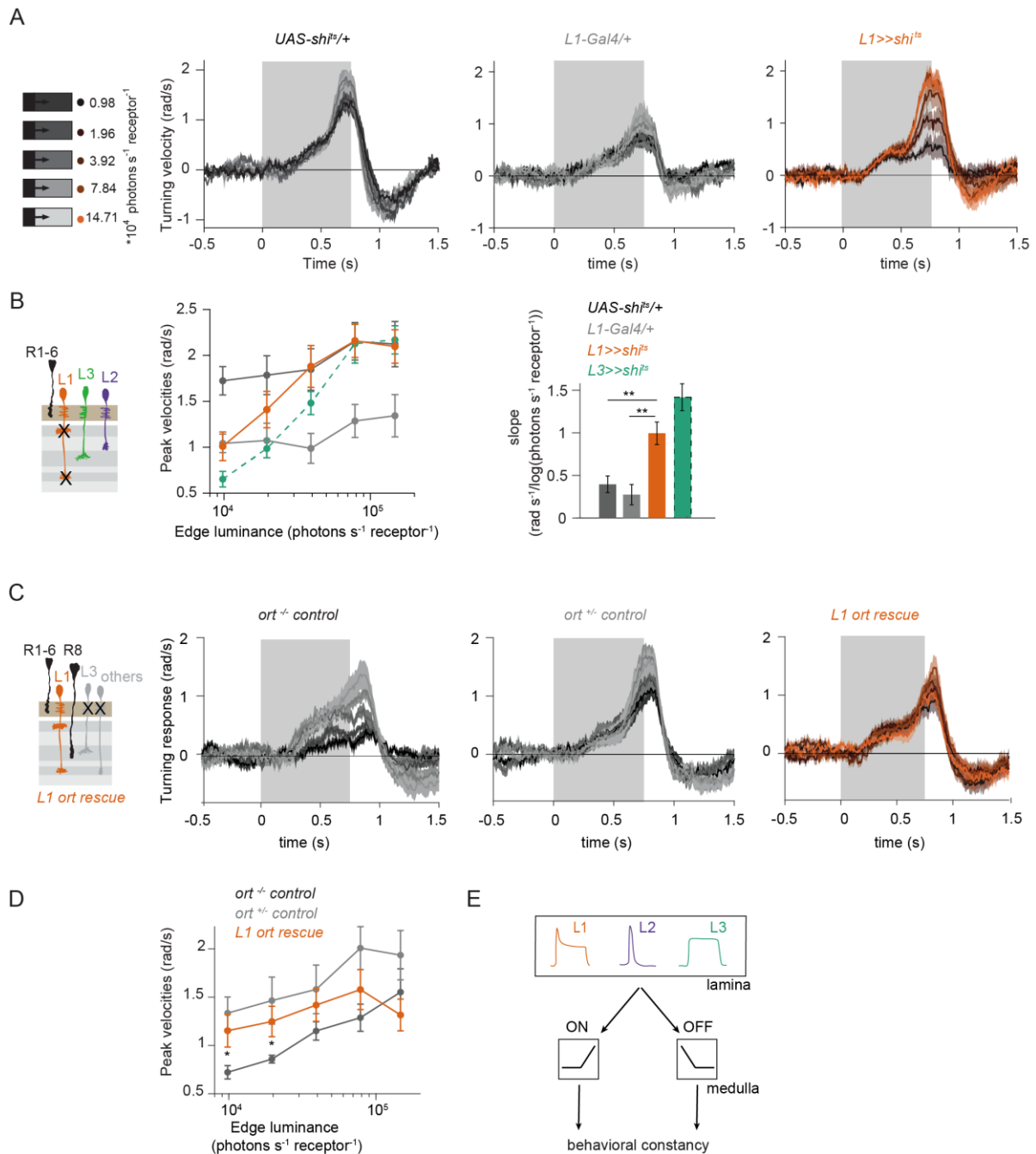
Figure 6: The L1 luminance signal is required and sufficient for OFF behavior. (A) Turning responses of L1-silenced flies (orange) and the controls (gray) to five OFF edges moving onto different backgrounds. **(B)** Peak velocities quantified for each of the five edges during the motion period, also including the peak velocities of L3-silenced flies (green dashed, re-quantified from the data in (Ketkar et al., 2020). Shown next to it is the relationship of the peak velocities with luminance, quantified as slopes of the linear fits to the data. **p < 0.01, two-tailed Student's t tests against both controls (not significant against the *L3>>shi^ts* slopes). Sample sizes are n = 7 *(L1-Gal4/+)* and n = 10 for other genotypes. **(C)** Schematics of the L1 ort rescue genotypes followed by its turning responses to the moving OFF edges. **(D)** Peak turning velocities of L1 ort rescue flies and the respective controls; *p<0.05, two-tailed Student's t tests against both controls. Sample sizes are n = 11 flies (*ort^-/-*control) and n =10 for other genotypes. The gray box region in (A) and (C) indicates motion duration. **(E)** Summary schematic. Lamina neurons L1-L3 distribute different visual features necessary for both ON and OFF pathways to guide contrast-constant behavior. Traces and plots show mean ± SEM.

Discussion

The present study establishes that contrast and luminance are basic visual features that interact with both ON and OFF pathways. In both pathways, the interaction between these features enables stable visual behaviors across changing conditions. The lamina neurons L1, L2 and L3 act as the circuit elements segregating both contrast and luminance information. Behavioral experiments show that luminance information is required for contrast constancy in both ON and OFF behaviors. While L1 and L3 provide contrast inputs to both ON and OFF pathways, L1 also encodes luminance, together with L3. Whereas L3 activity non-linearly increases with decreasing luminance, L1 shows a linear relationship with luminance. Luminance information from both neurons is differently used in ON and OFF pathways. Thus, L1, L2 and L3 are not ON or OFF pathways specific inputs, but they instead distribute the two most basic visual features, contrast and luminance, across pathways to enable behaviorally relevant computations.

Contrast constancy is a common feature of ON and OFF visual pathways, but with distinct implementations

Our work shows that visual behaviors guided by both ON and OFF pathways are luminance invariant. Similarly, luminance invariance has been shown in human perception of both ON and OFF contrasts, and in neural responses in cat LGN (Burkhardt et al., 1984; Mante et al., 2005). This argues that luminance invariance is a common feature of all visual systems, which is ethologically relevant for any species that relies on visual information for its survival in changing visual environments. Changing visual environments impose a common challenge onto the encoding of both ON and OFF contrasts, namely the contrasts are underestimated in sudden dim light. The L1 contrast-sensitive responses reflect such underestimation. Thus, both ON and OFF visual pathways would require a luminance-based correction to achieve luminance invariance, and such correction would in turn rely on luminance-sensitive neuronal signals themselves. We now confirm this hypothesis for both ON and OFF pathways. Specifically, luminance information from both L1 and L3 are required for luminance-invariant visual behaviors. However, the impact of the two neurons on behavior is pathway dependent. In the OFF pathway, losing either L1 or L3 function leads to a strong deviation from luminance invariance, such that the dim light stimuli are underestimated. On the contrary, ON motion-driven behavior only strongly deviates from invariance if both L1 and L3 neuron types are not functional. Furthermore, L2 neurons, which were formerly thought to be OFF pathway inputs, contribute contrast-sensitive information to ON behavior (Clark et al., 2011; Joesch et al., 2010; Silies et al., 2013). Notably, ON and OFF contrast constancy is not achieved symmetrically at every processing

stage. For example, in the vertebrate retina, ON RGCs encode a mixture of luminance-invariant and absolute (i.e. luminance-dependent) contrast, whereas OFF RGCs encode predominantly absolute contrast (Idrees and Münch, 2020). Thus, asymmetrical implementation of contrast-corrective mechanisms can be common across visual systems, too.

All lamina neurons are inputs to both ON and OFF pathways

L1, L2 and L3 all show different contrast and luminance sensitivities. These distinct neuronal properties are then differentially utilized across ON and OFF pathways. How does this fit with the established notion that L1 is an input to the ON and L2 and L3 are inputs to OFF pathways? The luminance-varying stimuli sets used here were able to pull out lamina neuron contributions that were not obvious with simpler stimuli. For example, our data show that L1 and L2 provide redundant contrast input to the ON pathway at 100% contrast and varying luminance. However, L1 is still strictly required for ON responses if different contrasts are mixed. This is consistent with a more complex ON pathway input architecture and hints at a role for the L1 pathway in contrast adaptation. Interestingly, Mi1, an important post-synaptic partner of L1, shows an almost instantaneous and strong contrast adaptation (Matulis et al., 2020).

All three lamina neuron types hyperpolarize to light onset and depolarize to light offset and are not contrast selective themselves. Contrast selectivity emerges downstream of these neurons: known post-synaptic partners of L1 acquire ON contrast selectivity due to inhibitory glutamatergic synapses, whereas cholinergic L2 and L3 synapses retain OFF contrast selectivity (Molina-Obando et al., 2019). While L3 was actually already suggested to be an ON pathway input based on connectomics (Borst et al., 2020), other synaptic connections that link L1 to downstream OFF-selective neurons, and link L2 and to downstream ON-selective neurons still have to be investigated in detail. However, it now becomes evident that a split in ON and OFF circuitry only truly exists in downstream medulla neurons and direction-selective cells. The luminance and contrast features encoded differently in L1, L2 and L3 lamina neurons are shared by both pathways. Importantly, the distinct features that are passed on by the specific inputs downstream of photoreceptors guide distinct behavioral roles.

L1 and L3 convey luminance information to multiple pathways

Behavioral experiments in combination with genetic manipulations show that both L1 and L3 neurons provide luminance information to to achieve luminance-invariant behaviors. This functional data is consistent with anatomical predictions suggesting a role for L3 in the ON

pathway based on synaptic contacts with ON-selective neurons (Takemura et al., 2013). L3 had mostly been considered an OFF pathway neuron because the OFF pathway neuron Tm9 receives its strongest input from L3 (Fisher et al., 2015; Shinomiya et al., 2014; Takemura et al., 2013). Remarkably, L3 itself actually makes most synaptic connections with the ON-pathway neuron Mi9. Further synapses of L3 with the ON-selective Mi1 neuron are similar in number to those with Tm9 (Takemura et al., 2013). Finally, L3 can potentially also convey information to the chromatic pathway, as Tm20 is its second strongest postsynaptic connection (Lin et al., 2016). There, L3 luminance sensitivity might play a relevant role in achieving color constancy, i.e., color recognition irrespective of illumination conditions. Altogether, anatomical and functional data indicate that it is time to redefine L3 as part of a luminance-encoding system rather than a mere OFF-pathway input.

A role of L1 beyond the ON pathway was less obvious based on anatomical data but is supported by functional connectivity studies showing that Tm9 properties rely in part on L1 input (Fisher et al., 2015), and that Tm9 together with other OFF pathway interneurons displays contrast-opponent receptive fields, adding evidence to the presence of ON information in the OFF pathway (Ramos-Traslosheros and Silies, 2021). Connectomics data did not identify any known OFF-pathway neurons postsynaptic to L1 and presynaptic to the OFF-motion selective neuron T5 (Takemura et al., 2013). L1 must therefore connect to the OFF pathway via interneurons. Among the strongest postsynaptic partners of L1 are the GABAergic interneurons C2 and C3 that connect to the OFF pathway (Takemura et al., 2013). Intercolumnar neurons downstream of L1, such as Dm neurons (Nern et al., 2015), could further carry information to OFF-selective neurons, likely through disinhibition from ON-selective inputs. In the vertebrate retina, intercolumnar amacrine cells mediate interaction between ON and OFF bipolar cells, which has been shown to extend the operating range of the OFF pathway (Manookin et al., 2008; Odermatt et al., 2012). Altogether, strategies appear to be shared across animals in which type of interneurons help to convey relevant features from one pathway to the other.

Neurons postsynaptic to photoreceptors encode contrast and luminance differently
Despite being postsynaptic to the same photoreceptor input, all lamina neurons respond differently to light stimuli. L1 was previously considered the ON pathway sibling of the contrast-sensitive L2, both with regard to its temporal filtering properties and at the transcriptome level (Clark et al., 2011; Tan et al., 2015). However, L1 calcium signals show a transient and a sustained response component, which are contrast- and luminance-sensitive, respectively. Compared to photoreceptors, which also carry both contrast and

luminance components, L1 still amplifies the contrast signals received from the photoreceptors, since its transient component is more pronounced than the one seen in the photoreceptor calcium traces (Gür et al., 2020). In other insect species, different types of lamina neurons have also been distinguished based on their physiological properties (Rusanen et al., 2018, 2017), although their specific luminance and contrast sensitivities are yet unknown.

The two luminance-sensitive neurons L1 and L3 differ in their luminance-encoding properties. L1's initial transient contrast response might reduce the operating range of the subsequent luminance-sensitive baseline. L3's calcium responses show little adaptation and can utilize most of its operating range to encode luminance. L3 seems to invest this wider operating range into amplifying the darkest luminance values selectively and non-linearly. Thus, a predominantly luminance-sensitive channel among LMCs may have evolved to selectively process stimuli in the low luminance range. The different linear and non-linear properties of L1 and L3 might further increase the dynamic range of luminance signaling (Odermatt et al., 2012). Together with the pure contrast sensitivity of L2, the first-order interneurons in flies exhibit a wide range of sensitivities with respect to contrast and luminance, and our data confirm the functional relevance of the differential sensitivities. Diversifying feature encoding through distinct temporal properties of first-order interneurons is a strategy employed to reliably handle wide luminance ranges.

Similarities and differences of peripheral processing strategies across species

In flies, three first-order interneurons feed contrast and luminance information into downstream circuitry. In the mouse retina, more than 30 functionally distinct bipolar types show a spectrum of temporal filter properties rather than a strict transient-sustained dichotomy, thus capturing a larger diversity of temporal information in parallel channels (e.g., (Baden et al., 2016; Ichinose et al., 2014; Odermatt et al., 2012)). Many bipolar cell types resemble L1, in that they have both luminance and contrast signals in distinct response components (e.g., (Oesch and Diamond, 2011)). However, the degree of transiency varies from cell type to cell type, and some predominantly sustained bipolar cell types are also found, closely resembling the luminance-sensitive L3 (e.g., (Awatramani and Slaughter, 2000; Ichinose et al., 2014)). Such diversification of feature extraction at the periphery has been shown to be computationally advantageous, especially when processing complex natural scenes (e.g. (Odermatt et al., 2012; Rieke and Rudd, 2009)). For example, during daylight, visual scenes can differ in intensity by 4 to 5 log units, whereas electrical signals in cone photoreceptors reach a dynamic range of only two orders of

magnitude (Naka and Rushton, 1966; Normann and Perlman, 1979; Pouli et al., 2010; Schnapf et al., 1990).

Although the vertebrate retina apparently has a much larger diversity of cell types to handle the wide and complex statistics of the visual environments, there is only a single layer of processing between photoreceptors and the first direction-selective cells, whereas in insects, there are two: the lamina and the medulla. It seems as if the combined properties of bipolar cells are spread across these two processing stages in the fly visual system: whereas some properties, such as diversity of temporal filtering starts in LMCs, contrast selectivity only emerges in medulla neurons and not directly in the first-order interneurons as it happens in bipolar cells. In both vertebrates and invertebrates, the emergence of ON selectivity occurs through inhibitory glutamatergic synapses, but whereas this happens at the photoreceptor-to-bipolar cell synapse in vertebrates, it happens one synapse further down between lamina and medulla neurons in flies (Masu et al., 1995; Molina-Obando et al., 2019). Taken together, LMCs and downstream medulla neurons combined appear to be the functional equivalents of vertebrate bipolar cell layers. Given the size limitations of the fly visual system to encode the same complex environment effectively, one benefit of this configuration with an extra layer could be that it allows more combinations. Furthermore, the photoreceptor-to-lamina synapse in the fly superposition eye already serves to spatially pool information from different photoreceptors (Braitenberg, 1967; Clandinin and Zipursky, 2002; Kirschfeld, 1967). In both visual systems, diversifying distinct information across several neurons could serve as a strategy to reliably respond to contrast when luminance conditions vary.

Methods

Experimental model

All flies were raised at 25 ºC and 65 % humidity on standard molasses-based fly food while being subjected to a 12:12h light-dark cycle. Two-photon experiments were conducted at room temperature (20 ºC) and behavioral experiments at 34 ºC. Female flies 2-4 days after eclosion were used for all experimental purposes. Lamina neuron driver lines used for genetic silencing and *ort* rescue experiments were *L3^{0595}-Gal4* (Silies et al., 2013), *L2^{21Dhh}-Gal4* and *L1^{C202a}-Gal4* (Rister et al., 2007), and *UAS-shi[ts], ort^1,ninaE^1* and *Df(3R)BSC809* were from BDSC (# 44222, 1946 and 27380). Since the *ort^1* mutant chromosomes also carries a mutation in *ninaE^1* (*Drosophila rhodopsin1*), we used the *ort^1* mutation in trans to a deficiency that uncovers the *ort* but not the *ninaE* locus. *UAS-ort* was first described in (Hong et al., 2006). For imaging experiments, GCaMP6f (BDSC #42747) was expressed using *L1^{c202a}-Gal4*, *L2^{21Dhh}-Gal4* (Rister et al., 2007), and *L3^{MH56}-Gal4* (Timofeev et al., 2012). Detailed genotypes are given in Table 1.

Table 1.: Genotypes used in this study.

Name	Genotype	Figure
Imaging		
L1>>GCaMP6f	*w+; L1^{c202a}-Gal4 / +; UAS-GCaMP6f / +*	Fig 1, 2
L2>>GCaMP6f	*w+; UAS-GCaMP6f / +; L2^{21Dhh}-Gal4 / +*	Fig 2
L3>>GCaMP6f	*w+; L3^{MH56}-Gal4 / +; UAS-GCaMP6f / +*	Fig 2
Behavior		
UAS-shibire^{ts} control	*w+; + / +; UAS-shi^{ts} / +*	Fig 2, 3,4, 5, 6, S1, S2
L3-Gal4 control	*w+; +/ +; L3^{0595}-Gal4 /+*	Fig 4
L3 silencing	*w+; +/ +; L3^{0595}-Gal4 /UAS- shi^{ts}*	Fig 4
L1-Gal4 control	*w+; L1^{c202a}-Gal4 / +; + /+*	Fig 3, 6, S1
L1 silencing	*w+; L1^{c202a}-Gal4 / +; + /UAS- shi^{ts}*	Fig 3, 6, S1

L1-Gal4, L3-Gal4 control	w+; L1^{c202a}-Gal4 / +; L3^{0595}-Gal4 /+	Fig 4
L1, L3 silencing	w+; L1^{c202a}-Gal4 / +; L3^{0595}-Gal4 /UAS- shi^{ts}	Fig 4
ort mutant	w+; UAS-ort / +; ort^1,ninaE^1 / Df(3R)BSC809	Fig 3, 4, 6
L3 ort +/- control	w+; + / +; L3^{0595}-Gal4, ort^1, ninaE^1 / +	Fig 4
L3 ort rescue	w+; UAS-ort / +; L3^{0595}-Gal4, ort^1,ninaE^1 / Df(3R)BSC809	Fig 4
L1 ort +/- control	w+; L1^{c202a}-Gal4 / +, ort^1, ninaE^1 / +	Fig 3, 6
L1 ort rescue	w+; UAS-ort / +; L1[c202a]; ort^1,ninaE^1 / Df(3R)BSC809	Fig 3, 6
L2-Gal4 control	w+; + /+; L2^{21Dhh}-Gal4 / +	Fig 5,S2
L2 silencing	w+; + / +; L2^{21Dhh}-Gal4 /UAS- shi^{ts}	Fig 5, S2
L1-Gal4, L2-Gal4 control	w+; L1^{c202a}-Gal4 / +; L2^{21Dhh}-Gal4 /+	Fig 5, S2
L1, L2 silencing	w+; L1^{c202a}-Gal4 / +; L2^{21Dhh}-Gal4 /UAS- shi^{ts}	Fig 5, S2

Behavioral experiments

Behavioral experiments were performed as described in (Ketkar et al., 2020). In brief, all experiments were conducted at 34 ºC, a restrictive temperature for Shibire^{ts} (Kitamoto, 2001). Female flies were cold anesthetized and glued to the tip of a needle at their thorax using UV-hardened Norland optical adhesive. A 3D micromanipulator positioned the fly above an air-cushioned polyurethane ball (Kugel-Winnie, Bamberg, Germany), 6 mm in diameter, and located at the center of a cylindrical LED arena that spanned 192º in azimuth and 80º in elevation (Reiser and Dickinson, 2008). The LED panels arena (IO Rodeo, CA, USA) consisted of 570 nm LEDs and was enclosed in a dark chamber. The pixel resolution was ~2º at the fly elevation. Rotation of the ball was sampled at 120 Hz with two wireless optical sensors (Logitech Anywhere MX 1, Lausanne, Switzerland), positioned toward the

center of the ball and at 90º to each other (setup described in (Seelig et al., 2010). Custom written C#-code was used to acquire ball movement data. MATLAB (Mathworks, MA, USA) was used to coordinate stimulus presentation and data acquisition. Data for each stimulus sequence were acquired for 15-20 minutes, depending on the number of distinct epochs in the sequence (see 'visual stimulation' for details).

Visual stimulation for behavior

The stimulation panels consist of green LEDs that can show 16 different, linearly spaced intensity levels. To measure the presented luminance, candela/m^2 values were first measured from the position of the fly using a LS-100 luminance meter (Konika Minolta, NJ, USA). Then, these values were transformed to photons incidence per photoreceptor per second, following the procedure described by (Dubs et al., 1981). The highest native LED luminance was approximately $11.77 * 10^5$ photons $* s^{-1} *$ photoreceptor^{-1} (corresponding to a measured luminance of 51.34 cd/m2), and the luminance meter read 0 candela/ m^2 when all LEDs were off. For all experiments, a 0.9 neutral density filter foil (Lee filters) was placed in front of the panels, such that the highest LED level corresponded to $14.71 * 10^4$ photons$*s^{-1}*$receptor^{-1}.

Fly behavior was measured in an open-loop paradigm where either ON or OFF edges were presented. For every set of ON or OFF edges, each epoch was presented for around 60 to 80 trials. Each trial consisted of an initial static pattern (i.e., the first frame of the upcoming pattern) shown for 500 ms followed by 750 ms of edge motion. Inter-trial intervals were 1s. All edges from a set were randomly interleaved and presented in a mirror-symmetric fashion (moving to the right, or to the left) to account for potential biases in individual flies or introduced when positioning on the ball.

The ON edge stimuli comprised four edges, each covering 48º arena space. All ON edges moved with the angular speed of 160º/s. Thus, within a 750 ms stimulus epoch, the edge motion repeated thrice: After each repetition, the now bright arena was reset to the pre-motion lower LED level, and the next repetition followed immediately, picking up from the positions where the edges terminated in the first repetition. This way, each edge virtually moved continuously. The following sets of ON edges were presented:

1. 100% contrast edges: Here, the edges were made of 5 different luminance values (i.e., five unique epochs), moving on a complete dark background. Thus, the pre-motion LED level was zero, and the edges assumed the intensities 7%, 14%, 27%, 53% or 100% of the highest LED intensity (corresponding to the luminances: 0.98, 1.96, 3.92, 7.84 or $14.71 * 10^4$ photons$*s^{-1}*$receptor^{-1} luminance). Thus, every epoch comprised 100% Michelson contrast. The inter-trial interval consisted of a dark screen.

2. Mixed-contrast edges – full range: The set comprised of seven distinct epochs, each with a different Michelson contrast value (11%, 25%, 33%, 43%, 67%, 82% and 100%). Here, the edge luminance was maintained constant at 67% of the highest LED intensity, across epochs, and the background luminance varied. The inter-trial interval showed a uniformly lit screen with luminance equivalent to the edge luminance.

3. Mixed-contrast edges – low contrast range: The set comprised of four distinct epochs, with contrasts from the range 9%, 18%, 27% and 36%. Here, edge luminances and background luminances both varied: The edge luminances assumed the intensities 80%, 87%, 93% and 100% of the highest LED intensity, whereas the background intensities were 67%, 60%, 53% and 47% of the highest LED intensity, respectively. The inter-trial interval consisted of a dark screen.

For the experiments concerning OFF edges, a set of five OFF edges comprising 100% Weber contrast was used as described in (Ketkar et al., 2020). Epoch consisted of a single OFF edge presented at one of five different uniformly lit backgrounds. The edge luminance was always ~zero, whereas the five different background luminances were 7%, 14%, 27%, 54% and 100% of the highest LED intensity (corresponding to five different background luminances: 0.98, 1.96, 3.92, 7.84 or 14.71 $*10^4$ photons$*$s$^{-1}*$receptor^{-1}). The inter-trial interval consisted of a dark screen.

Behavioral data analysis

Fly turning behavior was defined as yaw velocities that were derived as described in (Seelig et al., 2010), leading to a positive turn when flies turned in the direction of the stimulation and to a negative turn in the opposite case. Turning elicited by the same epoch moving either to the right or to the left were aggregated to compute the mean response of the fly to that epoch. Turning responses are presented as angular velocities (rad/s) averaged across flies ± SEM. Peak velocities were calculated over the stimulus motion period (750ms), shifted by 100 ms to account for a response delay, and relative to a baseline defined as the last 200 ms of the preceding inter-stimulus intervals. For the moving edges of 100% contrast and varying luminance, relation between peak velocities and luminance was assessed by fitting a straight line (V = a*log(luminance) + b) to the peak velocities of individual flies and quantifying the mean slope (a) ± SEM across flies. When comparing the slopes computed for behavior and L1 physiology, the two data types were first normalized for individual flies for behavior and individual regions of interest (ROIs) for L1 physiology (Figure 1E). For the *ort* rescue experiments, rescue efficiency was calculated at each stimulus luminance as

$$E_{rescue} = \frac{rescue - control^-}{control^+ - control^-}$$

where E_{rescue} is the fractional rescue efficiency, *rescue* is the mean peak velocity of the rescue genotype such as L1 rescue, *control⁻* is the mean peak velocity of the *ort* null mutant negative control and *control⁺* stands for the mean peak velocity of the positive heterozygous *ort¹* control (e.g., *L1-Gal4; ort¹/+*). Statistical significance of E_{rescue} differences was tested using a permutation test. Specifically, flies of the genotypes L1 ort rescue and L3 ort rescue were shuffled 1000 times and the difference between their rescue efficiencies was obtained each time. The difference values so obtained gave a probability distribution that approximated a normal distribution. The efficiency difference was considered significant when it corresponded to less than 5% probability on both tails of the distribution.

Mean turning of flies as well as the slopes from control and experimental genotypes were normal distributed as tested using a Kolmogorov-Smirnov test ($p > 0.05$). Two-tailed Student's t tests and Bonferroni-Holm correction were performed between genotypes. Data points were considered significantly different only when the experimental group significantly differed from both genetic controls. Flies with a baseline forward walking speed of less than 2 mm/s were discarded from the analysis. This resulted in rejection of approximately 25% of all flies.

Two-photon imaging

Female flies were anesthetized on ice before placing them onto a sheet of stainless-steel foil bearing a hole that fit the thorax and head of the flies. Flies they were head fixated using UV-sensitive glue (Bondic). The head of the fly was tilted downward, looking toward the stimulation screen and their back of the head was exposed to the microscope objective. To optically access the optic lobe, a small window was cut in the cuticle on the back of the head using sharp forceps. During imaging, the brain was perfused with a carboxygenated saline-sugar imaging solution composed of 103 mM NaCl, 3 mM KCl, 5 mM TES, 1 mM NaH2PO4, 4 mM MgCl2, 1.5 mM CaCl2,10 mM trehalose, 10 mM glucose, 7 mM sucrose, and 26 mM NaHCO3. Dissections were done in the same solution, but lacking calcium and sugars. The pH of the saline equilibrated near 7.3 when bubbled with 95% O2 / 5% CO2. The two-photon experiments for Figure 2 were performed using a Bruker Investigator microscope (Bruker, Madison,WI, USA), equipped with a 25x/NA1.1 objective (Nikon, Minato, Japan). An excitation laser (Spectraphysics Insight DS+) tuned to 920 nm was used to excite GCaMP6f, applying 5-15 mW of power at the sample. For experiments in Figure 1, a Bruker Ultima microscope, equipped with a 20x/NA1.0 objective (Leica, Jerusalem, Israel) was used. Here the excitation laser (YLMO-930 Menlo Systems, Martinsried, Germany) had a fixed 930 nm wavelength, and a power of 5-15 mW was applied at the sample.

In both setups, emitted light was sent through a SP680 shortpass filter, a 560 lpxr dichroic filter and a 525/70 emission filter. Data was acquired at a frame rate of ~10 to 15Hz and around 6–8x optical zoom, using PrairieView software.

Visual stimulation for imaging

For the staircase stimuli and light flashes of different luminances, the visual stimuli were generated by custom-written software using C++ and OpenGL and projected onto an 8cm x 8cm rear projection screen placed anterior to the fly and covering 60º of the fly visual system in azimuth and 60º in elevation. These experiments were performed with the Bruker Investigator microscope.

For ON-moving edges, the stimulus was generated by custom-written software using the Python package PsychoPy (Peirce, 2008), and then projected onto a 9cm x 9cm rear projection screen placed anterior to the fly at a 45º angle and covering 80º of the fly visual system in azimuth and 80º in elevation. These experiments were performed with the Bruker Ultima microscope.

Both stimuli were projected using a LightCrafter (Texas Instruments, Dallas, TX, USA), updating stimuli at a frame rate of 100 Hz. Before reaching the fly eye, stimuli were filtered by a 482/18 band pass filter and a ND1.0 neutral density filter (Thorlabs). The luminance values are measured using the same procedure described above for the behavioral experiments. The maximum luminance value measured at the fly position was $2.17*10^5$ photons s^{-1} photoreceptor^{-1} for the staircase and random luminance stimulation, and $2.4*10^5$ photons s^{-1} photoreceptor^{-1} for the ON-moving edge stimulation. The imaging and the visual stimulus presentation were synchronized as described previously (Freifeld et al., 2013).

<u>Staircase stimulation</u>

The stimulus consisted of 10s full-field flashes of 5 different luminances (0, 0.25, 0.5, 0.75 and 1∗ of the maximal luminance I$_{max}$). The different luminance epochs were presented first in an increasing order (from darkness to full brightness) then in a decreasing order (full brightness to darkness). This sequence was repeated ~3-5 times.

<u>Flashes of different luminances</u>

The stimulus consisted of 10s full-field flashes of 5 different luminances (0, 0.25, 0.5, 0.75 and 1∗ of the maximal luminance I$_{max}$). The order between the flashes was pseudo-randomized and the stimulus sequence was presented for ~300s.

<u>ON moving edges at different luminances</u>

Here, the edges were made of 6 different luminance values (corresponding to 0.16, 0.31, 0.62, 1.2, 1.8, 2.4 $*10^5$ photons$*$s$^{-1}*$receptor^{-1} luminance), moving on a dark background. The inter-stimulus interval was 4 seconds of darkness.

Two photon data analysis

<u>Staircase stimulation and randomized flashes of different luminances</u>

Data processing was performed offline using MATLAB R2019a (The MathWorks Inc., Natick, MA). To correct for motion artifacts, individual images were aligned to a reference image composed of a maximum intensity projection of the first 30 frames. The average intensity for manually selected ROIs was computed for each imaging frame and background subtracted to generate a time trace of the response. All responses and visual stimuli were interpolated at 10 Hz and trial averaged. Neural responses are shown as relative fluorescence intensity changes over time (ΔF/F0). To calculate ΔF/F0, the mean of the whole trace was used as F0. In some recordings, a minority of ROIs responded in opposite polarity (positively correlated with stimulus), as described previously (Fisher et al., 2015). These ROIs have their receptive fields outside the stimulation screen (Fisher et al., 2015; Freifeld et al., 2013). To discard these and other noisy ROIs, we only used ROIs that were negatively correlated (Spearman's rank correlation coefficient) with the stimulus. Plateau responses were calculated as the mean of the last 2 seconds within each luminance presentation. In the randomized flashes of different luminances, plateau response values of the highest luminance epoch were subtracted for each plateau response to get a comparable relationship between each neuron for visualization (this leads to 0 plateau response for each neuron in the highest luminance condition). Mutual information between luminance and response was calculated according to (Ross, 2014). To characterize the distinct luminance-response relationships of L1 and L3, the difference of Pearson correlation and Spearman's rank correlation was used as a non-linearity index. This value will reach zero if there is a strict linear relationship between luminance and response.

<u>ON moving edges at different luminances</u>

Data processing was performed offline using Python 2.7 (Van Rossum 1995). Motion correction was performed using the SIMA Python package's Hidden Markov Model based motion correction algorithm (Kaifosh et al., 2014). The average intensity for manually selected ROIs was computed for each imaging frame and background subtracted to generate a time trace of the response. To calculate ΔF/F0, the mean of the whole trace was used as F0. The traces were then trial averaged. Responses of ROIs for each epoch was calculated as the absolute difference between the mean of the full darkness background

epoch and the minimum of the ON edge presentation (minimum values are chosen because L1 neurons respond to ON stimuli with hyperpolarization).

Statistics

Throughout the analysis procedure, mean of quantified variables were calculated first for all ROIs within a fly, and then between flies. All statistical analysis was performed between flies. For normally distributed data sets, a two-tailed Student t test for unpaired (independent) samples was used. For other data sets, Wilcoxon rank-sum was used for statistical analysis. Normality was tested using Lilliefors test (p>0.05). One way ANOVA was used followed by multiple comparisons using the Bonferroni method for determining statistical significance between pairs of groups.

Acknowledgments

Competing interest:
The authors declare no competing interests.

Supplementary figures
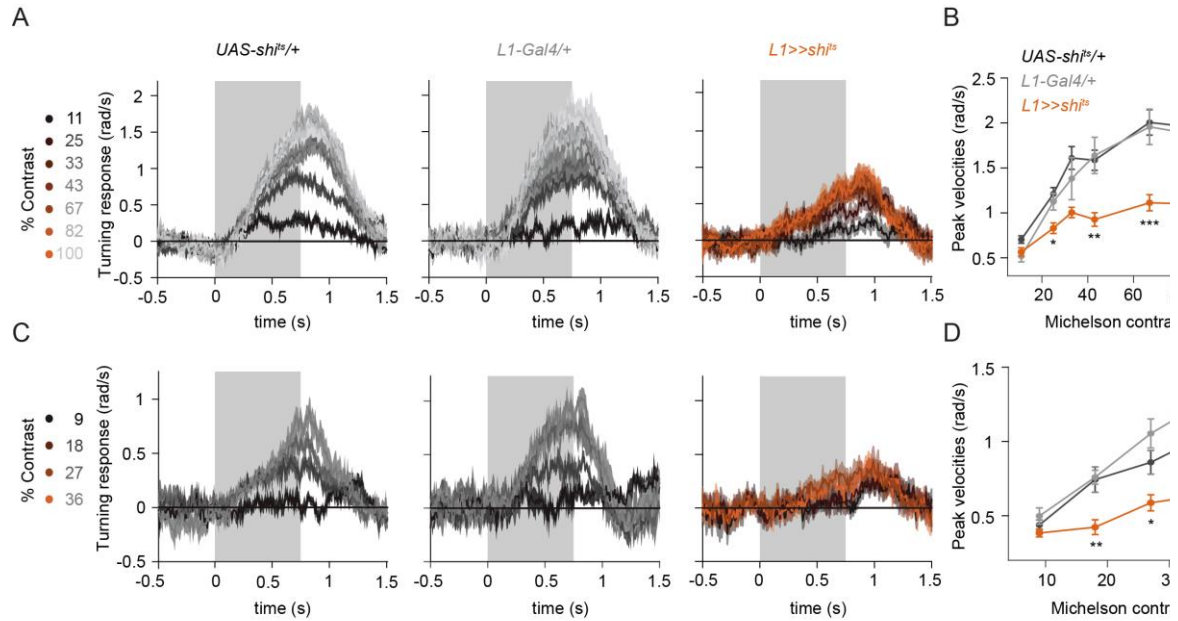
Figure S1: L1 is required for ON behavior across a range of contrasts. (A) Turning responses of the controls (gray) and L1-silenced flies (orange) in response to the moving ON edges of different contrasts, ranging from 11% to 100%. **(B)** Peak turning velocities quantified during the motion period, *p < 0.05, ***p < 0.01, ***p < 0.001, two-tailed Student's t tests against both controls. Sample sizes are n = 9 (*UAS-shi^ts/+, L1^c202a >>shi^ts*) and n = 5 (*L1^c202a-Gal4/+*). **(C)** Turning velocity time traces of the controls and L3-silenced flies in response to the moving ON edges of different contrasts, ranging from 9% to 36%. **(D)** Peak turning velocities quantified during the motion period, *p < 0.05, two-tailed Student's t tests against both controls. Sample sizes are n = 8 (*UAS-shi^ts/+*), n = 8 *(L1^c202a >>shi^ts*) and n = 5 (*L1^c202a -Gal4/+*). Traces and plots show mean ± SEM. The gray box region in (A) and (C) indicates motion duration.
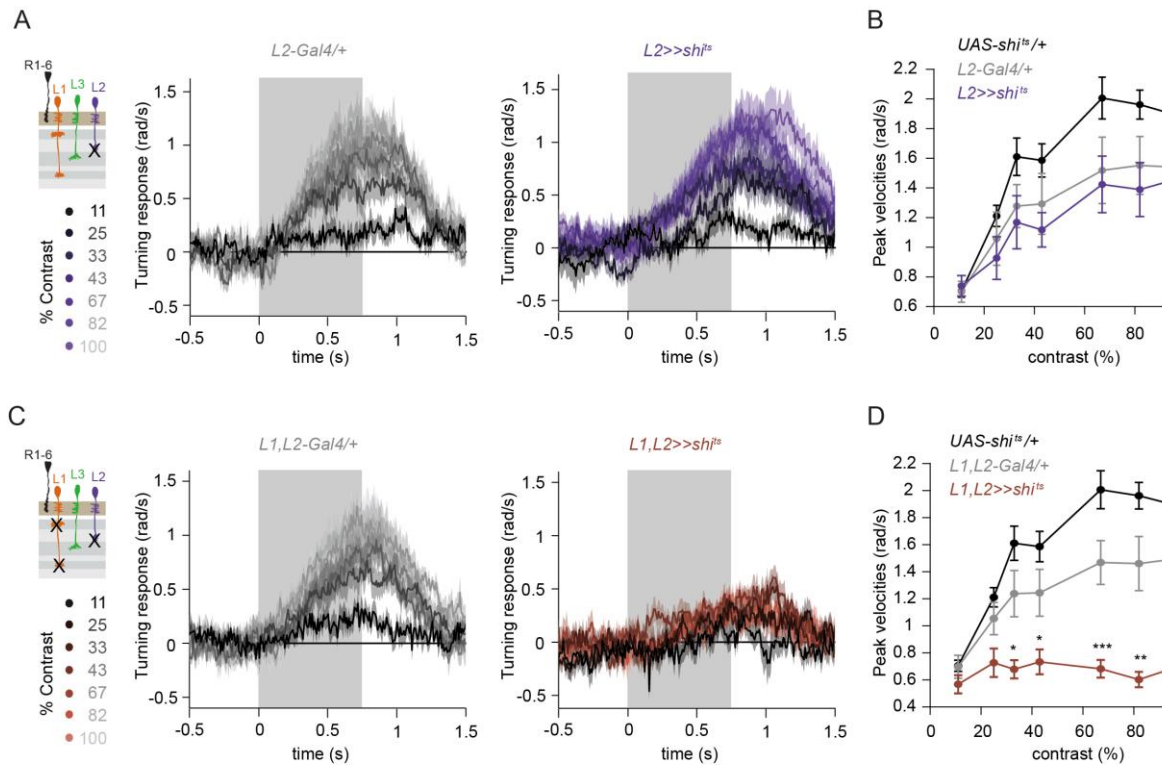
Figure S2: L1 and L2 together are required for ON behavior across a range of contrasts. (A) Turning velocity time traces of the Gal4 control (gray) and L2-silenced flies (purple) in response to the moving ON edges of different contrasts, ranging from 11% to 100%. **(B)** Peak turning velocities quantified during the motion period. Sample sizes are n = 9 (*UAS-shi^{ts}/+)*, n = 8 *(L2^{21Dhh} >>shi^{ts})* and n = 8 (*L2^{21Dhh}-Gal4/+*). **(C)** Turning velocity time traces of the Gal4 control and L1,L2-silenced flies (brown) in response to the moving ON edges of different contrasts, ranging from 11% to 100%. **(D)** Peak turning velocities quantified during the motion period, *p < 0.05, **p < 0.01, ***p < 0.001, two-tailed Student's t tests against both controls. Sample sizes are n = 9 (*UAS-shi^{ts}/+),*n = 8 *(L1,L2 >>shi^{ts})* and n = 9 (*L1,L2 -Gal4/+*). Traces and plots show mean ± SEM. The gray box region in (A) and (C) indicates motion duration.

4.   Parallel input pathways in fly visual circuitry enables robust neuronal responses required for visually guided behaviors

Manuscript in preparation / ongoing work

Authors and affiliations

Sebastian Molina-Obando[1,2], Juan F Vargas-Fique[1], Burak Gür[1,2], Miriam Henning[1] and Marion Silies[1]

[1] Institute of Developmental Biology and Neurobiology, Johannes-Gutenberg University Mainz, 55128 Mainz, Germany.

[2] Göttingen Graduate School for Neurosciences, Biophysics, and Molecular Biosciences (GGNB) and International Max Planck Research School (IMPRS) for Neurosciences at the University of Göttingen, 37077 Göttingen, Germany

Contribution statement

Conceptualization: **SMO** and MS

Methodology: **SMO**

Software: **SMO**

Investigation: **SMO**, JVF, BG, MH

Visualization: **SMO**

Supervision: MS

Writing—original draft: **SMO**

Writing—review & editing: **SMO**, MS

Funding acquisition: MS

SMO performed the imaging experiments and behavioral experiments in all figures (Figure 1-5). JVF, BG and MH contributed to experiments (Figure 3). **SMO** analyzed all data and wrote the manuscript draft. **SMO** composed all figures.

4.1   Introduction

Sensory systems are robust in detecting diverse sensory features despite being challenged by constantly changing conditions. The detection and processing of these features has classically been assigned to specific neuronal pathways. Thus, feature detection has been studied by looking at responses of distinct neurons and how the sensory signal is transformed after each synaptic connection. How neurons are connected in these pathways is studied in the field of connectomics. Comparing wiring diagrams, or connectomes, across animals and systems have revealed common connectivity characteristics (Barsotti et al., 2021). One ubiquitous aspect to highlight is the existence of multiple and parallel connections between neurons. Since parallel connections offers multiple ways to convey information between two points, it is hypothesized that such circuit architecture leads to a robust feature detection.

In the *Drosophila* ON pathway, a parallel connectivity implements contrast selectivity. In brief, ON selectivity arises in ON medulla neurons downstream of lamina inputs (Behnia et al., 2014; Strother et al., 2017; Yang et al., 2016). Lamina interneurons L1, L2 and L3, diversify and distribute contrast and luminance information in both pathways (Ketkar et al., 2021). The ON-pathway neuron Mi1 receives parallel inputs from L1 and L3 (Takemura et al., 2013). Since these two lamina neurons contact other medulla neurons as well, which directly or indirectly connect to Mi1, the L1 and L3 pathways are multisynaptic. Furthermore, the functional implementation of ON selectivity in Mi1 is also multisynaptic and involves a distributed action of glutamate-gated chloride channels (GluCls) (Molina-Obando et al., 2019). Thus, the extraction of ON uses a parallel and multisynaptic circuit architecture. Here we test if this architecture underlies robustness by individual disruption or recue of different Mi1 input pathways. Complementing physiological experiments, if function emerges from patterns of connectivity is being tested by analysis of connectivity. Graph theory, a field in mathematics studying graphs, is being used for that purpose (Schlegel et al., 2021; Shih et al., 2015). Considering a neural circuit as a graph with nodes (neurons) and edges (connections), analyses can uncover patterns of information flow as well as critical nodes -or hubs- where parallel inputs converge. Since the wiring diagram for the ON pathway is available (Takemura et al., 2015, 2013) and includes all ON-pathway neurons so far described (Arenz et al., 2017; Meier and Borst, 2019; Strother et al., 2017), we use graph theory to predict impairments in behavioral responses upon hub neuron disruption. Altogether, this study, either through cell- or gene-type specific manipulations and connectome analysis, tests how parallel input pathways implement a robust function.

Here, a connectome analysis reveals Mi1 as a critical hub neuron for information flow, followed by other neurons, like L5. Measuring fly optomotor responses while genetically silencing the activity of single neurons, we confirm that Mi1 is required for ON behavior, as previously shown (Strother et al., 2017), but using a wider range of contrast and luminance conditions. Moreover, the relative behavioral impact of silencing L5 compared to silencing Mi1, correlates with connectome prediction. Using 2-photon calcium imaging to measure Mi1 responses while silencing the L1 and/or the L3 pathway, we show that these input pathways are not required to implement ON responses. A further connectome analysis complemented by transsynaptic mapping of postsynaptic partners uncovers L2-to-Mi1 indirect pathways involving L5, Lawf2 and T1 as candidate interneurons. Furthermore, with a gain of function experiments, we show that the GluCl pathway is sufficient to implement ON responses in Mi1. Altogether, this work shows that individual input elements are sufficient but not necessarily required to implement ON responses in Mi1. Our study reveals parallel input pathways converging on Mi1 and suggest that they are part of a degenerate circuit architecture.

4.2   Results

4.2.1   Connectomics' analysis to predict function

<u>Mi1 is an anatomical hub in the ON pathway</u>

The functionality of highly interconnected networks specially depends on nodes that, based on their local and global connectivity, act as critical components (Bullmore and Bassett, 2011; Fornito et al., 2016; Sporns, 2018). To identify critical convergence nodes in the ON-pathway circuitry (Figure 1A), we used a published medulla dataset retrieved from <u>NeuroNLP.Medulla (fruitflybrain.org)</u>, and analyzed intracolumnar connectivity across seven different medulla columns (e.g., home column Figure 1A-B) (see methods for detailed analysis). We first asked how interconnected a neuron (node in the graph) is with respect to all other neurons by quantifying the number of first (direct), second and third order connected partners (Figure 1B-C) as well as respective synaptic counts (Figure 1D). Out of eight medulla neurons in the ON-pathway microcircuitry, we found that Mi1 is the neuron with the most first-order postsynaptic partners and connections. Analyzing first and second order connections, we found that L5 has the most second-order connected partners and respective synaptic counts and C2 with the most third-order connections. To have a more

precise measure of local vs global connectivity, as well as information flow, we performed a graph analysis of centrality (Figure 1E-G). We found that Mi1 is the node with the highest local connectivity (Figure 1E), the highest global connectivity (Figure 1F) and the highest influence on information flow (Figure 1G). Furthermore, Tm3 and L5, although not so relevant in global connectivity (Figure 1F), are the most critical nodes after Mi1 for local connectivity (Figure 1E) and information flow (Figure G). Tm3 is the second node with more first-order inputs to other neurons, and L5, the one with more second-order connections (Figure 1C). Altogether, this analysis show that Mi1 is the most critical neuron in the ON pathway circuitry, followed by L5 or Tm3.
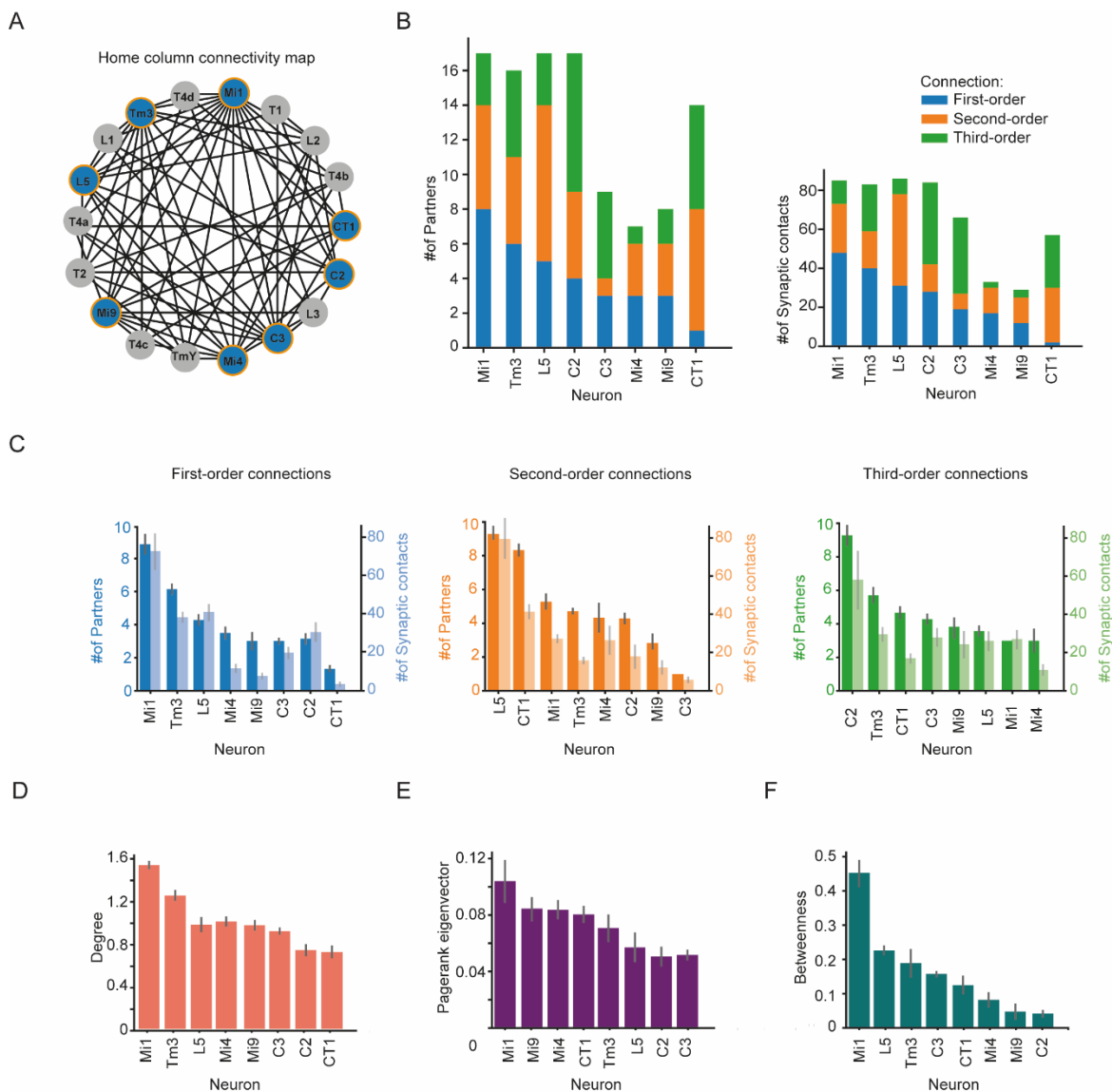
Figure 1: **Mi1 is an anatomical hub in the ON pathway. (A)** Network representation of the ON pathway circuit from the home column. Nodes of the network are neurons and edges their connections. All neurons included in the analysis are shown, with ON-pathway medulla neurons highlighted in blue. **(B)** Example quantification of first- (direct), second- and third-order connections in the home column. (C) Quantification of direct and indirect

number of partners and connections across seven medulla columns. **(D)** Degree of centrality to measure local connectivity. It gives for a node the fraction of nodes it is connected to, normalized by dividing by the maximum possible degree in a simple network n-1 where n is the number of nodes in the network (see methods). **(E)** PageRank eigenvector to measure unbiased global connectivity (see methods). **(F)** Betweenness centrality to measure information flow in a node (see methods). It is the sum of the fraction of all-pairs shortest paths that pass through the node.

4.2.2   Behavioral impact of circuit hub function

<u>Mi1 is required for ON behavior at different contrasts and luminances</u>

It has been proposed that function is an emergent property of network connectivity. If indeed this is true, and our connectome analysis allows to predict hub neurons for information processing, they should be functionally relevant for processing ON signals across conditions and their role be reflected in behavior. To test this, we measured visually guided ON behavior across different stimulus conditions while disrupting Mi1´s synaptic outputs. For that, we quantified turning behavior to visual motion stimuli of flies on a fly-on-a-ball assay. While doing so, we specifically silenced Mi1's activity by expressing Shibire[ts] (Kitamoto, 2001), a dominant-negative allele of dynamin that disrupts endocytosis and leads to neurotransmitter release disruption (Figure 2). First, we tested fly behavior with 100% Michaelson contrast ON edges moving at 5 different luminances. While control flies turned in the direction of the moving edge at all luminances, Mi1-silenced flies barely turned to the moving edge across conditions and their peak velocities were significantly impaired at all luminances (Figure 2A-B). To test if Mi1´s role generalizes to other contrasts steps, we showed the flies moving ON edges ranging from 11 to 100% Michaelson contrast (Figure 2 C-D). While control flies turned to all contrast steps and their response scaled with contrast, Mi1-silenced flies showed significant turning deficits at different contrasts steps (Figure 2C-D).

If the measures of connectivity and centrality allow to predict relative function between neurons, L5 should also contribute to ON behavior, but be less relevant as compared to Mi1. To test this, we measured visually guided ON behavior while disrupting L5 under the same conditions used with Mi1 silenced flies. Both control and L5 silenced flies turned equally fast to all ON moving edges at five different luminances (Figure 2E-F). When flies were shown different ON contrasts steps (Figure 2G), L5 silenced flies turned overall less than controls with peak quantifications showing significant differences at some contrasts (Figure 2H). Thus, L5 also contributes to contrast coding in the ON pathway. Importantly, the impact of silencing L5 is smaller compared to blocking the outputs of Mi1, confirming the prediction made by the connectome analysis. Altogether, our behavioral data confirm

that connectivity and centrality measures correlate with the functional importance of these neurons for ON behavior.
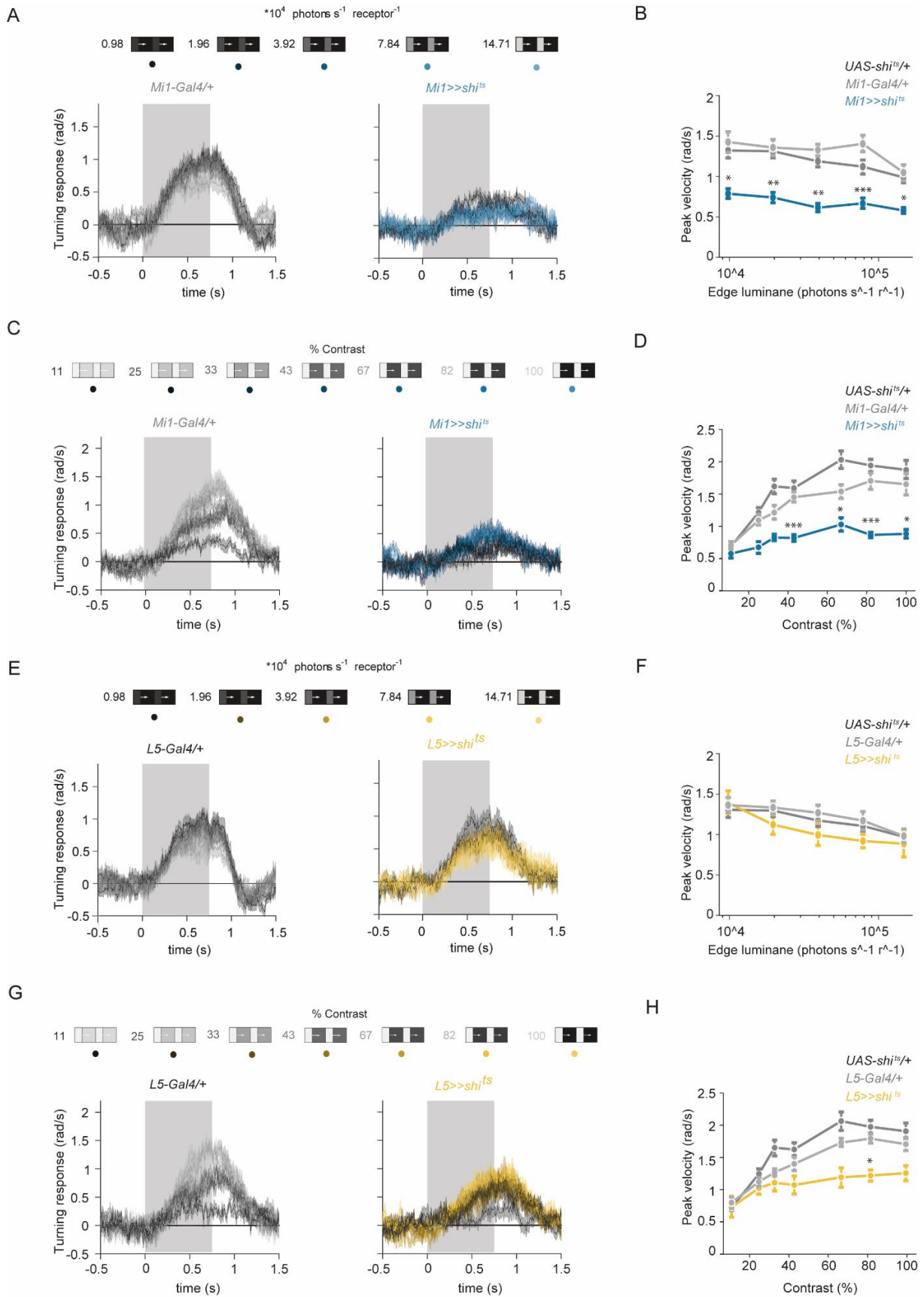
Figure 2: **Mi1 is required for ON behavior at different contrast and luminances. (A)** Turning responses of flies where Mi1 was silenced (blue) and Gal4 control (grey) color-coded according to 100% contrast ON edge at five different luminances. **(B)** Peak velocities quantified for each of the five edges during the motion period, *p < 0.05, **p < 0.01, ***p < 0.001, two-tailed Student's t tests against both Gal4 and UAS controls. Sample sizes are n = 8 *(Mi1>>shi^ts)*, n = 6 (*Mi1-Gal4/+*), and n = 10 (*UAS- shi^ts*). **(C)** Turning responses of the control (grey) and Mi1-silenced flies (blue) in response to the moving ON edges of different contrasts, ranging from 11% to 100%. **(D)** Peak turning velocities quantified during the motion period, *p < 0.05, ***p < 0.001, two-tailed Student's t tests against Gal4 and UAS controls. Sample sizes are n = 8 (*Mi1 -Gal4/+, Mi1 >>shi^ts*) and n = 9 (*UAS-shi^ts/+*). **(E)** Turning responses of flies where L5 was silenced (mustard) and Gal4 control (grey), color-coded according to 100% contrast ON edge at five different luminances. **(F)** Peak velocities quantified for each of the five edges during the motion period, *p < 0.05, **p < 0.01, ***p < 0.001, two-tailed Student's t tests against both Gal4 and UAS controls. Sample sizes are n = 8 *(L5>>shi^ts)*, n = 9 (*L5-Gal4/+*), and n = 10 (*UAS- shi^ts*). **(G)** Turning responses of the control (grey) and L5-silenced flies (mustard) in response to the moving ON edges of different contrasts, ranging from 11% to 100%. **(H)** Peak turning velocities quantified during the motion period, *p < 0.05, ***p < 0.001, two-tailed Student's t tests against both Gal4 and UAS controls. Sample sizes are n = 7 (*L5 -Gal4/+, Mi1 >>shi^ts*) and n = 9 (*UAS-shi^ts/+*).

4.2.3   Parallel inputs behind ON contrast detection

<u>L1 and L3 are not required for ON responses in Mi1</u>

Mi1 appears to be a critical convergence of parallel information from the lamina. If these different pathways are there to individually implement ON responses in Mi1, single pathway inputs would not be required for Mi1´s activity. To address this, we silenced the two first order (direct) inputs L1 or L3 while measuring Mi1 ON responses. For that, we visually stimulated the flies with 100% contrast 5 second ON flash while recording Mi1 calcium signals. Mi1 control responses to the ON flash show an initial transient peak followed by a plateau (Figure 3) (Behnia et al., 2014; Molina-Obando et al., 2019; Yang et al., 2016). L1-silenced flies show similar response trace as compared to controls and quantification of the ON step and the plateau amplitudes show no significant difference (Figure 3A-B). This shows that acute silencing of L1 is not required for Mi1 responses. Similarly, when L3 neurons were silenced, there was no change in response trace and quantification of ON step and plateau (Figure 3C-D) compared to controls, showing that this second direct lamina input is also not individually required. Interestingly, when L1 and L3 were silenced together, ON responses in Mi1 also remained (Figure 3 E-F), arguing that indirect inputs, independent of L1 and L3 function, are also required to implement ON responses in Mi1. Altogether, we show that the L1 and L3 pathway inputs are neither individually nor together required for Mi1 responses.
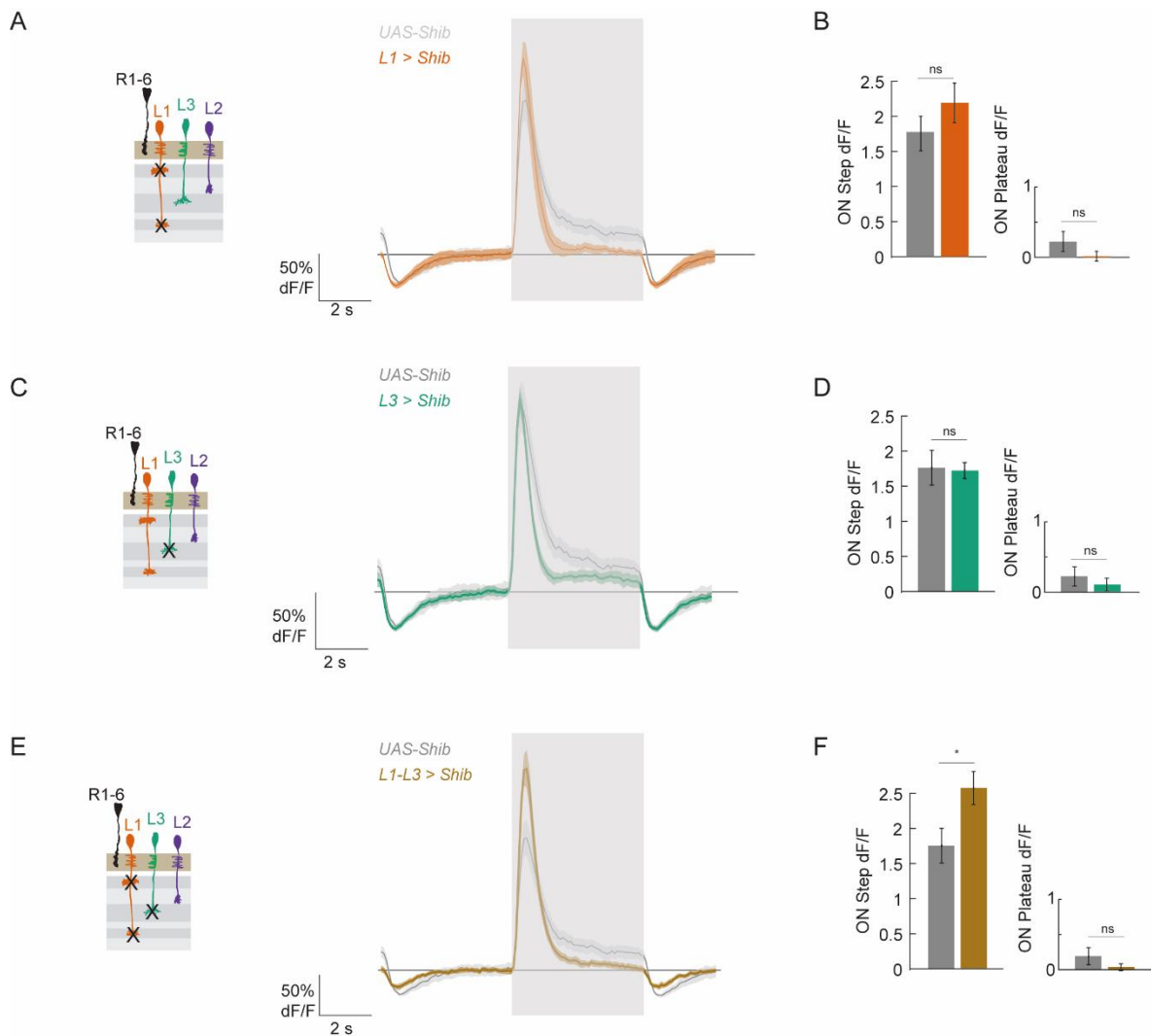
Figure 3: **L1 and L3 are not required for ON responses in Mi1. (A)** Mi1 ON calcium responses to a 5 second ON flash where L1 was silenced (orange) and its UAS control (grey). Sample sizes are n = 5(85) *(L1>>shi^{ts})*, and n = 8(92) (*UAS- shi^{ts}*). **(B)** Quantification of the ON step and plateau amplitudes, n.s. = p>0.05, two-tailed Student's t tests between L3 silencing and controls. **(C)** Mi1 ON calcium responses to a 5 second ON flash where L3 was silenced (green) and its UAS control (grey). Sample sizes are n = 7(70) *(L3>>shi^{ts})*, and n = 8(92) (*UAS- shi^{ts}*). **(D)** Quantification of the ON step and plateau amplitudes, n.s. = p>0.05, two-tailed Student's t tests between L3 silencing and controls. **(E)** Mi1 ON calcium responses to a 5 second ON flash where L1 and L3 were silenced (gold) and its UAS control (grey). Sample sizes are n = 7(82) *(L1,L3>>shi^{ts})*, and n = 8(92) (*UAS-Shib*). **(F)** Quantification of the ON step and plateau amplitudes, n.s. = p>0.05, two-tailed Student's t tests between L3 silencing and controls. Sample size shows #flies(#cells).

L5, T1 and Lawf2 are candidate interneurons connecting L2 and Mi1

In alignment with an implementation of function by different input pathways, Mi1 is highly interconnected with other neurons (Takemura et al., 2013). Recent behavioral experiments uncovered L2 as an ON-pathway input (Ketkar et al., 2021). Since L2 does not directly synapses onto and Mi1, indirect connections between L2 and Mi1 might implement ON

responses. To identify putative interneurons, we analyzed all neuronal paths from L2 to Mi1 (see methods). High network interconnectivity will allow to always find an indirect connection between all neurons in a circuit. The total number of uncovered paths and path length will eventually exceed what is biologically plausible. Therefore, we concentrated on shorter paths that included the maximum number of synapses. For that, for each path we summed the synaptic counts along the path and normalized this quantity by the path length (number of synapses along the path) before we ranked them. This analysis revealed T1 and L5 as candidate interneurons participating in significantly higher-ranked paths, with L5 as direct Mi1 input in both cases (Figure 4A). We also used a different approach to uncover interneurons directly downstream of L2 that might not be yet represented in the connectome. We used the genetic tool trans Tango (Talay et al., 2017) which allows the genetic labeling of postsynaptic neurons of L2. We marked L2 with myrGFP and its postsynaptic partners as revealed by transTango with tdTomato. This identified L5 and Lawf2 as neurons projecting to layers where Mi1 dendrites are located, and T1 as a neuron projecting to layer M2, where L5 projections lay (Figure 4B-C).
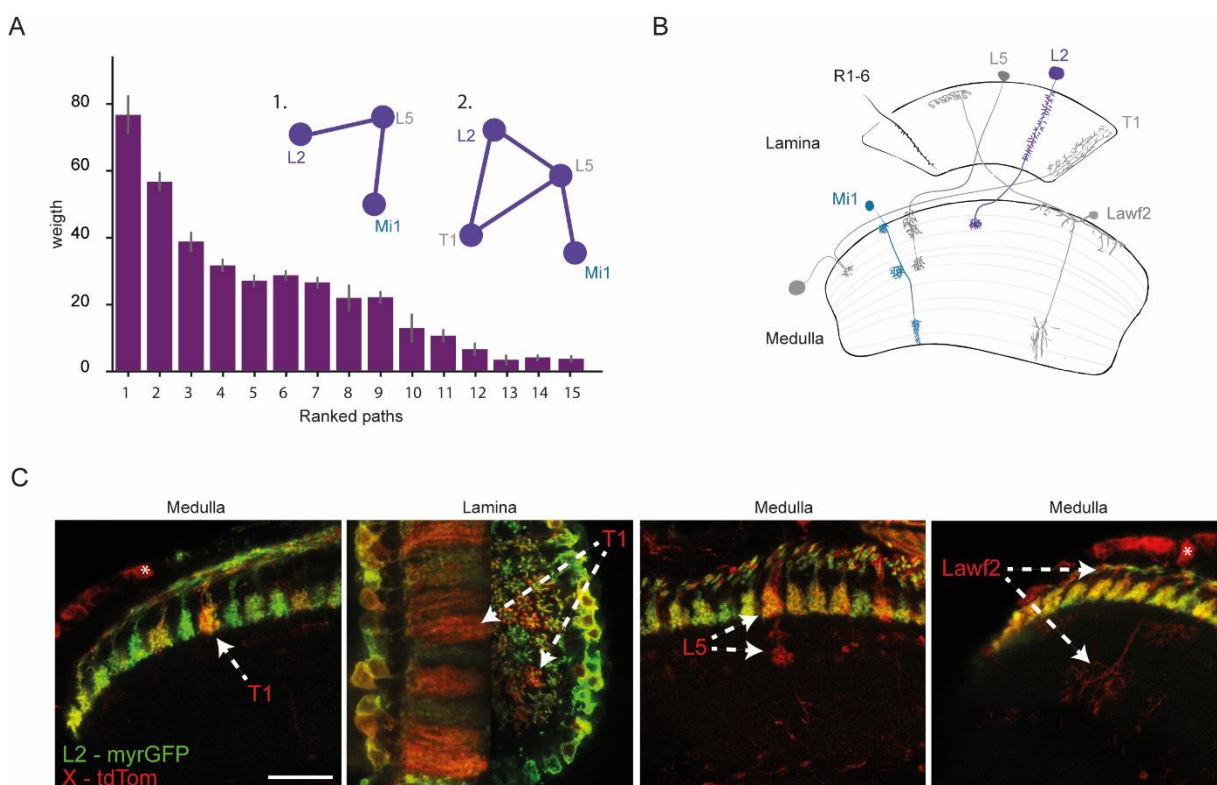
Figure 4. **L5 and T1 are candidate interneurons between L2 and Mi1. (A)** Weight-ranked neuronal paths between L2 and Mi1. Inset, path representation of significantly high-ranked paths. **(B)** Schematic of candidate neurons (gray) belonging to a functional input pathway between L2 (purple) and Mi1 (blue). **(C)** L2 (green) postsynaptic partners (red) uncovered by trans-Tango (Talay et al., 2017). White arrows point to the neuronal projections of identified postsynaptic partners. Asterisk marks the cell body. Scale bar = 20 um.

An Mi1 input pathway that is not required for ON responses is sufficient under distinct conditions

Parallel input pathways appear to be in place to implement ON responses in Mi1 neurons, and their individual action might implement ON responses. To test this, we next asked whether an input, although not being individually required to implement ON selectivity is sufficient. For that, we made use of the finding that ON responses in Mi1 are broadly dependent on the glutamate-gated chloride channel *GluClα* (Molina-Obando et al., 2019). We used this system to selectively restore *GluClα* just in Mi1 and thus asked whether just the direct glutamatergic inputs to Mi1 could be sufficient for Mi1 function. For that, we rescued *GluClα* expression in *GluClα* mutant flies specifically in Mi1 and compared Mi1 responses to a control condition with all inputs intact (Figure 5A). We first asked if both spatial and temporal properties of Mi1 could be rescued. Flies, adapted to an intermediate luminance level, were stimulated with 5° ternary noise bars in azimuth changing in luminance every 50ms (see methods). To extract space-time receptive fields (STRFs), we computed the response reverse correlation with the stimulation. Mean STRFs across neurons was computed by a center-alignment of response maximum of individual cells. For both control and rescue flies, Mi1 responses showed a positive correlation (red) with stimulus increments (ON) in the receptive field (RF) center, as previously described (Arenz et al., 2017), (Figure 5B, left). Time and space filters showed no differences between controls and rescued flies (Figure 5B, right). These data indicates that direct glutamatergic inputs are sufficient for ON spatial and temporal properties.

Robustness in feature detection implies that the circuit properly does its job despite of ever-changing conditions. To address this, we tested if these glutamatergic inputs were also sufficient under distinct, challenging scenarios. First, we measured Mi1 ON responses in suddenly changing luminances. For that, we visually stimulated flies with a 100% Michaelson contrast sinusoidal moving at 1 cycle per second (1hz) at five different luminances (Figure 5C). The sinusoidal wave moved for four seconds preceded and followed by 4 seconds of dark adaptation. Both control and rescued flies showed an increase in Mi1´s calcium response during stimulation bouts (increase in mean response) and their contrast responses followed the 1hz oscillation frequency of the stimulation (1hz osc.), generating 4 local maximums in four seconds (Figure 5C). To measure how well the response could follow the stimulation, we quantified the power of the 1hz component in Fourier space. Control and rescue flies elicited the same 1 Hz power and the same mean response amplitude across luminances (Figure 5D). This data first reveals that Mi1 elicits luminance-invariant responses to 100% contrasts, a computation that likely relies on several

inputs. Importantly, direct glutamatergic inputs can fully rescue response under changing conditions.

Since flies encounter not only changes in overall luminance but other conditions can challenge contrast detection in their natural environments, we then asked if a single input could also be sufficient to encode contrast responses at different noise levels. For that, we kept an intermediate level of luminance while presenting a 100% Michaelson contrast sinusoidal moving at 1 cycle per second (1hz) at five different noise levels. Mi1 responses scaled with noise, having higher 1 Hz oscillations at lower noise levels, while mean response across bouts remained constant (Figure 5E). Both control and rescue flies elicited the same 1 Hz power and the same mean response amplitude across contrasts (Figure 5F). This indicates that direct glutamatergic inputs are also sufficient to encode contrast responses at different levels of noise.

Our data and previous research have shown that Mi1 response to an ON flash has two components: a transient peak and a sustained plateau (Behnia et al., 2014; Molina-Obando et al., 2019; Yang et al., 2016). The plateau component suggest that Mi1 could carry information about overall luminance, as shown for the sustained components of lamina neurons L1 and L3 (Ketkar et al., 2021, 2020). To test if indeed Mi1 carries luminance information, we visually stimulated flies with different, randomly interleaved, luminance steps. The responses of single Mi1s, for both control and rescued conditions seem to increase and decrease following the stimulation (Figure 5G). To measure this, we quantified the response amplitude at the end of each stimulus luminance step (Figure 5H). Mi1 responses show a luminance dependency, being higher at high luminances. Importantly, responses were similar in both controls and rescued flies (Figure 5H), suggesting that direct glutamatergic inputs are also sufficient for luminance encoding. Taken together, these findings reveal that direct glutamatergic inputs to Mi1 are sufficient to implement ON responses under distinct conditions. In sum, our data supports that anatomically distinct parallel pathways can mediate the same (or very similar) function, here ON responses, in a critical ON pathway neuron which is required for visually guided ON behavior. This aligns with the idea that neuronal circuits are degenerate.

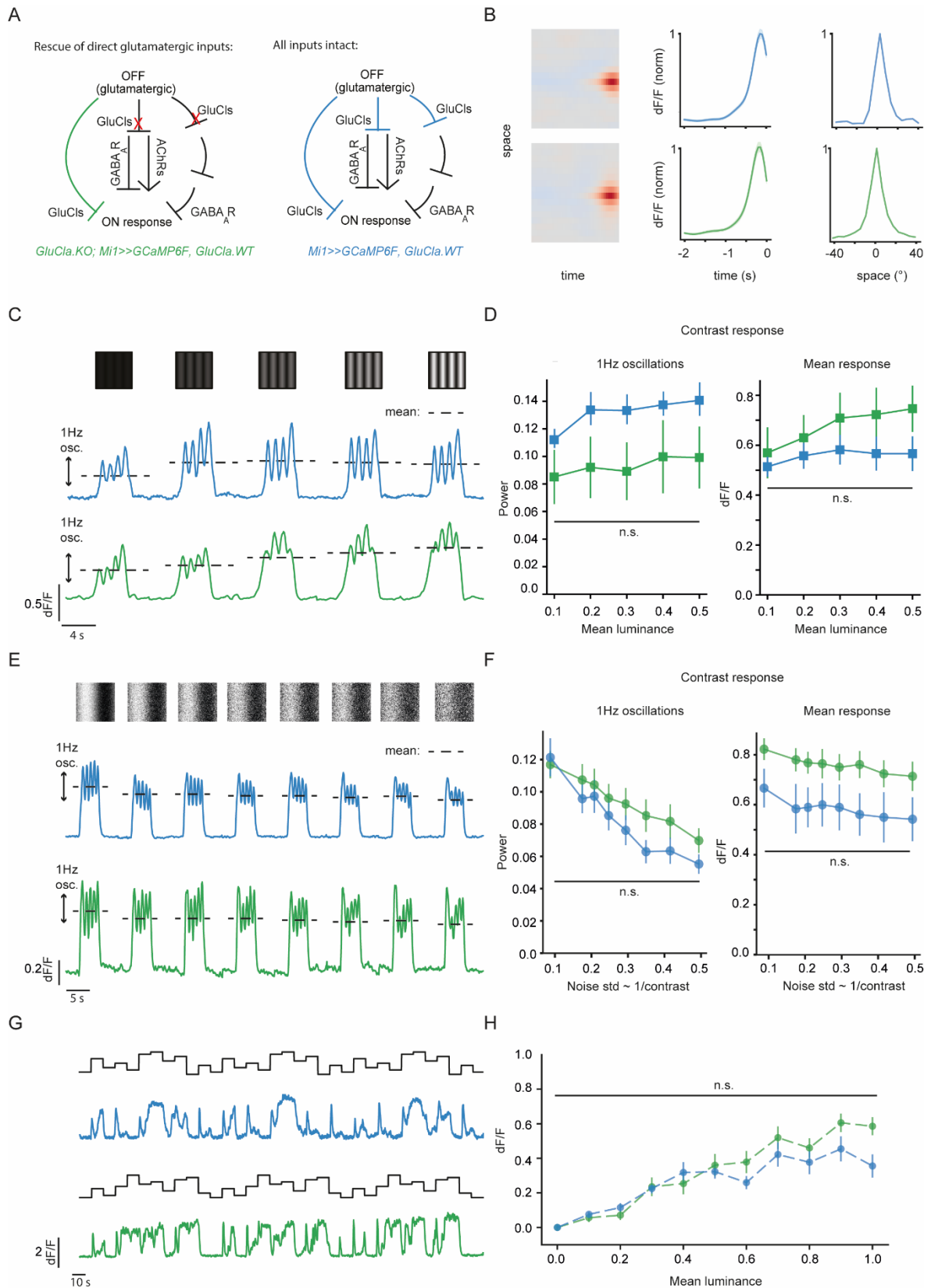Figure 5. **An Mi1 input pathway is sufficient for ON responses under distinct conditions. (A)** Schematic representation of the two compared circuit scenarios behind ON responses, based on the functional implementation of ON selectivity proposed in (Molina-Obando et al., 2019). Left, circuit schematic for rescue flies. Rescue of all direct *GluClα* -mediated inputs, in a *GluClα* mutant fly, is shown in green, whereas the

remaining disrupted inputs are marked with a red X. Right, circuit schematic for control flies. Intact *GluClα* - mediated inputs are in blue for the sake of comparison with rescue flies. For both circuit schematics, other cholinergic and GABAergic inputs are depicted in black, based on the current knowledge of neurotransmitter identity of, and receptor expression in ON-pathway neurons (Davis et al., 2020). **(B)** Space- time receptive fields (STRF) and filters of Mi1. Rescued flies in green, n= 11(97), control flies in blue, n=9(94). **(C)** Single region of interest (ROI) example traces of Mi1 responses to 100% Michaelson contrast moving sinusoidal at 5 different luminances for rescued flies (green) and controls (blue). **(D)** Quantification of 1hz response oscillations and baseline across conditions and genotypes. Rescued flies in green, n= 10(72), control flies in blue, n=10(68). **(E)** Single ROI example traces of Mi1 responses to a moving sinusoidal at 7 different noise levels for rescued flies (green) and controls (blue). **(F)** Quantification of 1hz response oscillations and baseline across conditions and genotypes. Rescued flies in green, n= 13(105), control flies in blue, n=12(67). **(G)** Single ROI example traces of Mi1 responses to 11 different luminance steps for rescued flies (green) and controls (blue). **(H)** Quantification of response amplitude of plateau responses across mean luminance. Rescued flies in green, n= 8(105), control flies in blue, n=6(52). Sample size indicates #of flies (#of cells). n.s. = p>0.05, two-tailed Student's t tests between rescued flies and controls.

4.3 Discussion

Our work uncovers Mi1 as a critical neuron in the ON pathway, being required for ON behavioral responses across contrasts and luminances. This aligns with a prediction using graph theory analysis. Direct, and parallel lamina input pathways downstream of L1 and L3 are not required for ON responses in Mi1. Further connectome analysis and neuronal labeling proposes L2 as an indirect input pathway engaging L5, T1 and/or Lawf2 interneurons. Finally, although direct glutamatergic inputs are not required, these inputs are sufficient for Mi1 ON responses properties under different scenarios. Altogether, we provide evidence that parallel connectivity is in place to implement ON responses and suggest that the ON-pathway circuit is degenerate.

<u>Prediction of function by connectivity</u>
Our connectome analysis predicted Mi1 as the most critical neuron in the ON-pathway microcircuitry, followed by other neurons, for example, L5 or Tm3. This prediction was then functionally confirmed by our behavioral experiments. Along the same lines, previous research also showed that silencing Mi1 has a greater impact in ON behavior than silencing Tm3 (Strother et al., 2017). Thus, the actual impact on visually guided behaviors in *Drosophila* correlates with graph theory measures, in the connectome of the visual circuitry. In this study, we have used as a main predictor of function the number of synaptic contacts between neurons. We ran some graph theory analyses of centrality that were relevant to capture a broad impact in the network by each neuron. Thus, we made emphasis in global

connectivity, testing the information flow in a network, and identifying critical hub neurons acting as main circuits outputs. However, we still lack some detail in how to predict function of specific parallel input pathways converging in the hub neuron. There are other types of analysis that could give an more detail description in that sense and which are also being used to identify the relationships between structure and function. For example, symmetric group factorization has been recently used in *Caenorhabditis elegans* neuronal network to assign broad functional categories to sectors of neuron and to predict the function of finer structures inside these sectors (Morone and Makse, 2019). Other graph theory analysis can be used to reveal other details of network components, such as using node polarity to identify main "senders" and "receivers", or edge betweenness to measure the importance of each connection, among others (Shih et al., 2015). Finally, attempts to reconcile the idea of "orders" (e.g., first-, second-, or third-order interneurons) into groups that are closer to the actual impact of synaptic strengths in the circuits also exist. For example, a probabilistic graph transversal model can be used to step through all neuronal connections and group neurons into different layers (Schlegel et al., 2021). We think that these new methods will help to bring connectomes analysis closer to physiological experiments and test if indeed function can be fully predicted by the underlying anatomy.

<u>The implementation of ON selectivity in the ON pathway is not L1-dependent</u>

Previous work in the field had assumed that L1 was the main lamina input to the ON-pathway (Borst et al., 2020; Clark and Demb, 2016; Yang and Clandinin, 2018) and, since L1 is the only glutamatergic lamina neuron (Davis et al., 2020; Takemura et al., 2011), that glutamatergic pathways implementing the signal inversion in the ON pathway where all downstream of L1 (Molina-Obando et al., 2019). However, in the second study we showed that L1 is not alone required for ON behavior across luminance and that L2 and L3 further contribute to ON behavior (Ketkar et al., 2021). Moreover, here we show that L1 is not required for ON responses in Mi1 (Figure 3). Altogether, this suggest that there is a wider implementation of the signal inversion in the ON pathway by glutamatergic synapses downstream of L2 and/or L3. Connectomics data support this idea. For example, indirect pathways to Mi1 include Mi9, a glutamatergic neuron depolarizing to OFF. Thus, an inhibitory input from Mi9 could also implement the signal inversion in the ON pathway, in addition to the direct glutamatergic Mi-input L1. Moreover, glutamatergic widefield neurons, which project to layers where L2, L3 and Mi1 neural projections locate, might provide direct glutamatergic inhibition to Mi1 (Davis et al., 2020; Nern et al., 2015). Similarly, in the vertebrate retina, GABAergic and glycinergic inhibitory neurons connect neurons that depolarize to OFF (OFF-BCs) to ON responding BCs. We suggest that the signal inversion

in the ON pathway relies on multiple OFF depolarizing neurons and that this might be a common architecture in the vertebrate retina too.

<u>Multiple pathways between two neurons</u>

L1 and L3 were neither individually nor together required for ON responses in Mi1. L2 is the remaining first-order interneuron that can pass information from photoreceptors to the downstream circuitry in the medulla. Since L2 is not a direct synaptic partner of Mi1, we looked at all indirect connection pathways (Figure 3) that might have a functional impact in Mi1 and found candidate interneurons L5, T1 and Lawf2. A functional characterization of these neurons does not exist but RNA seq data (Davis et al., 2020) suggests that Lawf2, L5 and T1 are GABAergic, whereas Lawf2 and L5 cholinergic. If the cholinergic L2 excites these neurons during OFF, an inhibitory GABAergic connection might be able to implement a signal inversion for an ON response. In fact, GABAergic inhibition has been shown to playing a role in establishing ON selectivity (Molina-Obando et al., 2019) but the GABAergic neurons behind have not been uncovered. The described neuronal paths between L2 and Mi1 remind to a recurrent circuit motif referred as to feedforward loop (FFL).

This deserves a bit of attention since network motifs, defined as recurrent and statistically significant subgraphs or patterns in that larger graph, the circuit (Masoudi-Nejad et al., 2012; Milo et al., 2004), are directly linked to function. In FFL motifs, two inputs, one regulating the other, joint together to regulate a third one. Depending on the type of interactions between pairs (e.g., excitation vs inhibition or ON vs OFF), the FFL motif can have eight possible combinations. Four of those combinations act coherently and can implement sign-sensitive delays. The other four, acting incoherently, can speed up the response time of the target following stimulus steps in one direction (e.g., OFF to ON) but not in the other direction (e.g., ON to OFF) (Mangan and Alon, 2003). In our network downstream of L2, the two main inputs -T1 and L5-, one regulating the other, jointly regulate Mi1. It is not possible though to make a prediction of which type of FFL (coherent or incoherent) they might implement since future experiments need to confirm T1 and L5 response polarity as well as the excitatory or inhibitory relationship between them and with Mi1. The detection of this specific network motif in one parallel input pathway motivates to employ advance analysis (Masoudi-Nejad et al., 2012) to uncover other type of motifs in all parallel input pathways. These analyses can complement graph theory analysis mentioned above, offering more power to test if function indeed emerges from anatomy.

Inputs can be sufficient but not required

A previous study showed that direct glutamatergic inputs through GluCls where not required for ON responses in Mi1 (Molina-Obando et al., 2019). Here we show that the same inputs are sufficient to rescue the temporal and spatial properties of Mi1 as well as its ON responses under various challenging conditions. It was striking that our reduced system kept a robust implementation of ON selectivity. In *Drosophila* behavior, similar functionality has been observed: the L1 and the L3 pathways although not being required, are sufficient to guide behavioral responses to ON (Ketkar et al., 2021). Importantly, for both cases, these parallel input pathways engage different neurons and neurotransmitter systems. Thus, they cannot be considered redundant. Instead, they are non-identical components performing the same function. This is referred to as degeneracy (Edelman and Gally, 2001; Tononi et al., 1999). In a degenerate circuit, distinct components support the stability of a single output and individual components contribute to the stability of multiple distinct outputs. Reinforcing the existence of degeneracy, in other neuronal systems it has been observed that several neurons often contribute to similar computations (Beverly et al., 2011; Koo et al., 2011; Trojanowski et al., 2014), and that neurons can also contribute to multiple computations within one or more circuits (Li et al., 2014; Liu et al., 2018). In these one-to-multiple and multiple-to-one relationships, inputs that are not required but sufficient provide stability and lead to robust neuronal responses.

4.4   Methods

Fly husbandry

All flies were raised at 25 ºC and 65 % humidity on standard molasses-based fly food while being subjected to a 12:12h light-dark cycle. Two-photon experiments were conducted at room temperature (20 ºC) and behavioral experiments at 34 ºC. Female flies 2-4 days after eclosion were used for all experimental purposes. Mi1 and L5 driver lines used for expression of UAS-*shi[ts] and UAS-GluCla*^{WT} constructs were a Gal4 split lines (Strother et al., 2017; Tuthill et al., 2013), and lamina neuron driver lines used for genetic silencing were *L3*^{0595}-*Gal4* (Silies et al., 2013) and *L1*^{C202a}-*Gal4* (Rister et al., 2007). *UAS-shi[ts], was* from BDSC (#27380) and UAS-GluCla^{WT} was developed in this study. We use GluCla disrupted (D) line (Molina-Obando et al., 2019) in trans to GluCla.MiMIC^{14426} null allele from BDSC (#59515) For imaging experiments, GCaMP6f (BDSC #42747) was expressed using *Mi1-LexA* line (Pfeiffer et al., 2010). For trans-Tango experiments, we used *L3*^{0595}-*Gal4* (Silies

et al., 2013), *L2²¹ᴰʰʰ-Gal4* and *L1ᶜ²⁰²ᵃ-Gal4* (Rister et al., 2007), and trans-Tango line was from BDSC (#77124). Detailed genotypes are given in Table 1.

Table 1.: Genotypes used in this study.

Name	Genotype	Figure
Behavior		
Mi1 silencing	*w+; R19F01-p65ADZpattP40 / +; R71D01- ZpGdbdattP2 / UAS- shi^{ts}*	Fig 2
Mi1-Gal4 control	*w+; R19F01-p65ADZpattP40 / +; R71D01- ZpGdbdattP2 / +*	Fig 2
L5 silencing	*w+; R64B07-p65ADZpattP40 / +; R37E10- ZpGdbdattP2 / UAS- shi^{ts}*	Fig 2
L5-Gal4 control	*w+; R64B07-p65ADZpattP40 / +; R37E10- ZpGdbdattP2 / +*	Fig 2
UAS-shibire^{ts} control	*w+; + / +; UAS-shi^{ts} / +*	Fig 2
2-photon calcium imaging		
L3 silencing	*w+; R19F01-LexAattP40, lexAop2-IVSGCaMP6fp10 su(Hw)attP5 / +; L3⁰⁵⁹⁵-Gal4 /UAS- shi^{ts}*	Fig 3
L1 silencing	*w+; L1^{c202a}-Gal4 / R19F01-LexAattP40, lexAop2-IVSGCaMP6fp10 su(Hw)attP5 ; + /UAS- shi^{ts}*	Fig 3
UAS-shibire^{ts} control	*w +; R19F01-LexAattP40, lexAop2-IVSGCaMP6fp10 su(Hw)attP5 /+ ; UAS-shi^{ts} / +*	Fig 3
L1, L3 silencing	*w+; L1^{c202a}-Gal4 / R19F01-LexAattP40, lexAop2-IVSGCaMP6fp10 su(Hw)attP5; L3⁰⁵⁹⁵-Gal4 /UAS- shi^{ts}*	Fig 3
Mi1 GluClα rescue	*w+; R19F01-LexAattP40, lexAop2-IVSGCaMP6fp10 su(Hw)attP5 / R19F01-p65ADZpattP40; GluClα^{FlpStop.D},UAS-GluClα^{WT}/ R71D01- ZpGdbdattP2, Mi{PTGFSTF.1}GluClα^{Mi14426}*	Fig 5
Mi1 control	*w+; R19F01-LexAattP40, lexAop2-IVSGCaMP6fp10 su(Hw)attP5 / R19F01-p65ADZpattP40; GluClα^{FlpStop.D},UAS-GluClα^{WT}/ R71D01- ZpGdbdattP2*	Fig 5

Confocal imaging		
L2 trans-Tango	*y[1] w[*] P{y[+t7.7] w[+mC]=UAS-myrGFP.QUAS-mtdTomato-3xHA}su(Hw)attP8; P{y[+t7.7] w[+mC]=trans-Tango}attP40/ +; L2^{21Dhh}-Gal4 /+*	Fig 4

Generation of transgenic lines

The transgenic line carrying the UAS-GluClα^{WT} cassette for gene overexpression was generated according to standard procedures. In brief, embryos carrying the attP1 construct on the third choromosome (3R, 87B13, BL34760) were injected with the UAS-GluClα^{WT} cassette and PhiC31 integrase. Embryos were dechorionated in 50% bleach (DanKlorix) for 3 min, followed by washing in a buffer (100 mM NaCl, 0.02% Triton X-100) for 3 min. Injections were done on a Nikon AZ100 microscope using a FemtoJet 4i (Eppendorf AG, Hamburg, Germany). The injection mix (20 µl) consisted of 10 µg of the UAS-GluClα^{WT} cassette, 6 µg of helper DNA (pBS130 containing the PhiC31 integrase) and 4 µl of 5x injection buffer (25 mM KCl, 0.5 mM NaH2PO4, pH 6.8, 1% phenol red [Sigma Aldrich]). Injection needles were pulled from quartz glass microcapillaries (10 cm length, 1.0mm outside diameter, 0.5mm inside diameter, Sutter Instruments, USA) using a P-2000 micropipette puller (Sutter Instruments, USA). Needles were sharpened using a capillary grinder (Bachofer, Germany). After injection, embryos were covered with 10S Voltalef oil and incubated at 18°C until larval hatching. Successful recombinase-mediated cassette insertion was scored by red eye color and verified by single fly PCR, testing for the present of the loss of the UAS-GluClα^{WT} cassette.

Connectome analysis

Connectome analysis was done with a custom-written code in Python 3.7 (Rossum and Drake, 2010), employing the graph analysis package Networkx (Hagberg et al., 2008). Briefly, a published connectome of seven medulla columns (Takemura et al., 2015, 2013) was used as data source to analyze the ON pathway circuit that implements ON direction selectivity. For that, lamina inputs L1-3, medulla intracolumnar neurons belonging or closely related to the ON pathway, and their common output neuron T4 were defined as nodes in a graph. All the corresponding synaptic counts between pairs were defined as edges in a graph, with higher numbers of synaptic counts representing smaller distances between nodes. Direct and indirect connection partners and synaptic counts were calculated for every node in the network. Moreover, three measured of centrality were perform per each graph. First, the node degree, one of the basic centrality measures, was used to calculate local connectivity. It is equal to the number of nodes neighbors, thus the more neighbors a

node has, the more it is central and highly connected. Second, eigenvector centrality was used to assess global connectivity. The eigenvector centrality takes into consideration the nodes degree but going a step further by also considering the degree of the neighbors. To avoid hub biases, the eingenvector centrality was Pageranked. This means that the number and quality of connections to a node was counted to determine a rough estimate of how important the node is. The underlying assumption is that more important nodes are likely to receive more connections from other nodes. And third, betweenness centrality was calculated as a measure for information flow. It measures the percentage of shortest paths where the node lies. Thus, a node with a high value for betweenness centrality will have more influence over the information passing between other nodes. This means that removing this node from the network will disrupt most of the connections between nodes. Finally, all possible paths between two nodes off interest (e.g., L2 and Mi1, Figure3) were extracted and ranked based on the assumption that the value of the collective synaptic weight in that path normalized by the length of the path will give an estimate of the strength or influence of the initial node (e.g., L2) through that path to the final node (e.g., Mi1).

Behavioral experiments

Behavioral experiments were performed as described in (Ketkar et al., 2020). In short, experiments were done at 34 ºC, a temperature for *shibire*^ts activation (Kitamoto, 2001). Female flies were anesthetized on ice and then glued at their thorax to the tip of a needle using UV-hardened Norland optical adhesive. A 3D micromanipulator positioned the fly above an air-cushioned polyurethane ball (Kugel-Winnie, Bamberg, Germany), 6 mm in diameter, and located at the center of a cylindrical LED arena that spanned 192º in azimuth and 80º in elevation (Reiser and Dickinson, 2008). The LED panels arena (IO Rodeo, CA, USA) consisted of 570 nm LEDs and was enclosed in a dark chamber. The pixel resolution was ~2º at the fly elevation. Rotation of the ball was sampled at 120 Hz with two wireless optical sensors (Logitech Anywhere MX 1, Lausanne, Switzerland), positioned toward the center of the ball and at 90º to each other (setup described in (Seelig et al., 2010). Custom written C#-code was used to acquire ball movement data. MATLAB (Mathworks, MA, USA) was used to coordinate stimulus presentation and data acquisition. Data for each stimulus sequence were acquired for 15-20 minutes, depending on the number of distinct epochs in the sequence (see 'visual stimulation' for details).

Visual stimulation for behavior

The stimulation panels consist of green LEDs that can show 16 different, linearly spaced intensity levels. To measure the presented luminance, candela/m^2 values were first measured from the position of the fly using a LS-100 luminance meter (Konika Minolta, NJ,

USA). Then, these values were transformed to photons incidence per photoreceptor per second, following the procedure described by (Dubs et al., 1981). The highest native LED luminance was approximately $11.77 * 10^5$ photons $* s^{-1} *$ photoreceptor^{-1} (corresponding to a measured luminance of 51.34 cd/m2), and the luminance meter read 0 candela/ m^2 when all LEDs were off. For all experiments, a 0.9 neutral density filter foil (Lee filters) was placed in front of the panels, such that the highest LED level corresponded to $14.71 *10^4$ photons*s^{-1}*receptor^{-1}.

Fly behavior was measured in an open-loop paradigm where either ON or OFF edges were presented. For every set of ON or OFF edges, each epoch was presented for around 60 to 80 trials. Each trial consisted of an initial static pattern (i.e., the first frame of the upcoming pattern) shown for 500 ms followed by 750 ms of edge motion. Inter-trial intervals were 1s. All edges from a set were randomly interleaved and presented in a mirror-symmetric fashion (moving to the right, or to the left) to account for potential biases in individual flies or introduced when positioning on the ball.

The ON edge stimuli comprised four edges, each covering 48º arena space. All ON edges moved with the angular speed of 160º/s. Thus, within a 750 ms stimulus epoch, the edge motion repeated thrice: After each repetition, the now bright arena was reset to the pre-motion lower LED level, and the next repetition followed immediately, picking up from the positions where the edges terminated in the first repetition. This way, each edge virtually moved continuously. The following sets of ON edges were presented:

1. 100% contrast edges: Here, the edges were made of 5 different luminance values (e.g., five unique epochs), moving on a complete dark background. Thus, the pre-motion LED level was zero, and the edges assumed the intensities 7%, 14%, 27%, 53% or 100% of the highest LED intensity (corresponding to the luminances: 0.98, 1.96, 3.92, 7.84 or $14.71 *10^4$ photons*s^{-1}*receptor^{-1} luminance). Thus, every epoch comprised 100% Michelson contrast. The inter-trial interval consisted of a dark screen.

2. Mixed-contrast edges – full range: The set comprised of seven distinct epochs, each with a different Michelson contrast value (11%, 25%, 33%, 43%, 67%, 82% and 100%). Here, the edge luminance was maintained constant at 67% of the highest LED intensity, across epochs, and the background luminance varied. The inter-trial interval showed a uniformly lit screen with luminance equivalent to the edge luminance.

Behavioral data analysis

Connectome analysis was used with custom-written code in Python 3.7 (Rossum and Drake, 2010). Fly turning behavior was defined as yaw velocities that were derived as described in (Seelig et al., 2010), leading to a positive turn when flies turned in the direction

of the stimulation and to a negative turn in the opposite case. Turning elicited by the same epoch moving either to the right or to the left were aggregated to compute the mean response of the fly to that epoch. Turning responses are presented as angular velocities (rad/s) averaged across flies ± SEM. Peak velocities were calculated over the stimulus motion period (750ms), shifted by 100 ms to account for a response delay, and relative to a baseline defined as the last 200 ms of the preceding inter-stimulus intervals.

Mean turning of flies from control and experimental genotypes were normal distributed as tested using a Shapiro-Wilk test ($p > 0.05$). Two-tailed Student's t tests and Bonferroni-Holm correction were performed between genotypes. Data points were considered significantly different only when the experimental group significantly differed from both genetic controls. Flies with a baseline forward walking speed of less than 3 mm/s were discarded from the analysis. This resulted in rejection of approximately 20% of all flies.

Two-photon imaging

Female flies were anesthetized on ice before placing them onto a sheet of stainless-steel foil bearing a hole that fit the thorax and head of the flies. Flies they were head fixated using UV-sensitive glue (Bondic). The head of the fly was tilted downward, looking toward the stimulation screen and their back of the head was exposed to the microscope objective. To optically access the optic lobe, a small window was cut in the cuticle on the back of the head using sharp forceps. During imaging, the brain was perfused with a carboxygenated saline-sugar imaging solution composed of 103 mM NaCl, 3 mM KCl, 5 mM TES, 1 mM NaH2PO4, 4 mM MgCl2, 1.5 mM CaCl2,10 mM trehalose, 10 mM glucose, 7 mM sucrose, and 26 mM NaHCO3. Dissections were done in the same solution, but lacking calcium and sugars. The pH of the saline equilibrated near 7.3 when bubbled with 95% O2 / 5% CO2. The two-photon experiments for Figure 3 were performed using a Bruker Investigator microscope (Bruker, Madison,WI, USA), equipped with a 25x/NA1.1 objective (Nikon, Minato, Japan). An excitation laser (Spectraphysics Insight DS+) tuned to 920 nm was used to excite GCaMP6f, applying 5-15 mW of power at the sample. For experiments in Figure 5, a Bruker Ultima microscope, equipped with a 20x/NA1.0 objective (Leica, Jerusalem, Israel) was used. Here the excitation laser (YLMO-930 Menlo Systems, Martinsried, Germany) had a fixed 930 nm wavelength, and a power of 5-15 mW was applied at the sample.

In both setups, emitted light was sent through a SP680 shortpass filter, a 560 lpxr dichroic filter and a 525/70 emission filter. Data was acquired at a frame rate of ~10 to 15Hz and around 6–8x optical zoom, using PrairieView software.

Visual stimulation for imaging

For the periodic full-filed flashes, the visual stimuli were generated by custom-written software using C++ and OpenGL and projected onto an 8cm x 8cm rear projection screen placed anterior to the fly and covering 60º of the fly visual system in azimuth and 60º in elevation. These experiments were performed with the Bruker Investigator microscope.

For all the rest, the stimuli were generated by custom-written software using the Python package PsychoPy (Peirce, 2008), and then projected onto a 9cm x 9cm rear projection screen placed anterior to the fly at a 45º angle and covering 80º of the fly visual system in azimuth and 80º in elevation. These experiments were performed with the Bruker Ultima microscope.

Both stimuli were projected using a LightCrafter (Texas Instruments, Dallas, TX, USA), updating stimuli at a frame rate of 100 Hz. Before reaching the fly eye, stimuli were filtered by a 482/18 band pass filter and a ND1.0 neutral density filter (Thorlabs). The luminance values are measured using the same procedure described above for the behavioral experiments. The maximum luminance value measured at the fly position was $2.17*10^5$ photons s^{-1} photoreceptor^{-1} for periodic full-filed flashes, and $2.4*10^5$ photons s^{-1} photoreceptor^{-1} for the rest. The imaging and the visual stimulus presentation were synchronized as described previously (Freifeld et al., 2013).

Periodic full-field flashes

The stimulus consisted of periodic, alternating full contrast ON and OFF flashes covering the whole screen, each lasting 5 s, were presented to the flies. Each stimulus epoch was presented for ~7 trials.

Flashes of different luminances

The stimulus consisted of 10s full-field flashes of 11 different luminances (0, 0.1, 0.2, 0.3, 0.4, 0.5, 0.6, 0.7, 0.8, 0.9 and 1* of the maximal luminance I_{max}). The order between the flashes was pseudo-randomized and the stimulus sequence was presented for ~440s.

Ternary white noise

Each frame consisted of 16 bars of 5° x 80° size tilted along elevation and spanning the whole screen of 80° x 80°. Each bar changed its contrast from frame to frame with equal probability of having either minimal, maximal, or intermediate contrast independent of all other bars. Frames were updated every 50 milliseconds. The duration of one epoch was 500s with 2s of grey interleave. Per fly the stimulus epoch was repeated twice.

Moving 1hz sinusoidal at different luminances

A 100% Michaelson contrast sinusoidal wave, with spatial wavelength of 30°, moved at 30° per second for 4 seconds. A complete dark screen was set as interstimulus interval for 4 seconds. Each epoch changed in mean luminance with 5 different value (0.1, 0.2, 0.3, 0.4, and 0.5 of the maximal luminance I_{max}), and the presentation order was randomized.

Moving 1hz sinusoidal at different noise levels

A sinusoidal wave, expanding the whole range of screen luminance, was first created for every epoch. Thus, the wave initially had a 100% Michaelson contrast and intermediate mean luminance (0.5 of the maximal luminance I_{max}). Then, to change contrast, noise values coming from a normal distribution were randomly added to the sinusoidal wave in space and time, yielding to a decrease in contrast when noise was higher. Different noise levels where chosen based on seven different normal distributions with same mean at zero but distinct standards deviations (0.08, 0.17, 0.2, 0.247, 0.29, 0.35, 0.41, 0.5). All waves had 30° of spatial wavelength and moved at 30° per second for 4 seconds. A complete dark screen was set as interstimulus interval for 4 seconds.

<u>Two photon data analysis</u>
Periodic full-field flashes

Data processing was performed offline using MATLAB R2019a (The MathWorks Inc., Natick, MA). To correct for motion artifacts, individual images were aligned to a reference image composed of a maximum intensity projection of the first 30 frames. The average intensity for manually selected ROIs was computed for each imaging frame and background subtracted to generate a time trace of the response. All responses and visual stimuli were interpolated at 10 Hz and trial averaged. Neural responses are shown as relative fluorescence intensity changes over time ($\Delta F/F0$). To calculate $\Delta F/F0$, the mean of the whole trace was used as F0. In some recordings, a minority of ROIs responded in opposite polarity (positively correlated with stimulus), as described previously (Fisher et al., 2015). These ROIs have their receptive fields outside the stimulation screen (Fisher et al., 2015; Freifeld et al., 2013). To discard these and other noisy ROIs, we only used ROIs that were negatively correlated (Spearman's rank correlation coefficient) with the stimulus and a standard deviation threshold of 0.2 was set during the 2 s before the onset of visual stimulation. Step responses were calculated as the difference between the mean response 500 ms before the onset of the stimulus and the peak $\Delta F/F_0$ during the stimulus epoch. Plateau responses were calculated as the difference between the mean response 500 ms before the onset of the stimulus and the mean of the last 500 ms of the stimulus epoch.

For the rest of the stimuli, data processing was performed offline using Python 3.7 (Van Rossum 1995). Motion correction was performed using the SIMA Python package's Hidden Markov Model based motion correction algorithm (Kaifosh et al., 2014). The average intensity for manually selected ROIs was computed for each imaging frame and background subtracted to generate a time trace of the response. To calculate ΔF/F0, the mean of the whole trace was used as F0, and the traces were then trial averaged.

Flashes of different luminances

In the randomized flashes of different luminances, plateau responses were calculated as the mean of the last 2 seconds within each luminance presentation. Values of the highest luminance epoch were subtracted for each plateau response to get a comparable relationship between each neuron for visualization (this leads to 0 plateau response for MI1 in the lowest luminance condition).

Ternary white noise

Space-time receptive fields (STRFs) were extracted from responses of single cell ROIs to the ternary white noise stimulus. The raw fluorescence (F) traces of single clusters were extrapolated to 20Hz matching the update rate of the ternary white noise stimulus. For ΔF/F0 calculation, F0 was defined as the baseline fluorescence, computed from averaging responses to gray interleaves. The extracted cell response was further centered around its mean and averaged across two stimulus repetitions. The stimulus was normalized to have values of -1, 0 and 1 for dark, grey and bright bars.

STRFs were extracted by computing the response reverse correlation with the stimulation. For this a sliding average of two seconds length was propagated backwards in time and weighted by the response of the cell at the start of the window. Given the response of the cell at time point t (rt), the time window of the stimulus (τ), the amount of total time points (T) and the stimulus snippet s(t-τ) the STRF is computed as follows:

$$STRF = \ 1/(T-\tau) \sum_{(t=\tau)}^{T} \text{rt} * s(t-\tau)$$

For visualization of space and time filters, we plotted the time or space response axis which passes through the response maximum along the spatial dimension.

Statistics

Throughout the analysis procedure, mean of quantified variables were calculated first for all ROIs within a fly, and then between flies. All statistical analysis was performed between flies. For normally distributed data sets, a two-tailed Student *t* test for unpaired (independent) samples was used. Normality was tested using a Shapiro-Wilk test ($p > 0.05$). One way ANOVA was used followed by multiple comparisons using the Bonferroni-Holm correction for determining statistical significance between pairs of groups.

Immunohistochemistry and confocal microscopy

Female flies were dissected 3-14 days after eclosion. Brains were removed in dissection solution and fixed in 2% paraformaldehyde in phosphate buffered lysine (PBL) for 50 minutes at room temperature. Subsequently, the brains were washed 3x for 5 min in phosphate buffered saline containing 0.3% Triton X-100 (PBT) adjusted to pH 7.2. For antibody staining, the samples were blocked in 10 % normal goat serum (NGS, Fisher Scientific GmbH, Schwerte, Germany) in PBT for 30 min at room temperature followed by incubation for 24 hours at 4ºC in the primary antibody solution (mouse mAb nc82,1:25, DSHB; chicken anti-GFP,1:2000, Abcam ab13970; rabbit anti-GABA, 1:200, Sigma-Aldrich, A2052). Primary antibodies (chicken anti-GFP polyclonal (1:20000), rabbit anti-dsRed (1:1000)) were removed by washing in PBT 3 times for 5 min and the brains were incubated in the secondary antibody (anti-chicken-Alexa488, anti-rabbit-Alexa594, all 1:200, Dianova) in the dark at 4˚C overnight. The samples were further washed with PBT (3 x 5 min) and mounted in Vectashield (Vector Laboratories, Burlingame). Serial optical sections were taken on a Leica SP8 microscope (Leica Microsystems) equipped with an oil immersion Plan-Apochromat 40x (NA = 1.3) objective and using the LAS AF 3 (Leica Application Suite Advanced Fluorescence) software. Z-stack images were taken at 1 µm intervals and 512 x 512-pixel resolution. Confocal stacks were rendered into two-dimensional images using Fiji (Schindelin et al., 2012). The images were then further processed using Illustrator CS5.1 (Adobe).

5.   General discussion

Visual systems must extract relevant features of the environment during early visual processing. Early features, such as contrast, need to be processed correctly also when the world around dynamically changes. This thesis investigates the molecular and neuronal mechanisms in early visual processing to achieve a robust feature extraction. I focus on contrast detection as a relevant feature that builds the basis for other more complex computations, such as motion detection. Specifically, I focus on those parallel inputs that implement a robust ON contrast selectivity and luminance-invariant contrast responses. These inputs are coming mainly from first-order lamina (L) interneurons that pass the signal from retinal photoreceptors to the first ON or OFF responding neurons in the medulla.

In the first study, I identified the mechanisms for the split in ON and OFF pathways in the *Drosophila* visual system. I showed that in circuitry downstream of the glutamatergic L1, broad expression of glutamate-gated chloride channels (GluCls) is required for the signal inversion in the ON pathway. ON pathway neurons are resilient to a cell-type-specific loss of GluCls, demonstrating that ON responses are computed in a distributed manner. In this multisynaptic computation, both GluCls as well as GABA-gated chloride channels are involved. In the second study, my colleagues and I showed how lamina neurons distribute luminance and contrast signals to downstream ON and OFF pathways to implement luminance-invariant contrast responses in behavior. First, we showed that, in *Drosophila*, ON contrast behavior is luminance-invariant as previously described for OFF. Both L1 and L3 carry luminance information, although L1 activity shows a linear relationship with luminance, whereas L3 activity non-linearly increases, being higher at low luminance levels. Both L1 and L2 carry relevant contrast information to both pathways. Although the neuronal implementation of luminance-invariant responses differs between the ON and OFF pathways, we showed that L1-3 neurons are not pathways specific as previously described but instead distribute contrast and luminance signals to both ON and OFF pathways to enable a stable behavior. In the third study, I showed that parallel inputs implement robust responses in the central ON pathway neuron Mi1. First, I predict and confirm the behavioral relevance of Mi1 as hub neuron in the ON pathway. Direct and parallel L1 and L3 inputs are not individually or together required for ON responses. Indirect inputs from L2 exists and might further implement responses in Mi1. Lastly, direct glutamatergic inputs that are not required (Molina-Obando et al., 2019) (first study), are sufficient to implement ON responses under different challenging conditions. In sum, we found that parallel connectivity

is in place in the early visual processing of contrast to implement robust neuronal responses and stable animal behavior.

Thus, either to implement contrast selectivity to light increments (ON) at the neuronal level or to guide stable contrast responses at the behavioral level, parallel input pathways are in place. The idea of having parallel input pathways that can individually implement function (are sufficient) and at the same time are not required for the function, provides a functional principle for the parallel brain architecture. Considering that brains across animals share this parallel arrangement of inputs in their neuronal circuits, and that they phase similar challenges when environmental conditions suddenly change, the above-mentioned functional principle can be a common strategy present in many other sensory systems too.

In the coming sections, I will discuss how these findings relate to the current understanding of visual processing, emphasizing the similarities and differences between invertebrates and vertebrates that lead to a remarkably similar feature extraction and robustness. First, I discuss the biological implementation of contrast across vertebrate and invertebrates, emphasizing in which point the first study shows similarities and differences across species. This part specially emphasizes the distributed implementation of feature extraction. Second, I discuss a novel role for the lamina neuropile, in which lamina interneurons encode both contrast and luminance in specific ways and are not cleanly segregated into ON versus OFF inputs, as previously thought. Finally, I discuss which can be a brain architecture behind robust and flexible responses or behaviors. I explore if the anatomical architecture of a wiring diagram suffices for an accurate functional prediction. I look at different circuit motifs that could be part of the architecture, as well as degeneracy as a theoretical framework to comprehend both the anatomical and the physiological evidence that the third study exposes.

5.1   Contrast detection across species

5.1.1   The biological implementation of ON-contrast responses

The solution to implement the split in ON and OFF pathways is similar between the vertebrate retina and the fly optic lobe. In both systems, a glutamatergic system triggers the signal inversion (Masu et al., 1995; Molina-Obando et al., 2019). Briefly, the glutamate release from the input neuron linearly increases with contrast, being higher for light offsets. On the postsynaptic neurons, glutamate inhibitory receptors are expressed and hyperpolarize the neurons. Since flies (invertebrates) and vertebrates are far apart in

evolution, the glutamatergic neurotransmitter system behind the inversion, either comes from an early common ancestor or is an outcome of converging evolution. How the signal inversion happens in other visual systems has not been described, but another invertebrate the nematode *Caenorhabditis elegans*, also utilizes glutamate in the ON pathway for the signal inversion, in this case in the olfactory system (Chalasani et al., 2007). Thus, the solution to implement a split for opposite pathways could be an even wider strategy used by different sensory systems in other animals as well. However, the mechanism between vertebrates and invertebrates differs in an important aspect: inhibitory glutamatergic receptors in invertebrates are ionotropic whereas in vertebrates are metabotropic. This distinction has mainly two functional implications: 1) the faster signaling of ionotropic receptors gives an advantage in the temporal coding of contrast, and 2) the secondary chemical cascades of metabotropic receptors give an advantage in signal amplification.

The first functional implication aligns with the fact that insect (invertebrate) vision is faster than, for example, that observed in humans (vertebrates). The flicker fusion frequency (FFF), which is the frequency at which ON-OFF light cycles cannot be longer detected as such, is higher in insects. Many mechanisms can contribute to a faster vision in insects. For example, in phototransduction, metarhodopsins can be reconverted back to light-sensitive rhodopsins faster in flies with higher wavelengths (red), whereas in vertebrates it requires a longer chemical process relying on enzymatic cascades. Similarly, differences and mechanisms underlying distinct temporal capabilities of sensory systems have also been observed in vertebrates vs invertebrates chemosensation (Kaupp, 2010; Silbering and Benton, 2010). Whereas ionotropic receptors are faster, it has been suggested that metabotropic receptors implement the signal amplification observed in bipolar cells (BCs) with respect to the photoreceptor signal (Shiells, 1994; Werblin and Dowling, 1969). However, the specific amplification role of metabotropic receptors in the ON pathway cannot been tested since the loss of these glutamate receptors abolishes ON responses in the first place (Masu et al., 1995). In the fly optic lobe, the signal from photoreceptors is also amplified in lamina neurons (Laughlin et al., 1987), although the biological mechanism has not been described, it does not involve metabotropic receptors, because lamina neurons responses are driven by histamine ionotropic receptors (Gengs et al., 2002). Amplification mechanisms in the fly rely on other mechanisms than in the expression of metabotropic neurotransmitter receptors.

Another striking difference between the vertebrate retina and the fly optic lobe is the described neuronal implementation of ON contrast detection. In the literature, it is described that the signal inversion in the vertebrate retina is implemented in the photoreceptor to ON-

BC synapse. In contrast, my work revealed that in flies, the implementation of ON selective responses is distributed and multisynaptic. Let's look carefully at the data that support the monosynaptic computation in vertebrates: 1) the experiments in mice have been done in non-conditional knock out animals in which genes coding for metabotropic glutamate receptors (mGluR6) (Masu et al., 1995) or other important genes in the signal transduction (Koike et al., 2010; Morgans et al., 2009; Shen et al., 2009) have been removed from all cells. And 2) although the expression of mGluR6 is specific to the OPL where ON-BCs project their dendrites (Masu et al., 1995) and photoreceptor are the main input of BCs, ON-BCs receive many more inputs that might covey signals relevant for an ON responses. For example, there are distinct types of BCs, both ON and OFF, that are highly interconnected through inhibitory interneurons. Crossover inhibition from the OFF pathway has the potential to introduce a signal inversion similarly as the OFF-responding photoreceptors do. In Drosophila, a ubiquitous loss of GluClα function also leads to a full loss of function, and expression data also supported the idea of a simple mechanisms mediating the signal inversion in the ON pathway. However, thanks to advance cell-type specific manipulations, we were able to uncover that ON selectivity is indeed a multisynaptic computation. Although we do not have direct knowledge of all different input pathways for a distributed signal inversion, we show that in involves two types of inhibitions: glutamatergic and GABAergic. This directly correlates with the existence of glutamatergic and GABAergic interneurons that expand horizontally, connecting to members of both the ON and the OFF pathways. Thus, crossover inhibitory signal might be also in place for a signal inversion in the ON-pathway. Together, our work on flies should motivate work in vertebrates to revisit the hypothesis that the emergency of ON selectivity might also be more distributed in the mouse retina.

5.1.2   Contrast extraction is implemented in a distributed manner

Contrast-selective neurons in both the vertebrate retina and the fly optic lobe have a lot of variability in their responses. In the vertebrate retina, although there are 14 anatomically defined BCs (Euler et al., 2014), a functional characterization uncovers many more subtypes (Franke et al., 2017). These subtypes have different temporal dynamics and rectification properties. Interestingly, what increases the functional variability -or diversity- are the lateral connections across pathways utilizing amacrine cells (ACs) as interneurons (Franke et al., 2017). This is an interesting property emerging from a highly interconnected circuitry. Having wider functional diversity across various neuronal subtypes that overlap their properties is interesting in two ways: 1) if one unit fails, there are others that can substitute its function, leading to robustness, and 2) if the environmental conditions

dynamically change, different functional units can together cover a wider range of signal detection, also leading to robust detection.

The *Drosophila* ON and OFF pathways also have distinct anatomically defined neurons with clearly different temporal and spatial properties (Arenz et al., 2017; Behnia et al., 2014; Strother et al., 2017; Yang et al., 2016). For example, in the ON pathway, Tm3 responds transiently to contrast. Mi1, on the other hand, has a sustained plateau after the transient peak that correlates with background luminance, and Mi4 responses are fully sustained during ON stimulation (Arenz et al., 2017). Similarly, in the OFF pathway there have the more transient Tm1, Tm2 or Tm4 vs the more sustained Tm9 (Arenz et al., 2017; Fisher et al., 2015; Ramos-Traslosheros and Silies, 2021; Serbe et al., 2016). This functionally diversity might reflect both their distinct lamina inputs as well as their lateral connections uncovered in the medulla wiring diagram. In the third study, we tried to elucidate the functional relevance of these parallel connections in the context of ON contrast detection. Our work suggests that having parallel inputs that are sufficient but not required for circuit function might be a principle leading to robustness. The functional implications of other parallel inputs still need to be investigated to check if the "sufficiency vs redundancy" principle is a general trait of all parallel inputs.

Implementing a feature in a distributed manner might be a strategy for other computations as well. For example, in motion detection in the ON pathway, the direction selective (DS) T4 receives parallel inputs. Direction selectivity emerges by comparing signals coming from neighboring photoreceptors over space and time (Ramos-Traslosheros et al., 2018). To fulfill most of the models that have been proposed to explain direction-selective responses, just two parallel inputs are sufficient. This is not what connectomics reveals. T4 receives inputs from at least Mi1, Tm3, Mi4, Mi9, C3 and CT1 (Meier and Borst, 2019; Takemura et al., 2013, 2017). Some of these inputs seem degenerate, for example Mi1, Mi9 and Tm3 are all inputs that can depolarize T4 during ON. Mi1 and Tm3 achieve this through direct excitation, and Mi9 through release of inhibition. Also, Mi4, C3 and CT1 are all inhibitory inputs to T4 during ON. Why to have so many inputs if two would suffice? All these neurons have at least slightly different temporal and spatial response, and although they still appear to overlap in function when it comes to different speed tuning of motion signals, have the combined potential to capture signal that might differ in space and time, leading to a robust detection of different moving objects (Figure 4).

5.2   Distribution of luminance and contrast information by the fly lamina

5.2.1   Lamina neurons are not members of ON and OFF contrast pathways

In the second study of this thesis, we show that lamina neurons are not pathway specific inputs but rather distribute their signals to both ON and OFF pathways. This deviates from how these inputs have been so far described. Briefly, in the *Drosophila* visual system, the ON and OFF contrast selective pathways, and their neuronal members, have been described from a motion detection pathway perspective. Recordings at lobula plate tangential cells (LPTCs), the wide field direction-selective output neurons of the optic lobe, and behavioral studies have been used to assess the overall contribution of single neurons to either ON or OFF motion detection. Early studies silencing different lamina neurons assigned L1 and L2 to the ON- and the OFF-motion pathways, respectively (Clark et al., 2011; Joesch et al., 2010). Nonetheless, it was observed that silencing more than one lamina neuron at the same time could enhance the phenotypes of individual silencing (Silies et al., 2013), arguing that there were interactions between pathways. This last study also described L3 as an OFF-pathway input. In parallel to this evidence, the physiological characterization of these neurons showed that L1 and L2 were functional siblings, having linear responses to contrast changes, whereas L3 differed from those two responding more rectified to light decrements (Clark et al., 2011; Silies et al., 2013). Together, the common view in the field was that the ON pathway had a single lamina input (L1), whereas the OFF pathway had two different ones (L2-3). Then, looking at the neuronal connectivity in the medulla (Takemura et al., 2013), two important contributions were made. 1) Neurons receiving most synaptic inputs from L1 clustered together in a single ON pathway, and the same for neurons downstream of L2 in a single OFF pathway. 2) Although not much emphasized in this paper, these pathways are highly interconnected, and L1 and L2-3 directly or indirectly contact neurons in both ON and OFF pathways. This anatomical evidence aligned with the mentioned pathway interaction (Silies et al., 2013).

Our study challenges the view of L1 being the major input to the ON and L2 and L3 being major inputs to the OFF pathway in two ways. First, we uncovered that L1 and L2 are not functional siblings inputs to two distinct pathways. L1, besides carrying a transient component, also shows a sustained plateau response which carries information about luminance. L2 does not have a luminance-sensitive component, thus is considered here as a pure contrast-sensitive input. Second, the lamina neurons L1 and L3 are individually sufficient for both ON and OFF behaviors. We further showed that L1 and L2 are together required for ON behavior. Thus, the distinct lamina neurons distribute contrast- and luminances-sensitive signals inherited from photoreceptors to both the ON and OFF pathways. This study helps to understand the role of the lamina in the fly optic lobe as an

extra layer of computation, compared to the vertebrate retina. Importantly, it hints to new hypothesis about how a circuit can create functional variability. For example, different combinations of L neurons inputs to downstream medulla neurons can increase their functional diversity. Since L1 and L3 carry different types of luminance information, a combination of those in distinct proportions might confer neurons to respond better in contextual dim light or equally good across a wider range of luminances. In the same line, a combination of L1 and L2 signals might give neurons different contrast sensitivity, conferring the lamina an important role in diversifying the two more basic visual features (luminance and contrast) between the peripheral photoreceptors and ON and OFF contrast selective neurons (Figure 4).
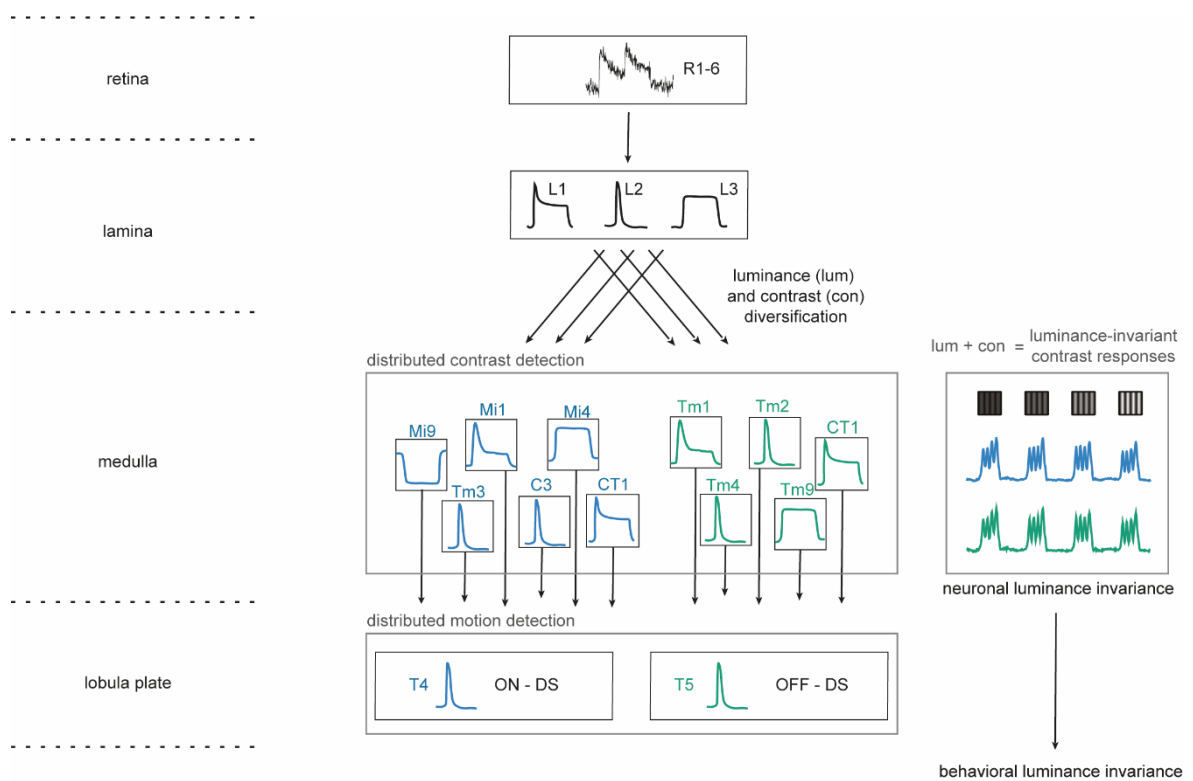

Figure 4: **Distributed feature extraction.** In the retina, photoreceptors send their signals to lamina first-order interneurons. In the lamina, neurons respond differently, diversifying luminance and contrast information. They distribute their signals to downstream neurons in the ON (blue) and OFF (green) pathways. (Left) In the medulla, second-order interneurons have different response dynamics and are cells in which contrast and luminance signals from the lamina first coincide. (Right) Sinusoidal gratings of 100% contrast, moving at different luminance backgound levels. Luminance-invariant contrast responses (blue and green traces) probably arise in ON and OFF pathway medulla neurons thanks to the scaling of contrast signals by luminance signals. Neuronal luminance-invariant responses will later guide luminance-invariant behavioral responses. In the lobula plate, direction selective (DS) cells receive multiple and parallel inputs from medulla neurons which implement motion detection.

5.2.2   Distinct implementation of luminance-invariant responses across pathways and systems

Since the contrast level of an object inform about its environmental relevance, this must be properly extracted also in dynamically changing conditions. Invariant responses to contrast under sudden changes in illumination is a common feature of ON and OFF visual pathways. Luminance-invariant contrast responses are also present in human perception (Burkhardt et al., 1984) as well as in neuronal responses of the cat lateral geniculate nucleus (LGN) (Mante et al., 2005). However, we only recently gained insights into the neuronal implementation of invariant ON and OFF contrast responses at very short time scales, faster than photoreceptor adaptation. In *Drosophila*, a luminance-sensitive neuron scales the contrast response to achieve luminance-invariant behavior to OFF contrast stimuli (Ketkar et al., 2020). Due to asymmetries between ON and OFF pathways across animals, including *Drosophila* (Behnia et al., 2014; Chichilnisky and Kalmar, 2002; Jin et al., 2011; Leonhardt et al., 2016; Ratliff et al., 2010), the same neuronal mechanism seemed unlikely for the ON pathway. In our second study, we show that for the ON pathway, luminance information is also the corrective signal for scaling the contrast response. However, the neuronal implementation of luminance-invariance in the two pathways is still not the same, as the OFF pathway is more sensitive to neuronal perturbations of the luminance-sensitive neurons L3 alone, whereas the ON pathways appears to rely on luminance information from both L1 and L3, at least in the tested luminance range. In the vertebrate retina, there are many cell types with a sustained response component (Awatramani and Slaughter, 2000; Ichinose and Hellmer, 2016; Normann and Werblin, 1974; Oesch and Diamond, 2011). These neurons have the potential to carry the luminance information inherited from photoreceptors to the downstream circuitry. Since photoreceptor adaptation (gain control) in the vertebrate retina is also too slow to explain invariant contrast responses upon sudden illumination changes, and since cones and rods contrast response scales with luminance (Brown and Rudd, 1998), a similar mechanism as the one in *Drosophila* might be in place. In any case, besides human perception, it also remains to be explored if animal contrast behavior is indeed luminance-invariant among other species.

5.3   Brain architecture for a robust function

5.3.1   Prediction of function by connectivity

The increasing amount of reconstructed wiring diagrams across animals and systems is a huge information source for understanding the brain. In the world of big data, we need to simplify information without losing important pieces when doing functional predictions. In

this thesis, I have used graph theory as a simplification strategy to convert a neuronal circuit to a graph. Using the number of connections as the relevant variable for measuring local and global connectivity as well as information flow led to the identification of crucial circuit nodes or hubs that correlated with their behavioral roles. This functional prediction is of course limited in that it ignores many other important variables. First, there is variability across individuals and a connectome only covers the anatomy of just one. Second, brains are plastic and change over time during development and aging (Meinertzhagen, 2001). Third, the relationship between number of connections and functional relevance is not linear, as assumed. For example, a small number of inhibitory connections can counteract the action of many more excitatory inputs, especially if they are close to the inhibitory source. This is referred to as divisive -or shunting- inhibition (Paulus and Rothwell, 2016). Finally, many other factors influence the functionality of a circuit, such as the existence of GAP junctions, excluded so far from current wiring diagrams, the secretion of neuromodulators with a great impact in physiology (Arenz et al., 2017; Marder, 2012), the temporal expression of clock genes (Hardin, 2005) and the interaction with glial cells (Bittern et al., 2021).

Some of these limitations are being addressed. First, although variability across individuals has not been studied in detailed, different connectomes from different individuals in the same brain regions have recently emerged (Scheffer et al., 2020; Takemura et al., 2015, 2013; Zheng et al., 2018), tools from comparing different dataset exist (Bates et al., 2020) and scientist begin to compare the wiring diagram across individuals (Schlegel et al., 2021; Takemura et al., 2015). Second, the first efforts in obtaining a connectome across development reveal the extent of circuit remodeling in the *Caenorhabditis elegans* brain (Witvliet et al., 2021). And third, some strategies, like Connect-seq (Hanchate et al., 2020), are emerging to determine the molecular identities of individual neurons in defined circuits. Or attempts for the co-registration of anatomy and physiology in the same specimen have been taken, by now only available for small brains of juveniles (Ohyama et al., 2015), transparent ones (Hildebrand et al., 2017) or microcircuits (Briggman et al., 2011). Thus, to overcome current limitations, great efforts and collaborations will be needed, as well as technological improvements in data registration and analysis that would allow to model the temporal and individual variability of this huge data sets.

5.3.2   Degeneracy in the brain: how to implement robustness

Nervous systems are known to be robust in implanting feature extraction and ultimately in guiding behavior. In the third study we showed that parallel input pathways contribute to a

robust feature extraction. First, individual pathways are not required and therefore others can cover its functionality. This avoids an easy function disruption if one pathway fails. Second, ON responses can be sufficiently implemented across varying conditions by a reduced system which includes only direct glutamatergic inputs. Similarly, we observe that animals can perform the same complex task despite of external or internal changes in conditions. For example, tracking movement performance of monkeys while measuring directional tuning of motor neurons has shown that the animal`s behavior is stable despite of variable neuron response properties, suggesting that for a given behavior, different combinations of neuronal activity associated with different synaptic strengths are in place (Rokni et al., 2007). Studies of songbirds also suggest significantly neuronal variability behind acoustic patterns that remain stable during years (Lombardino and Nottebohm, 2000). Thus, the activity of a neuronal population, rather than individual neuronal activity, turns out to be a better correlate of robust function. In those neuronal circuits, parallel connections are an anatomical trait that might explain how different neuronal representation arise in the same anatomical circuitry (Ding et al., 2016; Eschbach et al., 2021; Ohyama et al., 2015; Schlegel et al., 2021; Takemura et al., 2017). A theoretical framework has emerged to explain how a parallel circuit architecture might lead to robustness. Degeneracy, the ability of elements that are structurally different to independently perform the same function, could leads to robustness (Edelman and Gally, 2001; Tononi et al., 1999). If one considered that each parallel pathway can be define as structurally different element, degeneracy is in line with pathways being not required but sufficient, as found in our third study. Sufficiency ensures the independency for a robust function implementation, and not being required reflects that other element are there to implement the same or similar function in case any other pathway fails.

6.   Conclusions and outlook

The processing of any physical stimulus begins at the periphery of all brain sensory systems. Along visual features, simple features of the stimulus are extracted, which then are the basis for more complex ones. For example, our visual system first detects contrast to later detect motion. The saliency of different object around us depends on their contrast with respect to the background. To navigate, contrast, as an early feature, must be robustly extracted. From this thesis, investigating the mechanism for a robust extraction of contrast in early visual processing, I can conclude that:

1. Contrast detection is a circuit phenomenon which happens in a distributed manner, involving different cell types and neurotransmitter systems. Distributed mechanisms might be in place for other computations as well, such as motion detection.
2. Although the computation to become selective to ON contrast is similar across systems and animals, the molecular mechanisms between vertebrates and invertebrates are different.
3. ON contrast behavior in *Drosophila* is luminance-invariant, as previously described for OFF behavior (Ketkar et al., 2020).
4. The mechanism behind luminance-invariant contrast responses in both ON and OFF pathways involves the scaling of contrast responses by luminance-sensitive signals.
5. In *Drosophila*, different lamina inputs have asymmetric functional roles in the ON and the OFF pathway. Thus, the neuronal mechanism for a luminance-based correction is asymmetric across pathways.
6. The first-order lamina neurons are not ON and OFF pathway specific but rather distribute and diversify contrast and luminance signals inherited from photoreceptors across the downstream circuit in the medulla.
7. Graph analysis of information flow successfully identifies neurons that are behaviorally relevant ON pathway hubs.
8. Parallel input pathways in a distributed contrast extraction underlies robustness. They can be sufficient although there are not required.

Altogether, these conclusions open the possibility to test if a parallel circuit architecture and distributed coding is a general strategy for functional robustness. Besides to further explore the function of remaining parallel input pathways in ON selectivity, we can generalize testing if a similar strategy exists for other features as well, for example, OFF selectivity, luminance-

invariant contrast responses, or direction selectivity. In the next lines, I briefly mention how can we address this.

For a robust implementation of ON selectivity, we conclude that individual parallel input pathways are sufficient but not necessarily required. These two conditions -necessity and sufficiency- need to be checked for distinct neuronal pathways involved in all features mentioned above. Necessity is simple to check since different genetic tools for neuronal silencing exist, for example employing cell-type specific expression of Shibire[ts], Kir2.1 or tetanus toxin (Silies et al., 2014). However, to test sufficiency it is not trivial and potentially only works in very specific cases since it relies on rescuing gene expression in mutants. For example, it works for rescue experiments in lamina neurons, which all receive histaminergic input from photoreceptors, and therefore utilize a rare neurotransmitter. Mutant flies in which the histamine-gated chloride channel *ort* is lacking are blind. Rescuing *ort* expression in individual lamina neurons allows to test the specific contribution of each input pathway, as we did in the second study of this thesis. Thus, we can further test if L1-3 pathways are sufficient to implement distinct feature extraction (contrast selectivity, luminance-invariant contrast, direction selectivity) across ON and OFF pathway neurons. Rescue experiments also work in the ON pathway as used in the third study of this thesis. A *GluClα* mutant disrupts the activity in the ON but not in the OFF pathway. Thus, all pathways implementing ON responses are blocked in a *GluClα* mutant, and the overexpression of *GluCls* can rescue the function of individual input neurons. We can test if the GluCl pathway is sufficient to rescue other ON-pathway neurons besides Mi1 and consequently test if the activity of rescued neurons can implement distinct features in other interconnected neurons. In sum, we can use available genetic tools and the well described visual features in *Drosophila* to address the fundamental question of how brains achieve functional robustness.

Bibliography

Ache JM, Namiki S, Lee A, Branson K, Card GM. 2019. State-dependent decoupling of sensory and motor circuits underlies behavioral flexibility in Drosophila. *Nat Neurosci* **22**:1132–1139. doi:10.1038/s41593-019-0413-4

Agi E, Langen M, Altschuler SJ, Wu LF, Zimmermann T, Hiesinger PR. 2014. The Evolution and Development of Neural Superposition. *J Neurogenet* **28**:216–232. doi:10.3109/01677063.2014.922557

Arenz A, Drews MS, Richter FG, Ammer G, Borst A. 2017. The Temporal Tuning of the Drosophila Motion Detectors Is Determined by the Dynamics of Their Input Elements. *Curr Biol* **27**:929–944. doi:10.1016/j.cub.2017.01.051

Awatramani GB, Slaughter MM. 2000. Origin of Transient and Sustained Responses in Ganglion Cells of the Retina. *J Neurosci* **20**:7087–7095. doi:10.1523/JNEUROSCI.20-18-07087.2000

Baden T, Berens P, Franke K, Román Rosón M, Bethge M, Euler T. 2016. The functional diversity of retinal ganglion cells in the mouse. *Nature* **529**:345–350. doi:10.1038/nature16468

Barsotti E, Correia A, Cardona A. 2021. Neural architectures in the light of comparative connectomics. *Curr Opin Neurobiol* **71**:139–149. doi:10.1016/j.conb.2021.10.006

Bates AS, Manton JD, Jagannathan SR, Costa M, Schlegel P, Rohlfing T, Jefferis GS. 2020. The natverse, a versatile toolbox for combining and analysing neuroanatomical data. *eLife* **9**:e53350. doi:10.7554/eLife.53350

Baylor DA, Fuortes MGF, O'Bryan PM. 1971. Receptive fields of cones in the retina of the turtle. *J Physiol* **214**:265–294. doi:10.1113/jphysiol.1971.sp009432

Behnia R, Clark DA, Carter AG, Clandinin TR, Desplan C. 2014. Processing properties of on and off pathways for Drosophila motion detection. *Nature*. doi:10.1038/nature13427

Beverly M, Anbil S, Sengupta P. 2011. Degeneracy and Neuromodulation among Thermosensory Neurons Contribute to Robust Thermosensory Behaviors in Caenorhabditis elegans. *J Neurosci* **31**:11718–11727. doi:10.1523/JNEUROSCI.1098-11.2011

Bittern J, Pogodalla N, Ohm H, Brüser L, Kottmeier R, Schirmeier S, Klämbt C. 2021. Neuron–glia interaction in the Drosophila nervous system. *Dev Neurobiol* **81**:438–452. doi:10.1002/dneu.22737

Bloomfield SA, Dacheux RF. 2001. Rod Vision: Pathways and Processing in the Mammalian Retina. *Prog Retin Eye Res* **20**:351–384. doi:10.1016/S1350-9462(00)00031-8

Bock DD, Lee W-CA, Kerlin AM, Andermann ML, Hood G, Wetzel AW, Yurgenson S, Soucy ER, Kim HS, Reid RC. 2011. Network anatomy and in vivo physiology of visual cortical neurons. *Nature* **471**:177–182. doi:10.1038/nature09802

Boergens KM, Kapfer C, Helmstaedter M, Denk W, Borst A. 2018. Full reconstruction of large lobula plate tangential cells in Drosophila from a 3D EM dataset. *PLOS ONE* **13**:e0207828. doi:10.1371/journal.pone.0207828

Borghuis BG, Marvin JS, Looger LL, Demb JB. 2013. Two-Photon Imaging of Nonlinear Glutamate Release Dynamics at Bipolar Cell Synapses in the Mouse Retina. *J Neurosci* **33**:10972–10985. doi:10.1523/JNEUROSCI.1241-13.2013

Borst A, Haag J, Mauss AS. 2020. How fly neurons compute the direction of visual motion. *J Comp Physiol A* **206**:109–124. doi:10.1007/s00359-019-01375-9

Borst A, Helmstaedter M. 2015. Common circuit design in fly and mammalian motion vision. *Nat Neurosci* **18**:1067–1076. doi:10.1038/nn.4050

Braitenberg V. 1967. Patterns of projection in the visual system of the fly. I. Retina-lamina projections. *Exp Brain Res* **3**:271–298. doi:10.1007/BF00235589

Briggman KL, Bock DD. 2012. Volume electron microscopy for neuronal circuit reconstruction. *Curr Opin Neurobiol* **22**:154–161. doi:10.1016/j.conb.2011.10.022

Briggman KL, Helmstaedter M, Denk W. 2011. Wiring specificity in the direction-selectivity circuit of the retina. *Nature* **471**:183–188. doi:10.1038/nature09818

Brown LG, Rudd ME. 1998. Evidence for a noise gain control mechanism in human vision. *Vision Res* **38**:1925–1933. doi:10.1016/S0042-6989(97)00400-8

Buhmann J, Sheridan A, Malin-Mayor C, Schlegel P, Gerhard S, Kazimiers T, Krause R, Nguyen TM, Heinrich L, Lee W-CA, Wilson R, Saalfeld S, Jefferis GSXE, Bock DD, Turaga SC, Cook M, Funke J. 2021. Automatic detection of synaptic partners in a whole-brain Drosophila electron microscopy data set. *Nat Methods* **18**:771–774. doi:10.1038/s41592-021-01183-7

Bullmore ET, Bassett DS. 2011. Brain Graphs: Graphical Models of the Human Brain Connectome. *Annu Rev Clin Psychol* **7**:113–140. doi:10.1146/annurev-clinpsy-040510-143934

Burkhardt D. 1994. Light adaptation and photopigment bleaching in cone photoreceptors in situ in the retina of the turtle. *J Neurosci* **14**:1091–1105. doi:10.1523/JNEUROSCI.14-03-01091.1994

Burkhardt DA, Gottesman J, Kersten D, Legge GE. 1984. Symmetry and constancy in the perception of negative and positive luminance contrast. *J Opt Soc Am A* **1**:309. doi:10.1364/JOSAA.1.000309

Busse L, Ayaz A, Dhruv NT, Katzner S, Saleem AB, Scholvinck ML, Zaharia AD, Carandini M. 2011. The Detection of Visual Contrast in the Behaving Mouse. *J Neurosci* **31**:11351–11361. doi:10.1523/JNEUROSCI.6689-10.2011

Carandini M, Heeger DJ. 2012. Normalization as a canonical neural computation. *Nat Rev Neurosci* **13**:51–62. doi:10.1038/nrn3136

Chakravarthi A, Baird E, Dacke M, Kelber A. 2016. Spatial Vision in Bombus terrestris. *Front Behav Neurosci* **10**. doi:10.3389/fnbeh.2016.00017

Chalasani SH, Chronis N, Tsunozaki M, Gray JM, Ramot D, Goodman MB, Bargmann CI. 2007. Dissecting a circuit for olfactory behaviour in Caenorhabditis elegans. *Nature* **450**:63–70. doi:10.1038/nature06292

Chichilnisky EJ, Kalmar RS. 2002. Functional Asymmetries in ON and OFF Ganglion Cells of Primate Retina. *J Neurosci* **22**:2737–2747. doi:10.1523/JNEUROSCI.22-07-02737.2002

Choi S-Y, Borghuis B, Rea R, Levitan ES, Sterling P, Kramer RH. 2005. Encoding Light Intensity by the Cone Photoreceptor Synapse. *Neuron* **48**:555–562. doi:10.1016/j.neuron.2005.09.011

Clandinin TR, Zipursky SL. 2002. Making connections in the fly visual system. *Neuron* **35**:827–841. doi:10.1016/S0896-6273(02)00876-0

Clark DA, Bursztyn L, Horowitz MA, Schnitzer MJ, Clandinin TR. 2011. Defining the Computational Structure of the Motion Detector in Drosophila. *Neuron*. doi:10.1016/j.neuron.2011.05.023

Clark DA, Demb JB. 2016. Parallel Computations in Insect and Mammalian Visual Motion Processing. *Curr Biol* **26**:R1062–R1072. doi:10.1016/j.cub.2016.08.003

Clark DA, Fitzgerald JE, Ales JM, Gohl DM, Silies MA, Norcia AM, Clandinin TR. 2014. Flies and humans share a motion estimation strategy that exploits natural scene statistics. *Nat Neurosci* **17**:296–303. doi:10.1038/nn.3600

Clemens J, Schöneich S, Kostarakos K, Hennig RM, Hedwig B. 2021. A small, computationally flexible network produces the phenotypic diversity of song recognition in crickets. *eLife* **10**:e61475. doi:10.7554/eLife.61475

Collett TS. 1980. Some operating rules for the optomotor system of a hoverfly during voluntary flight. *J Comp Physiol A* **138**:271–282. doi:10.1007/BF00657045

Costa M, Manton JD, Ostrovsky AD, Prohaska S, Jefferis GSXE. 2016. NBLAST: Rapid, Sensitive Comparison of Neuronal Structure and Construction of Neuron Family Databases. *Neuron* **91**:293–311. doi:10.1016/j.neuron.2016.06.012

Crawford JD, Vilis T. 1991. Axes of eye rotation and Listing's law during rotations of the head. *J Neurophysiol* **65**:407–423. doi:10.1152/jn.1991.65.3.407

Dacey D, Packer OS, Diller L, Brainard D, Peterson B, Lee B. 2000. Center surround receptive field structure of cone bipolar cells in primate retina. *Vision Res* **40**:1801–1811. doi:10.1016/S0042-6989(00)00039-0

Dakin SC, Turnbull PRK. 2016. Similar contrast sensitivity functions measured using psychophysics and optokinetic nystagmus. *Sci Rep* **6**:34514. doi:10.1038/srep34514

Daly SJ, Normann RA. 1985. Temporal information processing in cones: Effects of light adaptation on temporal summation and modulation. *Vision Res* **25**:1197–1206. doi:10.1016/0042-6989(85)90034-3

Davis FP, Nern A, Picard S, Reiser MB, Rubin GM, Eddy SR, Henry GL. 2020. A genetic, genomic, and computational resource for exploring neural circuit function. *eLife* **9**:e50901. doi:10.7554/eLife.50901

Demb JB, Zaghloul K, Haarsma L, Sterling P. 2001. Bipolar Cells Contribute to Nonlinear Spatial Summation in the Brisk-Transient (Y) Ganglion Cell in Mammalian Retina. *J Neurosci* **21**:7447–7454. doi:10.1523/JNEUROSCI.21-19-07447.2001

Ding H, Smith RG, Poleg-Polsky A, Diamond JS, Briggman KL. 2016. Species-specific wiring for direction selectivity in the mammalian retina. *Nature* **535**:105–110. doi:10.1038/nature18609

Dubs A, Laughlin SB, Srinivasan MV. 1981. Single photon signals in fly photoreceptors and first order interneurones at behavioral threshold. *J Physiol* **317**:317–334. doi:10.1113/jphysiol.1981.sp013827

Dunn FA, Lankheet MJ, Rieke F. 2007. Light adaptation in cone vision involves switching between receptor and post-receptor sites. *Nature* **449**:603–606. doi:10.1038/nature06150

Eckstein N, Bates AS, Du M, Hartenstein V, Jefferis GSXE, Funke J. 2020. Neurotransmitter Classification from Electron Microscopy Images at Synaptic Sites in Drosophila (preprint). Neuroscience. doi:10.1101/2020.06.12.148775

Edelman GM, Gally JA. 2001. Degeneracy and complexity in biological systems. *Proc Natl Acad Sci* **98**:13763–13768. doi:10.1073/pnas.231499798

Eschbach C, Fushiki A, Winding M, Afonso B, Andrade IV, Cocanougher BT, Eichler K, Gepner R, Si G, Valdes-Aleman J, Fetter RD, Gershow M, Jefferis GS, Samuel AD, Truman JW, Cardona A, Zlatic M. 2021. Circuits for integrating learned and innate valences in the insect brain. *eLife* **10**:e62567. doi:10.7554/eLife.62567

Euler T, Haverkamp S, Schubert T, Baden T. 2014. Retinal bipolar cells: Elementary building blocks of vision. *Nat Rev Neurosci* **15**:507–519. doi:10.1038/nrn3783

Euler T, Schneider H, Wässle H. 1996. Glutamate Responses of Bipolar Cells in a Slice Preparation of the Rat Retina. *J Neurosci* **16**:2934–2944. doi:10.1523/JNEUROSCI.16-09-02934.1996

Fain GL, Matthews HR, Cornwall MC, Koutalos Y. 2001. Adaptation in Vertebrate Photoreceptors. *Physiol Rev* **81**:117–151. doi:10.1152/physrev.2001.81.1.117

Fechner GT. 1948. Elements of psychophysics, 1860. In: Dennis W, editor. Readings in the History of Psychology. East Norwalk: Appleton-Century-Crofts. pp. 206–213. doi:10.1037/11304-026

Fischbach KF, Dittrich APM. 1989. The optic lobe of Drosophila melanogaster. I. A Golgi analysis of wild-type structure. *Cell Tissue Res.* doi:10.1007/BF00218858

Fisher YE, Leong JCS, Sporar K, Ketkar MD, Gohl DM, Clandinin TR, Silies M. 2015. A Class of Visual Neurons with Wide-Field Properties Is Required for Local Motion Detection. *Curr Biol.* doi:10.1016/j.cub.2015.11.018

Fornito A, Zalesky A, Bullmore ET. 2016. Fundamentals of Brain Network Analysis. Elsevier. doi:10.1016/C2012-0-06036-X

Franceschini N, Kirschfeld K, Minke B. 1981. Fluorescence of Photoreceptor Cells Observed in Vivo. *Science* **213**:1264–1267. doi:10.1126/science.7268434

Franke K, Berens P, Schubert T, Bethge M, Euler T, Baden T. 2017. Inhibition decorrelates visual feature representations in the inner retina. *Nature* **542**:439–444. doi:10.1038/nature21394

Frazor RA, Geisler WS. 2006. Local luminance and contrast in natural images. *Vision Res* **46**:1585–1598. doi:10.1016/j.visres.2005.06.038

Freifeld L, Clark DA, Schnitzer MJ, Horowitz MA, Clandinin TR. 2013. GABAergic Lateral Interactions Tune the Early Stages of Visual Processing in Drosophila. *Neuron*. doi:10.1016/j.neuron.2013.04.024

Fu Y, Yau K-W. 2007. Phototransduction in mouse rods and cones. *Pflüg Arch - Eur J Physiol* **454**:805–819. doi:10.1007/s00424-006-0194-y

Gallio M, Ofstad TA, Macpherson LJ, Wang JW, Zuker CS. 2011. The Coding of Temperature in the Drosophila Brain. *Cell* **144**:614–624. doi:10.1016/j.cell.2011.01.028

Gengs C, Leung H-T, Skingsley DR, Iovchev MI, Yin Z, Semenov EP, Burg MG, Hardie RC, Pak WL. 2002. The Target of Drosophila Photoreceptor Synaptic Transmission Is a Histamine-gated Chloride Channel Encoded byort (hclA). *J Biol Chem* **277**:42113–42120. doi:10.1074/jbc.M207133200

Gjorgjieva J, Sompolinsky H, Meister M. 2014. Benefits of Pathway Splitting in Sensory Coding. *J Neurosci* **34**:12127–12144. doi:10.1523/JNEUROSCI.1032-14.2014

Gollisch T, Meister M. 2010. Eye Smarter than Scientists Believed: Neural Computations in Circuits of the Retina. *Neuron* **65**:150–164. doi:10.1016/j.neuron.2009.12.009

Götz KG. 1968. Flight control in Drosophila by visual perception of motion. *Kybernetik* **4**:199–208. doi:10.1007/BF00272517

Götz KG, Wehrhahn C. 1984. Optomotor control of the force of flight in Drosophila and Musca: I. Homology of wingbeat-inhibiting movement detectors. *Biol Cybern* **51**:129–134. doi:10.1007/BF00357926

Graham BJ, Hildebrand DGC, Kuan AT, Maniates-Selvin JT, Thomas LA, Shanny BL, Lee W-CA. 2019. High-throughput transmission electron microscopy with automated serial sectioning (preprint). Neuroscience. doi:10.1101/657346

Gür B, Sporar K, Lopez-Behling A, Silies M. 2020. Distinct expression of potassium channels regulates visual response properties of lamina neurons in Drosophila melanogaster. *J Comp Physiol A Neuroethol Sens Neural Behav Physiol* **206**:273–287. doi:10.1007/s00359-019-01385-7

Gutierrez GJ, O'Leary T, Marder E. 2013. Multiple Mechanisms Switch an Electrically Coupled, Synaptically Inhibited Neuron between Competing Rhythmic Oscillators. *Neuron* **77**:845–858. doi:10.1016/j.neuron.2013.01.016

Hagberg A, Swart P, Chult D. 2008. Exploring Network Structure, Dynamics, and Function Using NetworkX. Presented at the Proceedings of the 7th Python in Science Conference.

Hagins WA, Penn RD, Yoshikami S. 1970. Dark Current and Photocurrent in Retinal Rods. *Biophys J* **10**:380–412. doi:10.1016/S0006-3495(70)86308-1

Hanchate NK, Lee EJ, Ellis A, Kondoh K, Kuang D, Basom R, Trapnell C, Buck LB. 2020. Connect-seq to superimpose molecular on anatomical neural circuit maps. *Proc Natl Acad Sci* **117**:4375–4384. doi:10.1073/pnas.1912176117

Hardie RC. 1989. A histamine-activated chloride channel involved in neurotransmission at a photoreceptor synapse. *Nature* **339**:704–706. doi:10.1038/339704a0

Hardie RC, Raghu P. 2001. Visual transduction in Drosophila. *Nature* **413**:186–193. doi:10.1038/35093002

Hardin PE. 2005. The Circadian Timekeeping System of Drosophila. *Curr Biol* **15**:R714–R722. doi:10.1016/j.cub.2005.08.019

Hart N. 2001. Variations in cone photoreceptor abundance and the visual ecology of birds. *J Comp Physiol [A]* **187**:685–697. doi:10.1007/s00359-001-0240-3

Heinl S, Grabherr R. 2017. Systems biology of robustness and flexibility: Lactobacillus buchneri —A show case. *J Biotechnol* **257**:61–69. doi:10.1016/j.jbiotec.2017.01.007

Helmstaedter M, Briggman KL, Denk W. 2011. High-accuracy neurite reconstruction for high-throughput neuroanatomy. *Nat Neurosci* **14**:1081–1088. doi:10.1038/nn.2868

Henning M, Ramos-Traslosheros G, Gür B, Silies M. 2021. An optimal population code for global motion estimation in local direction-selective cells. *bioRxiv* 2021.03.17.435642. doi:10.1101/2021.03.17.435642

Hildebrand DGC, Cicconet M, Torres RM, Choi W, Quan TM, Moon J, Wetzel AW, Scott Champion A, Graham BJ, Randlett O, Plummer GS, Portugues R, Bianco IH, Saalfeld S, Baden AD, Lillaney K, Burns R, Vogelstein JT, Schier AF, Lee W-CA, Jeong W-K, Lichtman JW, Engert F. 2017. Whole-brain serial-section electron microscopy in larval zebrafish. *Nature* **545**:345–349. doi:10.1038/nature22356

Hong S-T, Bang S, Paik D, Kang J, Hwang S, Jeon K, Chun B, Hyun S, Lee Y, Kim J. 2006. Histamine and Its Receptors Modulate Temperature-Preference Behaviors in Drosophila. *J Neurosci* **26**:7245–7256. doi:10.1523/JNEUROSCI.5426-05.2006

Honma K, Hashimoto S, Nakao M, Honma S. 2003. Period and Phase Adjustments of Human Circadian Rhythms in the Real World. *J Biol Rhythms* **18**:261–270. doi:10.1177/0748730403018003008

Huang GB, Plaza S. 2014. Identifying Synapses Using Deep and Wide Multiscale Recursive Networks. *ArXiv14091789 Cs.*

Ichinose T, Fyk-Kolodziej B, Cohn J. 2014. Roles of ON Cone Bipolar Cell Subtypes in Temporal Coding in the Mouse Retina. *J Neurosci* **34**:8761–8771. doi:10.1523/JNEUROSCI.3965-13.2014

Ichinose T, Hellmer CB. 2016. Differential signalling and glutamate receptor compositions in the OFF bipolar cell types in the mouse retina: Temporal coding in the retinal OFF bipolar cells. *J Physiol* **594**:883–894. doi:10.1113/JP271458

Ichinose T, Lukasiewicz PD. 2007. Ambient Light Regulates Sodium Channel Activity to Dynamically Control Retinal Signaling. *J Neurosci* **27**:4756–4764. doi:10.1523/JNEUROSCI.0183-07.2007

Idrees S, Münch TA. 2020. Different contrast encoding in ON and OFF visual pathways (preprint). Neuroscience. doi:10.1101/2020.11.25.398230

Ikeda M, Nakano S, Giles AC, Costa WS, Gottschalk A, Mori I. 2018. Circuit Degeneracy Facilitates Robustness and Flexibility of Navigation Behavior in *C.elegans* (preprint). Neuroscience. doi:10.1101/385468

Jankowska E. 2001. Spinal interneuronal systems: identification, multifunctional character and reconfigurations in mammals. *J Physiol* **533**:31–40. doi:10.1111/j.1469-7793.2001.0031b.x

Januszewski M, Kornfeld J, Li PH, Pope A, Blakely T, Lindsey L, Maitin-Shepard J, Tyka M, Denk W, Jain V. 2018. High-precision automated reconstruction of neurons with flood-filling networks. *Nat Methods* **15**:605–610. doi:10.1038/s41592-018-0049-4

Jarrell TA, Wang Y, Bloniarz AE, Brittin CA, Xu M, Thomson JN, Albertson DG, Hall DH, Emmons SW. 2012. The Connectome of a Decision-Making Neural Network. *Science* **337**:437–444. doi:10.1126/science.1221762

Jin J, Wang Y, Lashgari R, Swadlow HA, Alonso J-M. 2011. Faster Thalamocortical Processing for Dark than Light Visual Targets. *J Neurosci* **31**:17471–17479. doi:10.1523/JNEUROSCI.2456-11.2011

Joesch M, Plett J, Borst A, Reiff DF. 2008. Response Properties of Motion-Sensitive Visual Interneurons in the Lobula Plate of Drosophila melanogaster. *Curr Biol* **18**:368–374. doi:10.1016/j.cub.2008.02.022

Joesch M, Schnell B, Raghu SV, Reiff DF, Borst A. 2010. ON and off pathways in Drosophila motion vision. *Nature.* doi:10.1038/nature09545

Jones EG. 1994. The neuron doctrine 1891. *J Hist Neurosci* **3**:3–20. doi:10.1080/09647049409525584

Juusola M, Uusitalo RO, Weckström M. 1995. Transfer of graded potentials at the photoreceptor-interneuron synapse. *J Gen Physiol* **105**:117–48.

Kaifosh P, Zaremba JD, Danielson NB, Losonczy A. 2014. SIMA: Python software for analysis of dynamic fluorescence imaging data, Frontiers in Neuroinformatics.

Kato S, Negishi K. 1979. Rod- and cone-bipolar cell responses in the carp retina. *Exp Eye Res* **28**:159–166. doi:10.1016/0014-4835(79)90128-3

Kaupp UB. 2010. Olfactory signalling in vertebrates and insects: differences and commonalities. *Nat Rev Neurosci* **11**:188–200. doi:10.1038/nrn2789

Kawamura S, Tachibanaki S. 2008. Rod and cone photoreceptors: Molecular basis of the difference in their physiology. *Comp Biochem Physiol A Mol Integr Physiol* **150**:369–377. doi:10.1016/j.cbpa.2008.04.600

Keleş MF, Mongeau JM, Frye MA. 2019. Object features and T4/T5 motion detectors modulate the dynamics of bar tracking by Drosophila. *J Exp Biol*. doi:10.1242/jeb.190017

Ketkar M, Gür B, Molina-Obando S, Ioannidou M, Martelli C, Silies M. 2021. First-order visual interneurons distribute distinct contrast and luminance information across ON and OFF pathways to achieve stable behavior (preprint). Neuroscience. doi:10.1101/2021.11.03.467156

Ketkar MD, Sporar K, Gür B, Ramos-Traslosheros G, Seifert M, Silies M. 2020. Luminance Information Is Required for the Accurate Estimation of Contrast in Rapidly Changing Visual Contexts. *Curr Biol*. doi:10.1016/j.cub.2019.12.038

Kirschfeld K. 1967. Die projektion der optischen umwelt auf das raster der rhabdomere im komplexauge von Musca. *Exp Brain Res* **3**:248–270. doi:10.1007/BF00235588

Kitamoto T. 2001. Conditional modification of behavior inDrosophila by targeted expression of a temperature-sensitiveshibire allele in defined neurons. *J Neurobiol* **47**:81–92. doi:10.1002/neu.1018

Kitano H. 2004. Biological robustness. *Nat Rev Genet* **5**:826–837. doi:10.1038/nrg1471

Knipple DC, Soderlund DM. 2010. The ligand-gated chloride channel gene family of Drosophila melanogaster. *Pestic Biochem Physiol* **97**:140–148. doi:10.1016/j.pestbp.2009.09.002

Koike C, Numata T, Ueda H, Mori Y, Furukawa T. 2010. TRPM1: A vertebrate TRP channel responsible for retinal ON bipolar function. *Cell Calcium* **48**:95–101. doi:10.1016/j.ceca.2010.08.004

Koo PK, Bian X, Sherlekar AL, Bunkers MR, Lints R. 2011. The Robustness of Caenorhabditis elegans Male Mating Behavior Depends on the Distributed Properties of Ray Sensory Neurons and Their Output through Core and Male-Specific Targets. *J Neurosci* **31**:7497–7510. doi:10.1523/JNEUROSCI.6153-10.2011

Laughlin S. 1981. Neural Principles in the Peripheral Visual Systems of Invertebrates. pp. 133–280. doi:10.1007/978-3-642-66907-1_2

Laughlin SB. 1989. The role of sensory adaptation in the retina. *J Exp Biol* **146**:39–62.

Laughlin SB, Hardie RC. 1978. Common strategies for light adaptation in the peripheral visual systems of fly and dragonfly. *J Comp Physiol* **128**:319–340. doi:10.1007/BF00657606

Laughlin SB, Howard J, Blakeslee B. 1987. Synaptic limitations to contrast coding in the retina of the blowfly *Calliphora*. *Proc R Soc Lond B Biol Sci* **231**:437–467. doi:10.1098/rspb.1987.0054

Lee K, Turner N, Macrina T, Wu J, Lu R, Seung HS. 2019. Convolutional nets for reconstructing neural circuits from brain images acquired by serial section electron microscopy. *Curr Opin Neurobiol* **55**:188–198. doi:10.1016/j.conb.2019.04.001

Lee W-CA, Bonin V, Reed M, Graham BJ, Hood G, Glattfelder K, Reid RC. 2016. Anatomy and function of an excitatory network in the visual cortex. *Nature* **532**:370–374. doi:10.1038/nature17192

Leonardo A. 2005. Degenerate coding in neural systems. *J Comp Physiol A* **191**:995–1010. doi:10.1007/s00359-005-0026-0

Leonhardt A, Ammer G, Meier M, Serbe E, Bahl A, Borst A. 2016. Asymmetry of Drosophila on and off motion detectors enhances real-world velocity estimation. *Nat Neurosci*. doi:10.1038/nn.4262

Li PH, Lindsey LF, Januszewski M, Tyka M, Maitin-Shepard J, Blakely T, Jain V. 2019. Automated Reconstruction of a Serial-Section EM Drosophila Brain with Flood-Filling Networks and Local Realignment. *Microsc Microanal* **25**:1364–1365. doi:10.1017/S1431927619007554

Li Z, Liu J, Zheng M, Xu XZS. 2014. Encoding of Both Analog- and Digital-like Behavioral Outputs by One C. elegans Interneuron. *Cell* **159**:751–765. doi:10.1016/j.cell.2014.09.056

Liang Z, Freed MA. 2010. The ON Pathway Rectifies the OFF Pathway of the Mammalian Retina. *J Neurosci* **30**:5533–5543. doi:10.1523/JNEUROSCI.4733-09.2010

Lin T-Y, Luo J, Shinomiya K, Ting C-Y, Lu Z, Meinertzhagen IA, Lee C-H. 2016. Mapping chromatic pathways in the *Drosophila* visual system: Chromatic Visual Circuits in the Fly's Lobula. *J Comp Neurol* **524**:213–227. doi:10.1002/cne.23857

Liu M, Sharma AK, Shaevitz JW, Leifer AM. 2018. Temporal processing and context dependency in Caenorhabditis elegans response to mechanosensation. *eLife* **7**:e36419. doi:10.7554/eLife.36419

Liu WW, Wilson RI. 2013. Glutamate is an inhibitory neurotransmitter in the Drosophila olfactory system. *Proc Natl Acad Sci* **110**:10294–10299. doi:10.1073/pnas.1220560110

Livingstone M, Hubel D. 1988. Segregation of form, color, movement, and depth: anatomy, physiology, and perception. *Science* **240**:740–749.

Lombardino AJ, Nottebohm F. 2000. Age at Deafening Affects the Stability of Learned Song in Adult Male Zebra Finches. *J Neurosci* **20**:5054–5064. doi:10.1523/JNEUROSCI.20-13-05054.2000

Macrina T, Lee K, Lu R, Turner NL, Wu J, Popovych S, Silversmith W, Kemnitz N, Bae JA, Castro MA, Dorkenwald S, Halageri A, Jia Z, Jordan C, Li K, Mitchell E, Mondal SS, Mu S, Nehoran B, Wong W, Yu S, Bodor AL, Brittain D, Buchanan J, Bumbarger DJ, Cobos E, Collman F, Elabbady L, Fahey PG, Froudarakis E, Kapner D, Kinn S, Mahalingam G, Papadopoulos S, Patel S, Schneider-Mizell CM, Sinz FH, Takeno M, Torres R, Yin W, Pitkow X, Reimer J, Tolias AS, Reid RC, Costa NM da, Seung HS. 2021. Petascale neural circuit reconstruction: automated methods (preprint). Neuroscience. doi:10.1101/2021.08.04.455162

Maddox J. 1994. Cocktail party effect made tolerable. *Nature* **369**:517–517. doi:10.1038/369517a0

Maisak MS, Haag J, Ammer G, Serbe E, Meier M, Leonhardt A, Schilling T, Bahl A, Rubin GM, Nern A, Dickson BJ, Reiff DF, Hopp E, Borst A. 2013. A directional tuning map of Drosophila elementary motion detectors. *Nature* **500**:212–216. doi:10.1038/nature12320

Mangan S, Alon U. 2003. Structure and function of the feed-forward loop network motif. *Proc Natl Acad Sci* **100**:11980–11985. doi:10.1073/pnas.2133841100

Manookin MB, Beaudoin DL, Ernst ZR, Flagel LJ, Demb JB. 2008. Disinhibition Combines with Excitation to Extend the Operating Range of the OFF Visual Pathway in Daylight. *J Neurosci* **28**:4136–4150. doi:10.1523/JNEUROSCI.4274-07.2008

Mante V, Frazor RA, Bonin V, Geisler WS, Carandini M. 2005. Independence of luminance and contrast in natural scenes and in the early visual system. *Nat Neurosci* **8**:1690–1697. doi:10.1038/nn1556

Marder E. 2012. Neuromodulation of Neuronal Circuits: Back to the Future. *Neuron* **76**:1–11. doi:10.1016/j.neuron.2012.09.010

Martemyanov KA, Sampath AP. 2017. The Transduction Cascade in Retinal ON-Bipolar Cells: Signal Processing and Disease. *Annu Rev Vis Sci* **3**:25–51. doi:10.1146/annurev-vision-102016-061338

Martin KAC. 1994. A Brief History of the "Feature Detector." *Cereb Cortex* **4**:1–7. doi:10.1093/cercor/4.1.1

Masland RH. 2012. The Neuronal Organization of the Retina. *Neuron* **76**:266–280. doi:10.1016/j.neuron.2012.10.002

Masoudi-Nejad A, Schreiber F, Kashani ZRM. 2012. Building blocks of biological networks: a review on major network motif discovery algorithms. *IET Syst Biol* **6**:164–174. doi:10.1049/iet-syb.2011.0011

Masu M, Iwakabe H, Tagawa Y, Miyoshi T, Yamashita M, Fukuda Y, Sasaki H, Hiroi K, Nakamura Y, Shigemoto R. 1995. Specific deficit of the ON response in visual transmission by targeted disruption of the mGluR6 gene. *Cell* **80**:757–765.

Matulis CA, Chen J, Gonzalez-Suarez AD, Behnia R, Clark DA. 2020. Heterogeneous Temporal Contrast Adaptation in Drosophila Direction-Selective Circuits. *Curr Biol.* doi:10.1016/j.cub.2019.11.077

Mauss AS, Vlasits A, Borst A, Feller M. 2017. Visual Circuits for Direction Selectivity. doi:10.1146/annurev-neuro-072116

Meier M, Borst A. 2019. Extreme Compartmentalization in a Drosophila Amacrine Cell. *Curr Biol* **29**:1545-1550.e2. doi:10.1016/j.cub.2019.03.070

Meinertzhagen IA. 2001. Plasticity in the insect nervous systemAdvances in Insect Physiology. Elsevier. pp. 84–167. doi:10.1016/S0065-2806(01)28009-6

Meinertzhagen IA, O'Neil SD. 1991. Synaptic organization of columnar elements in the lamina of the wild type in Drosophila melanogaster. *J Comp Neurol* **305**:232–263. doi:10.1002/cne.903050206

Meir E, von Dassow G, Munro E, Odell GM. 2002. Robustness, Flexibility, and the Role of Lateral Inhibition in the Neurogenic Network. *Curr Biol* **12**:778–786. doi:10.1016/S0960-9822(02)00839-4

Metzner W, Viete S. 1996. The neuronal basis of communication and orientation in the weakly electric fish,Eigenmannia: II. Electrolocation and avoidance of jamming by neighboring conspecifics. *Naturwissenschaften* **83**:71–77. doi:10.1007/BF01141873

Meyer B-U, Röricht S, Niehaus L. 1998. Morphology of acallosal brains as assessed by MRI in six patients leading a normal daily life. *J Neurol* **245**:106–110. doi:10.1007/s004150050187

MICrONS Consortium, Bae JA, Baptiste M, Bodor AL, Brittain D, Buchanan J, Bumbarger DJ, Castro MA, Celii B, Cobos E, Collman F, da Costa NM, Dorkenwald S, Elabbady L, Fahey PG, Fliss T, Froudarakis E, Gager J, Gamlin C, Halageri A, Hebditch J, Jia Z, Jordan C, Kapner D, Kemnitz N, Kinn S, Koolman S, Kuehner K, Lee K, Li K, Lu R, Macrina T, Mahalingam G, McReynolds S, Miranda E, Mitchell E, Mondal SS, Moore M, Mu S, Muhammad T, Nehoran B, Ogedengbe O, Papadopoulos C, Papadopoulos S, Patel S, Pitkow X, Popovych S, Ramos A, Reid RC, Reimer J, Schneider-Mizell CM, Seung HS, Silverman B, Silversmith W, Sterling A, Sinz FH, Smith CL, Suckow S, Takeno M, Tan ZH, Tolias AS, Torres R, Turner NL, Walker EY, Wang T, Williams G, Williams S, Willie K, Willie R, Wong W, Wu J, Xu C, Yang R, Yatsenko D, Ye F, Yin W, Yu S. 2021. Functional connectomics spanning multiple areas of mouse visual cortex (preprint). Neuroscience. doi:10.1101/2021.07.28.454025

Miller RF, Slaughter MM. 1986. Excitatory amino acid receptors of the retina: diversity of subtypes and conductance mechanisms. *Trends Neurosci* **9**:211–218. doi:10.1016/0166-2236(86)90061-5

Milo R, Itzkovitz S, Kashtan N, Levitt R, Shen-Orr S, Ayzenshtat I, Sheffer M, Alon U. 2004. Superfamilies of Evolved and Designed Networks. *Science* **303**:1538–1542. doi:10.1126/science.1089167

Molina-Obando S, Vargas-Fique JF, Henning M, Gür B, Schladt M, Akhtar J, Berger TK, Silies M. 2019. ON selectivity in the Drosophila visual system is a multisynaptic process involving both glutamatergic and GABAergic inhibition. doi:10.7554/eLife.49373.001

Morante J, Desplan C. 2008. The Color-Vision Circuit in the Medulla of Drosophila. *Curr Biol* **18**:553–565. doi:10.1016/j.cub.2008.02.075

Morgans CW, Zhang J, Jeffrey BG, Nelson SM, Burke NS, Duvoisin RM, Brown RL. 2009. TRPM1 is required for the depolarizing light response in retinal ON-bipolar cells. *Proc Natl Acad Sci* **106**:19174–19178. doi:10.1073/pnas.0908711106

Morone F, Makse HA. 2019. Symmetry group factorization reveals the structure-function relation in the neural connectome of Caenorhabditis elegans. *Nat Commun* **10**:4961. doi:10.1038/s41467-019-12675-8

Mronz M, Lehmann F-O. 2008. The free-flight response of *Drosophila* to motion of the visual environment. *J Exp Biol* **211**:2026–2045. doi:10.1242/jeb.008268

Naka KI, Rushton WAH. 1966. S-potentials from luminosity units in the retina of fish (Cyprinidae). *J Physiol* **185**:587–599. doi:10.1113/jphysiol.1966.sp008003

Nern A, Pfeiffer BD, Rubin GM. 2015. Optimized tools for multicolor stochastic labeling reveal diverse stereotyped cell arrangements in the fly visual system. *Proc Natl Acad Sci* **112**:E2967–E2976. doi:10.1073/pnas.1506763112

Nilsson DE. 1983. Evolutionary links between apposition and superposition optics in crustacean eyes. *Nature* **302**:818–821. doi:10.1038/302818a0

Normann RA, Perlman I. 1979. The effects of background illumination on the photoresponses of red and green cones. *J Physiol* **286**:491–507. doi:10.1113/jphysiol.1979.sp012633

Normann RA, Werblin FS. 1974. Control of Retinal Sensitivity I . Light and Dark Adaptation of. *J Gen Physiol* **63**:37–61. doi:10.1085/jgp.63.1.37

Odermatt B, Nikolaev A, Lagnado L. 2012. Encoding of Luminance and Contrast by Linear and Nonlinear Synapses in the Retina. *Neuron* **73**:758–773. doi:10.1016/j.neuron.2011.12.023

Oesch NW, Diamond JS. 2011. Ribbon synapses compute temporal contrast and encode luminance in retinal rod bipolar cells. *Nat Neurosci* **14**:1555–1561. doi:10.1038/nn.2945

Ohyama T, Schneider-Mizell CM, Fetter RD, Aleman JV, Franconville R, Rivera-Alba M, Mensh BD, Branson KM, Simpson JH, Truman JW, Cardona A, Zlatic M. 2015. A multilevel multimodal circuit enhances action selection in Drosophila. *Nature* **520**:633–639. doi:10.1038/nature14297

Okamoto H, Aizawa H. 2013. Fear and Anxiety Regulation by Conserved Affective Circuits. *Neuron* **78**:411–413. doi:10.1016/j.neuron.2013.04.031

Palmer C, Cheng S-Y, Seidemann E. 2007. Linking Neuronal and Behavioral Performance in a Reaction-Time Visual Detection Task. *J Neurosci* **27**:8122–8137. doi:10.1523/JNEUROSCI.1940-07.2007

Parmentier ML, Pin JP, Bockaert J, Grau Y. 1996. Cloning and functional expression of a Drosophila metabotropic glutamate receptor expressed in the embryonic CNS. *J Neurosci Off J Soc Neurosci* **16**:6687–6694.

Paulus W, Rothwell JC. 2016. Membrane resistance and shunting inhibition: where biophysics meets state-dependent human neurophysiology: Membrane resistance and shunting inhibition. *J Physiol* **594**:2719–2728. doi:10.1113/JP271452

Peichl L. 2005. Diversity of mammalian photoreceptor properties: Adaptations to habitat and lifestyle? *Anat Rec A Discov Mol Cell Evol Biol* **287A**:1001–1012. doi:10.1002/ar.a.20262

Peirce JW. 2008. Generating stimuli for neuroscience using PsychoPy. *Front Neuroinformatics* **2**. doi:10.3389/neuro.11.010.2008

Pfeiffer BD, Ngo TTB, Hibbard KL, Murphy C, Jenett A, Truman JW, Rubin GM. 2010. Refinement of tools for targeted gene expression in Drosophila. *Genetics* **186**:735–755. doi:10.1534/genetics.110.119917

Pouli T, Cunningham D, Reinhard E. 2010. Statistical regularities in low and high dynamic range imagesProceedings of the 7th Symposium on Applied Perception in Graphics and Visualization - APGV '10. Presented at the the 7th Symposium. Los Angeles, California: ACM Press. p. 9. doi:10.1145/1836248.1836250

Ramón y Cajal S, Sánchez D, Madrid UC de. 1915. Contribución al conocimiento de los centros nerviosos de los insectos. Madrid : Imprenta de Hijos de Nicolás Moya,.

Ramos-Traslosheros G, Henning M, Silies M. 2018. Bewegungssehen: Zellen, Schaltkreise und Algorithmen. *Neuroforum* **24**:85–96. doi:10.1515/nf-2017-0028

Ramos-Traslosheros G, Silies M. 2021. The physiological basis for contrast opponency in motion computation in Drosophila. *Nat Commun* **12**:1–16. doi:10.1038/s41467-021-24986-w

Ratliff CP, Borghuis BG, Kao Y-H, Sterling P, Balasubramanian V. 2010. Retina is structured to process an excess of darkness in natural scenes. *Proc Natl Acad Sci* **107**:17368–17373. doi:10.1073/pnas.1005846107

Reiser MB, Dickinson MH. 2008. A modular display system for insect behavioral neuroscience. *J Neurosci Methods* **167**:127–139. doi:10.1016/j.jneumeth.2007.07.019

Rieke F, Rudd ME. 2009. The Challenges Natural Images Pose for Visual Adaptation. *Neuron* **64**:605–616. doi:10.1016/j.neuron.2009.11.028

Rinner O, Rick JM, Neuhauss SCF. 2005. Contrast Sensitivity, Spatial and Temporal Tuning of the Larval Zebrafish Optokinetic Response. *Investig Opthalmology Vis Sci* **46**:137. doi:10.1167/iovs.04-0682

Rister J, Pauls D, Schnell B, Ting CY, Lee CH, Sinakevitch I, Morante J, Strausfeld NJ, Ito K, Heisenberg M. 2007. Dissection of the Peripheral Motion Channel in the Visual System of Drosophila melanogaster. *Neuron* **56**:155–170. doi:10.1016/j.neuron.2007.09.014

Roemschied FA, Pacheco DA, Ireland EC, Li X, Aragon MJ, Pang R, Murthy M. 2021. Flexible Circuit Mechanisms for Context-Dependent Song Sequencing (preprint). Neuroscience. doi:10.1101/2021.11.01.466727

Rogerson LE, Behrens C, Euler T, Berens P, Schubert T. 2017. Connectomics of synaptic microcircuits: lessons from the outer retina: Connectomics of synaptic microcircuits. *J Physiol* **595**:5517–5524. doi:10.1113/JP273671

Rokni U, Richardson AG, Bizzi E, Seung HS. 2007. Motor Learning with Unstable Neural Representations. *Neuron* **54**:653–666. doi:10.1016/j.neuron.2007.04.030

Ross BC. 2014. Mutual information between discrete and continuous data sets. *PLoS ONE* **9**:e87357–e87357. doi:10.1371/journal.pone.0087357

Rossum G van, Drake FL. 2010. The Python language reference, Release 3.0.1 [Repr.]. ed, Python documentation manual / Guido van Rossum; Fred L. Drake [ed.]. Hampton, NH: Python Software Foundation.

Ruderman DL. 1994. The statistics of natural images. *Netw Comput Neural Syst* **5**:517–548. doi:10.1088/0954-898X_5_4_006

Rusanen J, Frolov R, Weckström M, Kinoshita M, Arikawa K. 2018. Non-linear amplification of graded voltage signals in the first-order visual interneurons of the butterfly Papilio xuthus. *J Exp Biol* **221**:jeb179085–jeb179085. doi:10.1242/jeb.179085

Rusanen J, Vähäkainu A, Weckström M, Arikawa K. 2017. Characterization of the first-order visual interneurons in the visual system of the bumblebee (Bombus terrestris). *J Comp Physiol A Neuroethol Sens Neural Behav Physiol* **203**:903–913. doi:10.1007/s00359-017-1201-9

Saalfeld S, Fetter R, Cardona A, Tomancak P. 2012. Elastic volume reconstruction from series of ultra-thin microscopy sections. *Nat Methods* **9**:717–720. doi:10.1038/nmeth.2072

Sanes JR, Zipursky SL. 2010. Design Principles of Insect and Vertebrate Visual Systems. *Neuron* **66**:15–36. doi:10.1016/j.neuron.2010.01.018

Scheffer LK, Xu CS, Januszewski M, Lu Z, Takemura Shin-ya, Hayworth KJ, Huang GB, Shinomiya K, Maitlin-Shepard J, Berg S, Clements J, Hubbard PM, Katz WT, Umayam L, Zhao T, Ackerman D, Blakely T, Bogovic J, Dolafi T, Kainmueller D, Kawase T, Khairy KA, Leavitt L, Li PH, Lindsey L, Neubarth N, Olbris DJ, Otsuna H, Trautman ET, Ito M, Bates AS, Goldammer J, Wolff T, Svirskas R, Schlegel P, Neace E, Knecht CJ, Alvarado CX, Bailey DA, Ballinger S, Borycz JA, Canino BS, Cheatham N, Cook M, Dreher M, Duclos O, Eubanks B, Fairbanks K, Finley S, Forknall N, Francis A, Hopkins GP, Joyce EM, Kim S, Kirk NA, Kovalyak J, Lauchie SA, Lohff A, Maldonado C, Manley EA, McLin S, Mooney C, Ndama M, Ogundeyi O, Okeoma N, Ordish C, Padilla N, Patrick CM, Paterson T, Phillips EE, Phillips EM, Rampally N, Ribeiro C, Robertson MK, Rymer JT, Ryan SM, Sammons M, Scott AK, Scott AL, Shinomiya A, Smith C, Smith K, Smith NL, Sobeski MA, Suleiman A, Swift J, Takemura Satoko, Talebi I, Tarnogorska D, Tenshaw E, Tokhi T, Walsh JJ, Yang T, Horne JA, Li F, Parekh R, Rivlin PK, Jayaraman V, Costa M, Jefferis GS, Ito K, Saalfeld S, George R, Meinertzhagen IA, Rubin GM, Hess HF, Jain V, Plaza SM. 2020. A connectome and analysis of the adult Drosophila central brain. *eLife* **9**:e57443. doi:10.7554/eLife.57443

Schiller PH. 1996. On the specificity of neurons and visual areas. *Behav Brain Res* **76**:21–35. doi:10.1016/0166-4328(95)00186-7

Schindelin J, Arganda-Carreras I, Frise E, Kaynig V, Longair M, Pietzsch T, Preibisch S, Rueden C, Saalfeld S, Schmid B, Tinevez J-Y, White DJ, Hartenstein V, Eliceiri K, Tomancak P, Cardona A. 2012. Fiji: an open-source platform for biological-image analysis. *Nat Methods* **9**:676–682. doi:10.1038/nmeth.2019

Schlegel P, Bates AS, Stürner T, Jagannathan SR, Drummond N, Hsu J, Serratosa Capdevila L, Javier A, Marin EC, Barth-Maron A, Tamimi IF, Li F, Rubin GM, Plaza SM, Costa M, Jefferis GSXE. 2021. Information flow, cell types and stereotypy in a full olfactory connectome. *eLife* **10**:e66018. doi:10.7554/eLife.66018

Schnaitmann C, Haikala V, Abraham E, Oberhauser V, Thestrup T, Griesbeck O, Reiff DF. 2018. Color Processing in the Early Visual System of Drosophila. *Cell* **172**:318-330.e18. doi:10.1016/j.cell.2017.12.018

Schnapf JL, Nunn BJ, Meister M, Baylor DA. 1990. Visual transduction in cones of the monkey Macaca fascicularis. *J Physiol* **427**:681–713. doi:10.1113/jphysiol.1990.sp018193

Schneider-Mizell CM, Gerhard S, Longair M, Kazimiers T, Li F, Zwart MF, Champion A, Midgley FM, Fetter RD, Saalfeld S, Cardona A. 2016. Quantitative neuroanatomy for connectomics in Drosophila. *eLife* **5**:e12059. doi:10.7554/eLife.12059

Schnell B, Joesch M, Forstner F, Raghu SV, Otsuna H, Ito K, Borst A, Reiff DF. 2010. Processing of Horizontal Optic Flow in Three Visual Interneurons of the *Drosophila* Brain. *J Neurophysiol* **103**:1646–1657. doi:10.1152/jn.00950.2009

Scholl B, Gao X, Wehr M. 2010. Nonoverlapping sets of synapses drive on responses and off responses in auditory cortex. *Neuron* **65**:412–21. doi:10.1016/j.neuron.2010.01.020.

Schwartz G, Rieke F. 2011. Nonlinear spatial encoding by retinal ganglion cells: when 1 + 1 ≠ 2. *J Gen Physiol* **138**:283–290. doi:10.1085/jgp.201110629

Scott EK, Raabe T, Luo L. 2002. Structure of the vertical and horizontal system neurons of the lobula plate inDrosophila. *J Comp Neurol* **454**:470–481. doi:10.1002/cne.10467

Seelig JD, Chiappe ME, Dutta A, Osborne JE, Reiser MB, Jayaraman V. 2010. Two-photon calcium imaging from head-fixed Drosophila during optomotor walking behavior. *Nat Methods* **7**:535–40. doi:10.1038/nmeth.1468

Serbe E, Meier M, Leonhardt A, Borst A. 2016. Comprehensive Characterization of the Major Presynaptic Elements to the Drosophila OFF Motion Detector. *Neuron* **89**:829–841. doi:10.1016/j.neuron.2016.01.006

Shapley R, Enroth-Cugell C. 1984. Chapter 9 Visual adaptation and retinal gain controls. *Prog Retin Res* **3**:263–346. doi:10.1016/0278-4327(84)90011-7

Shekhar K, Lapan SW, Whitney IE, Tran NM, Macosko EZ, Kowalczyk M, Adiconis X, Levin JZ, Nemesh J, Goldman M, McCarroll SA, Cepko CL, Regev A, Sanes JR. 2016. Comprehensive Classification of Retinal Bipolar Neurons by Single-Cell Transcriptomics. *Cell* **166**:1308-1323.e30. doi:10.1016/j.cell.2016.07.054

Shen Y, Heimel JA, Kamermans M, Peachey NS, Gregg RG, Nawy S. 2009. A Transient Receptor Potential-Like Channel Mediates Synaptic Transmission in Rod Bipolar Cells. *J Neurosci* **29**:6088–6093. doi:10.1523/JNEUROSCI.0132-09.2009

Sheng Z, Choi S-Y, Dharia A, Li J, Sterling P, Kramer RH. 2007. Synaptic Ca2+ in Darkness Is Lower in Rods than Cones, Causing Slower Tonic Release of Vesicles. *J Neurosci* **27**:5033–5042. doi:10.1523/JNEUROSCI.5386-06.2007

Sheridan A, Nguyen T, Deb D, Lee W-CA, Saalfeld S, Turaga S, Manor U, Funke J. 2021. Local Shape Descriptors for Neuron Segmentation (preprint). Neuroscience. doi:10.1101/2021.01.18.427039

Shiells R. 1994. Retinal Synapses: Glutamate receptors for signal amplification. *Curr Biol* **4**:917–918. doi:10.1016/S0960-9822(00)00204-9

Shih C-T, Sporns O, Yuan S-L, Su T-S, Lin Y-J, Chuang C-C, Wang T-Y, Lo C-C, Greenspan RJ, Chiang A-S. 2015. Connectomics-Based Analysis of Information Flow in the Drosophila Brain. *Curr Biol* **25**:1249–1258. doi:10.1016/j.cub.2015.03.021

Shinomiya K, Huang G, Lu Z, Parag T, Xu CS, Aniceto R, Ansari N, Cheatham N, Lauchie S, Neace E, Ogundeyi O, Ordish C, Peel D, Shinomiya A, Smith C, Takemura S, Talebi I, Rivlin PK, Nern A, Scheffer LK, Plaza SM, Meinertzhagen IA. 2019. Comparisons between the ON- and OFF-edge motion pathways in the Drosophila brain. *eLife* **8**:e40025. doi:10.7554/eLife.40025

Shinomiya K, Karuppudurai T, Lin TY, Lu Z, Lee CH, Meinertzhagen IA. 2014. Candidate neural substrates for off-edge motion detection in drosophila. *Curr Biol*. doi:10.1016/j.cub.2014.03.051

Silbering AF, Benton R. 2010. Ionotropic and metabotropic mechanisms in chemoreception: 'chance or design'? *EMBO Rep* **11**:173–179. doi:10.1038/embor.2010.8

Silies M, Gohl DM, Clandinin TR. 2014. Motion-Detecting Circuits in Flies: Coming into View. *Annu Rev Neurosci* **37**:307–327. doi:10.1146/annurev-neuro-071013-013931

Silies M, Gohl DM, Fisher YE, Freifeld L, Clark DA, Clandinin TR. 2013. Modular Use of Peripheral Input Channels Tunes Motion-Detecting Circuitry. *Neuron*. doi:10.1016/j.neuron.2013.04.029

Skutt-Kakaria K, Reimers P, Currier TA, Werkhoven Z, de Bivort BL. 2019. A neural circuit basis for context-modulation of individual locomotor behavior (preprint). Neuroscience. doi:10.1101/797126

Sporns O. 2018. Graph theory methods: applications in brain networks. *Dialogues Clin Neurosci* **20**:111–120. doi:10.31887/DCNS.2018.20.2/osporns

Sterling P, Freed M. 2007. How robust is a neural circuit? *Vis Neurosci* **24**:563–571. doi:10.1017/S0952523807070526

Strausfeld NJ. 1976. Atlas of an insect brain. Berlin ; New York: Springer-Verlag.

Strother JA, Nern A, Reiser MB. 2014. Direct observation of on and off pathways in the drosophila visual system. *Curr Biol*. doi:10.1016/j.cub.2014.03.017

Strother JA, Wu ST, Wong AM, Nern A, Rogers EM, Le JQ, Rubin GM, Reiser MB. 2017. The Emergence of Directional Selectivity in the Visual Motion Pathway of Drosophila. *Neuron* **94**:168-182.e10. doi:10.1016/j.neuron.2017.03.010

Takemura S, Karuppudurai T, Ting C-Y, Lu Z, Lee C-H, Meinertzhagen IA. 2011. Cholinergic Circuits Integrate Neighboring Visual Signals in a Drosophila Motion Detection Pathway. *Curr Biol* **21**:2077–2084. doi:10.1016/j.cub.2011.10.053

Takemura Shin-ya, Bharioke A, Lu Z, Nern A, Vitaladevuni S, Rivlin PK, Katz WT, Olbris DJ, Plaza SM, Winston P, Zhao T, Horne JA, Fetter RD, Takemura Satoko, Blazek K, Chang LA, Ogundeyi O, Saunders MA, Shapiro V, Sigmund C, Rubin GM, Scheffer LK, Meinertzhagen IA, Chklovskii DB. 2013. A visual motion detection circuit suggested by Drosophila connectomics. *Nature*. doi:10.1038/nature12450

Takemura Shin-ya, Xu CS, Lu Z, Rivlin PK, Parag T, Olbris DJ, Plaza S, Zhao T, Katz WT, Umayam L, Weaver C, Hess HF, Horne JA, Nunez-Iglesias J, Aniceto R, Chang L-A, Lauchie S, Nasca A, Ogundeyi O, Sigmund C, Takemura Satoko, Tran J, Langille C, Lacheur KL, McLin S, Shinomiya A, Chklovskii DB, Meinertzhagen IA, Scheffer LK. 2015. Synaptic circuits and their variations within different columns in the visual system of Drosophila. *Proc Natl Acad Sci* **112**:13711–13716. doi:10.1073/pnas.1509820112

Takemura SY, Lu Z, Meinertzhagen IA. 2008. Synaptic circuits of the Drosophila optic lobe: The input terminals to the medulla. *J Comp Neurol* **509**:493–513. doi:10.1002/cne.21757

Takemura SY, Nern A, Chklovskii DB, Scheffer LK, Rubin GM, Meinertzhagen IA. 2017. The comprehensive connectome of a neural substrate for 'ON' motion detection in Drosophila. *eLife*. doi:10.7554/eLife.24394

Talay M, Richman EB, Snell NJ, Hartmann GG, Fisher JD, Sorkaç A, Santoyo JF, Chou-Freed C, Nair N, Johnson M, Szymanski JR, Barnea G. 2017. Transsynaptic Mapping of Second-Order Taste Neurons in Flies by trans-Tango. *Neuron* **96**:783-795.e4. doi:10.1016/j.neuron.2017.10.011

Tan L, Zhang KX, Pecot MY, Nagarkar-Jaiswal S, Lee PT, Takemura SY, McEwen JM, Nern A, Xu S, Tadros W, Chen Z, Zinn K, Bellen HJ, Morey M, Zipursky SL. 2015.

Ig Superfamily Ligand and Receptor Pairs Expressed in Synaptic Partners in Drosophila. *Cell* **163**:1756–1769. doi:10.1016/j.cell.2015.11.021

Thibos LN, Werblin FS. 1978. The properties of surround antagonism elicited by spinning windmill patterns in the mudpuppy retina. *J Physiol* **278**:101–116. doi:10.1113/jphysiol.1978.sp012295

Tichy H, Hellwig M. 2018. Independent processing of increments and decrements in odorant concentration by ON and OFF olfactory receptor neurons. *J Comp Physiol A* **204**:873–891. doi:10.1007/s00359-018-1289-6

Timofeev K, Joly W, Hadjieconomou D, Salecker I. 2012. Localized netrins act as positional cues to control layer-specific targeting of photoreceptor axons in drosophila. *Neuron* **75**:80–93. doi:10.1016/j.neuron.2012.04.037

Tononi G, Sporns O, Edelman GM. 1999. Measures of degeneracy and redundancy in biological networks. *Proc Natl Acad Sci* **96**:3257–3262. doi:10.1073/pnas.96.6.3257

Trojanowski NF, Padovan-Merhar O, Raizen DM, Fang-Yen C. 2014. Neural and genetic degeneracy underlies *Caenorhabditis elegans* feeding behavior. *J Neurophysiol* **112**:951–961. doi:10.1152/jn.00150.2014

Tsukamoto Y, Omi N. 2017. Classification of Mouse Retinal Bipolar Cells: Type-Specific Connectivity with Special Reference to Rod-Driven AII Amacrine Pathways. *Front Neuroanat* **11**:92. doi:10.3389/fnana.2017.00092

Tuthill JC, Nern A, Holtz SL, Rubin GM, Reiser MB. 2013. Contributions of the 12 Neuron Classes in the Fly Lamina to Motion Vision. *Neuron* **79**:128–140. doi:10.1016/j.neuron.2013.05.024

Van Hateren JH. 1997. Processing of natural time series of intensities by the visual system of the blowfly. *Vision Res* **37**:3407–3416. doi:10.1016/S0042-6989(97)00105-3

van Hateren JH, van der Schaaf A. 1998. Independent component filters of natural images compared with simple cells in primary visual cortex. *Proc R Soc Lond B Biol Sci* **265**:359–366. doi:10.1098/rspb.1998.0303

Vardi N. 1998. Alpha subunit of Go localizes in the dendritic tips of ON bipolar cells. *J Comp Neurol* **395**:43–52.

Varshney LR, Chen BL, Paniagua E, Hall DH, Chklovskii DB. 2011. Structural Properties of the Caenorhabditis elegans Neuronal Network. *PLoS Comput Biol* **7**:e1001066. doi:10.1371/journal.pcbi.1001066

Wei H, Kyung HY, Kim PJ, Desplan C. 2020. The diversity of lobula plate tangential cells (LPTCs) in the Drosophila motion vision system. *J Comp Physiol A* **206**:139–148. doi:10.1007/s00359-019-01380-y

Werblin FS, Dowling JE. 1969. Organization of the retina of the mudpuppy, Necturus maculosus. II. Intracellular recording. *J Neurophysiol* **32**:339–355. doi:10.1152/jn.1969.32.3.339

White JG, Southgate E, Thomson JN, Brenner S. 1986. The structure of the nervous system of the nematode *Caenorhabditis elegans*. *Philos Trans R Soc Lond B Biol Sci* **314**:1–340. doi:10.1098/rstb.1986.0056

Witvliet D, Mulcahy B, Mitchell JK, Meirovitch Y, Berger DR, Wu Y, Liu Y, Koh WX, Parvathala R, Holmyard D, Schalek RL, Shavit N, Chisholm AD, Lichtman JW, Samuel ADT, Zhen M. 2021. Connectomes across development reveal principles of brain maturation. *Nature* **596**:257–261. doi:10.1038/s41586-021-03778-8

Xu CS, Hayworth KJ, Lu Z, Grob P, Hassan AM, García-Cerdán JG, Niyogi KK, Nogales E, Weinberg RJ, Hess HF. 2017. Enhanced FIB-SEM systems for large-volume 3D imaging. *eLife* **6**:e25916. doi:10.7554/eLife.25916

Yang HH, Clandinin TR. 2018. Elementary Motion Detection in Drosophila : Algorithms and Mechanisms. *Annu Rev Vis Sci* **4**:143–163. doi:10.1146/annurev-vision-091517-034153

Yang HHH, St-Pierre F, Sun X, Ding X, Lin MZZ, Clandinin TRR. 2016. Subcellular Imaging of Voltage and Calcium Signals Reveals Neural Processing In Vivo. *Cell* **166**:245–257. doi:10.1016/j.cell.2016.05.031

Zhao T, Olbris DJ, Yu Y, Plaza SM. 2018. NeuTu: Software for Collaborative, Large-Scale, Segmentation-Based Connectome Reconstruction. *Front Neural Circuits* **12**:101. doi:10.3389/fncir.2018.00101

Zheng Z, Lauritzen JS, Perlman E, Robinson CG, Nichols M, Milkie D, Torrens O, Price J, Fisher CB, Sharifi N, Calle-Schuler SA, Kmecova L, Ali IJ, Karsh B, Trautman ET, Bogovic JA, Hanslovsky P, Jefferis GSXE, Kazhdan M, Khairy K, Saalfeld S, Fetter RD, Bock DD. 2018. A Complete Electron Microscopy Volume of the Brain of Adult Drosophila melanogaster. *Cell* **174**:730-743.e22. doi:10.1016/j.cell.2018.06.019

Appendix

i.   List of abbreviations

ON:	contrast increments
OFF:	contrast decrements
ON pathway:	group of neurons detecting contrast increments
OFF-pathway:	group of neurons detecting contrast decrements
OPL:	outer plexiform layer
IPL:	inner plexiform layer
RGCs.	retina ganglion cells
HCs:	horizontal cells
ACs:	amacrine cells
BCs:	bipolar cells
ON-RBCs:	ON rod bipolar cells
ON-CBCs:	ON cone bipolar cells
OFF-CBCs:	OFF cone bipolar cells
mGluR:	metabotropic glutamate receptors
TRP channels:	transient receptor potential channels
L:	lamina
M:	medulla
Lo:	lobula
LP:	lobula plate
GluCls:	glutamate-gated chloride channels
nAChRs:	nicotinic acetylcholine receptors
PLC:	phospholipase C
Ort receptors:	ora transientless receptors
HisCl1:	histamine chloride channel 1
Rdl:	resistance to dieldrin
STG:	somatogastric ganglion
FFL:	feed-forward loop
LGN:	lateral geniculate nucleus

ii.   List of figures

Figures in the general introduction and general discussion

Figures in manuscripts (first study excluded)

<u>Second study</u>

<u>Third study</u>

Declaration

Herewith I declare that I prepared the doctoral thesis **'Mechanisms for robust feature extraction in early visual processing**' on my own and with no other sources and aids than quoted.

Mainz, 31.12.2021

Sebastian M. Molina-Obando

Curriculum Vitae

Sebastian M. Molina-Obando

AG Silies
Institute of Developmental Biology
and Neurobiology (iDN)
Johannes Gutenberg University Mainz
+49 6131 39 36104
sebastian.molina.obando@gmail.com

EDUCATION

Apr' 17 – present	**PhD student** *International Max Planck Research School for Neurosciences, GGNB Neurosciences, George August University in Göttingen*, Germany.
Sep' 15 – Jul' 17	**M.Sc., in Neurosciences**, *George August University in Göttingen*, Germany.
Sep' 11 – Jul'1 5	**B.Sc., Biomedical Sciences**, Autonomous *University of Barcelona (UAB)*, Spain.
Sep' 07 – Jul' 10	**Diploma in Nursing,** Autonomous *University of Barcelona (UAB)*, Spain.
Sep' 05– Jul' 07	**High school studies**, *Scientific branch, IESS Princep de Viana, Barcelona, Spain*

RESEARCH EXPERIENCE

Apr' 17 – present	**PhD Thesis**, *University of Göttingen*, Visual processing lab, Dr. Marion Silies *Mechanism of robust detection in early visual processing. Two-photon and confocal microscopy, qRT-PCR, image processing, data analysis, fly genetics, behavioural experiments.*
Oct' 16 – Mar' 17	**Master Thesis**, *University of Göttingen*, Visual processing lab, Dr. Marion Silies *Molecular mechanisms that shape ON responses in the Drosophila visual system. Two-photon and confocal microscopy, image processing, data analysis, fly genetics.*
Mar' 16 – May ' 16	**Lab Rotation**, *University* of Göttingen, Synaptogenesis lab, Prof.Dr. Thomas Dresbach *Release probability in the presynapse of mover knock out and wild type neurons. Patch clamp, data analysis, immunostainings.*
Jan' 16 – Mar' 16	**Lab Rotation**, *MPI for experimental medicine*, Electrophisilogy lab, Prof.Dr. Luis Pardo *Voltage-gated potassium channels conductance measurements. Two-electrode voltage clamp, data analysis.*
Jan' 15–Jul' 15	**Lab Rotation**, *CRG (Center of genomics Regulation) Barcelona-Spain*. Cellular and Systems neurobiology Lab. Dr. Mara Dierssen. *Research in Down syndrome with mice models. Primary cell culture, confocal microscopy.*

PUBLICATIONS

2021	**Molina-Obando, S.*,** Madhura D Ketkar*, Burak Gür*, Maria Ioannidou1,3, and Marion Silies (2021, under review). First-order visual interneurons distribute distinct contrast and luminance information across ON and OFF pathways to achieve stable behavior. (*equal contribution)

2019   **Molina-Obando, S.,** Vargas-Fique, J.F., Henning, M., Gür, B., Schladt, M., Akhtar, J., Berger, T.K., and Silies, M. (2019). ON selectivity in the Drosophila visual system is a multisynaptic process involving both glutamatergic and GABAergic inhibition.

CONFERENCES / MEETINGS

Mar 2019   **13th Göttingen meeting of German Neuroscience Society,** Göttingen, (oral presentation):
"ON selectivity is a multisynaptic computation that depends on glutamatergic and GABAergic inhibition"

Oct 2018   **Flying Sense Symposium**, Göttingen, Germany (poster presentation):
"ON selectivity is a multisynaptic computation that depends on glutamatergic and GABAergic inhibition"

Jul 2018   **FENS Forum**, Berlin, Germany (poster presentation):
Molecular mechanisms that shape ON-pathway responses in Drosophila visual system

Jun 2018   **Neurizons**, Göttingen, Germany (poster presentation):
Molecular mechanisms that shape ON-pathway responses in Drosophila visual system

Oct 2017   **CSHL meeting: Neurobiology of Drosophila**, Cold Spring Harbor, New York

Sep 2017   **Bernstein Conference**: Computational Neuroscience, Göttingen, Germany

AWARDS AND SCHOLARSHIPS

2019   **Breaking News' 2nd Best Paper Award** at the 13th Göttingen meeting of German Neuroscience Society, Göttingen.

2015-2017   **Institute Max Planck Research School** (IMPRS) Scholarship
(Master program in Neuroscience)

COVERED TECHNIQUES

Physiology   Intracellular recordings, *in vivo* 2-photon calcium imaging
Molecular Biology   PCR, DNA/RNA extraction, qRT-PCR, Western Blot, Immunostainings, cell culture
Genetics   Construct/Vector design, transgenesis, fly genetics
Behavior   Fly-on-the-ball assay

COMPUTER SKILLS

Programming   MatLab, Python
Text and Graphics   LATEX, Open Office, Inkscape, Ape, ImageJ, Adobe Illustrator
OS   Windows

LANGUAGES

Spanish   Native
Catalan   Native
English   Fluent in speaking and writing
German   Advanced (C1)

OTHER WORK EXPERIENCE

Jul'15 – Sep'16   **Logistics**, *VCSsystem, Barcelona, Spain.*
Jul '14 – Sep '15   **Waitress Manager**, *Northwoods Inn, New York, USA*
Jul '12 – Sep '13   **Student Assistant**, *Autonomous University of Barcelona (UAB), Barcelona, Spain.*
Jul'11 – Sep '11   **Krankenpfleger (Nursing)**, *Altenhaus,* Kassel, Germany.
Apr'11 – May '11   **Usher**, *Renoir Cinemas,* Barcelona, Spain.
Jul'10 – Apr '11   **Assistant at MRI facility**, *Vall d'Hebron Hospital,* Barcelona, Spain.